INFORMATION TO USERS

While the most advanced technology has been used to photograph and reproduce this manuscript, the quality of the reproduction is heavily dependent upon the quality of the material submitted. For example:

- Manuscript pages may have indistinct print. In such cases, the best available copy has been filmed.

- Manuscripts may not always be complete. In such cases, a note will indicate that it is not possible to obtain missing pages.

- Copyrighted material may have been removed from the manuscript. In such cases, a note will indicate the deletion.

Oversize materials (e.g., maps, drawings, and charts) are photographed by sectioning the original, beginning at the upper left-hand corner and continuing from left to right in equal sections with small overlaps. Each oversize page is also filmed as one exposure and is available, for an additional charge, as a standard 35mm slide or as a 17"x 23" black and white photographic print.

Most photographs reproduce acceptably on positive microfilm or microfiche but lack the clarity on xerographic copies made from the microfilm. For an additional charge, 35mm slides of 6"x 9" black and white photographic prints are available for any photographs or illustrations that cannot be reproduced satisfactorily by xerography.

Myers, Matthew Ronald

EFFECT OF AIRFOIL MEAN LOADING ON HIGH-FREQUENCY GUST INTERACTION NOISE

The University of Arizona PH.D. 1987

EFFECT OF AIRFOIL MEAN LOADING ON HIGH-FREQUENCY GUST INTERACTION NOISE

by

Matthew Ronald Myers

A Dissertation Submitted to the Faculty of the

COMMITTEE ON APPLIED MATHEMATICS

In Partial Fulfillment of the Requirements
For the Degree of

DOCTOR OF PHILOSOPHY

In the Graduate College

THE UNIVERSITY OF ARIZONA

1 9 8 7

THE UNIVERSITY OF ARIZONA
GRADUATE COLLEGE

As members of the Final Examination Committee, we certify that we have read the dissertation prepared by Matthew Ronald Myers

entitled EFFECT OF AIRFOIL MEAN LOADING ON HIGH-FREQUENCY GUST INTERACTION NOISE

and recommend that it be accepted as fulfilling the dissertation requirement for the Degree of Doctor of Philosophy.

E.J. Kerschen	Date 1/5/87
T.F. Balsa	Date 8/25/86.
G. Lamb	Date 8/22/86
	Date
	Date

Final approval and acceptance of this dissertation is contingent upon the candidate's submission of the final copy of the dissertation to the Graduate College.

I hereby certify that I have read this dissertation prepared under my direction and recommend that it be accepted as fulfilling the dissertation requirement.

Dissertation Director	Date 1/5/87

STATEMENT BY AUTHOR

This dissertation has been submitted in partial fulfillment of requirements for an advanced degree at The University of Arizona and is deposited in the University Library to be made available to borrowers under rules of the Library.

Brief quotations from this dissertation are allowable without special permission, provided that accurate acknowledgment of source is made. Requests for permission for extended quotation from or reproduction of this manuscript in whole or in part may be granted by the head of the major department or the Dean of the Graduate College when in his or her judgment the proposed use of the material is in the interests of scholarship. In all other instances, however, permission must be obtained from the author.

SIGNED: Matthew Myers

ACKNOWLEDGMENT

I would like to thank my advisor, Ed Kerschen, for his friendship, his interest in my personal development, and his willingness to share with me his tremendous physical insight. I am grateful for the opportunity I had to work with Ed. I wish to thank George Lamb for many productive discussions on wave-propagation theory and complex analysis. A special acknowledgment goes to Thomas Balsa, who served as a consultant to our project in numerous crisis situations, and who provided me with a clear presentation of the aerodynamics principles upon which much of this work is based. I thank Harry Barrett for helping me prepare for the preliminary examination and for pointing out the optical analogs to the acoustic phenomena explored in this research.

I am deeply indebted to Eddie Envia for timely assistance with computer programming. Many of the graphs and figures were prepared by Layne Bownds and Lucy Coronado. I appreciate their careful efforts.

I am extremely thankful for the unending support and encouragement of my parents in all of my educational endeavors. Their belief in my potential strongly motivated me to undertake this project. The support and friendship of Roger and Pat Voss has been very valuable during my graduate career, particularly in times of discouragement. Finally, I owe so much to my wife, Kyle, for her involvement in every aspect of this dissertation. More importantly, I am grateful for her loving contributions to my educational, emotional and spiritual growth throughout the past five years.

TABLE OF CONTENTS

		Page
	LIST OF ILLUSTRATIONS	vi
	ABSTRACT	x
1.	INTRODUCTION	1
2.	DERIVATION OF THE DISTURBANCE EQUATIONS	8
3.	ANALYSIS FOR A FLAT PLATE	21
	3.1 Local-Leading-Edge Region	28
	3.1.1 Solution for H_0	30
	3.1.2 Solution for H_1	36
	3.1.3 Solution for H_2	41
	3.2 Outer Region	47
	3.2.1 Leading-Edge Ray Field	50
	3.2.2 Matching of Leading Edge Local and Outer Acoustic Solutions	54
	3.2.3 Trailing-Edge Ray Field	57
	3.3 Local-Trailing-Edge Region	59
	3.4 Transition Region	66
	3.4.1 Transition Solution in Geometric Farfield	73
	3.5 Total Farfield Solution	74
4.	ANALYSIS FOR A CAMBERED AIRFOIL	77
	4.1 Local-Leading-Edge Region	83
	4.2 Outer Region	84
	4.3 Local-Trailing-Edge Region	88
	4.4 Transition_C Region	92
	4.5 Transition_D Region	99
	4.6 Total Farfield Solution	101
5.	NUMERICAL RESULTS AND DISCUSSION	106
	5.1 Trends with Gust Orientation	110
	5.2 Behavior with Changing Mach Number	120
	5.2.1 Comparison with the Acoustic Analogy	142
	5.4 Mean Loading Effects	154

TABLE OF CONTENTS--Continued

Page

6. CONCLUSIONS 177

APPENDIX A: MEAN QUANTITIES FOR A SMALL-PERTURBATION, PERFECT-GAS FLOW 188

APPENDIX B: ASYMPTOTIC EXPANSION BY THE METHOD OF STEEPEST DESCENT 197

APPENDIX C: SOLUTION FOR H_{2C} 212

APPENDIX D: UNIFORM ASYMPTOTIC EXPANSION OF TRAILING-EDGE SCATTERED FIELD 218

APPENDIX E: FORMULA FOR ACOUSTIC POWER 227

REFERENCES 233

LIST OF ILLUSTRATIONS

Figure		Page
1.1	Unrolled channel model for the rotor-stator interaction	2
3.1	Flat-plate airfoil at incidence angle encountering a high-frequency convected disturbance	22
3.2	Flat-plate airfoil with asymptotic regions illustrated	27
3.3	Location of singularities in the transform plane for H_0	32
3.4	Location of singularities in the transform plane for H_2	44
4.1	Cambered airfoil encountering a high-frequency convected disturbance	78
4.2	Separation of incidence angle and camber effects for calculation of perturbation mean flow	80
4.3	Cambered airfoil with asymptotic regions illustrated	82
5.1	(a,b) Farfield pressure directivity patterns illustrating leading-edge-trailing-edge interactions. (a) Leading-edge field. (b) Trailing-edge field. $M_\infty = .6$, $kk_t = 7$	108
5.2	Power vs. gust orientation. $M_\infty = .6$, $kk_t = 2.5$	112
5.3	Power vs. gust orientation. $M_\infty = .6$, $kk_t = 5.6$	113
5.4	Power vs. gust orientation. $M_\infty = .6$, $kk_t = 9$	114

LIST OF ILLUSTRATIONS--continued

Page

5.5 Power vs. gust orientation. $M_\infty = .4$, $kk_t = 5.6$ 116

5.6 Power vs. gust orientation. $M_\infty = .8$, $kk_t = 5.6$ 117

5.7 Power vs. gust orientation curves illustrating symmetry with respect to α, k_{np}. $M_\infty = .6$, $kk_t = 5.6$ 119

5.8 Power vs. spanwise wavenumber. $k_{np}/k_t = 2$, $kk_t = 8$, $M_\infty = .6$ 121

5.9 Leading-edge power vs. Mach number. $k_{np}/k_t = 1$, $kk_t = 6$ 123

5.10 Leading-edge power vs. Mach number. $k_{np}/k_t = 2$, $kk_t = 6$ 124

5.11 Leading-edge power vs. Mach number. $k_{np}/k_t = -1$, $kk_t = 6$ 125

5.12 Power vs. Mach number for individual leading-edge solutions. $k_{np}/k_t = 2$ 127

5.13 Power vs. Mach number for "gust" and "compressibility" leading-edge solutions. $k_{np}/k_t = 2$ 129

5.14 Power vs. Mach number for "compressibility" and "combined gust" solutions. $k_{np}/k_t = 2$ 131

5.15 Power vs. Mach number for "compressiblity" and "combined gust" solutions. $k_{np}/k_t = 0$ 133

5.16 Power vs. Mach number for "compressibility" and "combined gust" solutions. $k_{np}/k_t = .5$ 134

5.17 Power vs. Mach number for "compressibility" and "combined gust" solutions. $k_{np}/k_t = 1$ 135

5.18 (a,b,c) Leading-edge pressure directivity patterns. $\alpha_i = 3°$, $kk_t = 6$, $k_{np}/k_t = 1.73$. (a) $M_\infty = 0$. (b) $M_\infty = .2$. (c) $M_\infty = .4$ 137

LIST OF ILLUSTRATIONS--continued

Page

5.19 (a,b) Leading-edge pressure directivity patterns. $\alpha_i = 3°$, $kk_t = 6$, $k_{np}/k_t = 1.73$. (a) $M_\infty = .6$. (b) $M_\infty = .8$ 138

5.20 (a,b,c) Leading-edge pressure directivity patterns. $\alpha_i = 3°$, $kk_t = 6$, $k_{np}/k_t = .577$. (a) $M_\infty = 0$. (b) $M_\infty = .2$. (c) $M_\infty = .4$ 139

5.21 (a,b) Leading-edge pressure directivity patterns. $\alpha_i = 3°$, $kk_t = 6$, $k_{np}/k_t = .577$. (a) $M_\infty = .6$. (b) $M_\infty = .8$ 140

5.22 Power vs. total mean loading. $M_\infty = .6$, $kk_t = 7$, $k_{np}/k_t = 1$ 157

5.23 Power vs. leading-edge flow strength. $M_\infty = .6$, $kk_t = 7$, $k_{np}/k_t = 1$ 159

5.24 Power vs. total mean loading. $M_\infty = .45$, $kk_t = 7$, $k_{np}/k_t = 1$ 160

5.25 Power vs. leading-edge flow strength. $M_\infty = .45$, $kk_t = 7$, $k_{np}/k_t = 1$ 161

5.26 Power vs. total mean loading. $M_\infty = .75$, $kk_t = 7$, $k_{np}/k_t = 1$ 162

5.27 Power vs. leading-edge flow strength. $M_\infty = .75$, $kk_t = 7$, $k_{np}/k_t = 1$ 163

5.28 Power vs. total mean loading. $M_\infty = .6$, $kk_t = 7$, $k_{np}/k_t = 0$ 164

5.29 Power vs. leading-edge flow strength. $M_\infty = .6$, $kk_t = 7$, $k_{np}/k_t = 0$ 165

5.30 Power vs. total mean loading. $M_\infty = .6$, $kk_t = 7$, $k_{np}/k_t = -1$ 166

5.31 Power vs. leading-edge flow strength. $M_\infty = .6$, $kk_t = 7$, $k_{np}/k_t = -1$ 167

5.32 Power vs. total mean loading. $M_\infty = .6$, $kk_t = 2.1$, $k_{np}/k_t = 1$ 168

LIST OF ILLUSTRATIONS--continued

Page

5.33 Power vs. leading-edge flow strength. $M_\infty = .6$, $kk_t = 2.1$, $k_{np}/k_t = 1$ 169

5.34 General form for power vs. leading-edge flow strength curve 170

5.35 (a,b,c) Total farfield pressure directivity patterns. $M_\infty = .6$, $k_{np}/k_t = .5$, $kk_t = 7.5$. (a) Flat plate at 0°. (b) NACA "1030" at 2.75°. (c) NACA "1530" at 4.1° 174

5.36 (a,b) Total farfield pressure directivity patterns. $M_\infty = .6$, $k_{np}/k_t = .5$, $kk_t = 7.5$. (a) Flat plate at 2.3°. (b) NACA "1030" at 5° 175

6.1 Thin airfoil with nonzero thickness 185

A.1 Mean flow around thin airfoil 189

B.1 Geometry for defining point on steepest descent path 201

B.2 Steepest descent path for integrals with acoustic phase 203

B.3 Branch cuts and contour of integration for hydrodynamic integral 206

B.4 Steepest descent path for integrals with hydrodynamic phase 208

D.1 Branch cuts and path of integration in the u-plane 220

D.2 Contour of integration and pole location in the s-plane 223

ABSTRACT

This dissertation investigates the effect of airfoil steady loading on the sound generated by the interaction of an isolated, zero-thickness airfoil with a high-frequency convected disturbance. The analysis is based on a linearization of the inviscid equations of motion about a nonuniform mean flow. The mean flow is assumed to be two-dimensional and subsonic. Throughout most of the dissertation, we assume that the Mach number is O(1), though in one section we concentrate on the leading-edge region and study the behavior of the sound field as the Mach number tends to zero. The small parameter representing the amount of airfoil camber and incidence angle, and the large parameter representing the ratio of airfoil chord to disturbance wavelength, are utilized in a singular perturbation analysis.

The analysis shows that essentially all of the sound is generated at the leading and trailing edges, in regions the size of the disturbance wavelength. The solution in the local-leading-edge region reveals several sound-generating mechanisms which do not exist for an airfoil with no mean loading. These mechanisms are not present at the trailing edge; the trailing edge is important only as a scatterer of the sound produced at the leading edge. The propagation of sound away from the airfoil edges is described by geometric acoustics, with the amplitude varying on the scale of the airfoil chord and the phase varying on the much smaller scale of the disturbance wavelength.

In addition, a diffraction-type transition region exists downstream of the airfoil.

Calculations of radiated acoustic power show that the sound field depends strongly on Mach number, gust characteristics, and airfoil steady loading. Small changes in these properties can produce large changes in radiated power levels. Most importantly, we find that the amount of power radiated correlates very well with the strength of the mean flow around the leading edge.

CHAPTER 1

INTRODUCTION

Convected disturbances, often called gusts, are disturbances to a fluid which move at the local mean-flow velocity. The interaction of these disturbances with airfoils is responsible for much of the noise generated by aircraft propulsion systems. Turbulence is a common example of a convected disturbance. The turbulent fluctuations encountered by an aircraft engine can be created externally in the atmosphere, or internally as an instability of the local flow through the engine. Another example is the entropy fluctuations created by temperature fluctuations in the combustion process. Perhaps the most important example of a gust is the velocity deficits of the wakes of rotating fan blades. These velocity deficits convect downstream and interact with neighboring components, generating sound in the process. In the context of the counter-rotating propellers currently under development, the neighboring component is another rotating fan, while for a turbofan engine the downstream component is a row of stationary or stator vanes. The rotor-stator interaction is worth examining in more detail.

Shown in Fig. (1.1) is an unrolled channel model for the rotor-stator interaction. The rotor blades and stator vanes appear as infinite rows of airfoils, with the rotor row translating vertically at a velocity U_{rotor}. If we consider a reference frame moving with the

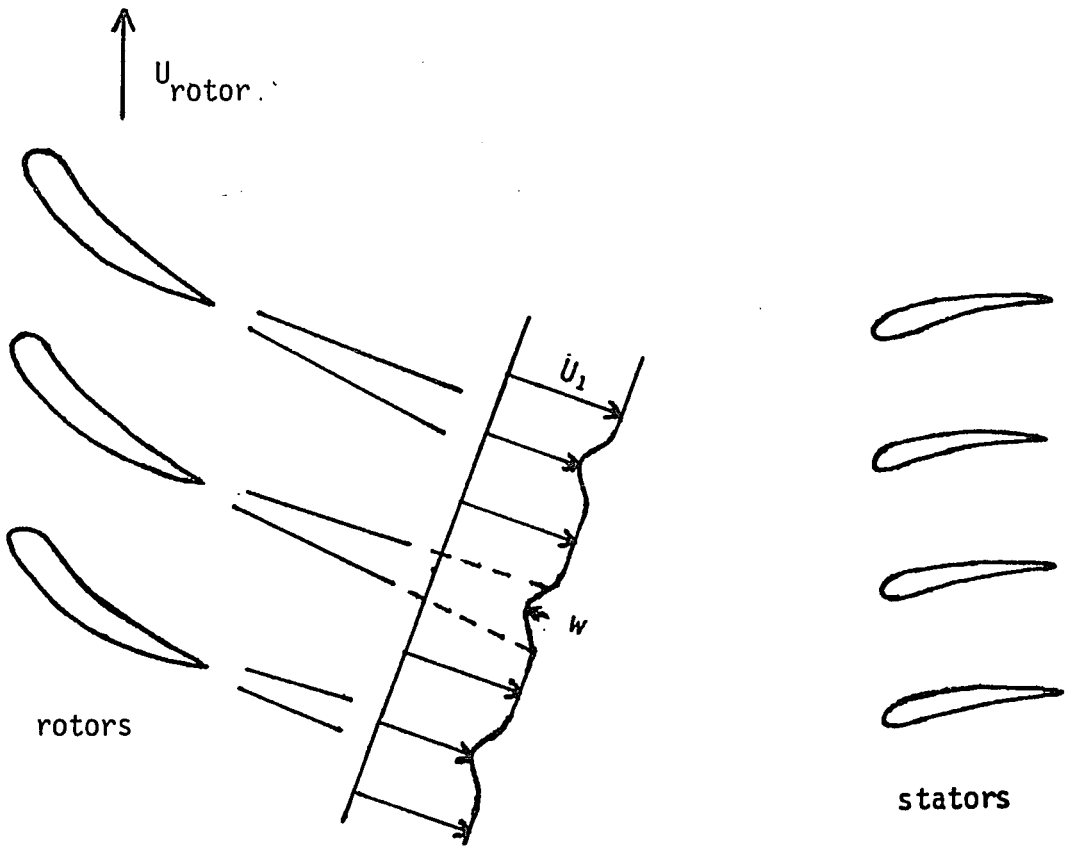

rotor wake pattern
as viewed in rotor
relative reference
frame

Fig. 1.1 Unrolled channel model for the rotor-stator interaction.

rotor, the steady flow behind the rotor row appears as shown in Fig. (1.1). This flow consists of a uniform velocity $\overline{U}_1$ plus the periodic deficit velocity $\overline{w}$ of the viscous wakes. In typical applications w is very small relative to U_1, and the deficits are essentially convected at the local mean flow speed U_1. To determine the velocity disturbance seen by an individual stator blade, we add the tangential velocity $\overline{U}_{rotor}$ to the velocity field shown behind the rotor row. The wake deficits then appear to the stators as an unsteady disturbance, due to the spatial periodicity in the moving frame. The interaction of the velocity deficits with the stators generates sound at the blade-passing frequency (the frequency at which the rotor blades pass a stator vane) and its higher harmonics. Turbulent gusts mentioned earlier contribute to the broadband noise produced by the engine.

Most analyses of airfoil-gust interactions have utilized the classical linearized approach, in which the total flow is represented as the sum of a uniform flow, an $O(\alpha)$ steady disturbance flow, and an $O(\varepsilon)$ unsteady disturbance. If one assumes that α and ε are both small but comparable, it is natural to neglect the $O(\alpha)$ corrections to the steady flow. The unsteady calculation then corresponds to small perturbations of a uniform flow, which simplifies the analysis considerably. However, in many turbomachinery applications the steady loading on the airfoils is considerable, and then the $O(\alpha)$ steady perturbation flow is large compared to the $O(\varepsilon)$ unsteady flow. It then becomes desirable to include the effects of the mean flow distortion of the unsteady motion.

The significance of steady loading effects on the noise generated by gust-airfoil interactions was first recognized by Ffowcs Williams and Hawkings (1969a). Their approach was based upon Lighthill's acoustic analogy. The acoustic analogy is a rearrangement of the equations of motion of fluid mechancis into a uniform-medium wave equation and a complicated source term. The source term is Lighthill's stress tensor, which actually depends on the pressure (or density) being solved for in the equation. Hence, one must have at least some prior knowledge about the source term and be able to model it in order to solve the wave equation. Ffowcs Williams and Hawkings modeled the interaction of the gust with the potential flow around the airfoil as a quadrupole source term. They used dimensional arguments to show that, at high subsonic Mach numbers, the quadrupole field should dominate the surface dipole field. Goldstein, Rosenbaum, and Albers (1974) and Mani (1974) utilized Ffowcs Williams' quadrupole formulation to produce actual prediction methods. In these methods the mean flow through the stator cascade was modeled as that due to a row of point vortices. Such an approximation is valid when the gust wavelength is long compared to the airfoil chord, but is inappropriate when the wavelength is small. In general, compact-source (or low-frequency) approximations can be used to model Lighthill's stress tensor when the disturbance wavelength is long compared to the airfoil chord (and the size of any source region away from the airfoil.) When the gust wavelength is short compared to the chord, i.e. in the high-frequency case, modeling in the acoustic analogy becomes much more

difficult. This is a serious drawback, since in modern aircraft engines many of the convected disturbances of interest are high frequency.

An alternative to the acoustic analogy is to consider linear unsteady disturbances of the nonuniform steady flow past the airfoil. This approach is often called rapid distortion theory, since it accounts for the rapid distortion of the gust by the nonuniform mean flow but neglects the slower-acting (under certain restrictions) viscous and nonlinear effects. The mean flows are typically irrotational in practical contexts. The first application of rapid distortion theory to the study of airfoil-gust interactions was presented by Goldstein and Atassi (1976). Their analysis assumed an incompressible mean flow and is useful for determining the sound field in the low-frequency limit.

Goldstein (1978) later extended rapid distortion theory to include compressible mean flows. Goldstein's formulation requires the solution of a linear convected wave equation with a specified source term and boundary conditions. The equation has variable coefficients, which accounts in a natural way for the nonuniform medium of propagation. In contrast, nonuniform propagation effects in the acoustic analogy appear as distributed source terms of the constant-coefficient wave equation.

Despite its linearity, Goldstein's equation is very difficult to solve. The variable coefficients and source term must in general be determined numerically. In order to obtain closed-form solutions, simplifications must be made. Kerschen and Balsa (1981) simplified the equations considerably by assuming the mean flow to be two-dimensional.

However, numerical methods are still required to evaluate the drift function (which will be defined later) appearing in the source term and boundary condition. When the mean flow is a small perturbation to a uniform flow, thin airfoil theory can be used to evaluate the drift function analytically. Kerschen and Myers (1986) simplified the equations of Kerschen and Balsa (1981) utilizing the small-perturbation mean-flow assumption. In the work of Kerschen and Myers, the mean-flow perturbation velocity, which is $O(\alpha)$ relative to the uniform flow, is large compared to the $O(\varepsilon)$ unsteady velocity. That is, $\varepsilon << \alpha << 1$.

An additional simplification arises in the high-frequency limit. In this case the boundary conditions at the airfoil leading and trailing edges can be satisfied iteratively. In the iterative scheme a leading-edge problem is first solved by assuming that the airfoil is infinite in the downstream direction. To correct the resulting error in the boundary condition along the wake, a trailing-edge problem is formulated in which the airfoil is infinite in the upstream direction. This correction gives the wrong boundary condition upstream of the airfoil, and another leading-edge problem arises to correct the upstream boundary condition. The scheme continues in this manner. For the case of a uniform mean flow, Landahl (1958) showed that the resulting series converges for all disturbance wavelengths. The high-frequency approximation has been developed for the case of a uniform mean flow by Adamczyk (1974), Amiet (1975,1976), and Martinez and Widnall (1980). Amiet (1976) showed that the unsteady lift on the airfoil is predicted to within ten percent accuracy by the first term in

the series, when the ratio of airfoil chord to acoustic wavelength is just 1/4. When one includes two terms in the series, the accuracy is even better.

In this dissertation we develop a closed-form asymptotic solution to Goldstein's equations, assuming a high-frequency gust and a mean flow which is two dimensional and nearly uniform. The small parameter representing the amount of mean loading on the airfoil, and the large parameter representing the ratio of the airfoil chord to the disturbance wavelength, are utilized in a singular-perturbation approach. The mean-flow Mach number is assumed to be O(1) and subsonic. We concentrate on a zero-thickness, isolated airfoil and indicate how the analysis can be extended to account for thickness and cascade effects.

In the following chapter we present Goldstein's equations and derive the simplified form of them for a two-dimensional, small-perturbation mean flow. In Chapter 3 the disturbance equations are solved for the case of a flat plate airfoil at a small incidence angle to the uniform stream. Chapter 4 extends the results to include airfoils with camber. Chapter 5 consists of a series of parametric studies on the formulas obtained in Chapters 3 and 4. Results of the parametric studies will be given in the form of acoustic power calculations and pressure directivity plots. In Chapter 6 we outline the future work required to extend our work into a complete noise prediction model. Chapter 6 also summarizes the conclusions of previous chapters, particularly those of Chapter 5.

CHAPTER 2

DERIVATION OF THE DISTURBANCE EQUATIONS

In this chapter we review the derivation of the equations in Goldstein's rapid distortion theory. We also examine transformations of the equations under several simplifying assumptions.

Goldstein's rapid distortion theory is concerned with the description of small-amplitude disturbances to a steady, compressible potential flow around an obstacle. The disturbances originate far upstream from the obstacle, where the mean flow is assumed to be uniform. Kovasznay (1953) described, and Goldstein (1978) recently reviewed, the nature of unsteady small-amplitude disturbances that may be imposed on a uniform flow. There are three types of disturbances: vorticity waves, acoustic waves, and entropy waves. Each of the three components to the unsteady motion is a solution of the governing equations and can be imposed independently of the others. We summarize the disturbances now.

The velocity field for the unsteady flow can be divided into two parts. The first part, often called a gust, is purely convected or "frozen in the flow". It has zero divergence and there are no pressure fluctuations associated with it. All of the fluid rotation or vorticity is associated with this field; hence it is often referred to as the vortical velocity. The second part is an irrotational field which contains pressure fluctuations, and for compressible flows is an

acoustic wave. The acoustic wave propagates at the speed of sound relative to the fluid.

In addition to the unsteady velocity, entropy fluctuations may be imposed on the flow. The entropy fluctuations are decoupled from the velocity and pressure but do produce density fluctuations. The entropy fluctuations are convected at the mean-flow speed, i.e, they are also "frozen in the fluid". The unsteadiness of all the disturbances is observed in the obstacle reference frame; the two convected fields will of course appear steady in a frame moving at the mean-flow speed.

Any acoustic waves present far upstream must be incoming waves, since waves generated near the obstacle decay to zero at infinity. Since we are interested in sound generation rather than scattering, we do not consider any incident acoustic waves. We impose convected vortical and entropic disturbances far upstream, which become distorted as they convect downstream due to the nonuniform mean flow around the obstacle. Calculation of the sound field generated by the interaction of the disturbances with the mean flow and the boundary is the main objective of this dissertation.

We now derive Goldstein's equation in a general form, without specifying the obstacle or making any assumptions about the convected disturbance. In Chapters 3 and 4 the obstacle and gust will be further specified. The assumptions we make here are that the fluid is an inviscid, non-heat-conducting, perfect gas. For most aeronautical applications, where the mean flow and turbulence Reynold's numbers are large, and the fluid is air, these assumptions are well justified.

The analysis begins with the inviscid equations of motion, which are

(momentum)
$$\rho \frac{D\overline{U}}{Dt} = -\nabla p \tag{2.1a}$$

(continuity)
$$\frac{D\rho}{Dt} + \rho \nabla\cdot\overline{U} = 0 \tag{2.1b}$$

(energy)
$$\frac{DS}{Dt} = 0 \quad , \tag{2.1c}$$

where
$$\frac{D}{Dt} = \frac{\partial}{\partial t} + \overline{U}\cdot\nabla \quad . \tag{2.1d}$$

Here ρ is the density, p the pressure, $\overline{U}$ the velocity, and S the entropy of the fluid. Overbars denote vectors. The following expression, which is a consequence of the perfect-gas equation of state ($p = \rho RT$) and the first law of thermodynamics, will also be utilized

$$S_1 - S_2 = c_v \ln(p_1/p_2) - c_p \ln(\rho_1/\rho_2) \quad . \tag{2.1e}$$

The subscripts 1 and 2 denote two thermodynamic states. The specific heats at constant volume and constant pressure, c_v and c_p, are assumed constant.

At upstream infinity the velocity and entropy fields have the form

$$\overline{U} = \overline{U}_\infty + \overline{u}'_\infty(\overline{x},t) \tag{2.2a}$$

$$S = s'_\infty(\overline{x}t) \tag{2.2b}$$

with

$$\frac{u'_\infty}{U_\infty} = O(\varepsilon) \qquad \text{and} \qquad \frac{s'_\infty}{c_p} = O(\varepsilon) \quad , \quad \varepsilon << 1 \quad . \qquad (2.2c)$$

Here the scalar velocities denote the magnitude of the vector quantities. Under the condition (2.2c), we anticipate a solution to Eqs. (2.1a,b,c) of the form

$$\overline{U} = \overline{U}_0(\overline{x}) + \overline{u}'(\overline{x},t) \qquad p = p_0(\overline{x}) + p'(\overline{x},t) \qquad (2.3a,b)$$

$$\rho = \rho_0(\overline{x}) + \rho'(\overline{x},t) \qquad S = s'(\overline{x},t) \quad , \qquad (2.3c,d)$$

with the unsteady quantities, denoted by primes, much smaller than the steady ones. The mean flow is the steady but nonuniform flow around the obstacle one would obtain if $\overline{u}'_\infty$ and s'_∞ were zero. The entropy for the mean flow is everywhere equal to a constant, which we take to be zero. Since viscosity is ignored and the steady flow at upstream infinity is assumed uniform, the mean flow is irrotational. The mean velocity can be expressed as the gradient of a potential function; we will utilize this property below and in Chapters 3 and 4.

Inserting Eqs. (2.3) into (2.1), neglecting squares of unsteady terms, and subtracting out the mean-flow equations, Goldstein obtained after several subsequent manipulations a set of linearized disturbance equations. (The states used in Eq. (2.1e) are the actual state and the mean-flow state.) The results are:

$$\frac{D_0 s'}{Dt} = 0 \qquad (2.4a)$$

$$\overline{u}' = \overline{v}' + \nabla G' \quad , \qquad (2.4b)$$

where

$$\overline{v}' = \frac{s'}{2c_p}\,\overline{U}_0 + \overline{v}^* \tag{2.4c}$$

with

$$\frac{D_0\overline{v}^*}{Dt} + \overline{v}^*\cdot\nabla\,\overline{U}_0 = 0 \quad , \tag{2.4d}$$

and the potential G' satisfies

$$\frac{D_0}{Dt}\left(\frac{1}{a_0^2}\frac{D_0G'}{Dt}\right) - \frac{1}{\rho_0}\nabla\cdot(\rho_0\nabla G') = \frac{1}{\rho_0}\nabla\cdot(\rho_0\overline{v}') \quad . \tag{2.4e}$$

The quantity a_0 is the speed of sound for the mean flow. The substantial derivative is with respect to the mean flow, i.e.,

$$\frac{D_0}{Dt} = \frac{\partial}{\partial t} + \overline{U}_0 \cdot \nabla \quad . \tag{2.4f}$$

The pressure is obtained from the relation

$$p' = -\rho_0\frac{D_0G'}{Dt} \quad , \tag{2.4g}$$

and the density is related to the pressure and entropy by

$$\rho' = p'/a_0^2 - \rho_0 s'/c_p \quad . \tag{2.4h}$$

The appropriate boundary condition on the body surface is

$$\overline{n}\cdot\nabla G' = -\overline{n}\cdot\overline{v}' \quad , \tag{2.4i}$$

where $\overline{n}$ is the normal to the surface. The radiation or outgoing wave condition applies at infinity.

Goldstein's velocity decomposition (2.4b) does not correspond to the classical decomposition of a vector field into solenoidal and irrotational parts, since in general $\overline{v}'$ is not divergence free. We will find that $\overline{v}'$ represents a velocity field convected at the local mean-flow speed, having the gust at upstream infinity as its initial condition. The acoustic field is contained in the potential G'. One can begin to see the nature of the sound field produced in gust-airfoil interactions by examining Eqs. (2.4). One mechanism for sound generation is the interaction of the gust $\overline{v}'$ with the boundary, as described by the boundary condition (2.4i). Another mechanism is the source term of the wave equation (2.4e). A volume source is produced in the fluid whenever there are significant changes in the momentum flux $\rho_0\overline{v}'$ associated with the convected disturbance. (Though, as we shall see, the source term does not always produce sound.) The sound generated propagates in a nonuniform medium as evidenced by the variable coefficients in Eq. (2.4e).

Equations (2.4a) and (2.4d), being first-order partial differential equations, can be solved by the method of characteristics. We will give the solution below. Equation (2.4e), however, is much more difficult to solve. Under general circumstances even the mean-flow quantities comprising the variable coefficients have to be determined numerically. In order to obtain an analytical solution, it is worth making some simplifying assumptions.

The assumption of two-dimensional mean flow produces significant simplifications. We consider a two-dimensional mean flow with $U_{0,i} = U_{0,i}(x_1,x_2)$, $i = 1,2$, and $U_{0,3} = 0$. Since the vorticity and

entropy fluctuations are convected along the mean-flow streamlines, it is convenient to introduce as orthogonal coordinates in the (x_1,x_2) plane the variables (ϕ,ψ), which are variations of the velocity potential and the stream function of the mean flow. The appropriate coordinate metrics are

$$h_\phi = 1/U_0 \qquad h_\psi = \rho_\infty/(\beta_\infty \rho_0 U_0) \quad , \tag{2.5}$$

where $\beta_\infty^2 = 1 - M_\infty^2$ and $M_\infty = U_\infty/a_\infty$ is the mean-flow Mach number at infinity. The β_∞ in the metric corresponds to a Prandtl-Glauert transformation, i.e.,

$$\phi = \phi_0 \qquad \psi = \beta_\infty \psi_0 \quad , \tag{2.6}$$

where ϕ_0 and ψ_0 are the actual mean-flow potential and streamfunction. The Prandtl-Glauert transformation will produce the final equation in canonical form. All of the analysis in the dissertation will be performed in the Prandtl-Glauert transformed, potential-streamline coordinates (ϕ,ψ). The final results will be transformed back into physical Cartesian coordinates for interpretation. Because we wish to allow the gust to be three-dimensional, we introduce the variable $\chi = U_\infty x_3$ as our third coordinate, where x_3 is the standard Cartesian coordinate. The factor of U_∞ is for dimensional consistency with the other coordinates. The metric for χ is $1/U_\infty$. In (ϕ,ψ,χ) space the substantial derivative becomes $D_0/Dt = \partial/\partial t + U_0^2 \partial/\partial\phi$.

Since the governing equations are linear, and the mean flow is uniform far upstream, an arbitrary upstream disturbance can be

represented as a superposition of harmonic waves. Hence we consider vortical and entropic disturbances having the following form far upstream

$$\left[\begin{matrix}\overline{v}' \\ s'\end{matrix}\right]\Bigg|_{\phi\to-\infty} = \left[\begin{matrix}U_\infty(A_t,A_n,A_3) \\ 2c_pB\end{matrix}\right] e^{i(k_t\phi + k_n\psi + k_3\chi - k_tU_\infty^2t)} \quad .(2.7a)$$

The quantities (A_t,A_nA_3) and (k_t,k_n,k_3) are the velocity-amplitude and wavevector components in (ϕ,ψ,χ) space. Far upstream where the flow is uniform the (ϕ,ψ,χ) direction vectors coincide with the standard Cartesian unit vectors. Under uniform-mean-flow conditions $\overline{v}'$ is solenoidal, so the wavevector and velocity components must satisfy the relation

$$A_t\ k_t + A_n\ k_n\ \beta_\infty + A_3\ k_3 = 0 \quad . \qquad (2.7b)$$

That is, the gust is a transverse wave. The factor β_∞ arising in (2.7b) comes from the metric h_ψ (see (2.5)) utilized in taking the divergence.

Equation (2.7a) is the initial condition for the equations (2.4a,d) governing the convected quantities. Kerschen and Balsa (1981) derived the solution to these equations in the (ϕ,ψ,χ) coordinate system. Separating Eq. (2.4d) into its three components, integrating the resulting first-order partial differential equations, and enforcing Eq. (2.7a), they showed that

$$\bar{v}'(\phi,\psi,\chi,t) = (v_t', v_n', v_3') \tag{2.8a}$$

$$v_t'/U_\infty = \left(A_t^* U_\infty/U_0 + BU_0/U_\infty \right) e^{i\sigma} \tag{2.8b}$$

$$v_n'/U_\infty = (\rho_0 U_0/\rho_\infty U_\infty)\left[A_n + \beta_\infty A_t^* \, \partial g/\partial\psi \right] e^{i\sigma} \tag{2.8c}$$

$$v_3'/U_\infty = A_3 \, e^{i\sigma} \tag{2.8d}$$

$$s' = 2c_p \, B \, e^{i\sigma} \tag{2.8e}$$

where

$$\sigma = k_t\phi + kg(\phi,\psi) + k_n\psi + k_3\chi - k_t U_\infty^2 t$$

$$A_t^* = A_t - B$$

and

$$g(\phi,\psi) = \int_{-\infty}^{\phi} \left[U_\infty^2/U_0^2(\zeta,\psi) - 1 \right] d\zeta \quad . \tag{2.8f}$$

The function $g(\phi,\psi)$ is Lighthill's Drift function, which represents the cumulative distortion of fluid material lines relative to uniform convection at speed U_∞.

We next simplify the wave equation (2.4e) for G', which at this point is the only remaining unknown. Because the mean flow and body shape are independent of the spanwise coordinate and time, we can factor the χ and t dependence out of Eqs. (2.4). Setting

$$s' = s \, e^{i(k_3 \chi - k_t U_\infty^2 t)} \tag{2.9a}$$

$$\bar{v}' = (v_t, v_n, v_3) \, e^{i(k_3 \chi - k_t U_\infty^2 t)} \tag{2.9b}$$

$$G' = G\, e^{i(k_3 x - k_t U_\infty^2 t)} \qquad (2.9c)$$

we obtain the following transformation of Eq. (2.4e):

$$\frac{\partial}{\partial\phi}(\beta_0^2\frac{\partial G}{\partial\phi}) + \frac{\partial}{\partial\psi}(\frac{\beta_\infty^2\rho_0^2}{\rho_\infty^2}\frac{\partial G}{\partial\psi}) + \frac{2ik_t(U_\infty^2)}{a_0^2}\frac{\partial G}{\partial\phi}$$

$$+ \frac{U_\infty^2}{a_0^2}\left[\frac{k_t^2U_\infty^2}{U_0^2} - \frac{k_3^2}{M_0^2} - 2ik_t \frac{\partial}{\partial\phi}(\log a_0) \right] G$$

$$= - \frac{\partial}{\partial\phi}(\frac{U_\infty}{U_0}v_t) - \frac{\partial}{\partial\psi}(\frac{\rho_0U_\infty\beta_\infty}{\rho_\infty U_0} v_n) - \frac{ik_3(U_\infty^2)}{U_0^2} v_3 \qquad (2.9d)$$

where M_0 is the local Mach number of the mean flow and $\beta_0^2 = (1 - M_0^2)$.

For a compressible flow, the mean-flow quantities which appear in Eq. (2.9d) must still be determined numerically, which precludes any possiblity of an analytical solution for G. Closed-form approximations for these quantities can be obtained with the further assumption that the mean flow is a small perturbation to a uniform flow. We require that the mean-flow perturbation (say $O(\alpha)$) is much larger than the $O(\varepsilon)$ unsteady disturbances. The small-perturbation, perfect-gas relations for the mean flow are derived in Appendix A. We quote the results here

$$U_0/U_\infty = 1 + q \qquad \text{where} \quad q = O(\alpha) \qquad (2.10a)$$

$$\frac{a_0}{a_\infty} = 1 - \frac{\gamma-1}{2}M_\infty^2\, q \qquad \frac{M_0}{M_\infty} = 1 + (1 + \frac{\gamma-1}{2}M_\infty^2)\, q \qquad (2.10b,c)$$

$$\frac{\beta_0}{\beta_\infty} = 1 - (1 + \frac{\gamma-1}{2} M_\infty^2) \frac{M_\infty^2}{\beta_\infty^2} q \qquad \frac{\rho_0}{\rho_\infty} = 1 - M_\infty^2\, q \qquad (2.10d,e)$$

Here γ is the ratio of the specific heats, c_p/c_v. The function $q(\phi,\psi)$ appearing in each relation is the $O(\alpha)$ perturbation to the normalized mean flow speed. As shown in Appendix A, it can be easily obtained in the complex variable formulation from the relation,

$$q(\phi,\psi) - i\mu(\phi,\psi) = F'(z) \quad , \tag{2.11a}$$

where

$$z = \frac{\phi+i\psi}{U_\infty} \tag{2.11b}$$

and F is the perturbation complex potential. The potential F is described in detail in Appendix A. The harmonic conjugate of q, μ, is $1/\beta_\infty$ times the mean flow angle relative to the uniform flow at upsteam infinity.

Using Eqs. (2.10) in Eq. (2.9d), making the following generalized Miles transformation,

$$h = G \exp(ik_t M_\infty^2 \phi/\beta_\infty^2) \exp(-M_\infty^2 q) \tag{2.12a}$$

$$= G \exp(ik_t M_\infty^2 \phi/\beta_\infty^2) [1 - M_\infty^2 q + O(\alpha^2)]$$

and neglecting terms of $O(\alpha^2)$, we obtain after a considerable amount of manipulation

$$\frac{\partial^2 h}{\partial \phi^2} + \frac{\partial^2 h}{\partial \psi^2} + w^2 (1 - 2\beta_\infty^2 q)\, h +$$

$$(\gamma+1)\frac{M_\infty^4}{\beta_\infty^2}\left[q\left[\frac{\partial^2 h}{\partial \psi^2} + 2i\delta\frac{\partial h}{\partial \phi} + (w^2+\delta^2)h\right] - \frac{\partial q}{\partial \phi}\left[\frac{\partial h}{\partial \phi} - i\delta h\right] \right] = S(\phi,\psi)\, e^{i\Omega} \tag{2.12b}$$

where

$$\delta = k_t/\beta_\infty^2 \qquad w^2 = (M_\infty \delta)^2 - (k_3/\beta_\infty)^2 \qquad \Omega = \delta\phi + k_\eta \psi + k_t g(\phi,\psi)$$

and

$$S(\phi,\psi) = 2\,[\, i(k_t A_t^*/\beta_\infty^2 - k_\eta A_\eta \beta_\infty)\, q + i(k_\eta A_t^* + k_t A_\eta/\beta_\infty)\, \mu$$

$$+ A_t^* M_\infty^2/\beta_\infty^2 \frac{\partial q}{\partial \phi} + A_\eta M_\infty^2/\beta_\infty \frac{\partial q}{\partial \psi}\,] \quad . \tag{2.12c}$$

For a small-perturbation mean flow, Eq. (2.8f) for the Drift function reduces to

$$g = -2\int_{-\infty}^{\phi} q(\gamma,\psi)\, d\gamma \quad ,$$

as one can see by expanding $U_\infty^2/U_0^2 = 1/(1+q)^2$. In terms of the complex potential this result becomes

$$g(\phi,\psi) = -2\ \mathrm{Re}\{\, F(z)\,\} \tag{2.12d}$$

where F(z) is the complex potential for the perturbation mean flow. The arbitrary constant in F(z) is chosen such that the Drift function vanishes at upstream infinity. The transformed boundary condition is

$$\left[\frac{\partial h}{\partial \psi} + M_\infty^2 \frac{\partial q}{\partial \psi} h\right]_{(\psi=\psi_0)} = -\left[\frac{A_n}{\beta_\infty}(1-M_\infty^2 q) - 2A_t^* \mu\right] e^{i\Omega} \quad , \quad (2.12e)$$

where $\psi = \psi_0$ on the body surface and the range of ϕ corresponds to the body length in the (ϕ,ψ) plane.

Eqs. (12) represent the final form of our governing equations for the modified unsteady-disturbance potential $h(\phi,\psi)$. All of the information about the sound field generated in gust-airfoil interactions will be obtained from simple operations on $h(\phi,\psi)$. To retain the advantages of a closed-form solution, in the next chapter we study the geometrically-simple case of a flat-plate airfoil at small incidence angle to the uniform stream at infinity. The gust wavelength is assumed short compared to the airfoil chord. In Chapter 4 the results of Chapter 3 are extended to include airfoils with camber.

CHAPTER 3

ANALYSIS FOR A FLAT PLATE

In this chapter the general results of Chapter 2 are applied to the following specific problem. We consider a flat plate of length 2b at mean incidence angle α to a uniform stream, interacting with a convected disturbance whose wavelength λ is short compared to the airfoil chord. The leading edge of the airfoil is located at the origin in the (x_1,x_2) plane. The problem is illustrated in Fig. (3.1). To solve Eqs. (2.12) for the modified acoustic potential h, we utilize the small-incidence angle and high-frequency assumptions in a perturbation method. To properly assess the magnitudes of the various quantities, we nondimensionalize all of our variables. The following list provides the relation between the previous variables and the new, nondimensional variables, which are superscripted by a dagger:

$$\phi = b\, U_\infty\, \phi^\dagger \qquad \psi = b\, U_\infty\, \psi^\dagger \qquad \chi = b\, U_\infty\, \chi^\dagger \quad (3.1a,b,c)$$

$$h = b\, U_\infty\, h^\dagger \qquad (3.1d)$$

$$(k_t\ ,k_n\ ,k_3) = (k_t{}^\dagger\ ,k_n{}^\dagger\ ,k_3{}^\dagger)\ \frac{2\,\pi}{U_\infty\,\lambda} \qquad (3.1e)$$

A set of nondimensional equations results by inserting Eqs. (3.1) into (2.12). The equations, with the daggers omitted from the variables for ease in writing, are

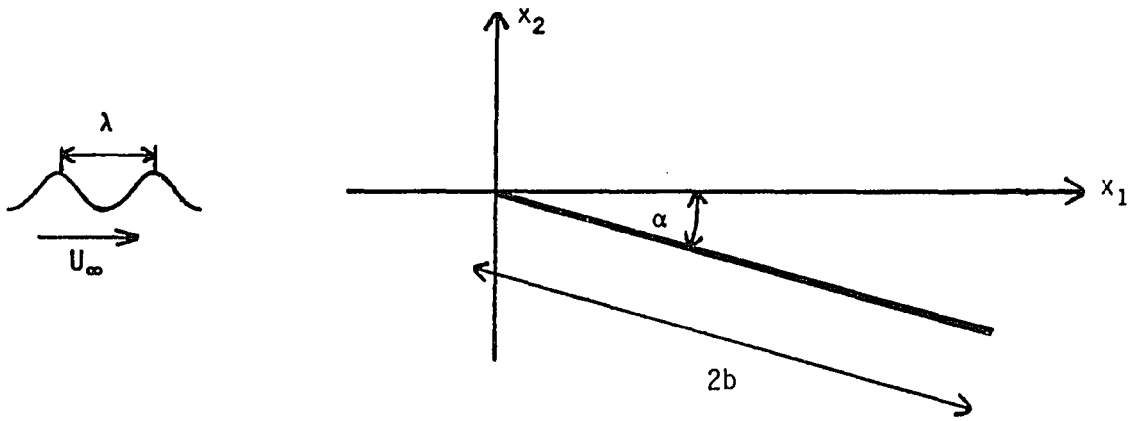

Fig. 3.1 Flat-plate airfoil at incidence angle encountering a high-frequency convected disturbance.

$$\frac{\partial^2 h}{\partial \phi^2} + \frac{\partial^2 h}{\partial \psi^2} + k^2 w^2 h - 2k^2 w^2 \beta_\infty^2 q h + \frac{(\gamma+1) M_\infty^4 q}{\beta_\infty^2}\left[\frac{\partial^2 h}{\partial \psi^2} + 2ik\delta \frac{\partial h}{\partial \phi} + k^2(w^2+\delta^2)h\right]$$

$$- \frac{(\gamma+1) M_\infty^4}{\beta_\infty^2} \frac{\partial q}{\partial \phi}\left[\frac{\partial h}{\partial \phi} - ik\delta h\right] = k e^{ik\Omega} S(\phi,\psi) \quad , \tag{3.2a}$$

where

$$S(\phi,\psi) = \frac{2}{\beta_\infty^2}[iq(A_t^* k_t - A_n k_n \beta_\infty^3) + i\beta_\infty \mu(\beta_\infty k_n A_t^* + A_n k_t)$$

$$+ \frac{A_t^* M_\infty^2}{k} \frac{\partial q}{\partial \phi} + \frac{A_n M_\infty^2 \beta_\infty}{k} \frac{\partial q}{\partial \psi}] \tag{3.2b}$$

and

$$\Omega = \delta\phi + k_n \psi + k_t g(\phi,\psi) \quad . \tag{3.2c}$$

The constant k appearing in the nondimensionalized equations is the high-frequency parameter, defined by

$$k = \frac{2\pi b}{\lambda}$$

The boundary condition is

$$\frac{\partial h}{\partial \psi} + M_\infty^2 \frac{\partial q}{\partial \psi} h = \left[-\frac{A_n}{\beta_\infty} + 2\mu A_t^* + \frac{A_n M_\infty^2 q}{\beta_\infty} \right] e^{ik\Omega} \quad . \tag{3.2d}$$

It is applied on the surface $\psi = \psi_0$. The precise location of the airfoil in the (ϕ,ψ) plane will be given below. The definitions of the wavenumbers w and δ, which appear throughout Eqs. (3.2), are repeated here for completeness:

$$w^2 = (\delta M_\infty)^2 - (k_3/\beta_\infty)^2 \qquad \delta = k_t/\beta_\infty^2 \quad .$$

Essentially, w is the wavenumber of the acoustic wave and δ the wavenumber of the convected wave.

The flow speed q, flow angle μ, and drift function g are obtained from the perturbation complex potential for the flow around the flat plate. The potential, which is obtained in Appendix A, is

$$F(z) = \frac{i\alpha}{\beta_\infty}\left[\log(z-1+\sqrt{z(z-2)}) + z - \sqrt{z(z-2)} - i\pi\right] \quad , \qquad (3.3a)$$

where $z = \phi + i\psi$. The arbitrary constant in F is chosen so that the drift function vanishes at upstream infinity. The expression for the drift function (Eq. (2.12d)) is

$$g(\phi,\psi) = -2\ \mathrm{Re}\ \{\ F(z)\ \} \quad . \qquad (3.3b)$$

The complex velocity is given by

$$q - i\mu = F'(z) = \frac{i\alpha}{\beta_\infty}\left[1 - \sqrt{\frac{z-2}{z}}\right] \quad . \qquad (3.3c)$$

The location of the airfoil in (ϕ,ψ) space can also be obtained from Eq. (3.3a). The Cartesian coordinates (x_1,x_2), nondimensionalized by the semi-chord b, are related to the potential-streamline coordinates (ϕ,ψ) (see Appendix A) by

$$z = \zeta + F(\zeta) + O(\alpha^2) \qquad (3.4a)$$

where $\zeta = x_1 + i\beta_\infty x_2$. Upon inserting the coordinates for the airfoil in physical space, $0 < x_1 < 2$, $x_2 = 0$, into (3.4a), we have the airfoil location in (ϕ,ψ) coordinates:

$$0 < \phi < 2 \pm \alpha\pi/\beta_\infty \qquad \psi = 0 \quad . \tag{3.4b}$$

The plus sign applies above the airfoil and the minus sign below. The location of the trailing edge is different above and below the airfoil due to the net circulation. The boundary condition (3.2d) is applied on the surface described by Eq. (3.4b)

Equations (3.2) through (3.4) provide the framework for an analytical study of the problem shown in Fig. (3.1). All of the variable coefficients in the differential equation and boundary condition have been obtained in closed form. The source term is also known analytically. The advantage of using (ϕ,ψ) coordinates appears in the boundary condition - the condition is applied at a constant value of one of the coordinates. A slight disadvantage of using (ϕ,ψ) coordinates has also emerged. This is the fact that the trailing edge is located at two separate locations. As a final word on the governing equations, we point out that while the large parameter k has been explicitly extracted from the quantities, the small parameter α has not. This choice will prove advantageous in the analysis of the cambered airfoil, where several small parameters emerge. Hence, in analyzing the above equations we remember that q, μ, g, and F are all $O(\alpha)$.

We now develop an asymptotic solution to Eqs. (3.2) for small α and large k, with $\alpha k = O(1)$. The asymptotic expansion has a singular-perturbation nature, and involves four different regions as illustrated in Fig. (3.2). The appropriate length scale in the local regions near the airfoil leading and trailing edges is the disturbance wavelength. Since we assume that M_∞ is O(1), the convective and acoustic wavelengths have the same order of magnitude. In the outer region away from the airfoil leading and trailing edges, the mean flow varies slowly compared to the disturbance wavelength and the solution has a multiple-scales or geometric-acoustics form. However, in a region of small angular extent downstream of the airfoil, the assumption of a slowly-varying amplitude and rapidly-varying phase becomes invalid. The trailing-edge geometric-acoustics solution becomes singular in this "transition" region, which is analogous to the transition region between illuminated and shadow regions in the corresponding optical problem. In the ϕ direction, the transition solution has the same multiple-scales behavior as in the outer region, i.e. it depends on both ϕ and $k\phi$, but in the ψ direction the dependence enters as $\sqrt{k\psi}$. A similarity solution will be developed in the transition region.

The condition $\alpha^2 k << 1$, satisfied by assuming $\alpha k = O(1)$, is utilized in the analysis. For a flat-plate airfoil, the shift in mean-flow stagnation point is $O(\alpha^2 b)$. Thus, the assumption $\alpha^2 k << 1$ implies that the shift of the mean-flow stagnation point is small compared to the disturbance wavelength. In practical terms, wavelengths so small that this assumption is violated probably do not contribute much to the

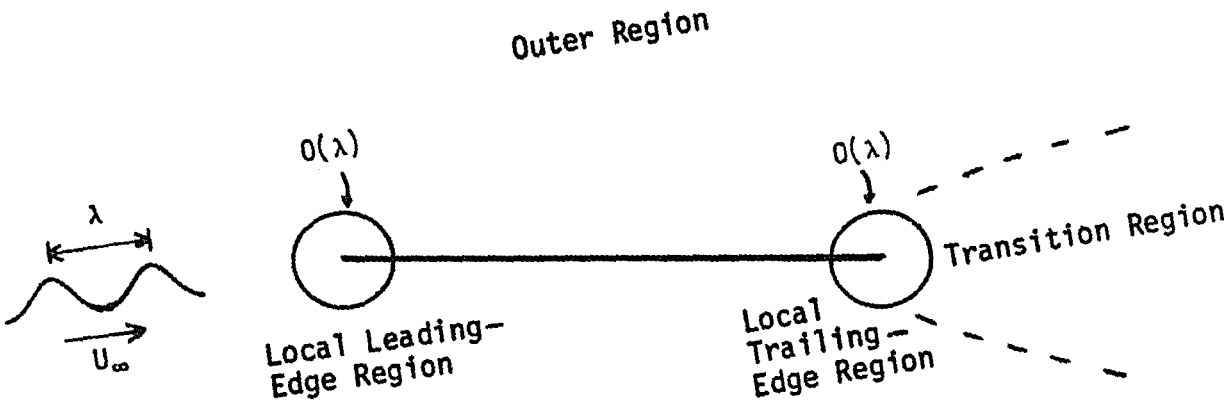

Fig. 3.2 Flat-plate airfoil with asymptotic regions illustrated.

sound field. For $\alpha^2 k << 1$, the mean-flow gradients are small when expressed in local-leading-edge coordinates. This property is utilized in developing the solution in the leading-edge region.

The following sections present the details of the analysis in the various regions. Throughout the chapter, upper-case letters will be used for local (leading- or trailing-edge) coordinates, potentials, and pressures. Lower case letters will be used in the outer region. The unsubscripted independent variables are referenced from the leading edge. Additional subscripted variables, both dependent and independent, will be defined in the course of the analysis.

3.1 Local Leading-Edge Region

In the local-leading-edge region, we introduce local coordinates, (Φ,Ψ), which scale on the disturbance wavelength and have their origin at the leading edge. The local coordinates are

$$\Phi = k\,\phi \qquad \Psi = k\,\psi \qquad Z = \Phi + i\Psi = R\,e^{i\theta}$$

The expansions of the mean-flow quantities in local coordinates, obtained from Eqs. (3.3), are

$$q - i\mu \sim \frac{\alpha\sqrt{k}\sqrt{2}}{\beta_\infty} R^{-1/2}\left(\cos\frac{\theta}{2} - i\sin\frac{\theta}{2}\right) \tag{3.5a}$$

$$g \sim -\frac{4\sqrt{2}\,\alpha}{\beta_\infty\sqrt{k}} R^{1/2}\cos\frac{\theta}{2} \quad . \tag{3.5b}$$

Utilizing these results in Eqs. (3.2), and writing the differential operators in local variables, we find that the asymptotic expansion in the leading-edge region has the form

$$H_{\ell}(\Phi, \Psi) = \frac{1}{k} \left[H_0 + \alpha\sqrt{k} \, (H_1 + H_2) \; + O \, (\alpha^2 k \, , \alpha) \right] \quad . \qquad (3.6)$$

The terms H_1 and H_2 are of equal importance, but have been separated because they represent different physical effects. H_1 contains the effects of the modified boundary conditions on the airfoil surface and the variations in mean-flow velocity and sound speed. H_2 arises from the volume source term, (3.2b). As we will show later, H_2 also arises in an acoustic-analogy approach in the local-leading-edge region, using the volume quadrupoles as the source in Lighthill's equation.

In leading-edge coordinates the airfoil body appears semi-infinite. The solutions are developed using Fourier transform techniques. In several instances the Wiener-Hopf technique must be utilized to obtain solutions to mixed boundary-value problems. To determine the noise radiated to the farfield, the important feature of these local solutions is their asymptotic behavior at distances many disturbance wavelengths away from the leading edge. We follow Van Dyke's (Van Dyke, 1975) matching rule, which involves expansion of the local solutions in outer coordinates. This asymptotic behavior is determined by the method of steepest descent.

3.1.1 Solution for H_0

The first term H_0 of the leading-edge solution satisfies the equations for the case of zero incidence angle. Here the noise generation is due solely to the blocking by the airfoil of the undistorted vortical-velocity component normal to the body surface. The governing equations are

$$D(H_0) = 0 \tag{3.7a}$$

$$\frac{\partial H_0}{\partial \Psi}\bigg|_{\Psi=0,\Phi>0} = -\frac{A_n\, e^{i\delta\Phi}}{\beta_\infty} \quad , \tag{3.7b}$$

where

$$D = \frac{\partial^2}{\partial \Phi^2} + \frac{\partial^2}{\partial \Psi^2} + w^2 \quad . \tag{3.7c}$$

Since the airfoil appears locally semi-infinite, the boundary condition is applied on the half-plane $\Phi > 0$.

The radiation condition is satisfied by assuming that w has a small positive imaginary part. We assume that δ has a small positive imaginary part to assure convergence in evaluating the Fourier transform of Eq. (3.7b). Equations (3.7) can be solved by the Wiener-Hopf technique. In the Wiener-Hopf technique, the boundary data for $\Phi <$ 0 and $\Phi >$ 0 are transformed and combined into a single equation. This equation is arranged with functions (some known, some unknown) analytic in the upper-half plane on one side of the equality and terms analytic in the lower half-plane on the other. The two sides of the equation

are equivalent on a strip in the transform plane, and therefore are analytic continuations of each other. The entire function formed by the two sides is uniquely determined by an edge condition. Typically, the entire function is shown to be bounded (using the edge condition), and hence by Liouville's theorem it is a constant. Once the entire function is known, the unknown functions on the left and right sides of the Wiener-Hopf equation, and hence the solution to the mixed boundary-value problem, can be determined. The details of the Wiener-Hopf argument, which utilize Fig. (3.3), are as follows.

We apply a Fourier transform on Φ, solve the resulting ordinary differential equation in terms of an unknown function of the transform variable, and write the inversion integral as

$$H_0 = \frac{\operatorname{sgn}\Psi}{\sqrt{2\pi}} \int_{-\infty}^{\infty} C(\lambda)\, e^{-i\lambda\Phi - |\Psi|\sqrt{\lambda^2 - w^2}}\, d\lambda \quad . \tag{3.8a}$$

The $\operatorname{sgn}\Psi$ function is necessary to satisfy the requirement that $\partial H_0/\partial\Psi$ be continuous across $\Psi = 0$. To solve for $C(\lambda)$ we utilize two conditions on $\Psi = 0$, one for $\Phi < 0$ and another for $\Phi > 0$. For $\Phi < 0$ continuity of the potential H_0 is imposed, i.e.,

$$\Delta H_0 = H_0 \Big|_{\Psi=0^-}^{\Psi=0^+} = 0 \quad \text{for } \Phi < 0 \quad . \tag{3.8b}$$

We utilize condition (3.8b) by taking the Fourier transform of the jump in potential across $\Psi = 0$. Since ΔH_0 is 0 for $\Phi < 0$, its Fourier transform is analytic in the upper half-plane. But from Eq. (3.8a), the Fourier transform of ΔH_0 is just 2 $C(\lambda)$. Hence $C(\lambda)$ is analytic in the

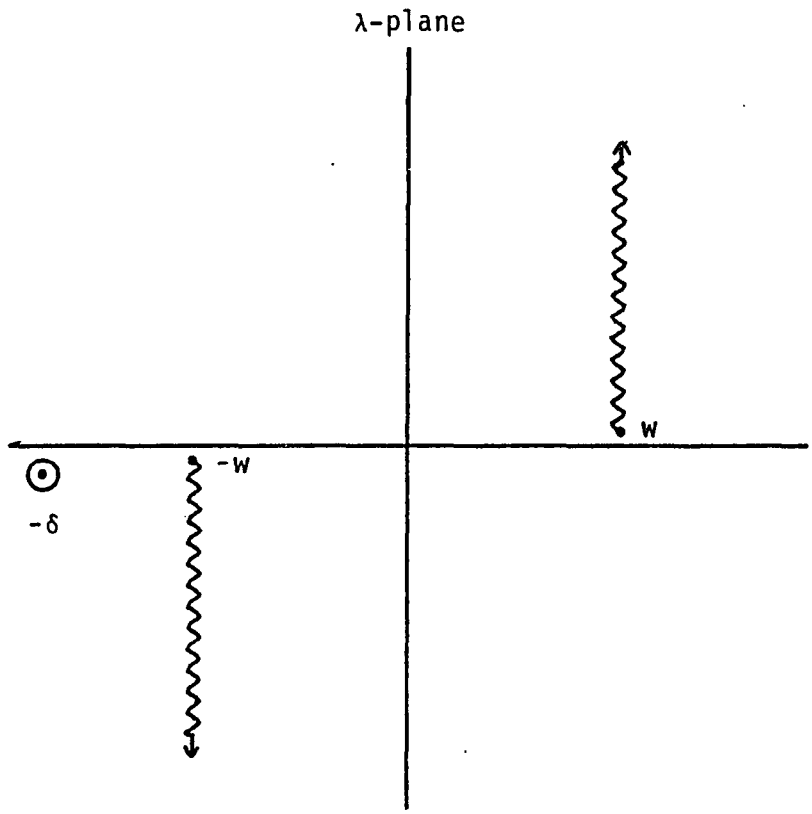

Fig. 3.3 Location of singularities in the transform plane for H_0.

upper half-plane, and we rename it $C_+(\lambda)$. The boundary condition enters as follows. Define a function $u(\Phi)$ by

$$u(\Phi) = \frac{\partial H_0}{\partial \Psi} \quad \text{for } \Phi < 0 \ ,$$
$$= 0 \qquad \text{for } \Phi > 0 \ . \tag{3.8c}$$

The Fourier transform of the normal velocity on $\Psi = 0$ is

$$\frac{\partial H_0}{\partial \Psi}\Big|_{\Psi=0} = U_-(\lambda) + \frac{1}{\sqrt{2\pi}} \int_0^\infty - \frac{A_n}{\beta_\infty} e^{i(\lambda+\delta)\Phi} \, d\Phi$$

$$= U_-(\lambda) - \frac{i}{\sqrt{2\pi}} \frac{A_n}{\beta_\infty} \frac{1}{\lambda+\delta} \ , \tag{3.8d}$$

where $U_-(\lambda)$ is the Fourier transform of $u(\Phi)$. The analyticity of $U_-(\lambda)$ in the lower half-plane results from Eq. (3.8c). Another expression for the Fourier transform of $\partial H_0/\partial \Psi$ on $\Psi = 0$ is obtained by differentiating (3.8a) through the integral sign and setting $\Psi = 0$. Equating the result with Eq. (3.8d), we have

$$- C_+(\lambda) \sqrt{\lambda^2 - w^2} = U_-(\lambda) - \frac{A_n \, i}{\sqrt{2\pi} \, \beta_\infty \, (\lambda+\delta)} \ , \tag{3.8e}$$

or

$$- C_+(\lambda) \sqrt{\lambda+w} = \frac{U_-(\lambda)}{\sqrt{\lambda-w}} - \frac{A_n \, i}{\sqrt{2\pi} \, \beta_\infty \, (\lambda+\delta) \sqrt{\lambda-w}} \ . \tag{3.8f}$$

The last term can be easily split into terms analytic in the upper and lower half-planes by adding and subtracting the pole. Proceeding in this manner and rearranging the terms in (3.8f), we obtain

$$- C_+(\lambda)\sqrt{\lambda+w} - \left[\frac{A_n}{\sqrt{2\pi}\,\beta_\infty\,(\lambda+\delta)\sqrt{\delta+w}}\right]_+$$

$$= \frac{U_-(\lambda)}{\sqrt{\lambda-w}} - \frac{A_n\, i}{\sqrt{2\pi}\,\beta_\infty}\left[\frac{1}{(\lambda+\delta)\sqrt{\lambda-w}} - \frac{i}{(\lambda+\delta)\sqrt{\delta+w}}\right]_- \quad . \qquad (3.8g)$$

The two sides of Eq. (3.8g) are equal on the strip $-\mathrm{Im}\{w\} < \mathrm{Im}\{\lambda\} < \mathrm{Im}\{w\}$. Hence, they are analytic continuations of each other and form an entire function. From the edge condition we will find that this entire function is bounded and therefore constant by Liouville's theorem.

The edge condition we require is that the velocity have at most an $R^{-1/2}$ singularity as $R \to 0$. (This singularity comes from the most singular eigenfunction that has an integrable velocity.) In terms of the potential, the behavior should be $R^{1/2}$ locally. Hence the transform U_- should decay as $\lambda^{-1/2}$, and C^+ as $\lambda^{-3/2}$ (see Noble (1958)). Utilizing these results, it is easily seen that both sides of (3.8g) approach 0 as $1/\lambda$ as $\lambda \to \infty$. Thus, the entire function defined by (3.8g) must be identically 0. Hence,

$$C_+(\lambda) = - \frac{A_n}{\sqrt{2\pi}\ \beta_\infty\ (\lambda+\delta)\ \sqrt{\delta+w}\ \sqrt{\lambda+w}}$$

and

$$H_0 = - \frac{A_n\ \mathrm{sgn}\ \psi}{\beta_\infty\ 2\ \pi\ \sqrt{\delta+w}} \int_{-\infty}^{\infty} \frac{e^{a(\lambda,\Phi,\Psi)}\ d\lambda}{(\lambda + \delta)\ \sqrt{\lambda + w}} \quad , \tag{3.9a}$$

where

$$a(\lambda,\Phi,\Psi) = - i\ \lambda\ \Phi - |\Psi|\ \sqrt{\lambda^2 - w^2} \quad . \tag{3.9b}$$

The pole corresponds to local hydrodynamic motion near the plate which does not radiate sound. The acoustic wave contributions are related to the branch points.

The asymptotic matching with the outer solution requires the expansion of Eq. (3.9) in outer coordinates. For convenience we use the polar form, with

$$r = \sqrt{\phi^2+\psi^2} = R/k \quad \text{and} \quad \theta = \arctan \frac{\psi}{\phi} = \arctan \frac{\Psi}{\Phi} \quad .$$

The method of steepest descent, which is outlined in Appendix B, can be utilized to obtain the asymptotic expansion for large k. The exponent $a(\lambda)$ contains a saddle point at $\lambda_0 = - w \cos \theta$, and after a transformation to the steepest-descent path (drawn in Appendix B), we obtain

$$H_0 \sim L_0(\theta) \frac{e^{ikwr}}{\sqrt{kr}} + O(k^{-3/2}) , \qquad (3.10a)$$

where

$$L_0(\theta) = - \frac{A_n \, e^{\frac{-i\pi}{4}} \cos\frac{\theta}{2}}{\sqrt{\pi(\delta+w)}\,(\delta - w\cos\theta)\,\beta_\infty} . \qquad (3.10b)$$

The formal matching process will be carried out after the outer solution is derived.

3.1.2 Solution for H_1

The function H_1 accounts for all $O(\alpha\sqrt{k})$ terms in the local-leading-edge region, except those arising from the volume source terms in Eq. (3.2a,b). The governing equations are:

$$D(H_1) = 2^{3/2} w^2 \beta_\infty R^{-1/2} \cos\frac{\theta}{2} H_0 - \frac{(\gamma+1)M_\infty^4\sqrt{2}\, R^{-1/2}\cos\frac{\theta}{2}}{\beta_\infty^3}$$

$$\times \left[\frac{\partial^2 H_0}{\partial\Psi^2} + 2i\delta\frac{\partial H_0}{\partial\Phi} + (w^2+\delta^2)\, H_0\right] + \frac{(\gamma+1)M_\infty^4 R^{-3/2}\cos\frac{3\theta}{2}}{\sqrt{2}\,\beta_\infty^3}\left[\frac{\partial H_0}{\partial\Phi} - i\,\delta\, H_0\right] \qquad (3.11a)$$

$$\left.\frac{\partial H_1}{\partial\Psi}\right|_{\Psi=0^{\pm},\ \Phi>0} = \pm\sqrt{2}\,\frac{A_n}{\beta_\infty^2}\left[M_\infty^2\Phi^{-1/2} + 4ik_t\Phi^{1/2}\right] e^{i\delta\Phi} , \qquad (3.11b)$$

where D is the Helmholtz operator of (3.7c). The source term in Eq. (3.11a), as well as the first term on the right-hand side of the

boundary condition, represent the effect of mean-flow variations on the acoustic propagation. (The first term in the boundary condition results from the factor $e^{-M^2 q}$ in the transformation from G to h. This term removes several first-order derivatives in the wave operator and in essence transforms some nonuniform-propagation effects from the operator to the boundary condition.) The second term in the boundary condition represents the phase distortion of the convected velocity disturbance by the local flow around the leading edge.

The source term in Eq. (3.11a) contains H_0, which is known only in the form of a Fourier transform. However, we note that the source term is the sum of products of harmonic functions with solutions to the Helmholtz equation. This property can be exploited to determine a particular solution in the following way. First we evaluate the derivatives of H_0 appearing in the source terms by differentiating under the integral sign. The source terms are then products of harmonic functions and integrals of the form $\int S(\lambda)\, e^{a(\lambda,\phi,\Psi)}\, d\lambda$. Now consider a function of the form

$$F(\Phi,\Psi) = f(\Phi,\Psi) \int C(\lambda)\, e^{a(\lambda,\phi,\Psi)}\, d\lambda \,, \tag{3.11c}$$

where f is harmonic and a is given by (3.9b). Applying the operator D to this function, we obtain

$$D(F) = -2i\frac{\partial f}{\partial \Phi} \int \lambda\, C\, e^{a(\lambda,\phi,\Psi)}\, d\lambda - \operatorname{sgn}\Psi\, \frac{\partial f}{\partial \Psi}\left[\int \sqrt{\lambda^2-w^2}\, C\, e^{a(\lambda,\phi,\Psi)} d\lambda\right] . \tag{3.11d}$$

The proper combinations of choices for the functions $f(\Phi,\Psi)$ and $C(\lambda)$ will produce a particular solution to (3.11a).

For example, to obtain a particular solution for the terms containing $R^{-1/2}\cos\frac{\theta}{2}$, we utilize the functions

$$f_1 = R^{1/2}\cos\frac{\theta}{2} \qquad \text{and} \qquad f_2 = R^{1/2}\sin\frac{\theta}{2} \quad .$$

According to (3.11c), we try a particular solution of the form

$$F = R^{1/2}\cos\frac{\theta}{2}\int C_1(\lambda)e^{a(\lambda,\Phi,\Psi)}\,d\lambda + R^{1/2}\sin\frac{\theta}{2}\int C_2(\lambda)e^{a(\lambda,\Phi,\Psi)}\,d\lambda \quad .$$

Equation (3.11d) then gives

$$DF = -i\cos\frac{\theta}{2}R^{-1/2}\int \lambda C_1(\lambda)e^{a}\,d\lambda - \frac{\operatorname{sgn}\Psi}{2}R^{-1/2}\sin\frac{\theta}{2}\int \sqrt{\lambda^2-w^2}\,C_1(\lambda)e^{a}\,d\lambda$$

$$+ i\sin\frac{\theta}{2}R^{-1/2}\int \lambda C_1(\lambda)e^{a}\,d\lambda - \frac{\operatorname{sgn}\Psi}{2}R^{-1/2}\cos\frac{\theta}{2}\int \sqrt{\lambda^2-w^2}\,C_2(\lambda)e^{a}\,d\lambda \qquad (3.11e)$$

Equating the coefficients of $R^{-1/2}\cos\frac{\theta}{2}$ in Eqs. (3.11e) and (3.11a), and setting the coefficients of $\sin\frac{\theta}{2}$ equal to zero, we obtain a set of linear, algebraic equations for $C_1(\lambda)$ and $C_2(\lambda)$. A similar procedure determines the particular solution for the terms containing $R^{-3/2}\cos\frac{3\theta}{2}$. The final result for the particular solution is:

$$H_{1p} = -\frac{A_n\sqrt{2}}{\sqrt{\pi}\sqrt{\delta+w}}\left\{i\sqrt{R}\left|\cos\frac{\theta}{2}\right|\int_{-\infty}^{\infty}\frac{\lambda(\lambda+\delta)}{\sqrt{\lambda+w}}\left[\frac{1}{(\lambda+\delta)^2}-\frac{(\gamma+1)M_\infty^4}{2\beta_\infty^4 w^2}\right]e^{a(\lambda,\phi,\Psi)}\,d\lambda\right.$$

$$+\sqrt{R}\sin\frac{\theta}{2}\int_{-\infty}^{\infty}(\lambda+\delta)\sqrt{\lambda-w}\left[\frac{1}{(\lambda+\delta)^2}-\frac{(\gamma+1)M_\infty^4}{2\beta_\infty^4 w^2}\right]e^{a(\lambda,\Phi,\Psi)}\,d\lambda$$

$$+\frac{(\gamma+1)M_\infty^4}{2\beta_\infty^4 w^2}\left[\frac{\left|\cos\frac{\theta}{2}\right|}{\sqrt{R}}\int_{-\infty}^{\infty}\frac{\lambda\, e^{a(\lambda,\Phi,\Psi)}\,d\lambda}{\sqrt{\lambda+w}}+i\,\frac{\sin\frac{\theta}{2}}{\sqrt{R}}\int_{-\infty}^{\infty}\right.$$

$$\left.\left.\times\sqrt{\lambda-w}\,e^{a(\lambda,\Phi,\Psi)}d\lambda\ \right]\right\}\ . \qquad (3.12a)$$

This particular solution does not satisfy the no-flow boundary condition. The normal velocity on the plate is

$$\left.\frac{\partial H_{1p}}{\partial\Psi}\right|_{\Psi=0} = \operatorname{sgn}\Psi\ A_n\sqrt{2}\left[\,2i\delta\,\Phi^{1/2}+\Phi^{-1/2}\,\right]e^{i\delta\Phi}\ .$$

This term must be incorporated into the boundary condition (3.11b) satisfied by the complementary solution. The complementary solution is a symmetric function of Ψ which can be determined directy by Fourier transforms. The solution is

$$H_{1c} = \frac{e^{i\pi/4}\,A_n}{\sqrt{2\pi}}\left[\int_{-\infty}^{\infty}\frac{e^{a(\lambda,\Phi,\Psi)}d\lambda}{(\lambda+\delta)^{3/2}\sqrt{\lambda^2-w^2}}-\left[\frac{M_\infty^2-\beta_\infty^2}{\beta_\infty^2}\right]\int_{-\infty}^{\infty}\frac{e^{a(\lambda,\Phi,\Psi)}d\lambda}{\sqrt{\lambda+\delta}\sqrt{\lambda^2-w^2}}\right] \qquad (3.12b)$$

Since the integral representations for H_{1p} and H_{1c} also contain the phase $a(\lambda,\Phi,\Psi)$, the asymptotic expansions of H_{1p} and H_{1c} for large k are similar to the expansion for H_0. The results, written in the outer polar coordinates (r,θ), are

$$H_{1p} \sim -i\sqrt{2kr}\,\cos\frac{\theta}{2}\left[2\beta_\infty w - \frac{(\gamma+1)M_\infty^4}{\beta_\infty^3 w}(\delta-w\cos\theta)^2\right] H_0 + O(\tfrac{1}{k}) \quad (3.13a)$$

$$H_{1c} \sim L_1(\theta)\ \frac{e^{ikwr}}{\sqrt{kr}} + O(k^{-3/2}) \quad , \quad (3.13b)$$

where

$$L_1(\theta) = \frac{A_n i}{\sqrt{w(\delta-w\cos\theta)}}\left[\frac{2\delta}{\delta-w\cos\theta} - \frac{\beta_\infty^2 w\cos\theta + M_\infty^2(\delta-w\cos\theta)}{\beta_\infty^2(\delta-w\cos\theta)}\right] \quad (3.13c)$$

and H_0 is the asymptotic expansion (3.10).

The asymptotic expansion in (3.13a) results from the effect of mean-flow variations on the acoustic propagation, and is singular with respect to H_0 as $kr \to \infty$. This singular term will later be shown to match with the phase distortion calculated by geometric acoustics. The result in (3.13b) represents additional noise generation due to nonuniform mean-flow effects. The first part of the directivity (3.13c) represents the sound generated by the distortion of the gust by the mean flow. This term exists even for incompressible flow, where M_∞ and hence w tend to zero. In fact, it is apparently infinite in the

incompressible limit. This curious result will be revisited in Chapter 5. The second term is a compressibility effect; it vanishes at low Mach number. This term represents additional sound generated by the scattering of the local acoustic field by the mean-flow gradients. Since mean-flow gradients in the local-leading-edge region occur on the same scale as the acoustic wavelength (for $M_\infty = O(1)$), scattering can produce additional sound.

3.1.3 Solution for H_2

The function H_2 accounts for the $O(\alpha\sqrt{k})$ volume source terms in the local-leading-edge region. The equations satisfied by H_2 are

$$D(H_2) = e^{i(\delta\,\Phi + k_\eta\,\Psi)}\left\{ R^{-1/2}\left[C_1\cos\frac{\theta}{2} + C_2\sin\frac{\theta}{2}\right]\right.$$

$$\left. + R^{-3/2}\left[C_3\cos\frac{3\theta}{2} + C_4\sin\frac{3\theta}{2}\right]\right\}\ , \qquad (3.14a)$$

$$\frac{\partial H_2}{\partial \psi}\bigg|_{\Phi>0,\Psi=0} = 0 \qquad (3.14b)$$

where

$$C_1 = 2^{3/2}i(\delta A_t^* - \beta_\infty A_\eta k_\eta)/\beta_\infty \qquad C_3 = -\sqrt{2}A_t^* M_\infty^2/\beta_\infty^3$$

$$C_2 = 2^{3/2}i(k_\eta A_t^* + \delta A_\eta \beta_\infty)/\beta_\infty \qquad C_4 = -\sqrt{2}A_\eta M_\infty^2/\beta_\infty^2\ . \qquad (3.14c)$$

The source terms in Eq. (3.14a) bear a strong resemblance to the quadrupole source terms in the acoustic-analogy model of Ffowcs Williams and Hawkings (1969b). We satisfy the no-flow boundary

condition on the airfoil surface, and thus H_2 also contains the scattering of the quadrupole field discussed by Ffowcs Williams and Hall (1970). The exact correspondence between our work and that of these authors will be discussed in Chapter 5.

A particular solution for H_2 is obtained by applying a double Fourier transform to Eq. (3.14a), followed by inversion on ψ through contour integration. The result is,

$$H_{2p} = \frac{e^{i\pi/4}\, e^{ik_\eta \Psi}}{8\sqrt{\pi}(\delta^2+k_\eta^2)} \int_{-\infty}^{\infty} \left[\frac{f_1(\lambda)}{\sqrt{\lambda+\delta'}} - \frac{\mathrm{sgn}(\psi) f_2(\lambda)}{\sqrt{\lambda+\delta}} \right] \frac{e^{hy(\lambda,\Phi,\Psi)}\, d\lambda}{(\lambda-\lambda_1)(\lambda-\lambda_2)}$$

$$- \frac{e^{i\pi/4}}{8\sqrt{\pi}(\delta^2+k_\eta^2)} \int_{-\infty}^{\infty} \left[\frac{(\lambda+\delta)f_1(\lambda)+ik_\eta f_2(\lambda)}{\sqrt{\lambda^2-w^2}} - \mathrm{sgn}(\psi) f_2(\lambda) \right] \frac{e^{a(\lambda,\Phi,\Psi)}\, d\lambda}{\sqrt{\lambda+\delta}\ (\lambda-\lambda_1)(\lambda-\lambda_2)} \ , \tag{3.15a}$$

where

$$hy(\lambda,\Phi,\Psi) = -i\lambda\Phi - |\Psi|\sqrt{(\lambda+\delta)(\lambda+\delta')} \ , \tag{3.15b}$$

$$f_1(\gamma) = [iC_2 - 2C_4(\gamma+\delta)](-\delta^2+k_\eta^2-w^2-2\delta\gamma) + [C_1 + 2iC_3(\gamma+\delta)]2ik_\eta(\gamma+\delta) \ , \tag{3.15c}$$

$$f_2(\gamma) = [iC_2 - 2C_4(\gamma+\delta)]2ik_\eta(\gamma+\delta) + [C_1+2iC_3(\gamma+\delta)](-\delta^2+k_\eta^2-w^2-2\delta\gamma) \ , \tag{3.15d}$$

and

$$\lambda_{1,2} = -\frac{\delta}{2}\left[\frac{\delta^2+k_n^2+w^2}{\delta^2+k_n^2}\right] \pm \frac{ik_n}{2}\left[\frac{\delta^2+k_n^2-w^2}{\delta^2+k_n^2}\right] \quad . \qquad (3.15e)$$

Here δ' is assumed to have a small negative imaginary part as contrasted to the small positive imaginary part in δ. The branch point at δ' has arisen from the complex representation of the absolute value function, i.e., $|\lambda+\delta| = \sqrt{\lambda+\delta}\ \sqrt{\lambda+\delta'}$. The poles and branch points contained in Eq. (3.15a) are shown in Fig. (3.4). The phase $hy(\lambda,\Phi,\Psi)$ is "hydrodynamic" as opposed to the "acoustic" phase $a(\lambda,\Phi,\Psi)$ defined earlier. That is, the solution many wavelengths from the local region represents a traveling acoustic wave when the integral contains the phase a and hydrodynamic or convected motion when the phase is hy. The functions f_1 and f_2 are quadratic functions of their arguments whose coefficients depend on the gust characteristics and mean-flow Mach number far upstream. The constants C_i, i=1...4, were defined in Eq. (3.14c).

It is interesting to note that the second part of Eq. (3.15a), with the phase $a(\lambda,\Phi,\Psi)$, is a solution to the homogeneous equation which serves to correct the edge condition at the leading edge. That is, in the absence of this homogeneous solution the particular solution asymptotically behaves like $R^{-1/2}$ for small R, while with it the behavior is $R^{1/2}$. The edge condition we impose on H_2 is that it be no more singular than the zero-incidence solution H_0, which locally went as $R^{1/2}$.

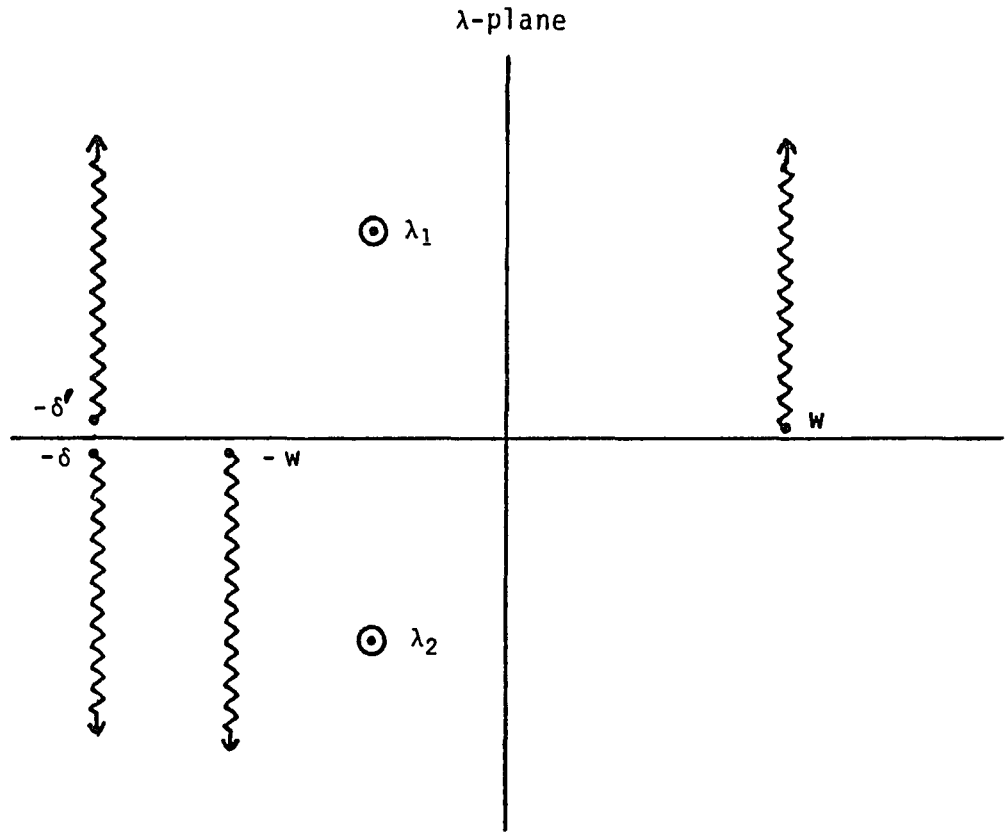

Fig. 3.4 Location of singularities in the transform plane for H_2.

The particular solution (3.15a) does not satisfy the no-flow boundary condition. To correct the boundary condition, we construct an additional complementary solution. The solution can be obtained by the Weiner-Hopf technique. The Weiner-Hopf procedure is nonstandard in this case because the vertical velocity $\partial H_{2p}/\partial\psi$ cannot be calculated directly, i.e., the integral defining $\partial H_{2p}/\partial\psi$ cannot be evaluated in closed form. The details are given in Appendix C; here we present the final form of the solution:

$$H_{2c} = \frac{-e^{i\pi/4}}{8\sqrt{\pi}(\delta^2+k_n^2)} \left\{ \int_{-\infty}^{\infty} \frac{(\lambda+\delta)f_1(\lambda) + ik_n f_2(\lambda+\delta)}{\sqrt{(\lambda+\delta)\ (\lambda^2-w^2)}\ (\lambda-\lambda_1)\ (\lambda-\lambda_2)}\ e^{a(\lambda,\Phi,\Psi)}\ d\lambda \right.$$

$$+ \operatorname{sgn}(\psi) \int_{-\infty}^{\infty} \left[4ik_n C_4 + 4i\delta C_3 - \frac{\sqrt{\lambda_1+w}\ f_2(\lambda_1)}{(\lambda_1-\lambda_2)\ \sqrt{\lambda_1+\delta}(\lambda-\lambda_1)} \right.$$

$$\left. \left. + \frac{(\lambda_2+\delta)\ f_2(\lambda_2) + ik_n f_1(\lambda_2)}{(\lambda_1-\lambda_2)\ (\lambda-\lambda_2)\ \sqrt{\lambda_2-w}\ \sqrt{\lambda_2+\delta}} + \frac{f_2(\lambda)}{\sqrt{\lambda+\delta}\ (\lambda-\lambda_1)\ (\lambda-\lambda_2)} \right] \frac{e^{a(\lambda,\Phi,\Psi)}d\lambda}{\sqrt{\lambda+w}} \right\} . \tag{3.16}$$

We now determine the asymptotic expansion of H_2 in outer coordinates. The terms in H_2 containing the acoustic phase $a(\lambda,\Phi,\Psi)$ can be expanded asymptotically by a saddle-point method. The phase $hy(\lambda,\Phi,\Psi)$ contains no saddle point, and the asymptotic expansion for the hydrodynamic terms is obtained by deforming the contour of integration onto two rays, along which the integral is endpoint dominated as

$kr \to \infty$. The details of the expansion techniques are discussed in Appendix B. The result is shown below:

$$H_2 = H_{2p} + H_{2c} \sim \frac{e^{ik(\delta\phi+k_\eta\psi)}}{\sqrt{kr}} \left[\frac{C_1\cos\frac{\theta}{2} + C_2\sin\frac{\theta}{2}}{\delta^2+k_\eta^2-w^2}\right] + \frac{L_2(\theta)\, e^{ikwr}}{\sqrt{kr}} + O(k^{-3/2}) \tag{3.17a}$$

where

$$L_2(\theta) = \frac{-i[(\delta-w\cos\theta)f_1(-w\cos\theta) + ik_\eta f_2(-w\cos\theta)]}{4\sqrt{2w}(\delta^2+k_\eta^2)\sqrt{\delta-w\cos\theta}(\lambda_1-w\cos\theta)(\lambda_2-w\cos\theta)} - \frac{\cos\frac{\theta}{2}}{4(\lambda_1-\lambda_2)(\delta^2+k_\eta^2)}$$

$$\times \left[4(\lambda_1-\lambda_2)(ik_\eta C_4+i\delta C_3) + \frac{\sqrt{\lambda_1+w}f_2(\lambda_1)}{\sqrt{\lambda_1+\delta}(\lambda_1+w\cos\theta)} - \frac{(\lambda_2+\delta)f_2(\lambda_2)+ik_\eta f_1(\lambda_2)}{(\lambda_2+w\cos\theta)\sqrt{\lambda_2-w}\sqrt{\lambda_2+\delta}}\right]. \tag{3.17b}$$

The term in (3.17a) containing the square brackets represents hydrodynamic motion; it matches with the particular solution in the outer region which is also non-propagating. The second term of the expansion in (3.17a) represents sound generated by the volume quadrupoles in the local-leading-edge region, and the scattering of this sound field by the sharp leading edge.

We have now completely solved for the first-order ($O(\alpha\sqrt{k})$) correction to the acoustic field in the local leading-edge region. The overall structure of our asymptotic series may be seen at this point

(with a little anticipation). We will retain the $O(1)$ and $O(\alpha\sqrt{k})$ leading-edge field, as well as the $O(1/\sqrt{k})$ trailing-edge field produced by the scattering of the $O(1)$ leading-edge field. Effects of size $O(\alpha, \alpha^2 k, 1/k)$ will be neglected. In solving for the fast-varying phase in the outer region, however, we must retain $O(\alpha)$ terms since they are multiplied by the large parameter k and the net result is an $O(\alpha k)$ phase variation. We assume $\alpha k = O(1)$.

Many effects not present for an airfoil at zero incidence have been uncovered by the analysis thus far. These include variations in the mean-flow convection-velocity and sound-speed, and modified boundary conditions, which are contained in H_1. In addition, the sound generated by the interaction of the convected disturbance with the nonuniform mean flow is contained in H_2. To understand how these effects propagate to the farfield, we now analyze the outer region.

3.2 Outer Region

In the outer region, the mean flow varies on the length scale of the airfoil chord, which is large compared to the disturbance wavelength. Thus, in this region we expect a multiple-scales type solution. The correct nondimensional equations are Eqs. (3.2), i.e., no rescaling is required.

The solution in the outer region consists of four parts, which we write as

$$h = h_p + h_c + h_\ell + h_t \quad .$$

The term h_p is a particular solution generated by the volume source term in Eq. (3.2a). This particular solution does not satisfy the boundary condition on the airfoil surface, and thus a complementary solution h_c is required. The additional contributions h_ℓ and h_t are necessary to account for the propagation into the outer region of the acoustic waves generated at the airfoil leading and trailing edges.

We solve first for h_p. In the source term of equation (3.2b), the phase $k\Omega$ varies rapidly compared to the amplitude $S(\phi,\psi)$. Thus it is natural to seek a particular solution that also contains this rapidly varying phase. Noting that the derivatives of the phase dominate those with respect to the amplitude, the following particular solution is easily found.

$$h_p = \frac{1}{k} \frac{S(\phi,\psi)e^{ik\Omega}}{\left[w^2 - (\frac{\partial\Omega}{\partial\phi})^2 - (\frac{\partial\Omega}{\partial\psi})^2\right]} + O(\alpha^2/k, \alpha/k^2) \quad . \tag{3.18}$$

The velocity fluctuations due to this solution are $O(\alpha)$ (recall that S is $O(\alpha)$). In constract, the pressure fluctuations are $O(\frac{\alpha}{k})$, since the pressure is obtained by taking the convective derivative and (3.18) contains a convective phase. Hence, only derivatives of the slowly-varying amplitude contribute to the pressure field.

The velocity normal to the body surface associated with the particular solution in (3.18) is

$$\left.\frac{\partial h_p}{\partial \psi}\right|_{\psi=0} = \frac{ik_n S(\phi,0)e^{ik\Omega(\phi,0)}}{w^2-\delta^2-k_n^2} + O(\alpha^2) \quad .$$

The velocity associated with the complementary solution h_c must cancel both this velocity and the gust velocity in Eq. (3.2d). That is,

$$\left.\frac{\partial h_{ch}}{\partial \psi}\right|_{\psi=0,0<\phi<2} = J(\phi)\, e^{ik\Omega(\phi,0)} \quad , \tag{3.19a}$$

where

$$J(\phi) = -\frac{A_n}{\beta_\infty} + \frac{2\alpha A_t}{\beta_\infty} + \frac{q(\phi,0)A_n M_\infty^2}{\beta_\infty} - \frac{ik_n S(\phi,0)}{w^2-\delta^2-k_n^2} \quad .$$

The complementary solution can also be easily derived by taking advantage of the fact that the derivatives with respect to the phase dominate those with respect to the amplitude. The result is

$$h_c = \frac{-\mathrm{sgn}(\psi)\, J(\phi)\, e^{-k|\psi|m(\phi)}\, e^{ik\Omega(\phi,0)}}{m(\phi)} \quad , \tag{3.19b}$$

where

$$m^2(\phi) = \left[\frac{\partial \Omega(\phi,0)}{\partial \phi}\right]^2 - w^2(1 - 2\beta_\infty^2 q(\phi,0)) \quad .$$

The solution applies for $0 < \phi < 2$. However, we will find in the local-trailing-edge analysis that h_c can be continued into the wake region, where $\phi > 2$. Note that h_c is exponentially small except when $\psi = O(1/k)$, i.e., very near the body (or wake).

The characteristics of h_c are similar to those of h_p. Both contain the phase $k\Omega$ which also appears in the vortical velocity $\bar{v}'$. Thus, although the disturbances corresponding to h_p and h_c are irrotational, these disturbances convect with the mean flow and are not sound waves.

Having found an outer particular solution which satisfies the boundary condition yet produces no sound waves, we conclude that all of the noise is generated in the local-leading-edge and local-trailing-edge regions. We have already investigated how sound is generated in the local-leading-edge region. The trailing edge produces additional sound by scattering acoustic waves produced at the leading edge, as we shall see shortly. The propagation of this locally-generated sound into the outer region is represented by the remaining outer solutions h_ℓ and h_t.

The large parameter k multiplies w in the governing equation (3.2a); hence we expect that the solutions h_ℓ and h_t will have a geometric-acoustics form. That is, the phase of the solutions will vary rapidly compared to the amplitude and the acoustic fields can be well described by rays. The rays emanate from the leading and trailing edges. We first concentrate on the leading-edge ray field.

3.2.1 Leading-Edge Ray Field

The asymptotic expansions of the local-leading-edge solutions in outer coordinates contained cylindrical acoustic waves emanating from the airfoil leading edge. We now develop the outer solution h_ℓ corresponding to these acoustic waves. The analysis utilizes the polar form (r,θ) of the outer coordinates (ϕ,ψ). Substituting the form

$$h_\ell = A_\ell(r,\theta)\, e^{ik\sigma_\ell(r,\theta)} \tag{3.20}$$

appropriate for geometric acoustics into Eq. (3.2a), and separating orders of k, we find the following variable-coefficient eikonal equation for σ_ℓ:

$$(\frac{\partial\sigma_\ell}{\partial r})^2 + \frac{1}{r^2}(\frac{\partial\sigma_\ell}{\partial\theta})^2 - w^2$$

$$+ q\left[2w^2\beta_\infty^2 + \frac{(\gamma+1)M_\infty^4}{\beta_\infty^2}\left[(\frac{\partial\sigma_\ell}{\partial\psi})^2 + 2\delta\frac{\partial\sigma_\ell}{\partial\phi} - \delta^2 - w^2\right]\right] = 0 \quad . \qquad (3.21)$$

It is natural to seek a perturbation series in α as a solution to (3.21), i.e., a solution of the form

$$\sigma_\ell = \sigma_{0\ell} + \sigma_{1\ell} + O(\alpha^2) \quad , \qquad (3.22)$$

where $\sigma_{0\ell}$ is $O(1)$ and $\sigma_{1\ell}$ is $O(\alpha)$. The leading term is

$$\sigma_{0\ell} = wr \quad ,$$

the cylindrical wave phase appropriate for a flat plate at zero incidence. Inserting (3.22) into (3.21), we obtain the following equation for the first-order correction to the phase in the outer region:

$$2w\frac{\partial\sigma_{1\ell}}{\partial r} + q\left[2w^2\beta_\infty^2 - \frac{(\gamma+1)M_\infty^4}{\beta_\infty^2}(\delta-w\cos\theta)^2\right] = 0 \qquad (3.23)$$

This equation can be easily integrated, with the result

$$\sigma_{1\ell} = \left[-\beta_\infty^2 w + \frac{(\gamma+1)M_\infty^4}{2\beta_\infty^2 w}(\delta-w\cos\theta)^2\right]\int_0^r q(r',\theta)dr' + g_1(\theta) \qquad (3.24)$$

The function $g_1(\theta)$ will be found to be zero in the matching with the local-leading-edge solution. The bracketed quantity appears repeatedly in our leading- and trailing-edge ray analysis. For convenience in future calculations, we set

$$V(\theta) = -\beta_\infty^2 w + \frac{(\gamma+1)M_\infty^4}{2\beta_\infty^2 w}(\delta - w\cos\theta)^2 \tag{3.25}$$

Equation (3.24) can be expressed in a more convenient form by utilizing the fact that the perturbation speed q is the real part of an analytic function:

$$\int_0^r q(r',\theta)dr' = \mathrm{Re}\int_0^r (q-i\mu)dr' = \mathrm{Re}\; e^{-i\theta}\int_0^z (q-i\mu)dz'$$

$$= \mathrm{Re}\;\{e^{-i\theta}F(re^{i\theta})\} \quad ,$$

where F is the complex potential for the mean perturbation flow and the arbitrary constant in F is chosen so that $F(0) = 0$. It turns out that, to $O(\alpha)$ accuracy, the constant utilized in Eq. (3.3a) is also appropriate here. The $O(\alpha)$ phase distortion can be written as

$$\sigma_{1\ell} = V(\theta)\;\mathrm{Re}\{e^{-i\theta}F(re^{-i\theta})\} \quad . \tag{3.26}$$

where F is given by Eq. (3.3a). The expansion of $\sigma_{1\ell}$ for $r >> 1$ will be required to determine the farfield solution. For $r >> 1$, Eq. (3.26) becomes

$$\sigma_{1\ell} \sim \frac{\alpha V(\theta)}{\beta_\infty}\left(\sin\theta(1+\log 2r) - (\theta-\pi)\cos\theta\right) + O(\tfrac{1}{r}) \quad . \tag{3.27}$$

The phase distortion $\sigma_{1\ell}$ is discontinuous across $\psi=0$ due to the differences in convection and sound speed above and below the airfoil.

The next correction to the phase in the outer region, $\sigma_{2\ell}$, is $O(\alpha^2)$. Since $\sigma_{2\ell}$ is multiplied by the large parameter k, the contribution to the phase associated with $\sigma_{2\ell}$ is $O(\alpha^2 k)$, which we are neglecting. Thus, to the desired accuracy, the phase is determined (except for the arbitrary function g_1) and we turn to the amplitude of the outer solution.

When we substituted (3.20) into (3.2) we found the eikonal equation at highest order. At the next order in k, the following equation for the amplitude results:

$$2\frac{\partial A_\ell}{\partial r}\frac{\partial \sigma_\ell}{\partial r} + \frac{A_\ell}{r}\frac{\partial \sigma_\ell}{\partial r} + O(\alpha,1/k) \text{ terms} = 0. \tag{3.28}$$

The relation $\sigma_\ell = wr + O(\alpha)$ is used in deriving this result. Equation (3.28) also can be written in the transport equation form:

$$\frac{\partial}{\partial r}(r^{1/2} A_\ell) = 0 \quad , \tag{3.29a}$$

which has solution

$$A_\ell = \frac{K_\ell(\theta)}{\sqrt{r}}. \tag{3.29b}$$

The standard geometric acoustics form is an amplitude expansion in powers of 1/k. Our perturbation approach has introduced the additional small parameter α, and the matching with the local-leading-edge

solution will show that a term of $O(\alpha\sqrt{k})$ must be included in the outer solution. The $O(\alpha\sqrt{k})$ amplitude term also satisfies Eq. (3.28), hence we can simply set

$$K_{\ell} = K_0(\theta) + \alpha\sqrt{k}\ K_I(\theta) \quad .$$

In the next section, we carry out the format matching process to determine $K_0(\theta)$ and $K_I(\theta)$.

3.2.2 Matching of Leading Edge Local and Outer Acoustic Solutions

The matching process is carried out utilizing Van Dyke's (1975) rule, which for our application may be written as follows. The two-term local expansion of the two-term outer solution must agree with the two-term outer expansion of the two-term local solution. Comparison of the expansions can be done in either local or outer coordinates; we choose local coordinates. Hence the outer expansion of the local solution must be rewritten in local coordinates. In the interest of brevity, we will present the matching only for the acoustic solutions. Matching of the hydrodynamic solutions only provides a consistency check, and does not affect the sound field.

The two-term outer-leading-edge acoustics solution, rewritten in local variables, is

$$h_{\ell} \sim \frac{\left[K_0(\theta) + \alpha\sqrt{k}\ K_I(\theta)\right] e^{i(wR+\sigma_{1\ell})}}{k\sqrt{R}} \quad , \qquad (3.30)$$

where r is replaced by R/k in the expression (3.26) for $\sigma_{1\ell}$. The two-term expansion of Eq. (3.30) for large k is

$$[h_\ell]_{local} \sim \frac{e^{iwR}}{k\sqrt{R}} \left\{ K_0(\theta) + \alpha\sqrt{k} \left[K_I(\theta) + \frac{i}{\beta_\infty} V(\theta)\, 2^{3/2} \cos\frac{\theta}{2}\, \sqrt{R}\, K_0(\theta) \right] \right\} . \tag{3.31}$$

Equation (31) is the two-term local expansion of the two-term outer solution.

The outer expansion of the local solution has been found in previous sections. Here we need only collect the previous results and rewrite them in local coordinates for comparison with Eq. (3.31). Combining the results of Eqs. (3.10), (3.13), and (3.17), and neglecting the hydrodynamic motion represented by the first term of (3.17a), we have

$$[H_\ell]_{outer} \sim \frac{e^{iwR}}{k\sqrt{R}} \left\{ L_0(\theta) + \right.$$

$$\left. \alpha\sqrt{k} \left[L_1(\theta) - i\sqrt{2R}\cos\frac{\theta}{2} \left[2\beta_\infty w - \frac{(\gamma+1)M_\infty^4(\delta - w\cos\theta)^2}{\beta_\infty^3 w} \right] L_0(\theta) + L_2(\theta) \right] \right\} \tag{3.32}$$

where L_0, L_1, and L_2 are the local leading-edge directivities defined in Eqs. (3.10), (3.13), and (3.17). The matching principle requires that Eqs. (3.31) and (3.32) be identical, i.e. that

$$K_0(\theta) = L_0(\theta) \quad \text{and} \quad K_I(\theta) = L_1(\theta) + L_2(\theta) \ . \tag{3.33}$$

The term in (3.32) containing $\sqrt{R}\ L_0(\theta)$, which was singular in the local region, matched to $\sigma_{1\ell}$. Hence, this singular term represents a local expansion of the outer phase distortion.

The complete leading-edge ray solution is,

$$h_\ell = L(\theta)\ \frac{e^{ik(wr\ +\ \sigma_{1\ell})}}{k^{3/2}\sqrt{r}}\quad , \tag{3.34a}$$

where

$$L(\theta) = L_0(\theta) + \alpha\sqrt{k}\ (\ L_1(\theta) + L_2(\theta)\ ) \tag{3.34b}$$

has been introduced for convenience in future calculations.

The pressure associated with the leading-edge ray field can be easily found now that the potential h is completely determined. Recall that the pressure is given by

$$p' = -\rho_0\ \frac{D_0G}{Dt} = \rho_\infty U_\infty^2\left[\frac{\partial h}{\partial \phi} - ik\delta h\right]\ e^{ik(-k_3X\ +\ k_tU_\infty^2t\ -\ \delta M_\infty^2\phi)} + O(\alpha)\ . \tag{3.35}$$

It proves convenient to work in terms of the modified pressure p, defined by

$$p = \frac{p'e^{ik(k_3x-k_tU_\infty^2t)}}{\rho_\infty U_\infty^2} = \left[\frac{\partial h}{\partial \phi} - ik\delta h\right]e^{-ik\delta M_\infty^2\phi}\quad . \tag{3.36}$$

The derivative $\partial h/\partial\phi$ in Eq. (3.36) is dominated by the derivative on the rapidly varying cylindrical wave phase ikwr. Hence, to the order of accuracy which we are retaining,

$$p = \left[h\ \frac{\partial}{\partial\phi}(ikwr) - ik\delta h\right]e^{-ik\delta M_\infty^2\phi} = -ik(\delta-w\cos\theta)e^{-ik\delta M_\infty^2\phi}h \quad . \quad (3.37)$$

Applying this result to the expression in Eq. (3.34), we find that the pressure for the leading-edge ray field is

$$p_\ell = -i(\delta-w\cos\theta)e^{-ik\delta M_\infty^2\phi}\ L(\theta)\ \frac{e^{ik(wr+\sigma_{1\ell})}}{\sqrt{kr}} + O(k^{-3/2},\alpha k^{-1/2}) \quad . \quad (3.38)$$

The effects of incidence angle on high-frequency gust interaction noise are contained in the directivity $L(\theta)$ and the distortion $\sigma_{1\ell}$ to the cylindrical wave phase. The relative importance of the various effects will be assessed after the trailing edge and total acoustic fields are found.

3.2.3 Trailing-Edge Ray Field

The trailing-edge ray field is derived in an identical manner to the leading-edge field; only the coordinate system changes. Hence

$$\sigma_t = wr_t + \sigma_{1t} \quad (3.39a)$$

where

$$\sigma_{1t} = \left[-\beta_\infty^2 w + \frac{(\gamma+1)M_\infty^4}{2\beta_\infty^2 w}(\delta - w\cos\theta_t)^2\right] \int_0^{r_t} q(r_t', \theta_t)\, dr_t' \qquad (3.39b)$$

$$= V(\theta_t)\ \mathrm{Re}\{e^{-i\theta_t} F_t(r_t e^{i\theta_t})\}$$

and (r_t, θ_t) are trailing-edge coordinates which will be defined shortly, in the local-trailing-edge analysis. The function F_t is the leading-edge complex potential F, rewritten in trailing-edge variables. The arbitrary constant associated with F_t is chosen so that F vanishes at the trailing edge. Ignoring $O(\alpha^2)$ terms, F_t is given by

$$F_t = \frac{i\alpha}{\beta_\infty}\left[\log(z_t + 1 + \sqrt{z_t(z_t+2)}) + z_t - \sqrt{z_t(z_t+2)}\right] , \qquad (3.39c)$$

where $z_t = r_t\, e^{i\theta_t}$ and $-\pi < \theta_t < \pi$. The expansion of σ_{1t} for $r_t >> 1$, to be utilized in the farfield solution, is

$$\sigma_{1t} \sim \frac{\alpha V(\theta_t)}{\beta_\infty}\left[-\theta_t\cos\theta_t + \sin\theta_t(-1+\log 2r_t)\right] . \qquad (3.39d)$$

The trailing-edge phase distortion is discontinuous across $\psi=0$ on the airfoil and in front of it, just as $\sigma_{1\ell}$ was discontinuous on the airfoil and behind it.

The amplitude of the trailing-edge ray field is given by the following general expression, analagous to (3.29b) in the leading-edge solution:

$$A_t = \frac{K_t(\theta_t)}{\sqrt{r_t}} + O(\alpha) \quad . \tag{3.40}$$

Here $K_t(\theta_t)$ is obtained by matching with the local trailing-edge region, which we now discuss.

3.3 Local Trailing Edge Region

Due to the net circulation around the airfoil, the trailing edge is located at different values of the coordinate ϕ above and below the airfoil. The location of the trailing edge is given by (Eq. (3.4b))

$$\phi = 2 \pm \frac{\alpha\pi}{\beta_\infty}, \quad \psi = 0 \quad , \tag{3.41a}$$

where the plus sign applies for $\psi = 0^+$ and the minus for $\psi = 0^-$. Thus the trailing-edge coordinates (ϕ_t, ψ_t) referred to in the trailing-edge ray field are measured from $(2+\alpha\pi/\beta_\infty, 0)$ above the airfoil and $(2-\alpha\pi/\beta_\infty, 0)$ below it. In the local-trailing-edge region we define coordinates which scale on the disturbance wavelength:

$$\Phi_t = k\,\phi_t, \quad \Psi_t = k\,\psi_t \quad . \tag{3.41b}$$

Like the outer coordinates, the local coordinates are defined differently above and below the airfoil.

We begin our analysis of the local-trailing-edge region by determining the effect of the interaction of the convected disturbance with the trailing edge. The local-trailing-edge expansion of the mean-flow perturbation speed is

$$q \sim \frac{i\alpha}{\beta_\infty}\left[1 - \sqrt{\frac{Z_t}{2k}}\right] + O(\alpha k^{-3/2})$$

where $Z_t = \Phi_t + i\Psi_t$. The interaction of this mean-flow velocity with the convected gust produces a source term similar to that in (3.14a) for the leading-edge, but O(1/k) weaker. (Since the variable part of q-iμ is O(1/k) weaker for the trailing edge.) Hence, to our order of approximation, the source term S in Eq. (3.2) can be neglected as a sound-generating mechanism in the local-trailing-edge region.

Though the volume source term is negligible, sound might still be generated by the interaction of the convected disturbance with the trailing edge through the change in boundary condition. The boundary condition (3.2d) and the homogeneous part of Eq. (3.2a), rewritten in local-trailing-edge coordinates, apply. However, the mean-flow perturbation quantities are $O(\alpha)$ or smaller and can be ignored. The governing equations, then, are simply

$$\frac{\partial^2 H_t}{\partial \Phi_t^2} + \frac{\partial^2 H_t}{\partial \Psi_t^2} + w^2 H_t = 0 \qquad (3.42a)$$

$$\left.\frac{\partial H_t}{\partial \Psi_t}\right|_{\Phi_t<0,\,\Psi_t=0^\pm} = \frac{-An}{B_\infty} e^{ik[\delta(2\pm\alpha\pi/\beta_\infty)+g(2,0^\pm)]} e^{i\delta\Phi_t} \qquad (3.42b)$$

Pressure continuous for $\Phi_t > 0$ (3.42c)

$$\left.\frac{\partial H_t}{\partial \Psi_t}\right|_{\Psi_t=0^\pm,\,\Phi_t=0^+} = \frac{-An}{B_\infty} e^{ik[\delta(2\pm\alpha\pi/\beta_\infty)+g(2,0^\pm)]} \qquad (3.42d)$$

The edge condition (3.42d) is the unsteady Kutta condition; it says that the total unsteady flow must leave the trailing edge tangentially.

The solution to equations (3.42) is

$$H_t = \frac{\operatorname{sgn}\Psi_t \; An}{\beta_\infty \sqrt{\delta^2-w^2}} \, e^{ik[\delta(2\pm\alpha\pi/\beta_\infty)+g(2,0^\pm)]} \, e^{-|\Psi_t| \sqrt{\delta^2-w^2}} \, e^{i\delta\Phi_t} \qquad (3.43)$$

as can be verified by direct substitution. Equation (3.43) is an extension into the local-trailing-edge region of the hydrodynamic solution (3.19b). It is at first somewhat surprising that Eq. (3.43) exhibits the same form for $\Phi_t < 0$ and $\Phi_t > 0$. This result is a consequence of the unsteady Kutta condition, which causes a wake of shed vorticity to be generated by the time-dependent motion. The shed vorticity in this "wake" is essentially a smooth continuation of bound vorticity in the airfoil which cancels the gust velocity $\overline{v^r}$. In the local-trailing-edge region, both the bound and shed vorticity convect at the free-stream speed, and hence no pressure fluctuations are generated. We conclude, then, that the interaction of the convected disturbance with the trailing edge produces no sound.‡

In contrast to the convected disturbance, there are pressure fluctuations associated with the leading-edge ray-acoustic field. In general the leading-edge ray field is different above and below the

---

‡It is important to note that the above result does not contradict current trailing-edge noise theories (Howe 1978). Our theory has ignored the presence of the boundary layer, and hence the vorticity is convected at free-stream speed. In constrast, trailing-edge noise theories consider boundary-layer turbulence, which convects at speeds less than the free-stream speed. In this situation, pressure fluctuations are generated and the trailing-edge region is a local sound source.

airfoil, and hence a pressure difference across the trailing edge is produced. A scattered field arises at the trailing edge to cancel this difference. The scattered field in the local-trailing-edge region becomes the source of the trailing-edge ray field in the outer region.

Referring to equation (3.38), the amplitude $L_0(\theta)$ of the wave from the leading edge is antisymmetric across $\psi = 0$ and therefore discontinuous across the wake. The phase $\sigma_{1\ell}$ is also discontinuous. Expanding the pressure p_ℓ (Eq. (3.38)) in local-trailing-edge coordinates, we obtain

$$p_\ell = \frac{-i(\delta-w)\, L(\theta)}{\sqrt{2k}}\, e^{ik(w-\delta M_\infty^2)(2\pm\alpha\pi/\beta)} + ik\sigma_{1\ell}(2,\theta) e^{i(w-\delta M_\infty^2)\Phi_t} + O(\alpha k^{-1/2}, k^{-3/2}) \quad . \tag{3.44}$$

where for $\psi > 0$ θ is set to zero and the plus sign is used, and for $\psi < 0$ θ is set to 2π and the minus sign is used. Equation (3.44) shows that the leading-edge ray field viewed in the local-trailing-edge region appears as a plane wave. The pressure jump across the wake is

$$p \Big|_{\psi=0^-}^{\psi=0^+} = \frac{\Delta_p}{\sqrt{k}}\, e^{i(w-\delta M_\infty^2)\Phi_t} \quad . \tag{3.45a}$$

The constant $\Delta_p/\sqrt{k}$ is the pressure jump at the trailing edge and is given by

$$\frac{\Delta_p}{\sqrt{k}} = \frac{i(w-\delta)e^{2ik(w-\delta M_\infty^2)}}{\sqrt{2k}} \left[L(0)e^{ik(w-\delta M_\infty^2)\alpha\pi/\beta_\infty} + ik\sigma_\ell(2,0) - L(2\pi)\, e^{-ik(w-\delta M_\infty^2)\alpha\pi/\beta_\infty} + ik\sigma_{1\ell}(2,2\pi) \right] \quad . \tag{3.45b}$$

We have extracted the factor $1/\sqrt{k}$, so that Δ_p is O(1).

The local-trailing-edge field generated to cancel (3.45a) satisfies the Helmholtz equation in local-trailing-edge variables:

$$\frac{\partial^2 H_t}{\partial \Phi_t^2} + \frac{\partial^2 H_t}{\partial \Psi_t^2} + w^2 H_t = 0 \quad . \tag{3.46a}$$

In constrast to the local-leading-edge region, here the nonuniform propagation effects are $O(\alpha)$ and can be neglected.

The condition of continuity of pressure is formulated using the definition of the modified pressure p given in Eq. (3.36) and the result of Eq. (3.45b). The condition is

$$e^{-iC_+}\left[\frac{\partial H_t}{\partial \Phi_t} - i\delta H_t\right]_{\Phi_t>0,\Psi_t=0^+} - e^{-iC_-}\left[\frac{\partial H_t}{\partial \Phi_t} - i\delta H_t\right]_{\Phi_t>0,\Psi_t=0^-}$$

$$= -\frac{\Delta_p\, e^{iw\Phi_t}}{k^{3/2}} \quad . \tag{3.46b}$$

The constant $C_\pm$ is defined by

$$C_\pm = k\delta M_\infty^2(2 \pm \alpha\pi/\beta_\infty) \tag{3.46c}$$

In addition to continuity of pressure, continuity of vertical velocity is also enforced across the wake, i.e.,

$$e^{-iC_+}\left.\frac{\partial H_t}{\partial \Psi_t}\right|_{\Phi_t>0,\Psi_t=0^+} - e^{-iC_-}\left.\frac{\partial H_t}{\partial \Psi_t}\right|_{\Phi_t>0,\Psi_t=0^-} = 0 \quad . \tag{3.46d}$$

Equation (3.46d) is a statement that the physical velocity $\partial G/\partial\psi$ rather than $\partial h/\partial\psi$ is continuous across the wake. The curious weighting factors in equations (3.46b) and (3.46d) arise from the discontinuity in ϕ across the wake, which enters in the transformation (2.12a) from G to h. The use of (ϕ,ψ) coordinates leads to some unintuitive forms for the equations in the trailing edge region. However, because of their extreme usefulness in describing convected disturbances and writing boundary conditions, we tolerate this inconvenience.

Equations (3.46) can be solved by the Wiener-Hopf technique, in an analogous manner to the leading edge half-plane problems. The result is

$$H_t = \frac{-\mathrm{sgn}(\psi)i\sqrt{2w}\Delta_p\, e^{iC_\pm}}{4\pi k^{3/2}} \int_{-\infty}^{\infty} \frac{e^{-i\lambda\Phi_t - |\Psi_t|\sqrt{\lambda^2-w^2}}\, d\lambda}{(\lambda+\delta)(\lambda+w)\sqrt{\lambda-w}} \quad . \qquad (3.47)$$

The plus sign in the constant $C_\pm$ applies for $\Psi_t > 0$ and the minus for $\Psi_t < 0$. The asymptotic expansion for O(1) values of the trailing edge angle θ_t can be obtained by the method of steepest descent. Equation (3.47) written in trailing edge outer variables and expanded for large k is

$$H_t \sim \frac{T(\theta_t)\, e^{ikwr_t}}{k^2\sqrt{r_t}} + O(k^{-3}) \quad , \qquad (3.48a)$$

where

$$T(\theta_t) = \frac{e^{-i\pi/4}\Delta_p \, \mathrm{sgn}(\psi) \, e^{iC_\pm}}{2\sqrt{\pi w(1-\cos\theta_t)}(\delta - w\cos\theta_t)} \quad . \tag{3.48b}$$

Equation (3.48b) is singluar for small θ_t. The method of steepest descent fails for small angles owing to the proximity of the saddle point at $\lambda = -w\cos\theta$ to the pole in Eq. (3.47) at $\lambda = -w$. A uniform asymptotic expansion is developed in Appendix D; here we quote the result:

$$H_t \sim \frac{-\mathrm{sgn}(\psi) \, e^{i\pi/4} \, \Delta_p \, e^{iC_\pm} \, e^{ikwr_t \cos\theta_t} \, E(\sqrt{kr_t w(1-\cos\theta_t)})}{k^{3/2}\sqrt{\pi}\,(\delta - w)}$$

$$- \frac{\mathrm{sgn}\psi \, \Delta_p \, e^{-i\pi/4} \, e^{iC_\pm}}{2\sqrt{\pi}\, k^{3/2}} \left[\frac{1}{\delta - w} - \frac{1}{\delta - w\cos\theta_t}\right] \frac{e^{ikwr_t}}{\sqrt{kwr_t(1-\cos\theta_t)}} \quad , \tag{3.49a}$$

where E is the Fresnel integral,

$$E(a) = \int_a^\infty e^{is^2} \, ds \quad . \tag{3.49b}$$

For O(1) values of θ_t, the asymptotic expansion of the Fresnel integral can be used to recover Eq. (3.48).

The amplitude of the trailing-edge ray field given in Eq. (3.40) is obtained by matching the trailing-edge ray solution with the local solution just described. Only the "geometric type" asymptotic expansion in Eq. (3.48) will match with the outer solution. The matching between the outer-trailing-edge and local-trailing-edge solutions is nearly identical to the matching carried out for the leading edge.

Comparing the one-term ray-expansion of the one-term local-solution with the one-term local-expansion of the one-term ray-solution, we find that the undetermined function $K_t(\theta_t)$ in equation (3.40) is simply $T(\theta_t)$. That is, the trailing-edge ray acoustics solution is

$$h_t = \frac{T(\theta_t)\, e^{ik(wr+\sigma_{1t})}}{k^{2/}\sqrt{r_t}} \quad , \tag{3.50}$$

where σ_{1t} is given in Eq. (3.39).

Like the local solution, the outer-trailing-edge solution is singular as θ_t approaches 0 or 2π. The singularity signifies that the geometric acoustics assumption of a slowly varying amplitude and rapidly vaying phase is violated for small values of θ_t. An improved description of the sound field is needed in this "transition" region, which is analagous to the zone in optical problems between illuminated and shadow regions. Our transition region is actually the union of two transition regions. For the wave on top of the airfoil, there exists an "illuminated" region above the airfoil, a "shadow" region below it, and a transition region between them. There exist similar regions for the wave below the airfoil, but with the illuminated and shadow regions reversed. The transition region is shown in Fig. (3.2).

3.4 Transition Region

The ray solution given by equation (3.50) becomes nonuniform when $\theta = O(1/\sqrt{k})$. That is, changes in the amplitude become as large as

changes in the phase. Guided by this nonuniformity, in the transition region we introduce the rescaled angular variable

$$\theta_{tn} = \sqrt{k}\ \theta_t \quad .$$

The radial variable r_t remains the same.

The governing equation is the homogeneous part of Eq. (3.2a), written in transition region variables:

$$\frac{1}{r_t}\frac{\partial}{\partial r_t}\left[r_t\ \frac{\partial h_{tn}}{\partial r_t}\right] + k\ \frac{\partial^2 h_{tn}}{\partial \theta_{tn}^2}$$

$$+ k^2 w^2 h_{tn} \ - 2k^2 w^2 \beta_\infty^2 q h_{tn}$$

$$+\frac{(\gamma+1)M_\infty^4 q}{\beta_\infty^2}\left[\frac{\partial^2 h_{tn}}{\partial \psi^2} + 2ik\frac{\partial h_{tn}}{\partial \phi_t} + k^2(w^2+\delta^2)h_{tn}\right]$$

$$- \frac{(\gamma+1)M_\infty^4 \alpha}{\beta_\infty^2}\frac{\partial q}{\partial \phi}\left[\frac{\partial h_{tn}}{\partial \phi_t} - ik\delta h_{tn}\right] = 0 \ , \qquad (3.51)$$

with

$$q = \frac{\alpha\ \theta_{tn}\ r_t^{1/2}}{\sqrt{k}\ \beta_\infty\ (2+r_t)^{3/2}} + O(\alpha k^{-3/2}) \quad ,$$

$$\frac{\partial}{\partial \psi} = \frac{\theta_{tn}}{\sqrt{k}}\ \frac{\partial}{\partial r_t} + \frac{\sqrt{k}}{r_t}\ \frac{\partial}{\partial \theta_{tn}} + O(\frac{1}{k}) \ ,$$

and

$$\frac{\partial}{\partial \phi_t} = \frac{\partial}{\partial r_t} - \frac{\theta_{tn}}{r_t} \frac{\partial}{\partial \theta_{tn}} + O(\frac{1}{k}) \ .$$

Like the local-trailing-edge solution, the transition solution must cancel the jump in pressure and vertical velocity across the wake due to the discontinuous leading-edge rays. However, in the transition region, the $1/\sqrt{r}$ decay of the leading-edge field, as well as nonuniform propagation effects, must be considered. The zero-jump pressure condition is

$$e^{-iC_+} \left[\frac{\partial h_{tn}}{\partial \phi_t} - ik\delta h_{tn}\right]_{\psi=0^+} - e^{-iC_-} \left[\frac{\partial h_{tn}}{\partial \phi_t} - ik\delta h_{tn}\right]_{\psi=0^-}$$

$$= -\sqrt{2}\ \Delta_p \frac{e^{ikw\phi_t}}{\sqrt{k}\sqrt{2+\phi_t}} \quad , \tag{3.52}$$

where $C_\pm$ and Δ_p are defined in equations (3.45) and (3.46). Along the wake, $\sigma_{1\ell}$ is $O(\alpha^2)$ and has therefore been ignored in the calculation of the pressure jump.

To calculate the vertical-velocity jump condition, we utilize the following relations.

$$\frac{\partial h_\ell}{\partial \psi}\bigg|_{\psi=0^\pm} = \frac{L(\theta=0,2\pi)\ e^{ik(w\phi+\sigma_{1\ell}(\phi,\theta=0,2\pi))}}{k^{3/2}\sqrt{\phi}} \frac{\partial \sigma_{1\ell}}{\partial \psi}(\phi,\theta=0,2\pi) \tag{3.53a}$$

$$\frac{\partial \sigma_{1\ell}}{\partial \psi}\bigg|_{\psi=0} = \frac{\partial \sigma_{1t}}{\partial \psi}\bigg|_{\psi=0} \quad \text{for} \quad \phi > 2 \ . \tag{3.53b}$$

Equation (3.53b) is valid because the difference between $\partial\sigma_{1\ell}/\partial\psi$ and $\partial\sigma_{1t}/\partial\psi$ along $\psi=0$ is an integral of $\partial q/\partial\psi$ on the airfoil. For a flat plate, $\partial q/\partial\psi$ is zero on the airfoil surface. Using Eqs. (3.53a) and (3.53b), we obtain the following jump condition for the vertical component of the acoustic-particle velocity.

$$\frac{e^{-iC_+}}{r_t}\frac{\partial h_{tn}}{\partial \theta_{tn}}\bigg|_{\theta_{tn}=0^+} - \frac{e^{-iC_-}}{r_t}\frac{\partial h_{tn}}{\partial \theta_{tn}}\bigg|_{\theta_{tn}=0^-}$$

$$= -\frac{1}{k}\frac{\sqrt{2}\ \Delta_p}{(w-\delta)}\frac{e^{ikw\phi_t}}{\sqrt{2+\phi_t}}\frac{\partial \sigma_{1t}}{\partial \psi}(\phi_t, \theta_t=0) \ . \tag{3.53c}$$

Here we have related the cluster of constants associated with the velocity jump to the pressure jump Δ_p. The explicit form for $\partial\sigma_{1t}/\partial\psi$ will not be required.

The final requirement on the transition solution is that it asymptotically match the ray solution as the transition angle θ_{tn} becomes large. That is, the small θ_t behavior of the ray solution must match the large θ_{tn} behavior of the transition solution.

In formulating a solution to the transition-region equations, we use the O(1) phase and $1/\sqrt{r}$ decay rate from the leading edge, and the $O(\alpha)$ phase distortion from the trailing edge. That is, we try a solution of the form

$$h_{tn} = \frac{e^{ik(wr+\sigma_{1t}-w(2\pm\alpha\pi/\beta_\infty))}}{k^{3/2}\sqrt{r}} \left[F_0(r_t,\theta_{tn}) + \alpha\sqrt{k}\, F_1(r_t,\theta_{tn})\right] \quad (3.54)$$

The magnitudes of the terms are forced into the solution by the jump conditions on $\psi = 0$. The relation between the leading edge and transition region variables is obtained from the law of cosines:

$$r = r_t + 2 \pm \alpha\pi/\beta_\infty - \frac{r_t\theta_{tn}^2}{k(r_t+2)} + O(1/k^2) \quad . \quad (3.55)$$

Inserting (3.54) into (3.51) and utilizing (3.55), we find the following reduced equations for F_0 and F_1.

The function F_0 satisfies

$$2iw\frac{\partial F_0}{\partial r_t} - \frac{4iw\theta_{tn}}{r_t(r_t+2)}\frac{\partial F_0}{\partial\theta_{tn}} + \frac{1}{r_t^2}\frac{\partial^2 F_0}{\partial\theta_{tn}^2} = 0 \quad (3.56a)$$

$$e^{-iC_+} F_0\Big|_{\theta_{tn}=0^+} - e^{-iC_-} F_0\Big|_{\theta_{tn}=0^-} = \frac{i\sqrt{2}\,\Delta p}{w-\delta} \quad (3.56b)$$

$$e^{-iC_+}\frac{\partial F_0}{\partial\theta_{tn}}\Big|_{\theta_{tn}=0^+} - e^{-iC_-}\frac{\partial F_0}{\partial\theta_{tn}}\Big|_{\theta_{tn}=0^-} = 0 \quad (3.56c)$$

To solve equations (3.56) we introduce the similarity variable

$$\eta = \sqrt{\frac{wr_t}{r_t+2}}\,|\theta_{tn}| \quad . \quad (3.57)$$

The differential equation then takes the form

$$-2i\eta \frac{dF_0}{d\eta} + \frac{d^2F_0}{d\eta^2} = 0 \quad . \tag{3.58}$$

This ordinary differential equation can be integrated twice, with the result

$$F_0 = b_1 E(\eta) + b_2 \quad , \tag{3.59}$$

where E is the Fresnel integral defined in equation (3.49b) of the local-trailing-edge analysis. The constant b_2 can be set to zero in anticipation of the matching with the trailing-edge ray solution. The other constant, b_1, is chosen to satisfy the conditions on $\psi = 0$. Equations (3.56b) and (3.56c) require that

$$b_1 = \frac{e^{i\pi/4} \sqrt{2} \Delta_p \operatorname{sgn}(\psi) e^{iC_\pm}}{(w-\delta)\sqrt{\pi}} \quad . \tag{3.60}$$

The $O(\alpha\sqrt{k})$ term in the transition region satisfies

$$2iw\frac{\partial F_1}{\partial r_t} - \frac{4iw\theta_{tn}}{r_t(r_t+2)} \frac{\partial F_1}{\partial \theta_{tn}} + \frac{1}{r_t^2} \frac{\partial^2 F_1}{\partial \theta_{tn}^2}$$

$$\left[-\frac{2i}{r_t^2} \frac{\partial F_0}{\partial \theta_{tn}} - \frac{4 F_0 w}{r_t(r_t+2)}\right] \frac{\theta_{tn} V(0)}{\beta_\infty} \int_0^{r_t} \frac{s^{1/2}\, ds}{(2+s)^{3/2}} = 0 \tag{3.61a}$$

$$e^{-iC_+} F_1 \Big|_{\theta_{tn}=0^+} - e^{-iC_-} F_1 \Big|_{\theta_{tn}=0^-} = 0 \tag{3.61b}$$

$$e^{-iC_+} \left.\frac{\partial F_1}{\partial \theta_{tn}}\right|_{\theta_{tn}=0^+} - e^{-iC_-} \left.\frac{\partial F_1}{\partial \theta_{tn}}\right|_{\theta_{tn}=0^-} = 0 \qquad (3.61c)$$

where $V(\theta_t)$ appearing in Eq. (3.61a) is defined in Eq. (3.25). The integral appearing in Eq. (3.61a) results from the integral representation (3.39b) for σ_{1t}.

Unfortunately, the inhomogeneous equation (3.61a) has no similarity solution as the homogeneous equation (3.56a) did. We have been unable to obtain an analytical solution to (3.61) for arbitrary values of r_t. However, when $r_t >> 1$ (i.e. in the geometric farfield), the equation simplifies enough so that an asymptotic solution can be found. Before developing this solution, we indicate how one would approach problem (3.61) numerically for general r_t. Since the differential equation is parabolic, a marching scheme in r_t would be used. The initial condition is the solution to (3.61) in the local-leading-edge region, which could be obtained similarly to (3.59) since the right-hand side of (3.61a) is locally negligible. The boundary condition on $\theta_{tn} = 0$ is given, and the other condition utilizes the small-θ_t expansion of the ray solution. One might require that the difference between the numerical solution and the small-θ_t expansion of the ray solution go to zero for large enough θ_{tn}.

Such a numerical approach would not be difficult to implement (at least in principle). However, since only the second order term F_1 is affected, and only in a small $(O(1/\sqrt{k}))$ region, we did not consider the investigation worthwhile. In addition, most of the solution in the farfield can be determined. We now consider the farfield case.

3.4.1 Transition Solution in Geometric Farfield

For $r_t >> 1$ the $O(1/r^2)$ terms in (3.61a) can be neglected and the equation reduces to

$$2iw\frac{\partial F_1}{\partial r_t} = 0 \quad . \tag{3.62}$$

Equation (3.62) has the solution

$$F_1(r_t,\theta_{tn}) \sim G_1(\theta_{tn}) + O(1/r_t) \quad . \tag{3.63}$$

The function G_1 must be determined by matching with a solution for $r_t = O(1)$. Such a solution is unavailable. However, we note that for the choice $G_1 = 0$, the boundary conditions (3.61b) and (3.61c) are automatically satisfied. The matching between the transition and ray solutions is easily done since the transition solution (3.54) contains the phase distortion σ_{1t} of the ray field. Realizing that there is some arbitrariness remaining in G_1, we set it equal to zero. The transition solution for large r_t then is

$$h_{tn} \sim \frac{\mathrm{sgn}(\psi)\, e^{iC_\pm}\, e^{i\pi/4}\, \sqrt{2}\, \Delta_p}{k^{3/2}\,(w-\delta)\,\sqrt{\pi}}\, \frac{e^{ik(wr_t - w\theta_{tn}^2/k + \sigma_{1t})}\, E(\sqrt{w}\,|\theta_{tn}|)}{\sqrt{r_t}} \quad . \tag{3.64}$$

At this point we have determined the solution to the convected wave equation (3.2) in all of the asymptotic regions. We now expand the various solutions for large r and compose a total farfield solution.

3.5 Total Farfield Solution

We first combine the transition solution with the trailing-edge-ray field to form a uniformly valid trailing edge solution for $r_t >> 1$. Utilizing equations (3.39) and (3.48b), we can readily write the farfield expansion of the trailing edge ray field. It is

$$h_t \sim \frac{e^{-i\pi/4}\ \Delta p\ \mathrm{sgn}(\psi)\ e^{iC_\pm}}{k^2\ 2\sqrt{\pi}\ (\delta - w\cos\theta_t)\ \sqrt{w(1-\cos\theta_t)}\ \sqrt{r_t}}\ e^{ik(wr_t + \sigma_{1t})} \quad , \tag{3.65a}$$

where

$$\sigma_{1t} = \frac{\alpha V(\theta_t)}{\beta_\infty}\left[-\theta_t\cos\theta_t + \sin\theta_t(-1+\log 2r_t)\right] \ . \tag{3.65b}$$

A composite expansion can be formed by adding the ray solution to the transition solution and subtracting the common expansion. The common is the ray-expansion of the transition solution or, equivalently, the transition-expansion of the ray solution. It is perhaps easier to look at equations (3.64) and (3.65) and guess an expression which contains both. Either approach leads to the following formula for the trailing-edge sound field, valid for all trailing-edge angles:

$$h_{ttn} = \frac{-\mathrm{sgn}(\psi)\, e^{iC_{\pm}} \sqrt{2}\, e^{i\pi/4}\, \Delta_p\, e^{ikw(r_t - 2(1-\cos\theta_t))}}{k^{3/2}\sqrt{\pi}\,(\delta - w\cos\theta_t)\sqrt{r_t}}$$

$$\times \left(E(\sqrt{2kw(1-\cos\theta_t)})\, e^{ik\sigma_{1t}}\right) \qquad (3.66)$$

with σ_{1t} given in Eq. (3.65b).

The farfield expansion of the leading edge ray field can be obtained by combining equations (3.27) and (3.34). The result is

$$h_{\ell} \sim \frac{L(\theta)}{k^{3/2}\sqrt{r}}\, e^{ik(wr + \sigma_{1\ell})} \qquad (3.66a)$$

with

$$\sigma_{1\ell} \sim -\frac{\alpha V(\theta)}{\beta_{\infty}} \left[(\theta-\pi)\cos\theta - \sin\theta(1+\log 2r) \right] \quad . \qquad (3.66b)$$

The total farfield solution is the sum of h_{ℓ} and h_{ttn}. Before adding the two terms we refer the trailing edge solution to the leading edge, using the relations

$$r_t = r - (2 + \mathrm{sgn}(\psi)\alpha\pi/\beta_{\infty})\cos\theta + O(1/r)$$

$$\theta_t = \theta - \pi + \pi\,\mathrm{sgn}(\psi) + O(1/r) \quad .$$

The total farfield solution is then

$$h \sim \frac{L(\theta)\, e^{ik(wr+\sigma_{1\ell})}}{k^{3/2}\sqrt{r}} - \frac{\mathrm{sgn}(\psi)\, e^{iC_{\pm}}\sqrt{2}\, e^{i\pi/4}\, \Delta_p}{k^{3/2}\sqrt{\pi}\sqrt{r}} \cdot$$

$$\times \frac{e^{ikw[r-2-\alpha\pi \mathrm{sgn}(\psi)\cos\theta/\beta_\infty]}\, E(\sqrt{2kw(1-\cos\theta)})\, e^{ik\sigma_{1t}}}{\delta - w\cos\theta} \quad . \quad (3.67a)$$

The total pressure in the farfield, obtained from Eq. (3.37), is

$$p \sim \frac{-i\, L(\theta)\, (\delta - w\cos\theta)\, e^{ik(wr-\delta M_\infty^2\phi+\sigma_{1\ell})}}{k^{1/2}\sqrt{r}} - \frac{\mathrm{sgn}(\psi)\, e^{iC_{\pm}}\sqrt{2}\, e^{-i\pi/4}\, \Delta_p}{k^{1/2}\sqrt{\pi r}}$$

$$\times e^{ikw[r-2-\alpha\pi\ \mathrm{sgn}(\psi)\cos\theta/\beta_\infty]-ik\delta M_\infty^2\phi}\, E(\sqrt{2kw(1-\cos\theta)})\, e^{ik\sigma_{1t}} \quad (3.67b)$$

Analysis of these formulas is deferred until the end of Chapter 4, where generalizations to include effects of camber will have been made.

CHAPTER 4

ANALYSIS FOR A CAMBERED AIRFOIL

This chapter generalizes the results of Chapter 3 to include airfoil camber. The problem we consider is portrayed in Fig. (4.1). A cambered airfoil at incidence angle α_i encounters a convected disturbance whose wavelength is short compared to the airfoil chord. As in Chapter 3, we introduce the large parameter $k=2\pi b/\lambda$ representing the ratio of airfoil size to disturbance wavelength. The amount of camber of the airfoil, measured by the parameter d/b, and the incidence angle α_i are both assumed to be $O(\alpha)$, where $\alpha << 1$ and $\alpha k = O(1)$. Note that we have changed the incidence angle notation from α to α_i. This change is to accomodate additional small parameters that will soon arise, which we will label α with an appropriate subscript.

The nondimensional equations (3.2) apply whenever the mean flow is a small perturbation to a uniform flow, and the gust wavelength is short compared to the body length. Hence, they are the appropriate governing equations for this problem as well. The difference between the equations for a cambered airfoil and those for a flat plate is contained in the flow speed q, the flow angle μ, and the drift function g. These quantities are all obtained from the complex potential F.

The function F is obtained by transforming the compressible potential to an incompressible one through a Prandtl-Glauert transformation, as described in Appendix I. For a flat plate, the

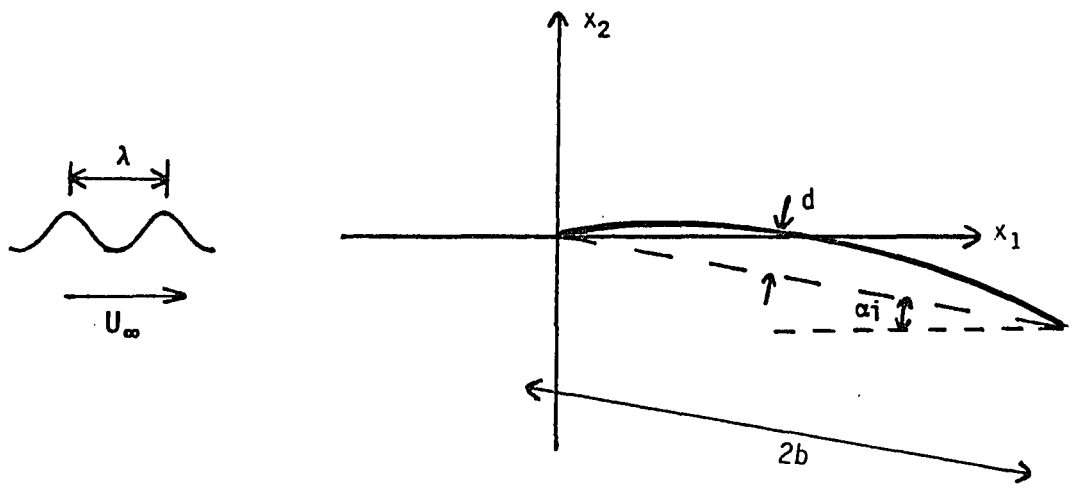

Fig. 4.1 Cambered airfoil encountering a high-frequency convected disturbance.

incompressible potential can be obtained by conformal mapping. For a general cambered airfoil no such mapping exists in closed form. However, since we only need the mean flow quantities accurate to $O(\alpha)$, approximate results from thin airfoil theory can be used. We utilize the result of Cheng and Rott (1954). They showed that, for incompressible flow, the complex velocity is given by

$$q - i\mu = -\frac{i}{\pi}\sqrt{\frac{\zeta^i - L}{\zeta^i}} \int_0^L \sqrt{\frac{s}{L-s}}\, \frac{N'(s)}{\zeta^i - s} ds + O(\alpha^2) \quad , \tag{4.1}$$

where $\zeta^i = x_1 + ix_2$ and the airfoil shape is given by $x_2 = N(x_1)$. The prime denotes differentiation. To calculate the mean flow perturbation quantities the effects of camber and incidence can be superposed. That is, we can set $N(x_1) = -\alpha_i x_1 + \eta(x_1)$, as depicted in Fig. (4.2). We now apply a Prandtl-Glauert transformation to convert the incompressible results to a compressible flow, and switch to nondimensional potential-streamline coordinates. Under these operations (4.1) becomes

$$q - i\mu = \frac{i\alpha_i}{\beta_\infty}\left[1 - \sqrt{\frac{z-2}{z}}\right] -$$

$$\frac{i}{\pi\beta_\infty}\sqrt{\frac{z-2}{z}} \int_0^2 \sqrt{\frac{s}{2-s}}\, \frac{\eta'(s)}{z-s}\, ds + O(\alpha^2) \quad , \tag{4.2}$$

where $z = \phi + i\psi$. In nondimensional form the airfoil shape function $\eta(s)$ is $O(\alpha)$.

A drawback of result (4.2) is that an integral over the body shape is required to determine the mean velocity at an arbitrary point

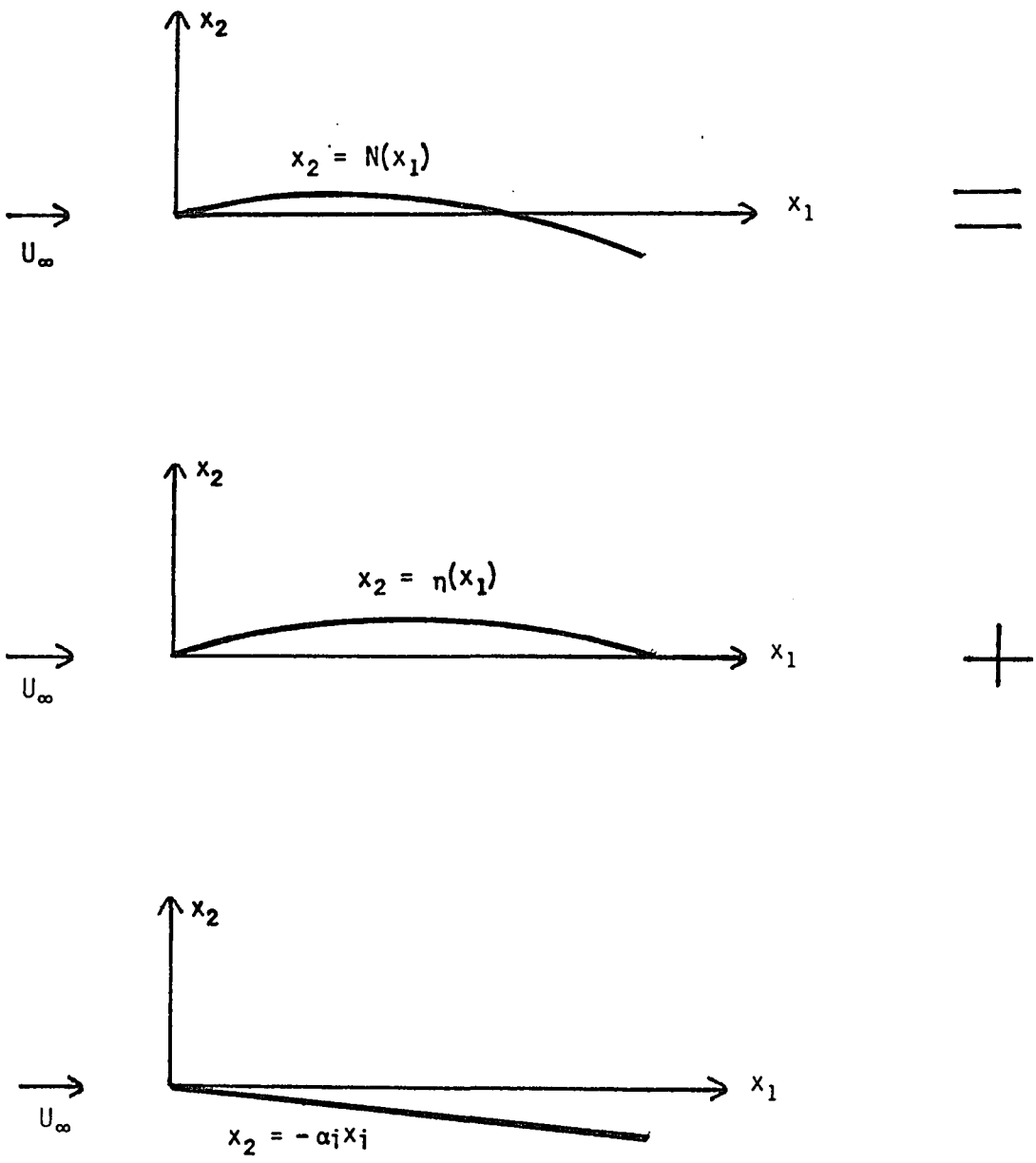

Fig. 4.2 Separation of incidence angle and camber effects for calculation of perturbation mean flow.

in space. An additional integral over space is required to determine the potential. Even the location of the trailing edge in (ϕ,ψ) space is not apparent from equation (4.2). However, we will find that to determine most quantities of interest, such as the farfield sound, only a few numerical integrations are required. This is a consequence of the localization of the sound generating regions. That is, to determine most of the information about the sound field, we need only know the mean flow characteristics in the local-leading-edge and local-trailing-edge regions. In these regions local approximations to Eq. (4.2) can be used.

Our approach to solving Eqs. (3.2) is again through an asymptotic series for large k and small α. The asymptotic regions utilized in the singular perturbation analysis are shown in Fig. (4.3). There are several changes from the corresponding figure for the flat plate. First, we have renamed the downstream transition region "Transition$_p$", for "planar", since it is related to the diffraction by a plane and is independent of curvature effects (at least to first order.) It exists even for a flat plate. A new transition region has also emerged due to surface curvature effects. It lies above and below the airfoil. We label it "Transition$_c$" for "curvature". This new region will be described in detail in the course of the analysis.

In the first few sections, we indicate the required modifications to the flat plate theory in the asymptotic regions common to flat-plate and cambered airfoils. We then show the need for a new region to generalize the leading-edge ray field, and we derive the

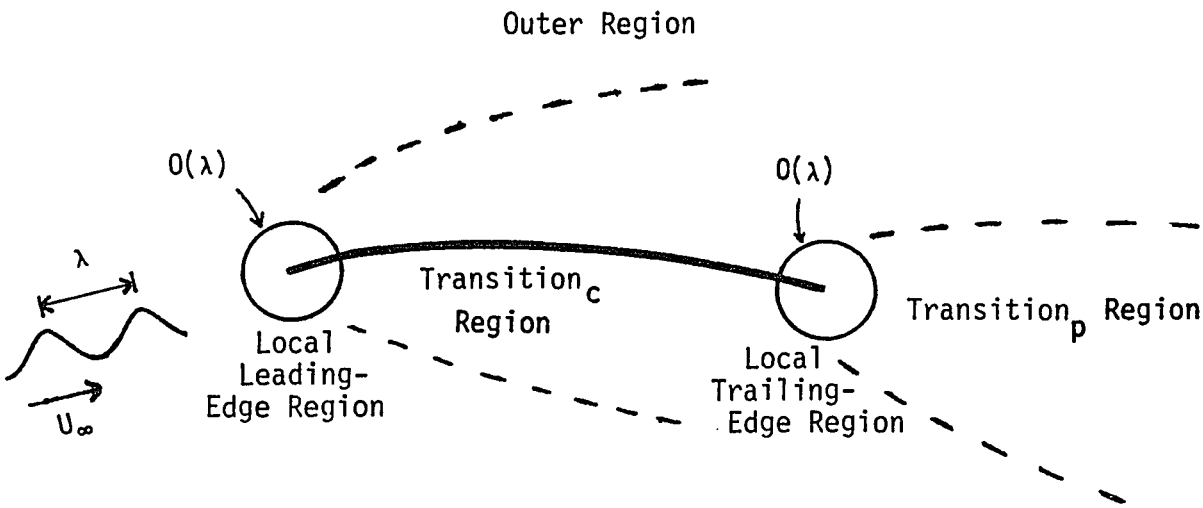

Fig. 4.3 Cambered airfoil with asymptotic regions illustrated.

necessary modifications to the solution. Finally, we will collect the solutions from the various asymptotic regions to form the total farfield expression.

4.1 Local Leading Edge Region

The local-leading-edge expansion of the mean-flow perturbation velocity can be readily obtained from Eq. (4.2). Inserting the local coordinate $Z = kz$ into (4.2) we obtain

$$q - i\mu = \left[\frac{\alpha_i \sqrt{k}}{\beta_\infty} - \frac{\sqrt{k}}{\beta_\infty \pi} \int_0^2 \frac{n'(s)ds}{\sqrt{s(2-s)}} \right] \sqrt{\frac{2}{Z}} + O(\alpha, \alpha^2 k) \quad . \tag{4.3}$$

For most airfoils of interest, the shape $n(s)$ goes to zero fast enough near the leading and trailing edges that we can integrate once by parts. We then have

$$q - i\mu = \frac{\alpha_{eff} \sqrt{k}}{\beta_\infty} \sqrt{\frac{2}{Z}} \quad , \tag{4.4a}$$

where

$$\alpha_{eff} = \alpha_i - \alpha_{1c} \quad , \tag{4.4b}$$

and

$$\alpha_{1c} = \frac{1}{\pi} \int_0^2 \frac{(1 - s)\, n(s)\, ds}{[\, s\,(2-s)\,]^{3/2}} \quad . \tag{4.4c}$$

The behavior of the mean flow in the local-leading-edge region is evident from Eqs. (4.4). The inverse-square-root flow around the leading

edge dominates, but with a modified strength compared to that for a flat plate. Thus α_{eff} is a measure of the strength of the local flow around the leading edge. It will be shown later to be a dominant correlating parameter for the sound power level.

By using the effective incidence angle α_{eff} in place of α_i in our local analysis for the flat plate, the results previously derived for the acoustic field can be used here directly. Hence, the asymptotic expansion of the local-leading-edge potential for a cambered airfoil is

$$h_\ell \sim \left[L_0(\theta) + \alpha_{eff}\sqrt{K}\,(L_1(\theta) + L_2(\theta)) \right] \frac{e^{iKwr}}{\sqrt{Kr}} \quad , \qquad (4.5)$$

where L_0, L_1, and L_2 are defined in Eqs. (3.10), (3.13), and (3.17). We emphasize that additional effects due to camber enter only through the single parameter $\alpha_{eff} = \alpha_i - \alpha_{1C}$. For many airfoils of practical interest α_{1C} is positive, so that the effective incidence angle is less than the incidence angle relative to the mean flow at infinity. This leads to several interesting features for the outer acoustic field, which will be discussed later.

4.2 Outer Region

The geometric acoustics solution was derived in a very general form in the flat-plate analysis. The $O(\alpha)$ phase distortion was shown to be an integral of the flow speed q. The integral could be expressed in terms of the complex potential F as (see (3.26))

$$\sigma_{1\ell} = V(\theta)\ \mathrm{Re}\{e^{-i\theta}F(re^{-i\theta})\} \quad , \qquad (4.6)$$

where $V(\theta)$ is defined in (3.25). The same result applied to the trailing-edge phase distortion σ_{1t}, when (r,θ) was replaced by the trailing-edge outer variables (r_t, θ_t) and the constant in F was adjusted so that F vanished for $r_t = 0$. For a cambered airfoil determination of σ_1 is cumbersome, since q and F must in general be obtained by numerical integration at each point in space. However, we are ultimately interested only in knowing σ_1 in the geometric farfield, i.e. for $r >> 1$. In this limit we can reduce the problem to the calculation of two integrals over the body shape, independent of observer location. This is done as follows.

The complex potential for the cambered airfoil at zero incidence is

$$F_C(z) = -\frac{i}{\beta_\infty \pi} \int_0^z dz' \sqrt{\frac{z'-2}{z'}} \int_0^2 ds \sqrt{\frac{s}{2-s}} \frac{\eta'(s)}{z'-s} \quad . \tag{4.7}$$

The reader is reminded that the prime on the η denotes differentiation. Switching the order of integration we obtain

$$F_C(z) = -\frac{i}{\beta_\infty \pi} \int_0^2 ds\, \eta'(s) \sqrt{\frac{s}{2-s}} \int_0^z \sqrt{\frac{z'-2}{z'}} \frac{dz'}{z'-s} \quad .$$

The integration on z', which we call I_2, can be done in closed form. The result is

$$I_2 = \log\left[\frac{1 + \sqrt{(z'-2)/z'}}{1 - \sqrt{(z'-2)/z'}}\right] -$$

$$\sqrt{\frac{s-2}{s}}\,\log\left[\frac{\sqrt{(s-2)/s} + \sqrt{(z'-2)/z'}}{\sqrt{(s-2)/s} - \sqrt{(z'-2)/z'}}\right]$$

Evaluating I_2 at the limits 0 and z, integrating with respect to s the term which is an exact differential, and utilizing the fact that $\eta(2) = \eta(0) = 0$, we obtain

$$F_C(z) = \frac{-i}{\beta_\infty \pi}\int_0^2 \eta'(s)\sqrt{\frac{s}{2-s}}\left[\log\left[\frac{1 + \sqrt{(z-2)/z}}{1 - \sqrt{(z-2)/z}}\right] -\right.$$

$$\left.\sqrt{\frac{s-2}{s}}\log\left[\frac{\sqrt{(s-2)/s} + \sqrt{(z-2)/z}}{\sqrt{(s-2)/s} - \sqrt{(z-2)/z}}\right] - i\pi\right] ds \qquad (4.8)$$

This is the expression for the $O(\alpha)$ complex potential for the cambered airfoil. For large r, the z dependence can be separated from the integral. Integrating by parts the term containing the second logarithm and utilizing $\eta(2) = \eta(0) = 0$, we obtain

$$F_C \sim \frac{i}{\beta_\infty}\left[\alpha_{2C}(\log 2r + i(\theta-\pi)) - \alpha_{3C}\right] \qquad (4.9a)$$

where

$$\alpha_{2C} = \frac{1}{\pi}\int_0^2 \frac{\eta(s)ds}{s^{1/2}(2-s)^{3/2}}\,, \qquad (4.9b)$$

$$\alpha_{3C} = \frac{1}{\pi}\int_0^2 \frac{\eta(s)ds}{\sqrt{s(s-2)}} \quad , \tag{4.9c}$$

and (r,θ) are the polar coordinates of the observation point referenced from the leading edge.

Using Eqs. (4.6) and (4.9) we can calculate the phase distortions $\sigma_{1\ell}$ and σ_{1t} in the geometric farfield. Including the contribution from the flat plate, the asymptotic form of $\sigma_{1\ell}$ for $r >> L$ is

$$\sigma_{1\ell} \sim \frac{V(\theta)}{\beta_\infty}\left[\alpha_g \sin\theta \log 2r - \alpha_g (\theta-\pi)\cos\theta + (\alpha_i-\alpha_{3C})\sin\theta\right] , \tag{4.10a}$$

where

$$\alpha_g = \alpha_i + \alpha_{2C} \quad . \tag{4.10b}$$

The corresponding result for the trailing-edge ray field is obtained by inserting trailing-edge coordinates into (4.8) and expanding for large r_t. Accounting for the slight difference in branch cut orientation in trailing-edge coordinates, we find

$$\sigma_{1t}(\theta_t) \sim \frac{V(\theta_t)}{\beta_\infty}\left[\alpha_g \sin\theta_t \log 2r_t - \alpha_g \theta_t \cos\theta_t - (\alpha_i + \alpha_{3C})\sin\theta_t\right] \tag{4.10c}$$

The only numerical integrations required to determine the phase distortion of the far field sound are those defining α_{2C} and α_{3C}.

Derivation of the amplitude equation ((3.28)) was also done very generally in Chapter 3. The asymptotic matching here is identical

to that performed for the flat plate. Again we find that the directivity of the leading-edge ray field is just $L(\theta)$, the directivity produced in the local leading-edge region. Hence the expression for the leading-edge ray field in the $r >> 1$ limit is

$$h_\ell \sim \left[L_0(\theta) + \alpha_{eff}\sqrt{k}\,(L_1(\theta) + L_2(\theta)) \right] \frac{e^{ik(wr + \sigma_{1\ell})}}{k^{3/2}\sqrt{r}} \quad , \quad (4.11)$$

with $\sigma_{1\ell}$ given in (4.10c). Similarly, we find that the trailing-edge solution in the farfield limit is

$$h_t \sim T(\theta_t) \frac{e^{ik(\,wr_t + \sigma_{1t}\,)}}{k^{3/2}\sqrt{r}} \quad , \quad (4.12)$$

where σ_{1t} is given in (4.10c). The amplitude T is the directivity of the local trailing-edge scattered field, which we now discuss.

4.3 Local-Trailing-Edge-Region

Since mean flow effects do not enter into the differential equation in the local-trailing-edge region, the transformation from flat plate to camber solution is immediate. The only complication arises in finding the location of the trailing edge in (ϕ,ψ) space, which is used in calculating the pressure jump in the leading-edge field at the trailing edge. We use the relation (Eq. (3.4a))

$$z = \zeta + F(\zeta) \quad (4.13)$$

to determine the trailing-edge location. Here $z = \phi + i\psi$ and $\zeta = x_1 + i\beta_\infty x_2$. The potential F is the sum of Eq. (4.8) for camber plus (3.3a) for the flat plate. Putting $\zeta = 2$ in (4.13) gives

$$\text{trailing-edge location} = \left(2 \pm \frac{\alpha_g \pi}{\beta_\infty}\ ,\ 0\right) \quad , \tag{4.14}$$

where α_g is defined in (4.10b). The parameter $\alpha_g \pi/\beta_\infty$ is the nondimensional circulation around the airfoil, i.e., it is the lift coeffiecient. Hence, the shift in trailing-edge location in (ϕ,ψ) coordinates is just mean lift coefficient for the airfoil. Equation (4.14) represents the origin of the trailing-edge coordinate-system, from which the variables (r_t,θ_t) are referenced.

The local-trailing-edge solution for the cambered airfoil is obtained from the flat plate result by replacing α with α_g everywhere in Eq. (3.47). The asymptotic expansion of the result is

$$H_t \sim \frac{T(\theta_t)\ e^{ikwr_t}}{k^2\sqrt{r_t}} \quad , \tag{4.15a}$$

where

$$T(\theta_t) = \frac{\mathrm{sgn}(\psi)\ \Delta_p\ e^{i(-\pi/4\ +\ C_\pm)}}{2\sqrt{\pi w(1-\cos\theta_t)}\ (\delta - w\cos\theta_t)} \quad . \tag{4.15b}$$

The quantities Δ_p and $C_\pm$ are as defined for the flat plate ((3.45b) and (3.46c)) but with α replaced by α_g. Substitution of Eq. (4.15b) for $T(\theta_t)$ into (4.12) completes the expression for the trailing-edge ray field.

The ray-field analysis for both the flat plate and cambered airfoils tacitly assumed that the acoustic waves generated at the leading and trailing edges satisfied the boundary condition on the airfoil. In other words, it was assumed that the acoustic propagation was tangent to the airfoil. To check this assumption, we calculate the normal velocity $\partial h/\partial \psi$ on the body for the leading-edge rays. The leading-edge ray field has the form

$$h_\ell \sim \frac{L(\theta)}{k^{3/2}\sqrt{r}} e^{ik(wr + \sigma_{1\ell})} \quad . \tag{4.16}$$

The normal velocity on the body upper surface is proportional to

$$\frac{\partial h_\ell}{\partial \psi}\bigg|_{\psi=0^+} = \frac{L(0)}{k^{3/2}\sqrt{r}} e^{ik(\, wr + \sigma_{1\ell}(r,0)\,)} \frac{1}{r} \frac{\partial \sigma_{1\ell}}{\partial \theta}\bigg|_{\theta=0} . \tag{4.17}$$

(The derivative $dL/d\theta$ is zero for $\theta = 0, 2\pi$.) The derivative of the phase distortion on the body is

$$\frac{\partial \sigma_{1\ell}}{\partial \theta}\bigg|_{\theta=0} = V(0) \int_0^r \frac{\partial q}{\partial \theta}(r',0)\, dr' \quad . \tag{4.18}$$

By the Cauchy-Riemann conditions, Eq. (4.18) may be written

$$V(0) \int_0^r r' \frac{\partial \mu}{\partial r'}(r',0)\, dr' \quad . \tag{4.19}$$

After one integration by parts we have

$$V(0) \left[\mu\, r - \int_0^r \mu(r',0)\, dr' \right] \quad . \tag{4.20a}$$

It is most meaningful to analyze this formula in the physical (x_1,x_2) space. Since μ is $O(\alpha)$, we can replace the potential-streamline coordinates (ϕ,ψ) by $(x_1,\beta_\infty x_2)$ and introduce no additional error. On the airfoil, the flow angle μ is equal to the body slope $\eta'(x_1)$. Hence Eq. (4.20a) says that $\frac{\partial h_\ell}{\partial \psi}$ is proportional to

$$x_1\, \eta'(x_1) - \eta(x_1) \quad . \tag{4.20b}$$

This quantity, which is essentially the reciprocal of the radius of curvature of the airfoil, is zero for a flat plate but nonzero for a cambered airfoil.

Thus, for the flat-plate airfoil analyzed in Chapter 3, the leading-edge ray field automatically satisfied the no-flow boundary condition on the airfoil surface. However, for the cambered airfoil under consideration here, the leading-edge ray field (4.11) fails to satisfy the boundary condition. A similar difficulty is present in the trailing-edge ray field (4.12), but there the error appears in higher order terms than are being considered. Mathematically, the inability to satisfy the correct boundary condition arises from neglect of the second derivative with respect to θ in the eikonal equation.

A more general geometric theory of diffraction must account for such phenomena such as "creeping waves" (waves decaying exponentially in the direction of propagation) on top of the body, and "whispering galleries" (multiple reflections from the surface) on the bottom. Such phenomena are very complicated to describe mathematically. Fortunately, the length of our airfoil is short

compared to its radius of curvature, and our problem contains only transition regions between the ray description and the creeping-wave or whispering-gallery descriptions. The transition zones provide a description of the leading-edge sound field for shallow angles, where the ray theory breaks down. We combine the transition regions above and below into the "transition$_c$" region, because the two are mathematically very similar. The transition$_c$ region is shown in Fig. (4.3)).

The major concern with the boundary-condition error in Eq. (4.20b) is that the leading-edge ray theory may have not predicted the sound field incident upon the trailing edge correctly. In that case, the strength of the scattered field would be incorrectly predicted. However, by finding the correct shallow angle description for h_ℓ, we will now show that to the desired accuracy the scattered field was correctly calculated by ray theory.

4.4 Transition$_c$ Region

We first consider the simpler "tangent gas" version of our full equation, by setting $\gamma=-1$ in equation (3.2). This step will ease the amount of writing considerably but not change the essence of the problem. The extension of the result for a perfect gas is given after the tangent-gas solution. With $\gamma=-1$, Eq. (3.2) becomes

$$\nabla^2 h + k^2 w^2 \left(1 - 2\beta_\infty^2 q \right) h = 0 \quad . \tag{4.21}$$

We write the operator in polar variables and expand q in a Taylor series for small θ. Equation (4.21) then becomes

$$\frac{1}{r}\frac{\partial h}{\partial r} + \frac{\partial^2 h}{\partial r^2} + \frac{1}{r^2}\frac{\partial^2 h}{\partial \theta^2} + k^2 w^2 \left[1 - 2\beta_\infty^2 \left[q(r,0) + \theta \frac{\partial q}{\partial \theta}(r,0) + \ldots\right]\right] h = 0 \; . \tag{4.22}$$

(We concentrate on the upper airfoil surface, where $\theta \approx 0$. The analysis for the lower surface ($\theta \approx 2\pi$) is similar.) As a starting point in determining the solution, we retain the part of Eq. (4.16) that does satisfy the boundary condition. We also set the amplitude $L(\theta)$ equal to $L(0)$, since $L(\theta) = L(0) + O(\theta^2)$ for small θ. Thus, we attempt a solution of the form

$$h_{tn,c} = \frac{L(0)}{k^{3/2}\sqrt{r}} e^{ik(\, wr + \sigma_{1\ell}(r,0)\,)} j(r,\theta) \quad . \tag{4.23}$$

The expression for $\sigma_{1\ell}$ (Eq. (3.24)) for a "tangent gas" is

$$\sigma_{1\ell}(r,0) = -\beta_\infty^2 w \int_0^r q(r',0)\, dr' \tag{4.24}$$

The boundary condtion on j is

$$\frac{\partial j}{\partial \theta}\bigg|_{\theta=0} = 0 \quad . \tag{4.25}$$

The condition that $h_{tn,c}$ match the ray field h_ℓ for O(1) values of θ is also imposed. Inserting (4.23) into (4.22) and neglecting $O(\theta^2)$ terms, we find

$$2ikw \frac{\partial j}{\partial r} \frac{(e^{ik\sigma_{1\ell}(r,0)})}{\sqrt{r}} + \frac{\partial^2}{\partial r^2}\left[j \frac{(e^{ik\sigma_{1\ell}(r,0)})}{\sqrt{r}} \right] + \frac{1}{r} \frac{\partial}{\partial r}\left[j \frac{(e^{ik\sigma_{1\ell}(r,0)})}{\sqrt{r}} \right]$$

$$+ \frac{1}{r^2} \frac{(e^{ikw\sigma_{1\ell}(r,0)})}{\sqrt{r}} \frac{\partial^2 j}{\partial \theta^2} - 2\, k^2\, w^2\, \beta_\infty^2 \theta \frac{\partial q}{\partial \theta}(r,0)\, j \frac{(e^{ik\sigma_{1\ell}(r,0)})}{\sqrt{r}} = 0 \qquad (4.26)$$

No fast variation in the r-direction is anticipated, hence, the second and third terms can be neglected since they are not multiplied by the large parameter k. Also, in this analysis it is worthwhile to extract the small parameter $\alpha_c = d/b$ (see Fig. (4.1)) from the flow speed q. Our new reduced equation is

$$2ikw \frac{\partial j}{\partial r} + \frac{1}{r^2} \frac{\partial^2 j}{\partial \theta^2} - 2\, k^2\, w^2\, \beta_\infty^2\, \alpha_c\, \theta\, Q_\theta(r,0)\, j = 0 \quad , \qquad (4.27)$$

where $q = \alpha_c\, Q$ and the subscript on Q denotes differentiation.

We now make use of the small-camber, or large radius of curvature, assumption. For small α_c and θ, the first two terms in Eq. (4.25) should balance. This fact suggests making the change of variable,

$$\nu = \sqrt{k}\, \theta \quad , \qquad (4.28)$$

which implies that the size of the transition region is $O(1/\sqrt{k})$. In terms of ν, (4.25) becomes

$$2\, i\, w \frac{\partial j}{\partial r} + \frac{1}{r^2} \frac{\partial^2 j}{\partial \nu^2} - 2\, k\, \alpha_c\, w^2\, \beta_\infty^2 \frac{\nu}{\sqrt{k}} Q_\theta(r,0)\, j = 0 \quad . \qquad (4.29)$$

Since we assume α_c k is O(1), the last term is $O(\frac{1}{\sqrt{k}})$ and a sensible solution to attempt is

$$j = 1 + \frac{j_1(r,\nu)}{\sqrt{k}} \quad . \tag{4.30}$$

The equation for j_1 is

$$2\ i\ w\ \frac{\partial j_1}{\partial r} + \frac{1}{r^2}\ \frac{\partial^2 j_1}{\partial \nu^2} = 2\ \alpha_c\ k\ w^2\ \beta_\infty^2\ Q_\theta(r,0) \quad . \tag{4.31}$$

The boundary condition

$$\frac{\partial j_1}{\partial \nu}\ \Big|_{\nu=0} = 0$$

and the matching condition as $\nu \to \infty$ also apply.

One can easily verify that equation (4.31) possesses the following particular solution.

$$j_{1p} = -i\ k\ \alpha_c\ w\ \beta_\infty^2\ \nu \int_0^r Q_\theta(r',0)\ dr' \quad . \tag{4.32}$$

This solution is just the second term in the expansion for small θ of the ray-acoustic field h_ℓ. Hence, the matching condition will be satisfied. The particular solution does not satisfy the boundary condition, however, and a homogeneous solution satisfying

$$\frac{\partial j_{1h}}{\partial r} + \frac{1}{2\ i\ w\ r^2}\ \frac{\partial^2 j_{1h}}{\partial \nu^2} = 0 \tag{4.33a}$$

$$\left.\frac{\partial j_{1h}}{\partial \nu}\right|_{\nu=0} = i\,k\,w\,\alpha_c\,\beta_\infty^2 \int_0^r Q_\theta(r',0)\,dr' = M(r) \qquad (4.33b)$$

$$j_{1h} \to 0 \text{ as } \nu \to \infty \qquad (4.33c)$$

is required.

A solution to Eqs. (4.33) can be obtained by obtained by applying a cosine transform on the ν variable and utilizing Eq. (4.33b), which results in the following first-order ordinary differential equation in r.

$$\frac{\partial J}{\partial r} + \frac{1}{2iwr^2}\left[-\sqrt{\frac{2}{\pi}}\,M(r) - \xi^2\,J\right] = 0 \quad , \qquad (4.34)$$

where ξ and J are the transform independent and dependent variables. The function M(r) is defined in (4.33b). We integrate (4.34) and apply the inverse transform to obtain the solution

$$j_{1h}(r,\nu) = \frac{2}{\pi}\int_0^\infty d\xi\,\cos\xi\theta\; e^{-\xi^2/2iwr} \int_0^r d\rho\;\frac{M(\rho)}{2\,i\,w\,\rho^2}\; e^{\xi^2/2iw\rho} \quad . \qquad (4.35)$$

Switching the order of integration and performing the integration on ξ, we arrive at the simpler form

$$j_{1h} = \frac{e^{-i\pi/4}}{\sqrt{\pi}} \int_0^r \frac{M(\rho)}{2\,i\,w\,\rho^2}\sqrt{\frac{2\,w\,r\,\rho}{r-\rho}}\; e^{i\nu^2 wr\rho/2(r-\rho)}\,d\rho \quad . \qquad (4.36)$$

The final version, obtained by making the change of variable,

$$s = \frac{w\, r\, \rho}{2\,(r - \rho)} \quad . \tag{4.37}$$

is

$$j_{1h} = \frac{e^{-i\pi/4}}{2\sqrt{\pi}} \int_0^\infty N(r,s)\, \sqrt{s}\, e^{i\nu^2 s}\, ds \quad , \tag{4.38a}$$

where

$$N(r,s) = \frac{1}{s^2}\, M_{\frac{2rs}{2s+wr}} \quad . \tag{4.38b}$$

Since $M(t) = O(t^2)$ as $t \to 0$, the integral in (4.38a) does not diverge.

The asymptotic behavior of (4.38a) as $\nu \to \infty$ can be obtained by deforming the contour of integration from the positive real to the positive imaginary axis. The integral is dominated by the contribution from the origin, and the asymptotic expansion is

$$j_{1h} \sim \frac{1}{4}\, N(r,0)\, \nu^{-3} \quad . \tag{4.39}$$

In outer variables, j_{1h} is $O(k^{-3/2})$ and hence small enough to satisfy the matching requirement.

To derive the transition$_c$ solution for a perfect gas, we must consider the terms in the differential operator of Eq. (3.2a) that are not present in (4.21). However, several simplifications can be made. In the transition$_c$ region, the variable coefficients in the additional operators can be replaced by their values at $\theta = 0$. Also, the derivatives contained in these additional terms affect only the rapidly-varying phase ikwr, to the desired accuracy. The final result is that

to change our "tangent gas" result to apply for a perfect gas, we simply replace the quantity $-B_\infty^2 w$ appearing in (4.24), (4.32), and (4.33b) with $V(0)$. The function $V(\theta)$ is defined in Eq. (3.25).

We have verified that the transition$_c$ solution formed by equations (4.23), (4.30), (4.32), and (4.38a) appropriately corrects the ray solution for small angles. The size of the region in which the transition$_c$ solution is required is $\theta = O(1/\sqrt{k})$. Most importantly, we have shown that the pressure field incident upon the trailing edge, and hence the strength of the scattered field, were correctly predicted by the ray theory. The ray-theory result is sufficiently accurate because the corrections due to body curvature effects are contained in the term j_1, which is negligible in determining the strength of the scattered field (since the scattered field is weaker than the incident field by $1/\sqrt{k}$).

The question remains as to how this transition$_c$ solution should be extended downstream beyond the airfoil trailing edge. The choice is somewhat arbitrary, since any error in the wake jump conditions made by a particular choice of the extension can be corrected by the "transition$_p$" solution. A natural extension is to simply continue satisfying $\partial h/\partial\psi = 0$ on $\psi = 0$, clear to downstream infinity. This is the extension we make. Continuity of velocity across the wake is automatically satisfied. The pressure jump across the wake, obtained from Eq. (3.52), is

$$e^{-iC_+}\left[\frac{\partial h_{tn,c}}{\partial \phi_t} - ik\delta h_{tn,c}\right]_{(\psi=0^+)} - e^{-iC_-}\left[\frac{\partial h_{tn,c}}{\partial \phi_t} - ik\delta h_{tn,c}\right]_{(\psi=0^-)} =$$

$$\frac{-\sqrt{2}\, e^{ikw\phi_t}\, \Delta_p}{\sqrt{k}\,\sqrt{2+\phi_t}}\left[1 + \frac{j_1(2+\phi_t,0)}{\sqrt{k}}\right] . \qquad (4.40)$$

Here Δ_p is the pressure jump at the trailing edge and is given by (3.45b), with α replaced by α_g. Equation (4.40) becomes the boundary condition for the "transition$_p$" solution, which we now describe.

4.5 Transition$_p$ Region

Neither the differential equation nor the boundary condition in the transition$_p$-region contain effects of camber to first order, except in the location of the trailing edge. Hence, the leading term is identical to the first term in Eq. (3.54), with the parameter α replaced by α_g. To derive the equation for the next order term, it is necessary to calculate the perturbation velocity $q - i\mu$. In general this cannot be done in closed form; however, it can again be done in the farfield.

The expansion of $q - i\mu$ for large r_t is obtained from Eq. (4.2) by setting $\frac{1}{z-s}$ equal to $\frac{1}{z}$, which can then be taken outside the integral. The mean flow perturbation velocity, including both camber and incidence angle effects, has the following form for $|z| >> L$:

$$q - i\mu \sim \frac{i\alpha_i}{\beta_\infty z} + \frac{i}{\beta_\infty z}\left[\frac{1}{\pi}\int_0^2 \frac{n(s)\, ds}{s^{1/2}\,(2-s)^{3/2}}\right] = \frac{i\alpha_g}{\beta_\infty z} . \qquad (4.41a)$$

When rewritten in transition-region variables Eq. (4.41a) becomes

$$q - i\mu = \frac{i\alpha_g e^{-i\theta_{tn}/\sqrt{k}}}{\beta_\infty r_t} \sim \frac{\alpha_g}{\beta_\infty r_t}\left[i + \frac{\theta_{tn}}{\sqrt{k}}\right] \qquad (4.41b)$$

This expression is identical to the complex velocity for the flat plate, except that the circulation α_g appears instead of the incidence angle α. Hence the differential equation, and the particular solution, can be obtained by analogy with the flat-plate results (3.62) and (3.63). Unfortunately, the boundary condition (4.40) is not easily satisfied, since the large r behavior of the function j_{1h} is not easily extracted. What probably happens is that the complementary solution required to satisfy the boundary condition effectively cancels j_{1h}. We say this because the flat-plate farfield result satisfied continuity of pressure and velocity across the wake. Since the farfield problem formulations are entirely analagous for the cambered and flat-plate airfoils, we expect the solutions to be similar. This problem requires more careful analysis. However, realizing that there is a certain degree of arbitrariness at this order due to our inablity to match for small r, and the fact that any error affects only the second order ($O(\alpha\sqrt{k})$) term in a small ($O(1/\sqrt{k})$) angular region, we simply take the term that is analagous to the flat plate result as our farfield solution. The total transition$_p$ solution then is

$$h_{tn,p} \sim \frac{\mathrm{sgn}(\psi)\, e^{iC_\pm}\, e^{i\pi/4}\, \sqrt{2}\, \Delta_p}{k^{3/2}\,(w-\delta)\,\sqrt{\pi}} \; \frac{e^{ik(wr_t - w\theta_{tn}^2/k + \sigma_{1t})}\; E(\sqrt{w}\;|\theta_{tn}|)}{\sqrt{r_t}} \tag{4.42}$$

with Δ_p and $C_\pm$ defined in (3.45) and (3.46) but as functions of α_g instead of α. The fresnel integral E is defined in Eq. (3.49b), and σ_{1t} is given in (4.10c).

4.6 Total Farfield Solution

A uniformly valid trailing-edge solution, which includes the trailing-edge ray field and the transition$_p$ solution, can be constructed by analogy with Eq. (3.66). We proceed instead to the total solution, of which the uniform trailing-edge solution is the second term. The total solution is

$$h \sim \frac{L_0(\theta) + \alpha_{eff}\sqrt{k}\;(L_1(\theta) + L_2(\theta))}{k^{3/2}\,\sqrt{r}}\; e^{ik(wr+\sigma_{1\ell})}$$

$$- \frac{\sqrt{2}\; e^{i\pi/4}\; \mathrm{sgn}\,\psi\; e^{iC_\pm}\;\; \Delta_p}{k^{3/2}\,\sqrt{\pi r}}\; \frac{e^{ikw(r-(2\pm\alpha_g\pi/\beta_\infty)\cos\theta)}\;\; e^{ik\sigma_{1t}}}{\delta - w\cos\theta}$$

$$\left[e^{-2ikw(1-\cos\theta)}\; E(\sqrt{2kw(1-\cos\theta)})\;\right] \tag{4.43a}$$

The variables (r,θ) are referenced from the leading edge. The corresponding equation for pressure is

$$p \sim \frac{-i(\delta-w\cos\theta)\left[L_0(\theta)+\alpha_{eff}\sqrt{k}\ (L_1(\theta)+L_2(\theta))\right]}{k^{1/2}\sqrt{r}}\ e^{ik(wr-\delta M_\infty^2\phi+\sigma_{1\ell})}$$

$$-\frac{\sqrt{2}\ e^{-i\pi/4}\ \mathrm{sgn}\psi\ e^{iC_\pm}\ \Delta p}{k^{1/2}\sqrt{\pi r}}\ e^{ikw(r-(2\pm\alpha_g\ \pi/\beta_\infty)\ \cos\theta)-ik\delta M_\infty^2\phi}$$

$$\times\ e^{ik\sigma_{1t}}\left[e^{-2ikw(1-\cos\theta)}\ E(\sqrt{2kw(1-\cos\theta)})\right] \qquad (4.43b)$$

As these constitute our most important results, we repeat the definitions of several of the quantities involved:

$$E(a) = \int_a^\infty e^{is^2}\,ds$$

$$\sigma_{1t} = \frac{V(\theta)}{\beta_\infty}\left[\alpha_g \sin\theta \log 2r-\alpha_g(\theta-\pi)\cos\theta-\alpha_g\pi\,\mathrm{sgn}\psi\ \cos\theta-(\alpha_i+\alpha_{3C})\sin\theta\right]$$

$$\sigma_{1\ell} = \frac{V(\theta)}{\beta_\infty}\left[\alpha_g \sin\theta \log 2r - \alpha_g\ (\theta-\pi)\ \cos\theta + (\alpha_i - \alpha_{3C})\ \sin\theta\ \right]$$

$$V(\theta) = -\ w\ \beta_\infty^2 + \frac{(\gamma+1)\ M_\infty^4\ (\delta-w\cos\theta)^2}{2\ \beta_\infty^2\ w}$$

$C_\pm = k\ \delta\ M_\infty^2\ (2 \pm \alpha_g\pi/\beta_\infty) = k\ \delta\ M_\infty^2$ times trailing edge location

$$\Delta p = \frac{i\ (w-\delta)}{\sqrt{2}}\left[\ L(0)\ e^{iC_2} - L(2\pi)\ e^{-iC_2}\ \right] e^{2ik(w\ -\ \delta M_\infty^2)}$$

$$C_2 = k\left[\ \alpha_g\ \pi\ (w\ -\ \delta M_\infty^2) + \sigma_{1\ell}(2,0^+)\ \right]$$

$$\alpha_{eff} = \alpha_i\ -\ \alpha_{1c}$$

$$\alpha_g = \alpha_i + \alpha_{2c}$$

An extensive parametric study will be performed on Eqs. (4.43) in the next chapter. Here we make some observations about the result which summarize comments made in previous sections.

The two terms comprising (4.43a) are the leading-edge and trailing-edge fields. Both contain the cylindrical wave phase (ikwr) and decay rate ($1/k^{3/2}\sqrt{r}$) that would be present for an unloaded airfoil. The first term contains the directivity $L_0 + \alpha_{eff}\,(L_1 + L_2)$ of the local-leading edge solution, indicating that the sound is produced in the local-leading-edge region. In the propagation to the farfield only the phase is distorted, through the term $\sigma_{1\ell}$. The trailing-edge contribution is proportional to Δ_p, the pressure jump in the leading-edge field at the trailing edge. This verifies the assertion that the trailing edge generates sound only by scattering the leading-edge field. For shallow angles the Fresnel integral description of the trailing-edge solution is required, but when $(1-\cos\theta)$ is $O(1)$, the asymptotic expansion of the Fresnel integral may be used to reduce the bracketed quantity to

$$\frac{i}{2\sqrt{2kw(1-\cos\theta)}} \quad . \tag{4.44}$$

The trailing-edge solution then takes a geometric-acoustics form, similar to that of the leading edge. The directivity of the trailing-edge ray field is the directivity of the local-trailing-edge region. Equation (4.44) shows that, except at small angles, the trailing-edge

field is weaker than the leading edge field that it scatters by $1/\sqrt{k}$. Hence, in our theory where $\alpha k = O(1)$, the $O(1)$ and $O(\alpha\sqrt{k})$ leading-edge terms are retained along with the $O(1/\sqrt{k})$ trailing-edge field, which arises from the scattering of the $O(1)$ leading-edge field. The scattering of the $O(\alpha\sqrt{k})$ leading-edge field can be neglected, since we do not include effects of order α, $\alpha^2 k$, and $1/k$. However, for convenience, we include the full leading-edge directivity $L(\theta)$ in the definition of Δ_p.

In determining the character of the farfield sound, the phase differences between the leading-edge and trailing-edge ray fields control the destructive and constructive interference. The phase of the trailing-edge sound field, relative to that for the leading edge, is given by

$$k \left[w \left(2 \pm \alpha_g \pi/\beta_\infty \right) \cos\theta + \sigma_{1\ell} - \sigma_{1t} \right] .$$

The part $\left(2 \pm \alpha_g \pi /\beta_\infty \right) \cos\theta$ is simply the difference in path lengths to the observation point from the leading and trailing edges. In the limit of uniform mean flow this term is the only difference in phase between leading and trailing edge radiation. For variable-mean flow the additional phase difference

$$\sigma_{1t} - \sigma_{1\ell} = \frac{V(\theta)}{\beta_\infty \left[-\alpha_g \pi \, \mathrm{sgn}\psi \cos\theta - 2 \alpha_i \sin\theta \right]} , \qquad (4.45)$$

which accounts for the nonuniform medium of propagation, also exists.

The influence of airfoil mean loading is contained in the incidence angle α_i and the three camber parameters α_{1C}, α_{2C}, and α_{3C}. However, several combinations of the incidence angle and camber parameters have emerged. It was found that $\alpha_{eff} = \alpha_i - \alpha_{1C}$ measures the strength of the mean flow around the leading edge and the magnitude of the correction to the local acoustic field due to nonuniform mean flow effects. The parameter $\alpha_g = \alpha_i + \alpha_{2C}$ represents the circulation or total lift on the airfoil. It appears throughout the phases of the various fields. The parameter α_{3C} is relatively unimportant, since it cancels out in the phase difference $\sigma_{1\ell} - \sigma_{1t}$. Notice that the incidence angle α_i appears by itself in only one term, the second half of $\sigma_{1\ell} - \sigma_{1t}$. Thus the dualism between camber and incidence angle present in the other small parameters does not extend to this one term. The term $-2\,\alpha_i \sin\theta$ in (4.45) represents a difference in path lengths to the observation point, from the trailing-edges of a cambered airfoil at zero incidence and a flat plate at incidence angle α_i. The effects on the sound field as the small parameters are varied constitutes an important part of our numerical study of Eqs. (4.43). We now turn to that study.

CHAPTER 5

NUMERICAL RESULTS AND DISCUSSION

This chapter is a numerical investigation of formulas (4.43) for the acoustic farfield generated by the interaction of a loaded airfoil with a high-frequency disturbance. The dependence of the sound field on the gust, mean flow, and airfoil characteristics will be analyzed through a series of computerized parametric studies.

The parameters contained in (4.43) form a ten-dimensional space. Five of the six gust-velocity and wavevector components (A_t, A_n, A_3, k_t, k_n, k_3) can be independently varied, as well as the entropy fluctuation B. The Mach number M_∞ and the three loading parameters α_i, α_{1C}, α_{2C} complete the space. With such a large number of variables, it is impossible to systematically study all possible parameter combinations, or even all of the combinations of practical interest. To make the number of variables more manageable, we do not consider entropy variations. We will also concentrate on entirely two-dimensional gusts, i.e., ones for which $k_3 = A_3 = 0$. Finally, most of the calculations will involve flat-plate airfoils. Justification for this (besides convenience) will be given in Section C below.

The most important quantifier of the sound field is the amount of acoustic power radiated. The main emphasis of our parametric study is on the change in radiated power as the above parameters vary. The formula for acoustic power, in the case of non-zero mean flow, is given

in Appendix E. Our results will be expressed in terms of the normalized power, defined by

$$\text{Normalized Power} = \frac{\text{Power/Span}}{\frac{1}{2}\rho_\infty U_\infty^3 b\, \varepsilon^2} \quad , \tag{5.1}$$

where ε is the magnitude of $|\overline{A}|$. Since the governing equations are a linear function of the disturbance amplitude, we can factor ε out and assume $|\overline{A}|$ is O(1).

Changes in the sound field will also be studied through farfield pressure-directivity patterns. As we see from Eq. (4.43b), in the farfield limit the radial dependence of our solution can be factored out. We plot the directivity factor as a function of the polar angle in physical space. In the farfield, the angles in physical and (ϕ,ψ) space are related by

$$\cos\theta = \frac{\cos\xi}{\sqrt{1-M_\infty^2\sin^2\xi}} \tag{5.2a}$$

$$\sin\theta = \frac{\beta_\infty \sin\xi}{\sqrt{1 - M_\infty^2\sin^2\xi}} \quad , \tag{5.2b}$$

where $\theta = \arctan(\psi/\phi)$ is the angle in (ϕ,ψ) space and $\xi = \arctan(x_2/x_1)$ the physical angle. The directivity pattern represents the angular distribution of the farfield pressure. Sample directivity patterns are shown in Figs. (5.1a,b). In these and all of the directivity patterns, the leading edge of the airfoil is located at the

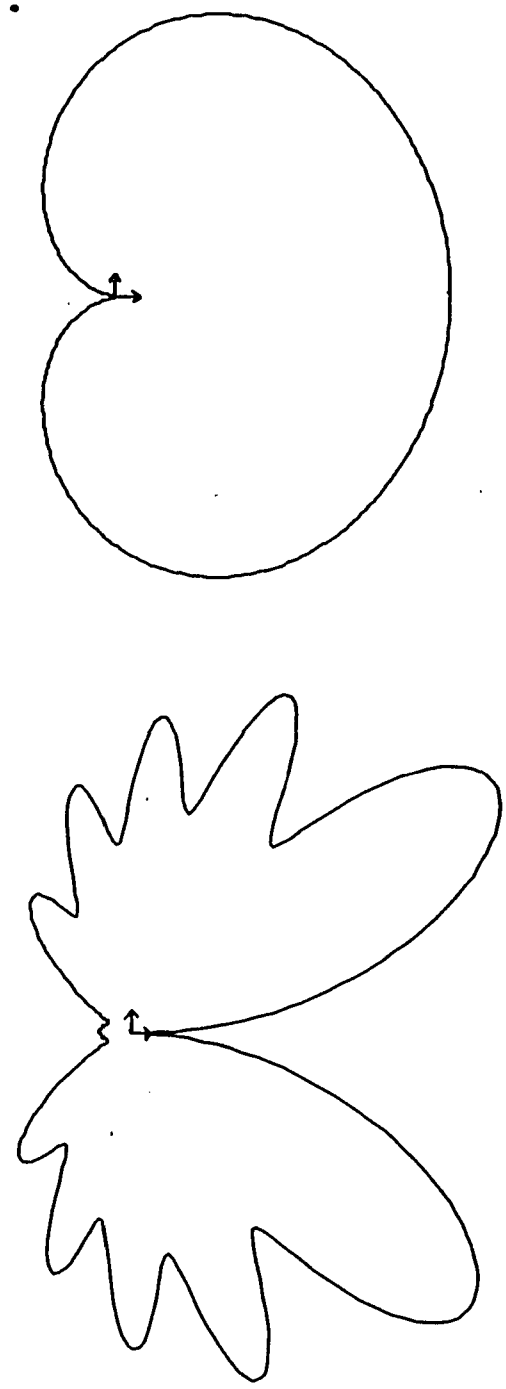

Fig. 5.1 (a,b) Farfield pressure directivity patterns illustrating leading-edge-trailing-edge interactions. (a) Leading-edge field. (b) Total field. $M_\infty = .6$, $kk_t = 7$.

origin of the coordinate system drawn in the figure. These patterns arise from the interaction of an unloaded airfoil with a convected disturbance. Figure (5.1a) shows the pressure distribution of the leading-edge field alone. Plotted is the $\cos\theta/2$ pattern of Eq. (3.10b) (converted to pressure). The distortion of the cardioid is due to the transformation from (ϕ,ψ) to (x_1,x_2) coordinates. Figure (5.1b) illustrates the leading-edge-trailing-edge interaction. For small angles the trailing-edge field cancels the antisymmetric leading-edge field. For larger angles the constructive and destructive interference between the leading-edge field and weaker trailing-edge field can be observed.

Our investigation into the influence of the different parameters on the sound field is divided into three sections. In Section 5.1, we study the effect of varying the orientation of a two-dimensional gust. We also briefly look at the cut-off phenomenon for a three-dimensional gust interacting with a loaded airfoil. In Section 5.2, we analyze the behavior of the sound field as the Mach number is changed. At this point it is appropriate to compare our approach with the acoustic analogy. We give a brief derivation of the acoustic-analogy equations appropriate for our problem, and compare this approach with the rapid-distortion-theory formulation we have used. Section 5.3 is an investigation of how the sound field changes as the mean loading on the airfoil is varied. The mean loading will be varied by changing both incidence angle and camber. We begin by looking at gust-orientation effects.

5.1 Trends with Gust Orientation

In varying the gust orientation, we must satisfy the solenoidal-gust condition far upstream. This condition is

$$A_t\, k_t + A_n\, k_n\, \beta_\infty + A_3\, k_3 = 0 \quad . \tag{5.3}$$

For interpretation of results, it is most convenient to work in terms of the physical wavenumber $k_{np} = \beta_\infty\, k_n$ rather than the Prandtl-Glauert wavenumber k_n. In this way, all of our gusts will be identified by physical quantities. Since far upstream the (ϕ,ψ) and (x_1,x_2) unit vectors coincide, one can physically visualize the gusts we consider by thinking in Cartesian coordinates. In terms of the physical wavenumber, and for a two-dimensional gust, Eq. (5.3) is

$$A_t\, k_t + A_n\, k_{np} = 0 \quad . \tag{5.4}$$

Another requirement that must be satisfied as the input disturbance is varied is the high-frequency condition, $k \cdot k_t >> 1$. Actually, this condition can be relaxed considerably. Amiet (1975) has given some justification for using the value $kw = k \cdot k_t M_\infty / \beta_\infty^2 = \pi/4$ as the dividing line between high and low frequencies. When a trailing-edge correction is included, as is the case for us, the lower limit can be decreased even further. Amiet's criterion does not apply directly to loaded airfoils, but we will use it as a rough lower limit. The upper limit of $k \cdot k_t$ is determined by the criterion $\alpha k \cdot k_t = O(1)$ (or $\alpha^2 k \cdot k_t << 1$.) We take $2 < k \cdot k_t < 12$ for most of our analysis. The desire to describe a right-going disturbance poses a final restriction

of k_t. A time dependence of $\exp(-i\omega t) = \exp(-ik_t U_\infty^2 t)$ was assumed, hence, we suppose $k_t > 0$.

Since the magnitude of the gust velocity may be factored out of the equations, we can assume without loss of generality that $A_t^2 + A_n^2 = 1$. Under this condition, and the continuity requirement (5.4), only two degrees of freedom are left for a two-dimensional gust. It is then possible to perform a thorough study on the effects of gust orientation by fixing k_t and varying k_{np}. We fix k_t to exclude the effects of changing frequency, allowing us to isolate the influence of gust orientation. Thus our calculations are performed at constant horizontal wavenumber rather than constant wavevector magnitude. The results of three sets of calculations, for $k \cdot k_t = 2.5$, 5.6, and 9.0, are shown in Figs. (5.2), (5.3), and (5.4). In each case, the airfoil is a flat plate, and three different incidence angles are considered for each k_t.

The most striking feature of the plots is that all curves reach a sharp peak between k_{np}/k_t equal 0 and 1. The peak for the unloaded case is easily understood. When k_{np} is equal to zero, the normal velocity component A_n is maximum. Because the only effect contained in the unloaded solution H_0 is the blocking of the gust velocity component normal to the body, one would expect a maximum in power output at $k_{np} = 0$. Likewise, the solution H_1 due to gust-distortion and nonuniform-propagation effects depends only on the gust parameters k_t and A_n, for fixed Mach number. The increase in power as k_{np}/k_t increases from zero, then, is due to the solution H_2 arising from the

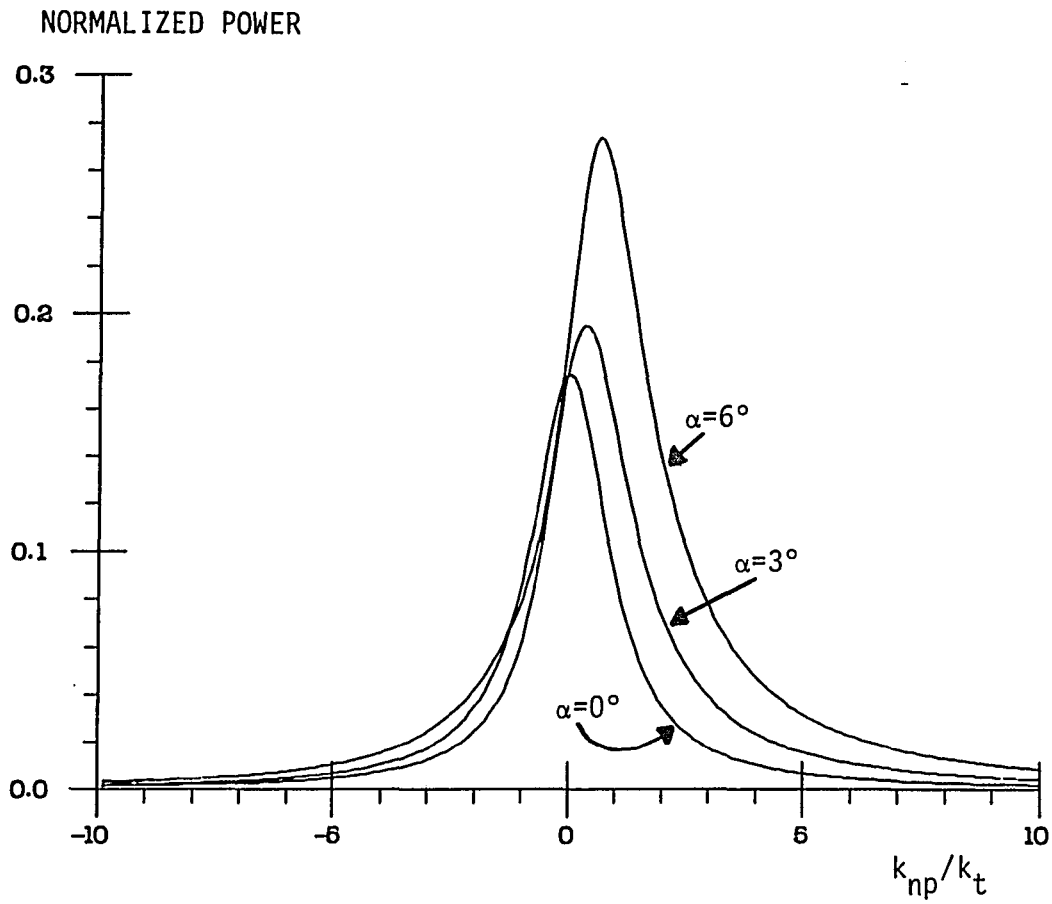

Fig. 5.2 Power vs. gust orientation. $M_\infty = .6$, $kk_t = 2.5$.

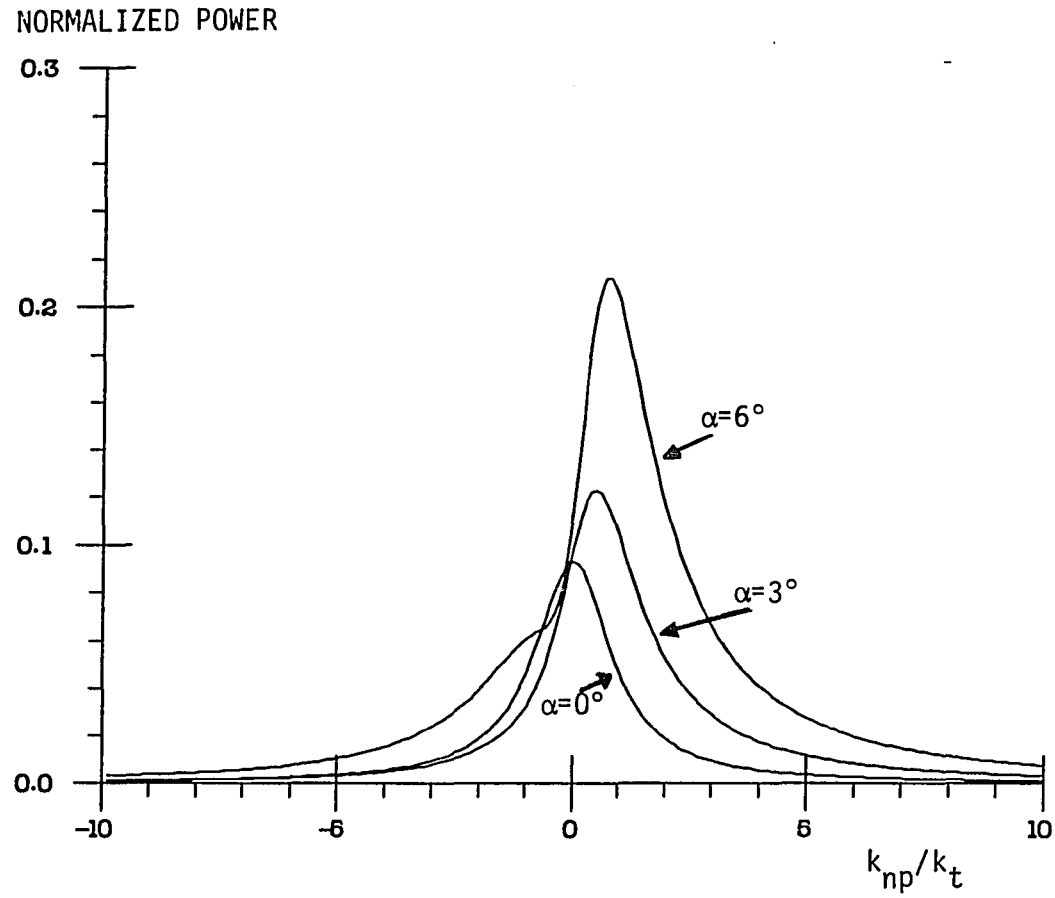

Fig. 5.3 Power vs. gust orientation. $M_\infty = .6$, $kk_t = 5.6$.

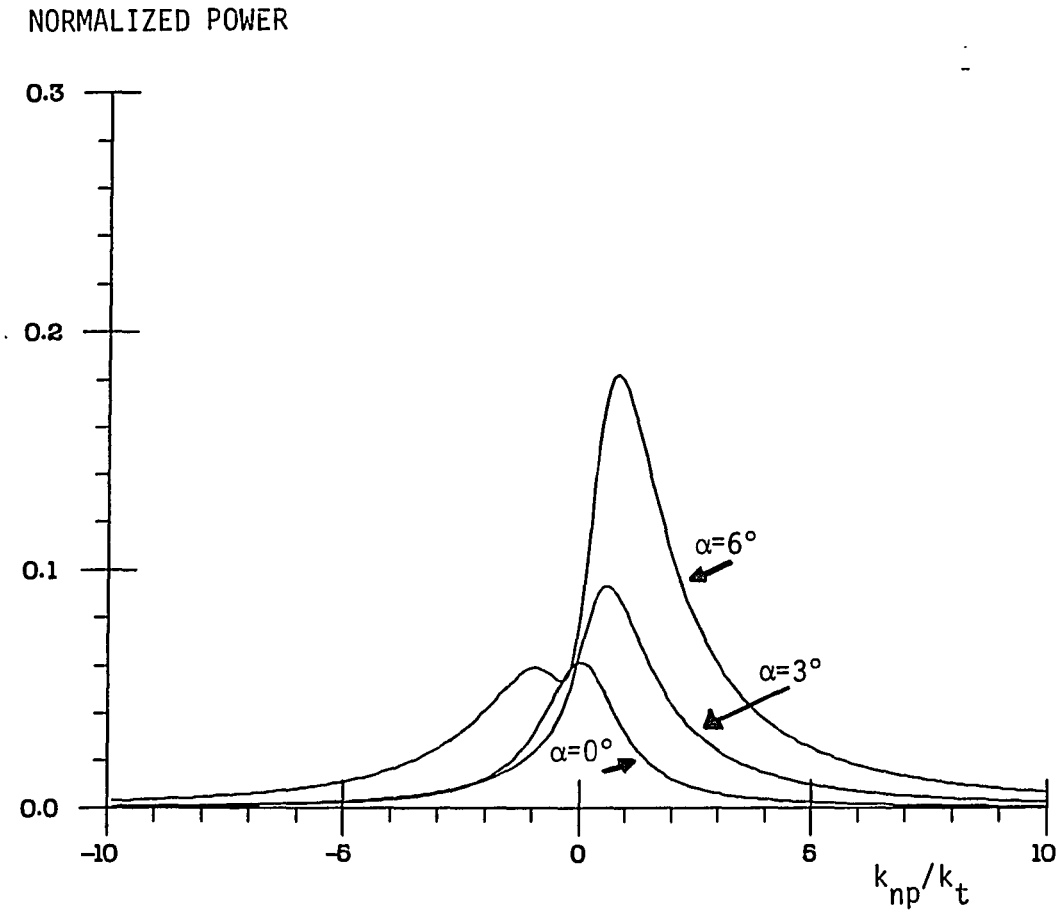

Fig. 5.4 Power vs. gust orientation. $M_\infty = .6$, $kk_t = 9$.

volume source in Goldstein's wave equation. The peaks of the curves shift to the right with increasing loading on the airfoil. The shift is actually considerable; a change in the peak from k_{np}/k_t equal 0 to 1 corresponds to a 45 degree rotation by the wavevector. The scale on the plots is misleading in this regard. Interestingly, the shift of the maximum to the right seems to be independent of the wavenumber k_t, at least at this Mach number. This is a bit suprising, since the volume source is strongly dependent upon k_t.

As $k \cdot k_t$ increases, the radiated power goes down due to the increase in frequency, but loading effects become more important relative to the no-loading case. Part of the explanation for this phenomenon is the reduction in interference from the trailing edge, since the strength of the trailing-edge scattered field decreases with loading. The dependence of the scattered field intensity on loading will be discussed in Section 5.3.

We repeated the calculations for $k \cdot k_t = 5.6$ at Mach numbers of 0.4 and 0.8. The results are shown in Figs. (5.5) and (5.6). The effect of increased Mach number for the loaded airfoil is substantial, as one can see from a comparison of Figs. (5.5), (5.3), and (5.6). Note the difference in scale. The important mechanisms behind the increase in power with Mach number will be identified in Section 5.2. The tendency of the curves is to shift to the right with increases in Mach number, as was the case for increases in loading. This is to be expected, since the more compressible the flow is, the larger (i.e. more cambered or at higher incidence) the airfoils appear. The $1/\beta_\infty$ in front of all of the

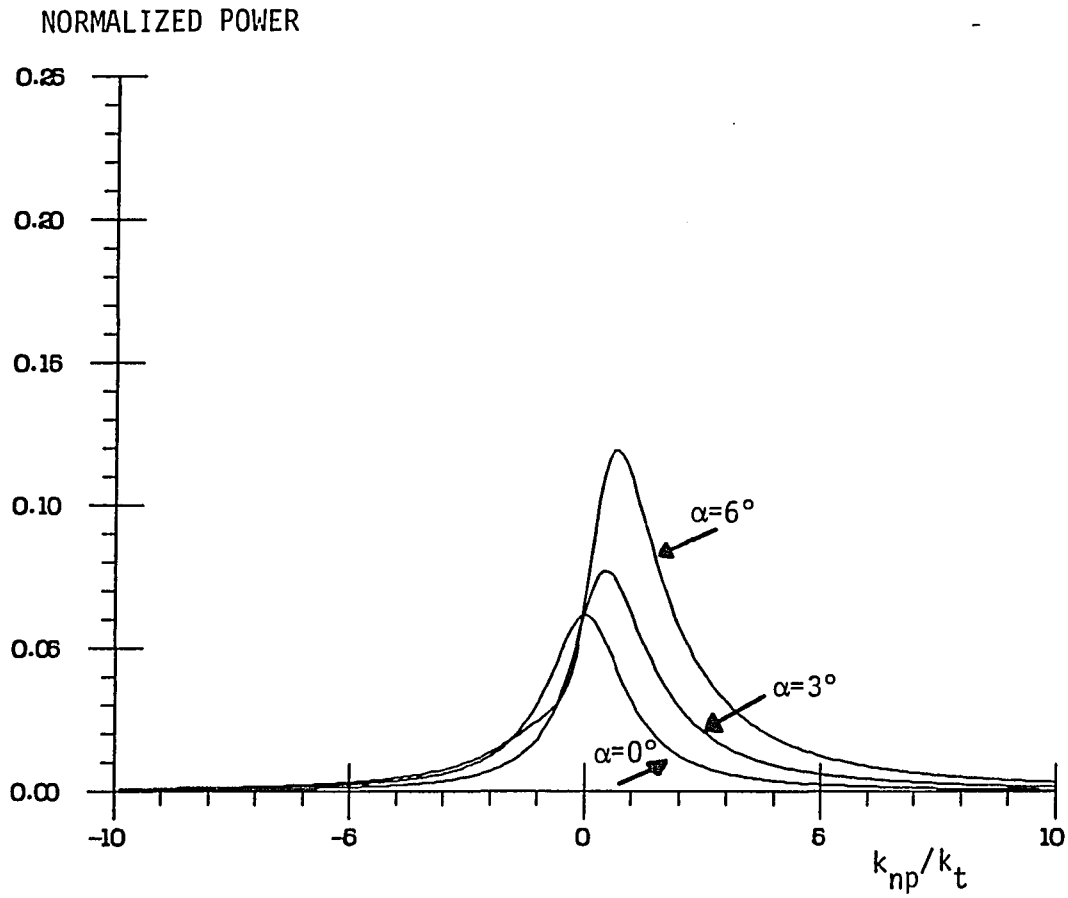

Fig. 5.5 Power vs. gust orientation. $M_\infty = .4$, $kk_t = 5.6$.

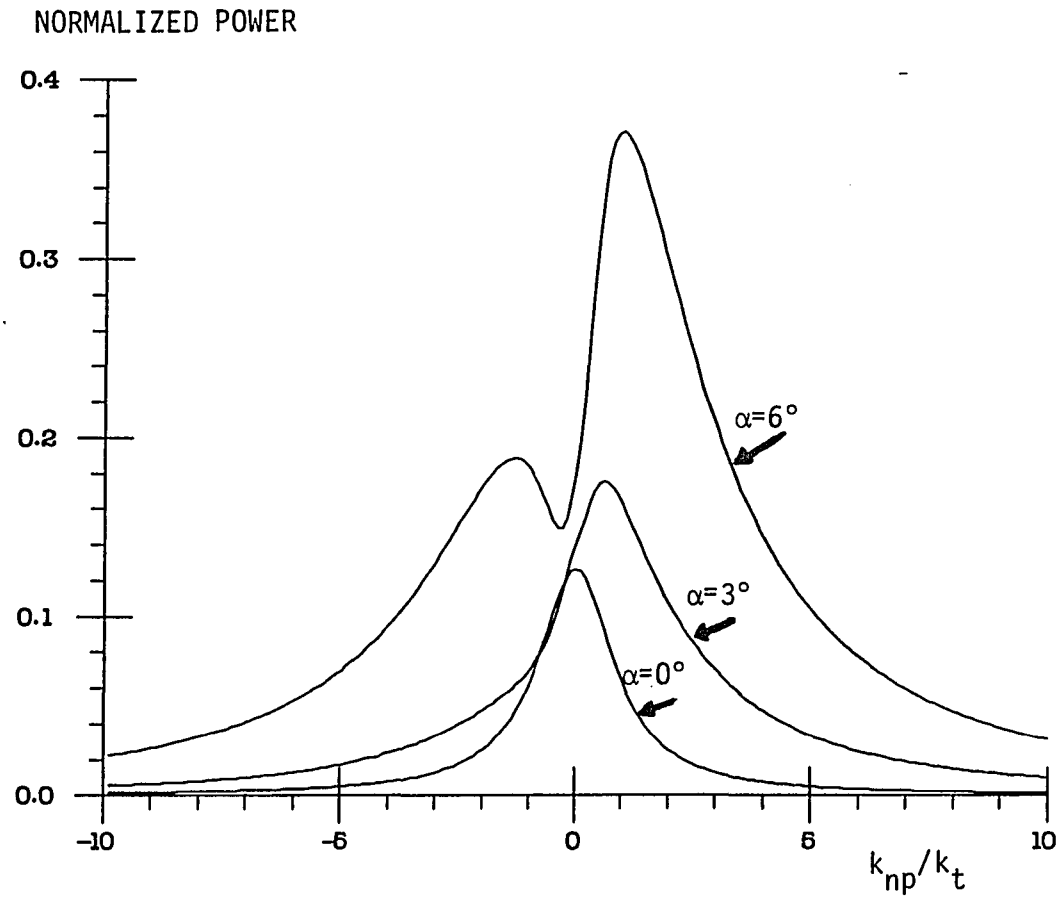

Fig. 5.6 Power vs. gust orientation. $M_\infty = .8$, $kk_t = 5.6$.

loading parameters is evidence of the similarity between increases in loading and increases in compressibility. The origin of the second peak in the power plot at Mach number 0.8, and in Fig. (5.4) where $M_\infty = 0.6$ and $k \cdot k_t = 9$, is not understood at this time.

Another interesting feature of the sound field is the symmetry with respect to incidence angle and gust orientation. Physically, a flat plate at incidence angle α encountering a convected disturbance whose wavevector makes an angle υ with the real axis is equivalent to a flat plate at angle $-\alpha$ encountering a disturbance with wavevector at angle $-\upsilon$. Shown in Fig. (5.7) is the power produced under the conditions of Fig. (5.3), but for $\alpha = 3°$ and $-3°$. The two curves are symmetric about the $k_\eta = 0$ axis. Thus, the data described so far for positive incidence angles may be obtained for negative incidence angles by reflecting the curves across the $k_\eta = 0$ axis. An additional consequence of the symmetry property is that for a gust with $k_\eta = 0$, (one with purely vertical velocity fluctuations), the power is a quadratic function of the incidence angle α near $\alpha = 0$. This is because the sound field must change in the same way whether the incidence angle is raised or lowered, as there is no directional preference to the gust. Hence for $k_\eta = 0$, the power is equal to the power for an unloaded airfoil plus $O(\alpha^2)$, and the power curves should all intersect the $k_\eta = 0$ axis near the point where the unloaded solution does. This is indeed the case, as we see from Figs. (5.2) through (5.6).

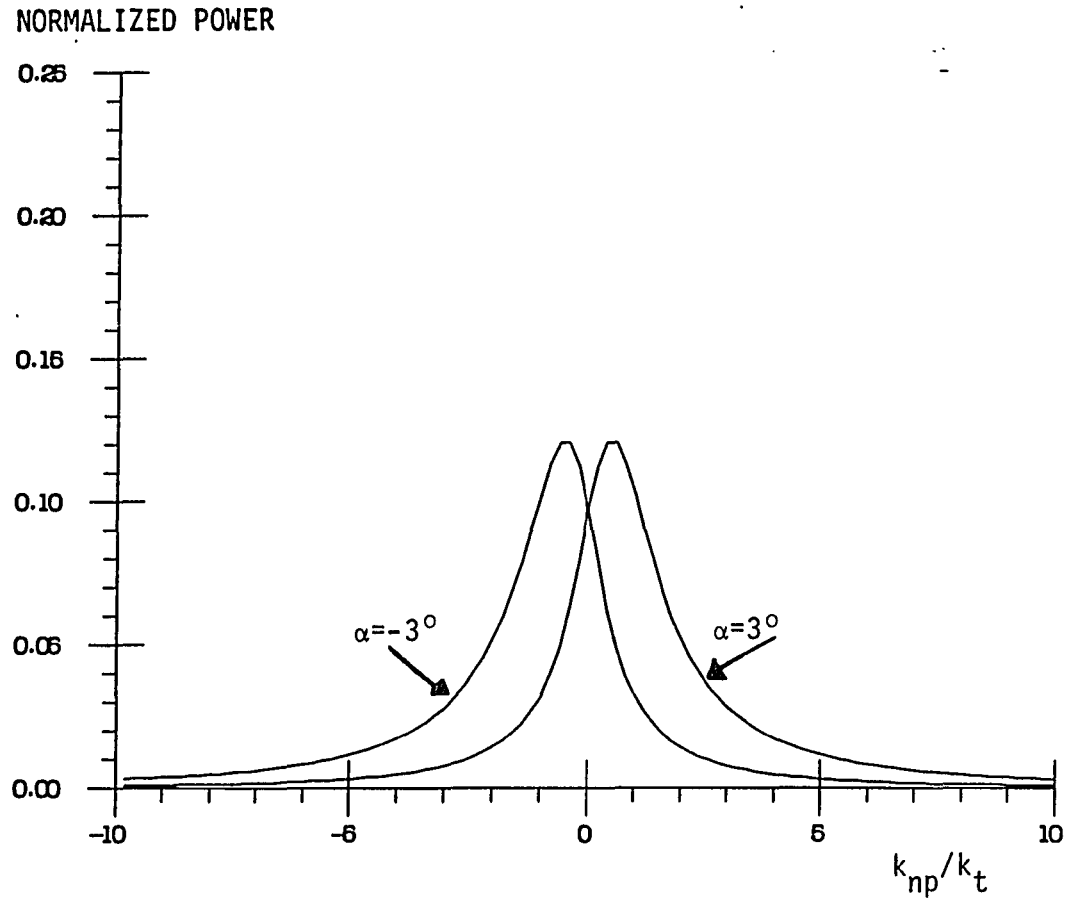

Fig. 5.7 Power vs. gust orientation curves illustrating symmetry with respect to α, k_{np}. $M_\infty = .6$, $kk_t = 5.6$.

As a final investigation into gust-orientation effects, we consider a three-dimensional gust. We wish to observe the effect of increasing k_3 while keeping A_3 zero. The sound field is much like that for a two-dimensional gust, except that the effective frequency decreases. (See (2.12b).) As k_3 increases, the interaction angle between the gust wavefront and the leading edge of the infinite-span airfoil increases from 0 degrees, and the trace speed of the gust along the edge of the airfoil decreases. When the trace speed becomes subsonic there is no more sound generated, i.e., cut-off is reached. As the acoustic wavenumber w approaches zero, care must be taken in interpreting our high-frequency solution. This issue is discussed in Section 5.2. Here we simply allow w to go to zero, as we are most interested in how rapidly the power drops with small changes in k_3, particularly for non-zero incidence. The power vs. k_3 curves are shown in Fig. (5.8) for α_i = 0, 3, and 6 degrees. We see that except near cut-off, the decrease in power with increasing k_3 is slight, although it is more for larger values of airfoil incidence.

5.2 Behavior with Changing Mach Number

To study the effect of changing the Mach number, we want to examine our solution for the widest range of subsonic Mach numbers, including the limit as M_∞ tends to zero. When the Mach number approaches zero, the acoustic wavelength becomes long compared to the airfoil chord. This fact does not affect our leading-edge solution, which is essentially a gust-scattering problem. (We continue to assume that $k \cdot k_t$ is large, i.e., that the gust wavelength is short compared to

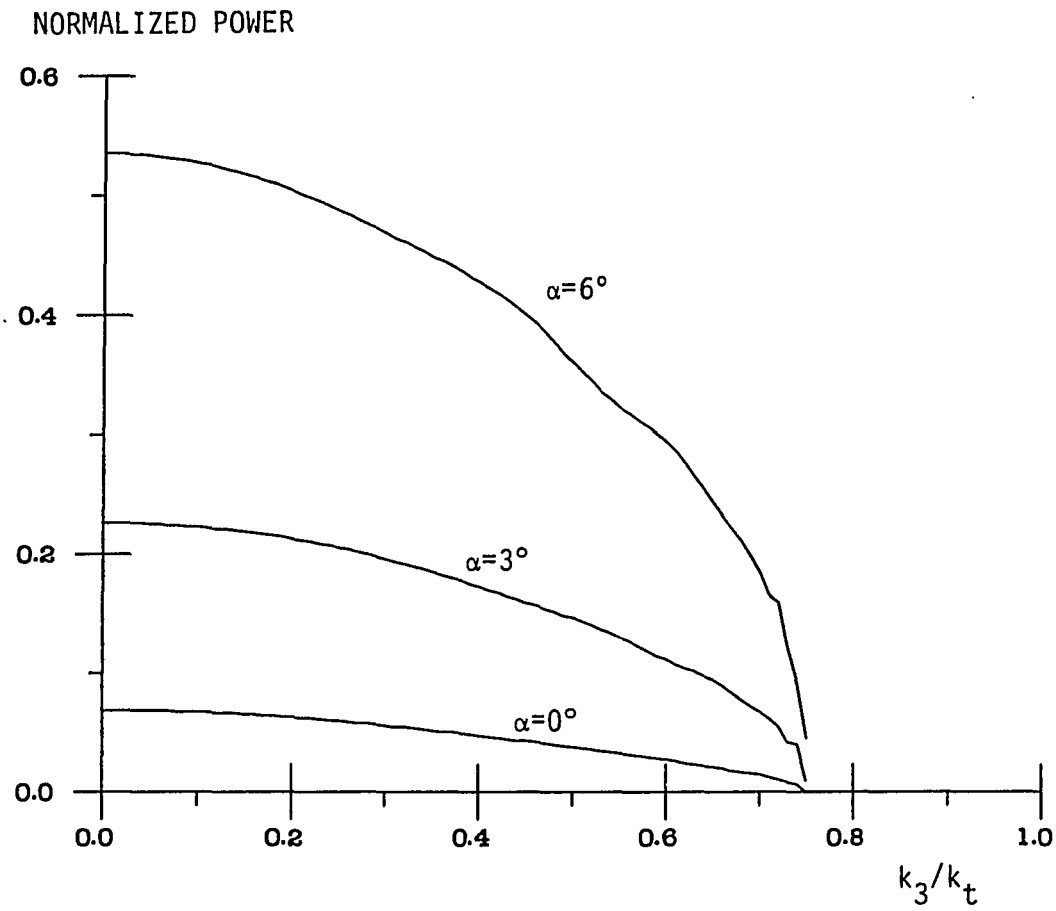

Fig. 5.8 Power vs. spanwise wavenumber. $k_{np}/k_t = 2$, $kk_t = 8$, $M_\infty = .6$.

the airfoil chord.) However, subsequent steps in the iteration scheme for high frequencies (described in Chapter 1) involve the scattering of acoustic waves. As the acoustic wavelength increases, the iterations converge more slowly. One can see the slow convergence in the trailing-edge part of solution (4.43). For large kw the asymptotic expansion of the Fresnel integral can be used for most angles, and the trailing-edge contribution is $O(1/\sqrt{k})$ relative to the leading edge. When kw is small, though, the asymptotic expansion is inapplicable and the function remains O(1).

In order to avoid the issue of series convergence associated with the trailing-edge correction, we consider only the leading-edge solution in this section. This also allows us to isolate the sound-generating mechanims, since the trailing edge serves only to scatter leading-edge sound. Our problem is now equivalent to the scattering of a convected disturbance by a semi-infinite plate.

In Figs. (5.9), (5.10), and (5.11), we plot the amount of power radiated by the leading edge alone as a function of Mach number. Curves are drawn for three different incidence angles for each of the three gust orientations. The trend with increasing Mach number is clear from these plots. For a loaded airfoil, the normalized power increases linearly at low Mach numbers and very rapidly at higher Mach numbers. For an unloaded airfoil, the power increases approximately linearly at all Mach numbers. The radiated power is greatest for k_{np}/k_t near 1, consistent with the conclusions of Section 5.1. The reader is reminded that normalized power is plotted. Actual power contains an additional U_∞^3 (or M_∞^3) dependence.

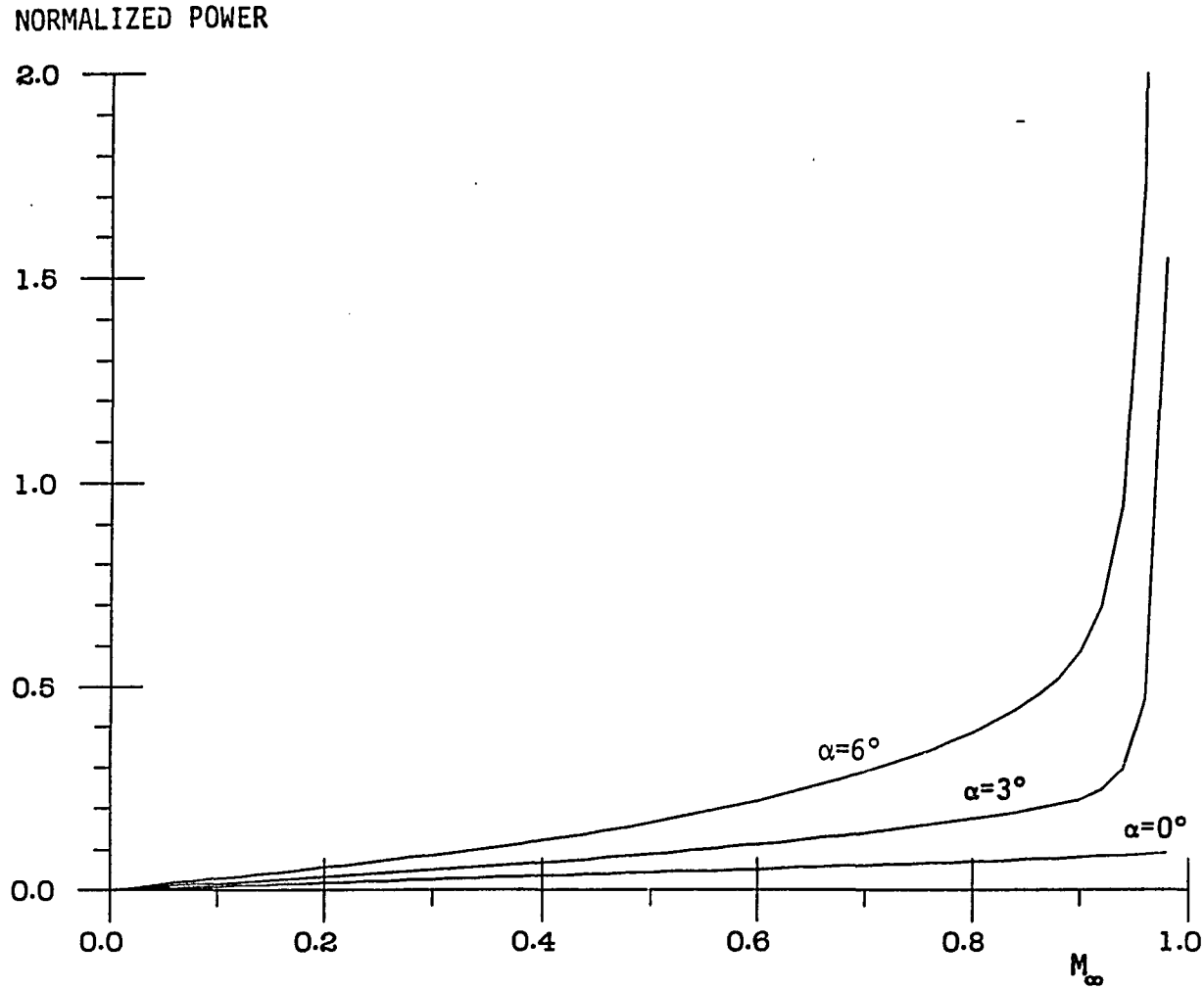

Fig. 5.9 Leading-edge power vs. Mach number. $k_{np}/k_t = 1$, $kk_t = 6$.

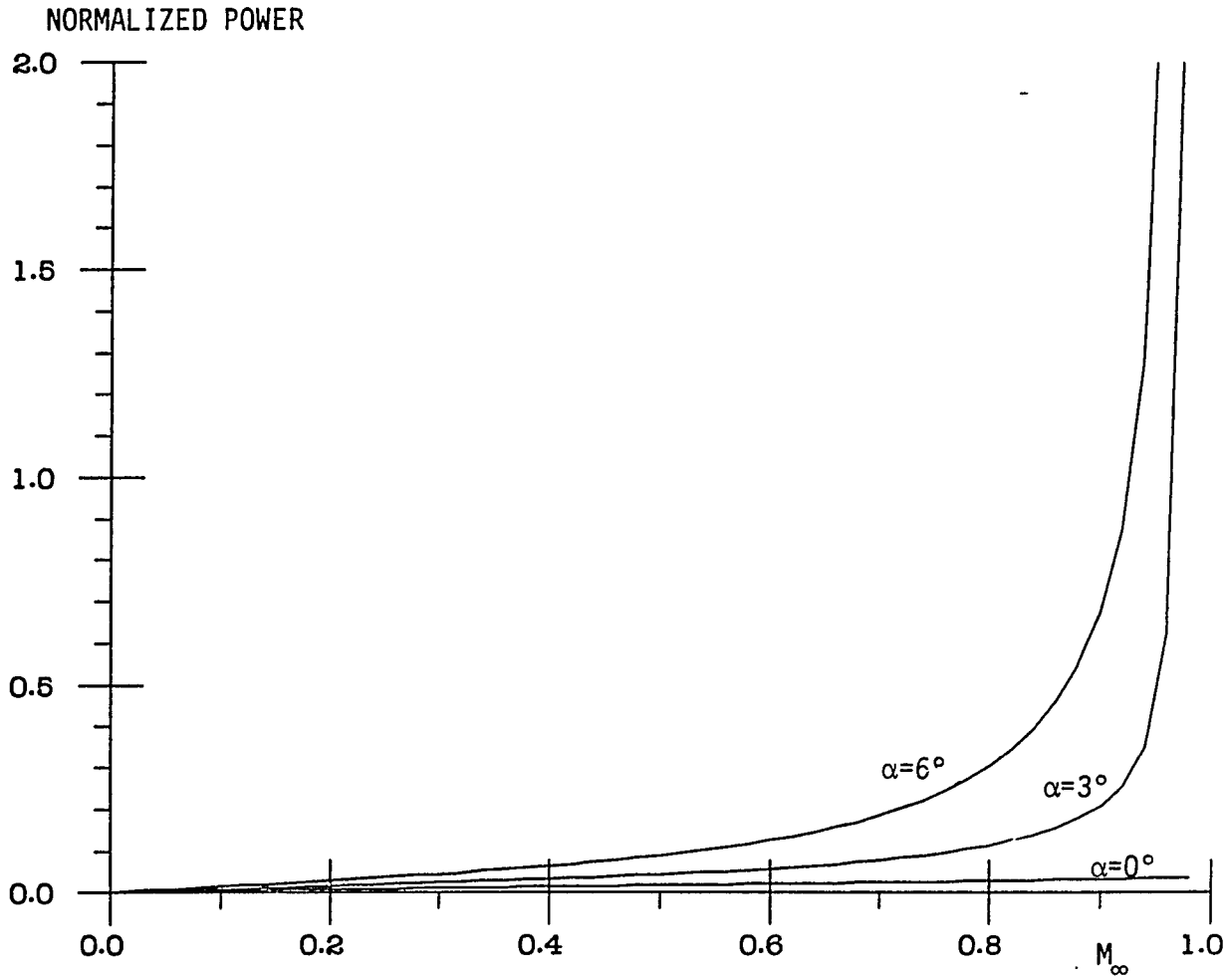

Fig. 5.10 Leading-edge power vs. Mach number. $k_{np}/k_t = 2$, $kk_t = 6$.

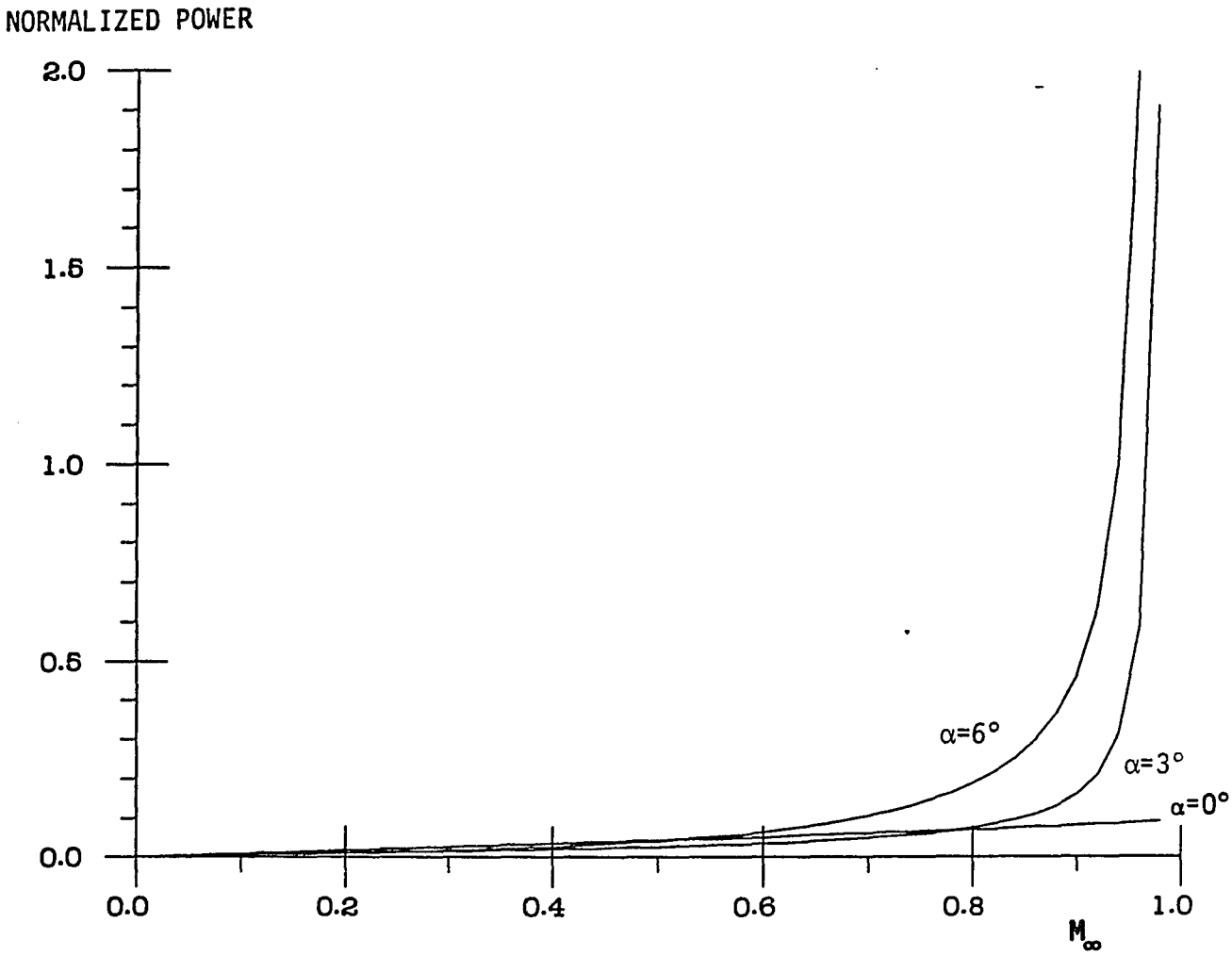

Fig. 5.11 Leading-edge power vs. Mach number. $k_{np}/k_t = -1$, $kk_t = 6$.

The mechanisms responsible for the increase in sound power level with increasing Mach number can be identified through an analysis of our local-leading-edge solutions H_0, H_1, and H_2. The function H_1 accounts for nonuniform-propagation effects, as well as blocking by the airfoil surface of the gust velocity distortions. The function H_2, representing the interaction of the gust with the nonuniform mean flow, arises from the presence of the volume source term

$$\frac{1}{\rho_0} \nabla\cdot(\rho_0 \overline{v}') \quad . \tag{5.5}$$

Due to the single divergence, the source term has the mathematical form of a dipole. In terms of pressure, the source is a quadrupole. We assess the relative efficiency of H_1 and H_2 as sound-generating mechanisms by plotting the power associated with each of them divided by the power for the unloaded-solution H_0. The plots are given in Fig. (5.12), for $k_{np}/k_t = 2$. The functions H_1 and H_2 are not multiplied by the small parameter $\alpha\sqrt{k}$.

The rapid increase in power as M_∞ approaches one is expected, since small incidence angles produce substantial flow distortions at high Mach numbers. In fact, the linearized mean-flow description is invalid at transonic Mach numbers. The singularities at small M_∞ are more surprising. To understand the nature of these singularities, we further divide our solution. We split H_1 and H_2 into "compressiblility" and "gust" parts, the compressibility parts being those that vanish at low Mach numbers. For H_1, the division is made into the first and

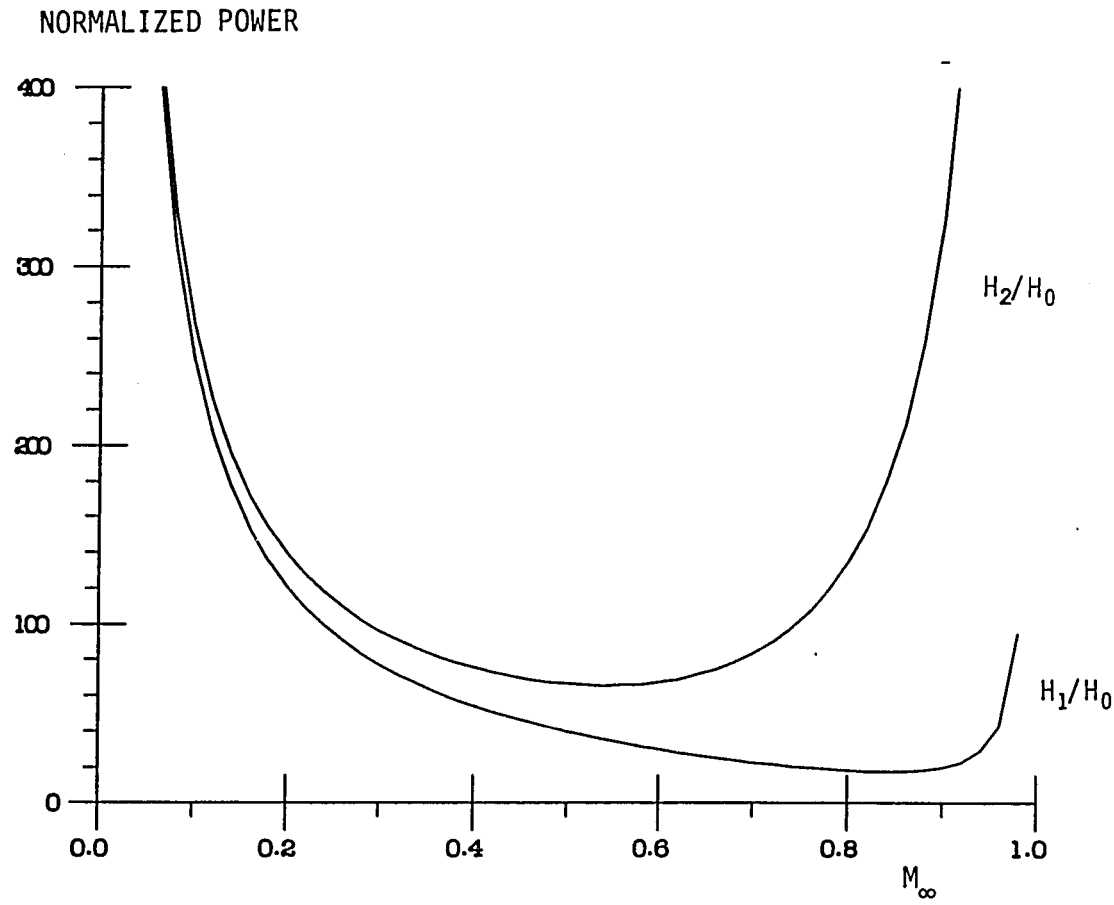

Fig. 5.12 Power vs. Mach number for individual leading-edge solutions. $k_{np}/k_t = 2$.

second terms of Eq. (3.13c). The second term vanishes at low Mach numbers and is the compressibility part; we label it H_{1CO}. The first term is the gust component, which we label H_{1g}. To split H_2 we expanded the source (5.5):

$$\frac{1}{\rho_0}\,\nabla\cdot(\rho_0\overline{v}') = \nabla\cdot\overline{v}' + \frac{1}{\rho_0}\,\overline{v}'\cdot\nabla\rho_0 \quad . \tag{5.6}$$

The density gradients in the second term vanish at low Mach number, while the first term is nonzero at all Mach numbers since $\overline{v}'$ is not solenoidal. The second term of Eq. (5.6) corresponds to the source term

$$R^{-3/2}\left[\, C_3\cos\frac{3\theta}{2} + C_4\sin\frac{3\theta}{2}\,\right] e^{i(\delta\Phi+k_n\Psi)} \tag{5.7a}$$

in Eq. (3.14a) for the modified potential H_2. Expression (5.7a) gives rise to the compressibility solution H_{2CO}. The term

$$R^{-1/2}\left[C_1\cos\frac{\theta}{2} + C_2\sin\frac{\theta}{2}\,\right] e^{i(\delta\Phi+k_n\Psi)} \tag{5.7b}$$

appearing in (3.14a) corresponds to the first term in (5.6) and gives rise to the gust solution H_{2g}. The powers generated by the four separate solutions H_{1CO}, H_{1g}, H_{2CO}, and H_{2g} are shown in Fig. (5.13). We see that both gust solutions are singular as M_∞ tends to zero, while both compressibility terms vanish in this limit.

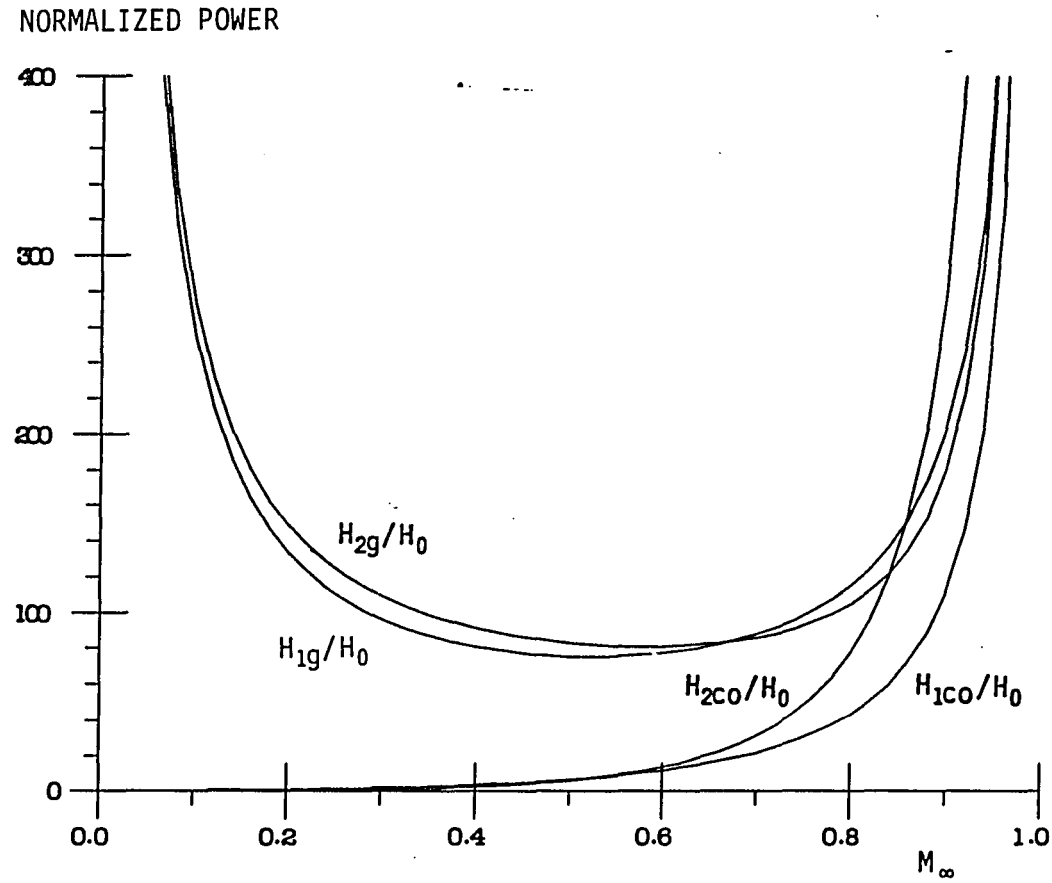

Fig. 5.13 Power vs. Mach number for "gust" and "compressibility" leading-edge solutions. $k_{np}/k_t = 2$.

In the low-Mach-number limit, H_{2g} can be studied analytically. As M_∞ approaches zero the farfield pressure corresponding to H_{2g} tends to

$$\frac{2 A_n e^{ik_t r}}{\sqrt{M_\infty k_t r}} \quad , \tag{5.8}$$

which is the farfield of a two-dimensional monopole. (Eq. (5.8) is for the dimensionless pressure; dimensional pressure is proportional to $M_\infty^{3/2}$.) The monopole field is stronger than the surface-generated field H_0 (a "three-halves pole") by a factor of $1/\sqrt{M_\infty}$. The ratio of the powers associated with H_{2g} and H_0, shown in Fig. (5.13), behaves as $1/M_\infty$. Upon inspection of Eq. (5.7b), the reason for the monopole is evident. The volume source does not satisfy conservation of mass (the volume integral over all space is nonzero, as one can verify by direct integration), and hence is not a really a dipole source but actually a monopole.

Physically there is no mass source in the fluid, and a monopole description acoustic field is incorrect. The problem arises from considering the volume source, which produces H_{1g}, separately from the surface sourse (see the boundary condition (3.11b)), which produces H_{2g}. Indeed, the farfield pressure associated with H_{1g} is the negative of (5.8), i.e., a monopole in H_{1g} cancels the one in H_{2g}. The logical succeeding step is to combine H_{1g} and H_{2g} into the total gust solution H_{12g}. The power associated with H_{12g} is shown in Fig. (5.14), along with the compressibility solutions. The new gust solution is bounded with

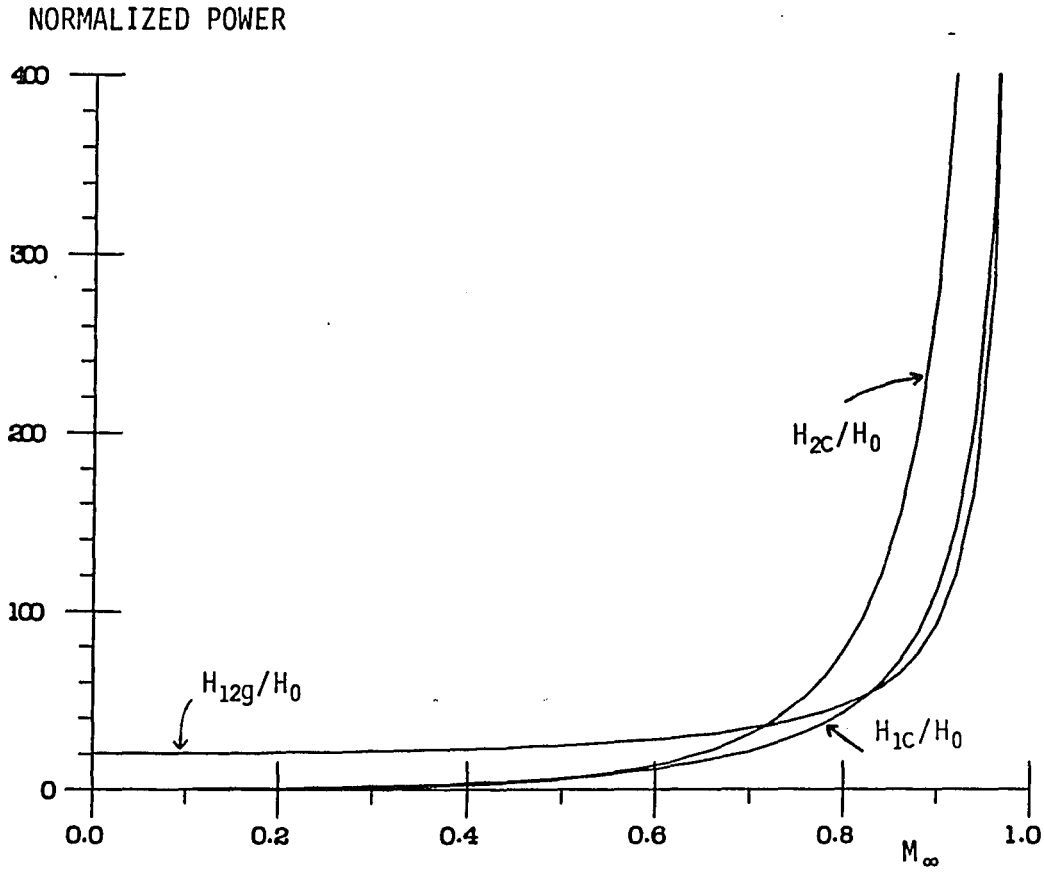

Fig. 5.14 Power vs. Mach number for "compressibility" and "combined gust" solutions. $k_{np}/k_t = 2$.

respect to H_0 for low Mach numbers, indicating that its leading-order behavior is that due to a "three-halves pole," whose pressure is proportional to M_∞^0 (M_∞^2 in dimensional form). The second-order term in the small-M_∞ expansion for H_{12g} is a dipole, proportional to $M_\infty^{1/2}$. Similar power calculations were performed for k_{np}/k_t values of 0, 0.5, and 1.0. The plots are shown in Figs. (5.15), (5.16), and (5.17).

The data contained in Figs. (5.14)-(5.17) cover a wide range of parameters of practical interest. Because the magnitude of the individual solutions was taken in computing powers, the results apply for negative values of k_{np}/k_t as well. The calculation for H_{1c} is completely general, since this solution depends only on the quantities A_n and k_t, and in the same way as the unloaded solution H_0. Hence, the power curve for H_{1c} is identical on all of Figs. (5.14)-(5.17). Since the small parameter $\alpha\sqrt{k}$ could be factored out, the graphs apply for all values of loading. One need only scale them by the small parameter to determine the effects of Mach number on the field for a loaded airfoil. The trends in Figs. (5.14)-(5.17) with increasing k_{np}/k_t are consistent with what was observed in Section 5.1. For very small k_{np}/k_t (gust velocities almost normal to the airfoil surface), and Mach numbers below about 0.6, the total power is approximately what one would get for an unloaded airfoil. However, loading effects become important with very small changes in k_{np}/k_t. When k_{np}/k_t is equal to 0.5, the ratio of the power for H_{12g} to that for H_0 is equal to 5 at a Mach number of zero. For $M_\infty = 0.6$ the ratio of the powers is 10.

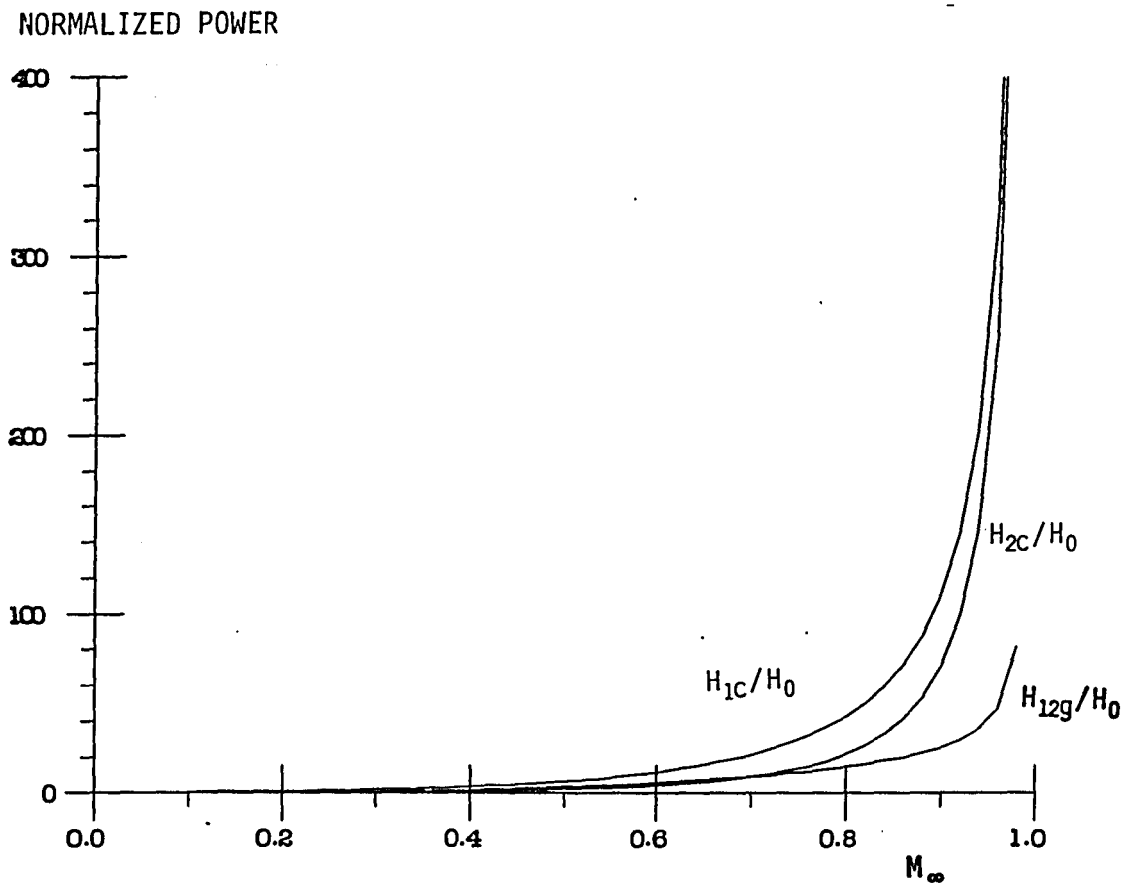

Fig. 5.15 Power vs. Mach number for "compressiblity" and "combined gust" solutions. $k_{np}/k_t = 0$.

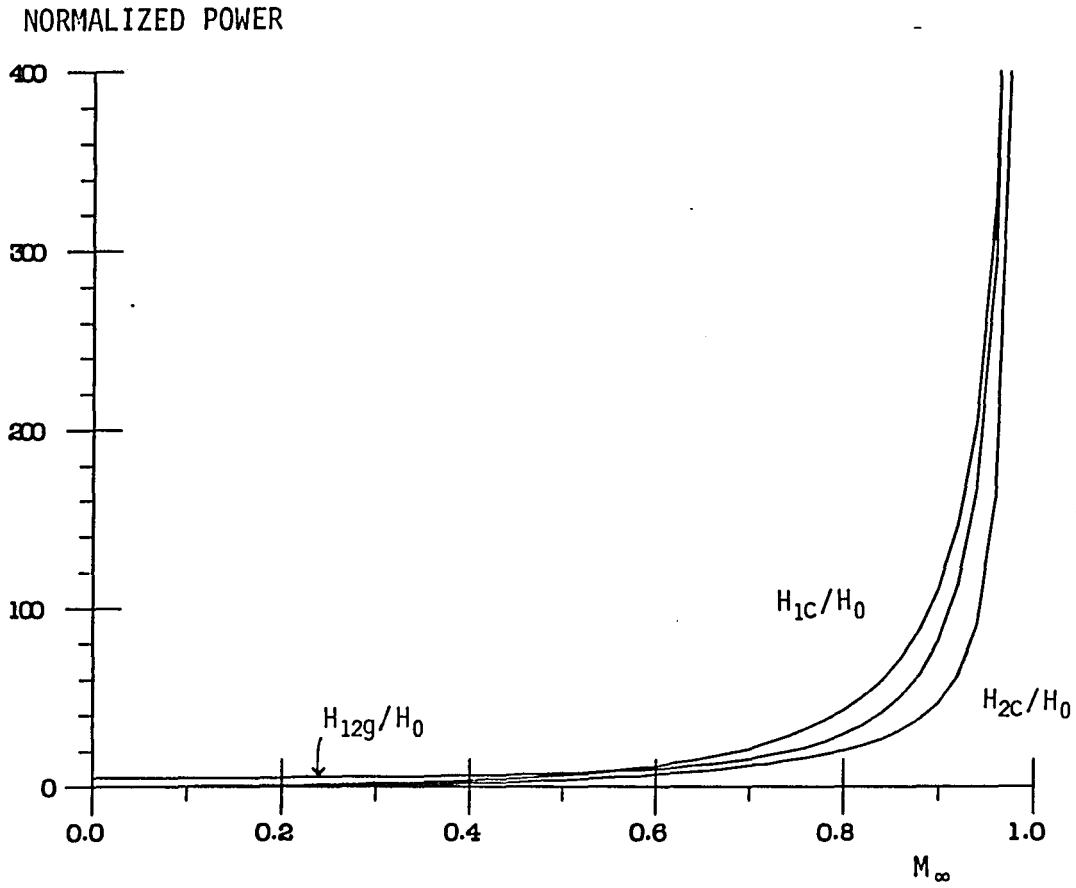

Fig. 5.16 Power vs. Mach number for "compressibility" and "combined gust" solutions. $k_{np}/k_t = .5$.

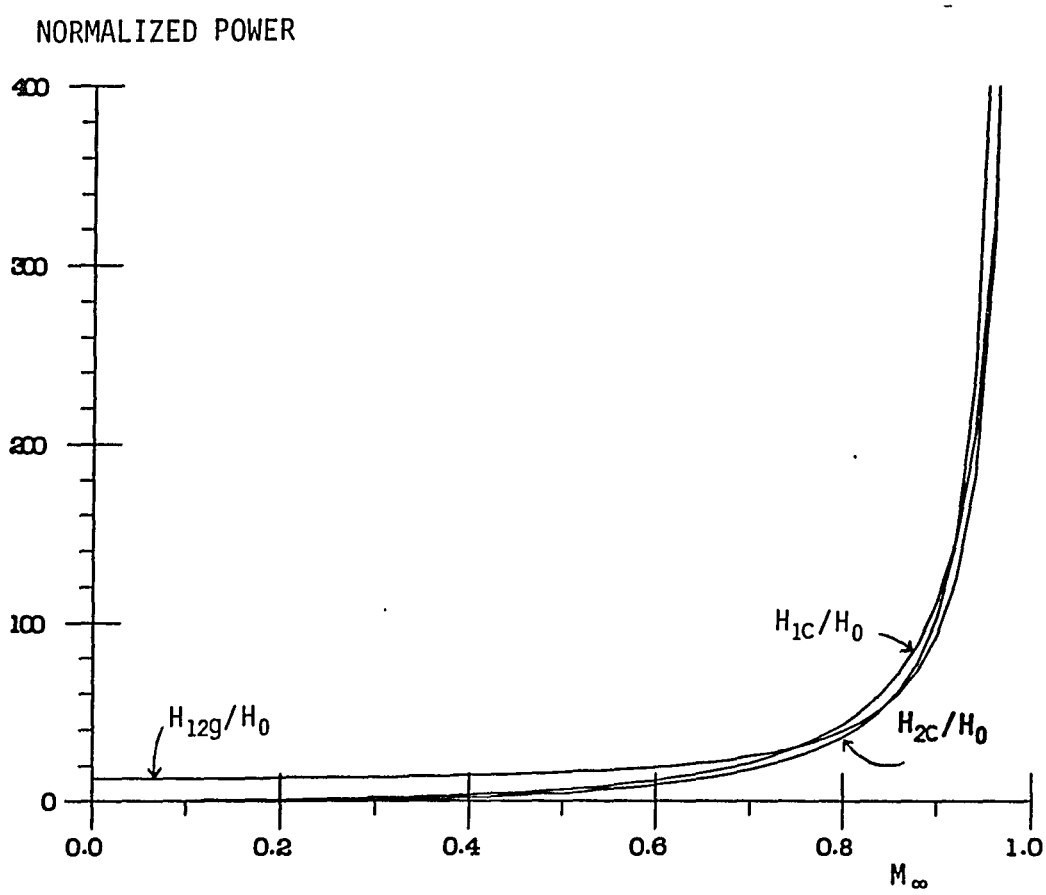

Fig. 5.17 Power vs. Mach number for "compressibility" and "combined gust" solutions. $k_{np}/k_t = 1$.

Interestingly, the power curve for the gust solution is almost independent of Mach number until M_∞ reaches about 0.5.

From Figs. (5.14)-(5.17), the following general comments can be made about the behavior of the sound field with Mach-number variation. Compressibility effects are negligible until the Mach number reaches about 0.5. Compressibility effects become very important as the Mach number increases beyond 0.5, though the small-perturbation mean flow assumption is invalid very close to $M_\infty = 1$. For k_{np}/k_t less than one, sound generation due to local scattering of acoustic waves, described by H_{1C}, is the dominant compressibility effect. For k_{np}/k_t greater than one, the interaction of mean density gradients with the convected disturbance, contained in H_{2C}, is the strongest compressibility sound source. Gust distortion effects are important at all Mach numbers, except for very small values of k_{np}/k_t. For Mach numbers less than 0.5, the importance of gust-distortion effects relative to the zero-loading solution hardly changes with Mach number. At an M_∞ of about 0.5 or 0.6, gust-distortion effects begin to produce large increases in power over the unloaded case.

The effects of Mach number variation just described can also be qualitatively seen in pressure directivity patterns. In Figs. (5.18)-(5.21), leading-edge pressure directivity patterns are displayed for $k \cdot k_t = 6$ and $\alpha = 3°$. Total patterns are shown, i.e., $P_0+\alpha\sqrt{k}\ (P_1+P_2)$. In Figs. (5.18a,b,c) and (5.19a,b), k_{np}/k_t is 1.73 and the Mach number assumes the values 0.0, 0.2, 0.4, 0.6, and 0.8. The same Mach numbers apply in Figs. (5.20a,b,c) and (5.21a,b), but there k_{np}/k_t is equal to -.577. We first examine the case where k_{np}/k_t is 1.73.

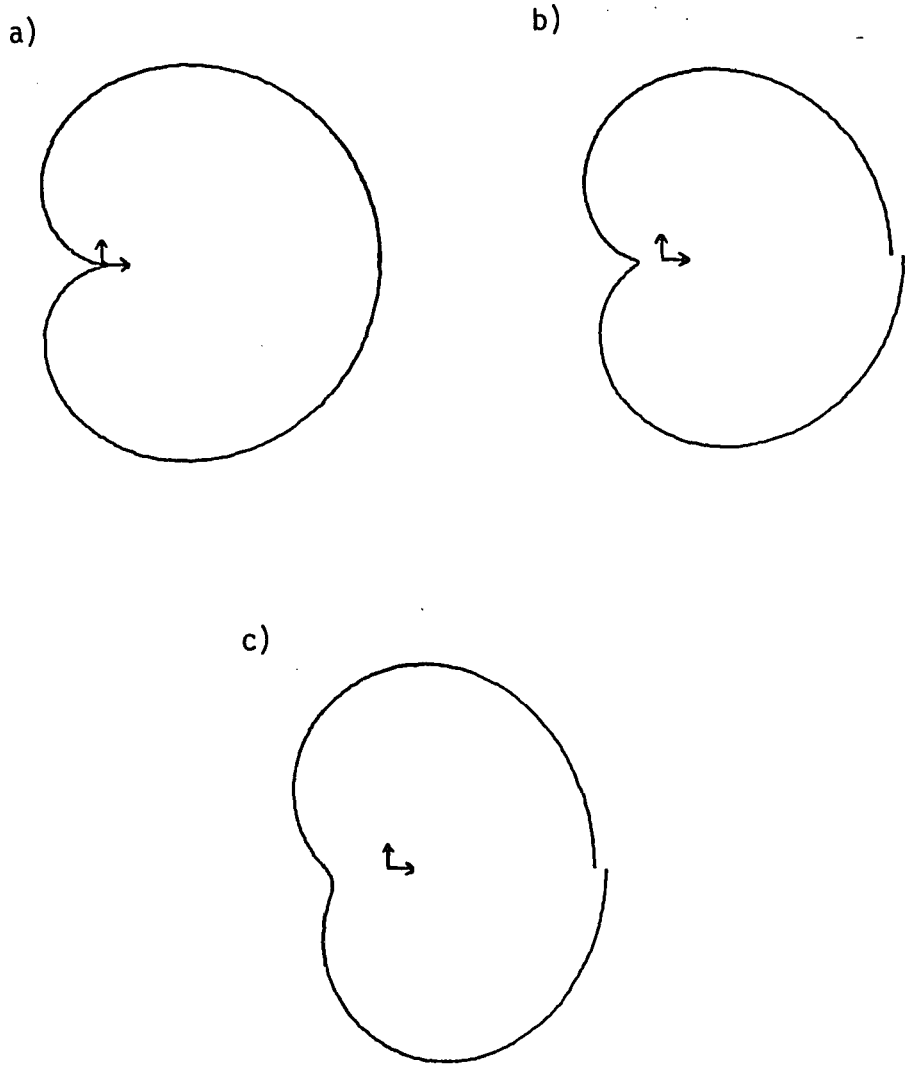

Fig. 5.18 (a,b,c) Leading-edge pressure directivity patterns. $\alpha_i = 3°$, $kk_t = 6$, $k_{np}/k_t = 1.73$. (a) $M_\infty = 0$. (b) $M_\infty = .2$. (c) $M_\infty = .4$.

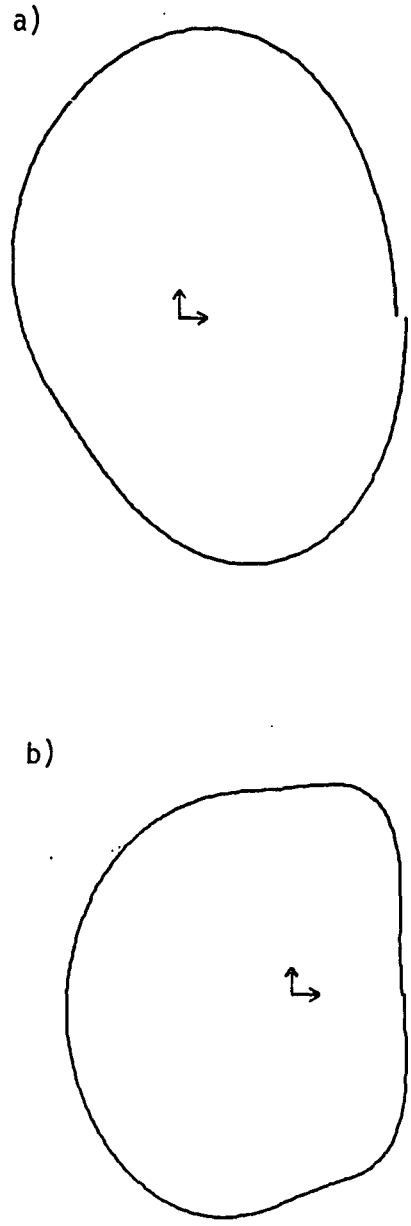

Fig. 5.19 (a,b) Leading-edge pressure directivity patterns. $\alpha_i = 3°$, $kk_t = 6$, $k_{np}/k_t = 1.73$. (a) $M_\infty = .6$. (b) $M_\infty = .8$.

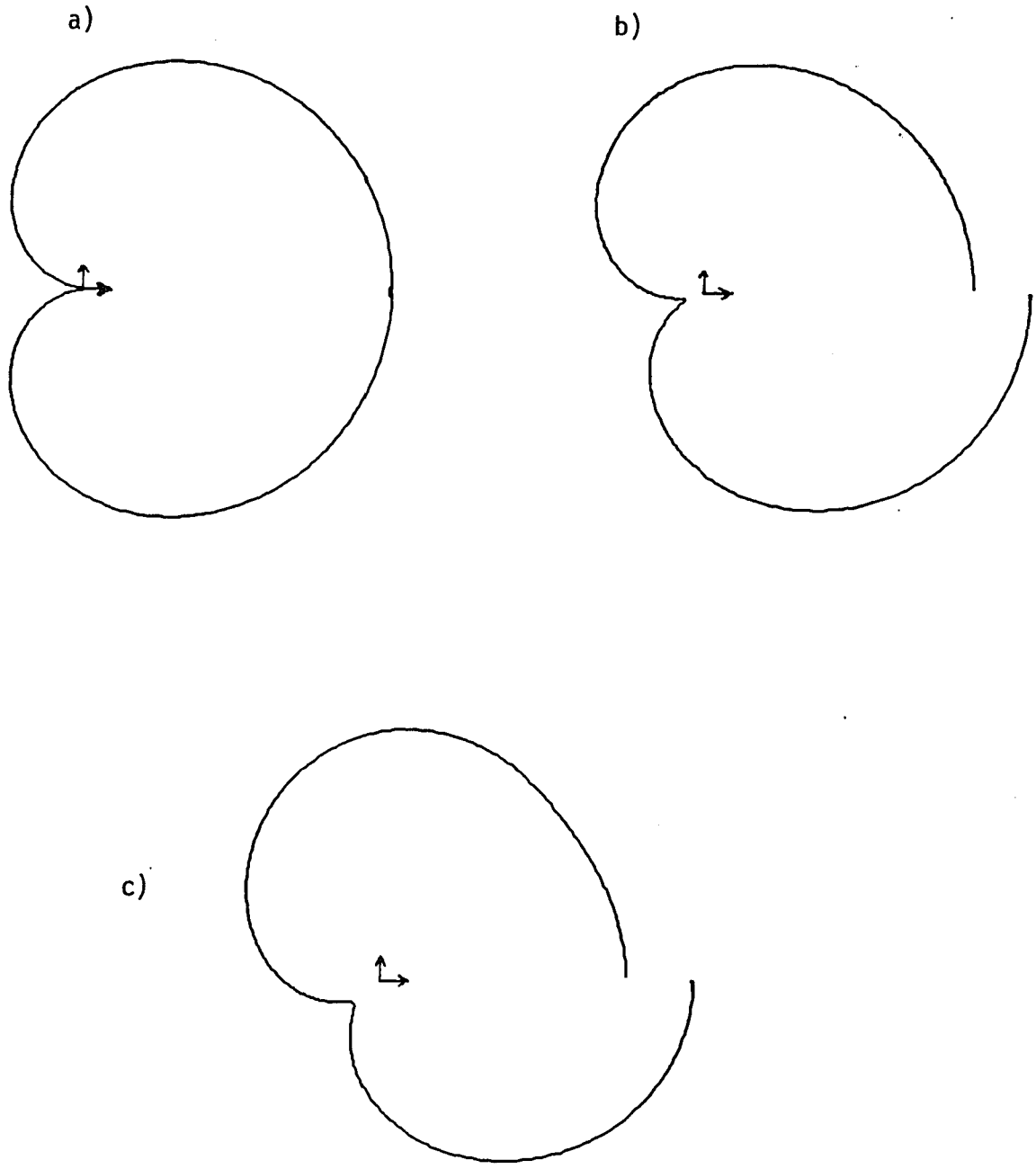

Fig. 5.20 (a,b,c) Leading-edge pressure directivity patterns. $\alpha_i = 3°$, $kk_t = 6$, $k_{np}/k_t = -.577$. (a) $M_\infty = 0.$ (b) $M_\infty = .2.$ (c) $M_\infty = .4.$

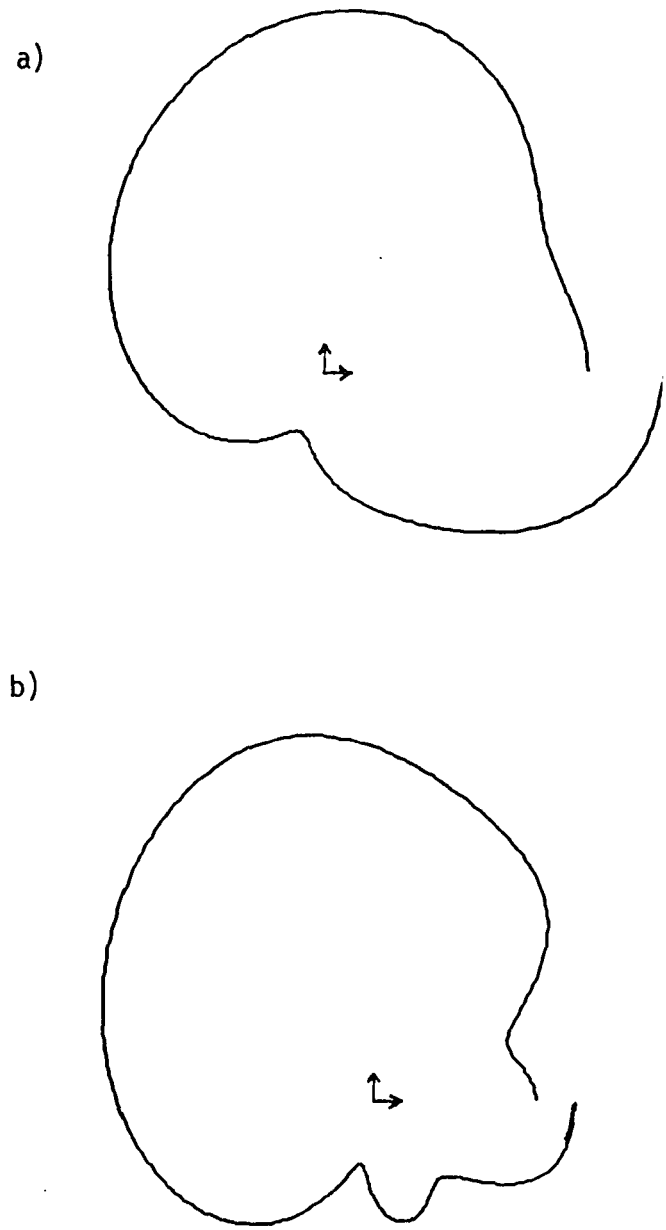

Fig. 5.21 (a,b) Leading-edge pressure directivity patterns. $\alpha_i = 3°$, $kk_t = 6$, $k_{np}/k_t = -.577$. (a) $M_\infty = .6$. (b) $M_\infty = .8$.

The pattern in Fig. (5.18) is a cardioid, having the $\cos \frac{\theta}{2}$ functional form in Prandtl-Glauert space. This pattern is due to the "three-halves pole" fields arising from the no-loading solution H_0 and the part of H_{12g} representing the scattering of the volume source by the airfoil. The solution H_{12g} also contains a dipole component; it is $O(\sqrt{M_\infty})$ weaker than the "three-halves" pole and distorts slightly the cardioid of Fig. (5.18a) at low Mach numbers, as we see in Figs. (5.18b,c). Notice the small amount of upstream radiation and slight jump across the wake in pressure magnitude. At higher relative Mach numbers, compressibility effects enter and distort the directivity patterns considerably more. In Figs. (5.19a,b) for Mach numbers .6 and .8, the profile is stretched in the y-direction, and there is a significant amount of upstream radiation relative to the $M_\infty = 0$ case.

The trend is similar but more extreme in Figs. (5.20) and (5.21) for $k_{np}/k_t = -.577$. The jump in pressure magnitude across the wake at the low Mach numbers .2 and .4 is greater for $k_{np}/k_t = -.577$ than it was for $k_{np}/k_t = 1.73$. The pattern is also beginning to show asymmetry at $M_\infty = .4$. The plot for $M_\infty = .6$ (Fig. (5.21a)) shows much more radiation above the airfoil than below it, considerable upstream radiation, and a significant jump in pressure magnitude across the wake. Almost all of the characteristics of the $M_\infty = 0$ plot of Fig. (5.20a) are gone. At $M_\infty = .8$, compressibility effects dominate and the pattern is completely different from the incompressible result. The radiation is almost entirely above the airfoil, and lobes have begun to appear below the airfoil.

The division of our solution into H_{1c}, H_{2c}, and H_{12g} made our originally singular solutions for H_1 and H_2 understandable. Part of the motivation for our original decomposition was to separate volume source effects, for comparison with the acoustic analogy. We now briefly describe an acoustic-analogy approach to our problem.

5.2.1 Comparison with the Acoustic Analogy

Here we present the general theory of Ffowcs Williams and Hawkings (1969a), and apply it to our specific problem. We assume no entropy fluctuations are present.

The acoustic-analogy approach is based on Lighthill's equation, which for an inviscid gas (assuming also that the acoustic pressure is equal to the density times the speed-of-sound squared) is

$$\frac{\partial^2 \rho'}{\partial t^2} - a_\infty^2 \nabla^2 \rho' = \frac{\partial^2}{\partial x_i \partial x_j} (\rho u_i u_j) \quad . \tag{5.9}$$

Here ρ is the total density, u_i the total velocity, and $\rho' = \rho - \rho_0$ is the acoustic density. Also, for this analysis Cartesian rather than potential-streamline coordinates will be used. We decompose the velocity field into a uniform flow in the x-direction plus a small correction term:

$$u_i = U_\infty \delta_{1i} + \hat{u}_i \quad . \tag{5.10}$$

Inserting Eq. (5.10) into (5.9) we obtain the convective form of Lighthill's equation,

$$\left[\frac{\partial}{\partial t} + U_\infty \frac{\partial}{\partial x}\right]^2 \rho' - a_\infty^2 \nabla^2 \rho' = \frac{\partial^2}{\partial x_i \partial x_j} (\rho \hat{u}_i \hat{u}_j) \quad . \qquad (5.11)$$

We now further decompose the velocity field by writing $\hat{u}_i$ as the sum of a steady-potential-flow perturbation velocity plus a vortical disturbance:

$$\hat{u}_i = u_i^p(\overline{x}) + u_i^s(\overline{x},t) \quad . \qquad (5.12)$$

If mean-flow effects on the vortical disturbance are not accounted for (as is likely in an acoustic-analogy approach), the vortical disturbance is simply convected at the mean-flow speed U_∞. The disturbance remains solenoidal and is hence given the superscript "s". The mean-flow perturbation velocity u_i^p is $O(\alpha)$ (except in the local-leading-edge region, where it is $O(\alpha\sqrt{k})$) relative to U_∞, and the vortical disturbance is assumed to be $O(\varepsilon)$ with $\varepsilon << \alpha$. Inserting Eq. (5.12) into the source term of (5.11), we find that several combinations arise. The square of u_i^p results in a steady source term which produces no sound (only a higher correction to the mean flow) and is not of interest to us. The nonlinear unsteady source term is $O(\varepsilon^2)$ and can be neglected. The important term is the $O(\alpha\varepsilon)$ interaction of the nonuniform mean flow with the vortical disturbance. With this source term Lighthill's equation is,

$$\frac{1}{a_\infty^2}\left[\frac{\partial}{\partial t} + U_\infty \frac{\partial}{\partial x}\right]^2 p' - \nabla^2 p' = 2\rho \frac{\partial^2}{\partial x_i \partial x_j} (u_i^p u_j^s) \quad , \qquad (5.13)$$

where we have switched dependent variable to the acoustic pressure p' ($= a_\infty^2 \rho'$) for convenience. Since terms of higher order than $\alpha\varepsilon$ are negelected, the total density ρ appearing in the source can be replaced by its value far from the airfoil, ρ_∞. Also, it is advantageous to perform the differentiation in the source and make use of the solenoidality of u_i^S. We then have

$$\frac{1}{a_\infty^2}\left[\frac{\partial}{\partial t} + U_\infty \frac{\partial}{\partial x}\right] p' - \nabla^2 p' = 2\,\rho_\infty \left[\frac{\partial u_j^S}{\partial x_i}\frac{\partial u_i^P}{\partial x_j} + u_j^S \frac{\partial^2 u_i^P}{\partial x_i \partial x_j}\right] . \quad (5.14)$$

One can determine the influence of nonuniform mean flow on the acoustic field via the acoustic analogy by solving Eq. (5.14) along with the no-flow boundary condition on the body and the radiation condition at infinity. Ffowcs Williams and Hall (1970) utilized this approach to study the sound generation by turbulent flow in the vicinity of a scattering half plane. Mani (1974) and Goldstein (1974) also used the approach to calculate fan noise due to inlet turbulence. In these two investigations the potential flow through the rotor cascade was modeled as that due to an infinite row of point vortices. Vorticity distortion and non-uniform propagation effects are not generally included in theories based on the acoustic analogy.

In order to compare the acoustic-analogy approach with rapid-distortion theory, we must convert Goldstein's equation (2.4e) to an equation for the acoustic pressure. This is accomplished by operating on both sides with $-\rho_0 D_0/Dt$. Such an operation yields many terms representing nonuniform propagation effects on the left side of

the equation. Ignoring these terms and retaining only the uniform-medium wave operator (but keeping the complete source term), we have

$$\frac{1}{a_\infty^2}\left[\frac{\partial}{\partial t} + U_\infty \frac{\partial}{\partial x}\right] p' - \nabla^2 p' = -\rho_0 \frac{D_0}{Dt}\left[\frac{1}{\rho_0}\frac{\partial}{\partial x_i}(\rho_0 v_i')\right] \quad . \tag{5.15}$$

Here v_i' is the convected disturbance of Eq. (2.8). It is convenient to expand the derivative of the product in the source term and rewrite the source as

$$-\rho_0 \frac{D_0}{Dt}\left[\frac{\partial v_i'}{\partial x_i} + \frac{v_i'}{\rho_0}\frac{\partial \rho_0}{\partial x_i}\right] \quad . \tag{5.16}$$

The first term in Eq. (5.16), which we'll temporarily label source_1, can be written as

$$-\rho_0 \frac{\partial}{\partial x_i}\frac{D_0 v_i'}{Dt} + \rho_0 \frac{\partial u_j^p}{\partial x_i}\frac{\partial v_i'}{\partial x_j} \quad , \tag{5.17}$$

where we have utilized the mean-flow decomposition $U_{0i} = U_\infty \delta_{1i} + u_i^p$. The convected disturbance satisfies the linearized momentum equation (see Eq. (2.4d))

$$\frac{D_0 v_i'}{Dt} + v_j' \frac{\partial}{\partial x_j} u_i^p = 0 \quad .$$

Utilizing this result in Eq. (5.17), we obtain

$$\text{source}_1 = \rho_0 \frac{\partial}{\partial x_i}\left[v_j' \frac{\partial}{\partial x_j} u_i^p\right] + \rho_0 \frac{\partial u_j^p}{\partial x_i}\frac{\partial v_i'}{\partial x_j} \quad . \tag{5.18}$$

The second term in Eq. (5.18), which we call source_2, can to $O(\alpha\varepsilon)$ accuracy be written as

$$\text{source}_2 = -v_i' \frac{\partial}{\partial x_i} \frac{D_\infty \rho_0}{Dt} \quad . \tag{5.19}$$

By the mean-flow continuity equation,

$$\frac{D_\infty \rho_0}{Dt} = - \rho_\infty \frac{\partial u_j^p}{\partial x_j} \quad .$$

Hence the second term in the source becomes

$$\text{source}_2 = \rho_0 \, v_i' \frac{\partial}{\partial x_i} \frac{\partial u_j^p}{\partial x_j} \quad . \tag{5.20}$$

Adding the results of Eqs. (5.18) and (5.20) and utilizing $\rho_0 = \rho_\infty + O(\alpha)$ to replace the mean density with the uniform flow value, we obtain the following equation for the acoustic pressure

$$\frac{1}{a_\infty^2} \left[\frac{\partial}{\partial t} + U_\infty \frac{\partial}{\partial x} \right]^2 p' - \nabla^2 p' = 2 \rho_\infty \left[\frac{\partial v_j'}{\partial x_i} \frac{\partial u_i^p}{\partial x_j} + v_j' \frac{\partial^2 u_i^p}{\partial x_i \partial x_j} \right] \quad . \tag{5.21}$$

The difference between Eq. (5.21) of rapid-distortion theory and Eq. (5.14) obtained from the acoustic analogy lies in the representation of the vortical disturbance. In general the two representations are unequal since rapid-distortion theory accounts for the distortion of the gust by the nonuniform mean flow. However, in the local-leading-edge region, where the sound generation is concentrated, a close

correspondence can be made. We now examine the local-leading-edge expansion of the expression for the convected disturbance.

The local-leading-edge expansion of the drift function, given in Eq. (3.5b), is

$$g \sim \frac{-4\sqrt{2}\,\alpha}{\beta_\infty \sqrt{k}} R^{1/2} \cos\theta/2 \quad .$$

Hence the drift function in the local-leading-edge region is zero to the desired order of accuracy. Also, locally the gust amplitude can be approximated by its value at upstream infinity:

$$|\overline{v}'| = |\overline{v}'_\infty| + O(\alpha\sqrt{k}) \quad .$$

Hence in the local-leading-edge region Eq. (2.8) for the convected disturbance becomes

$$\overline{v}' = (A_t, A_\eta, A_z)\, e^{i(k_t(\Phi - kU_\infty^2 t) + k_\eta \Psi + kk_3 x_3)} + O(\alpha\sqrt{k}) \quad , \qquad (5.22)$$

where (Φ,Ψ) are the local coordinates introduced before Eq. (3.5) and all variables are nondimensional. (Recall that in Chapter 2, dimensional variables were used.) In the local-leading-edge region,

$$\Phi = X_1 + O(\alpha^2 k) \quad , \qquad (5.23)$$

and

$$\Psi = \beta_\infty X_2 + O(\alpha^2 k) \quad , \qquad (5.24)$$

where $X_1 = kx_1$ and $X_2 = kx_2$ and (x_1,x_2) are the standard Cartesian coordinates. Since the physical wavenumber is $\beta_\infty k_\eta$, the local-

leading-edge expansion for the phase in (5.22) is

$$k[k_t\ (x_1 - U_\infty t) + k_{np}\ x_2 + k_3 x_3] \quad . \tag{5.25}$$

This is the phase for a solenoidal gust. From Eqs. (5.22) and (5.25) we can conclude that locally, $\overline{v'} = u_j^s$ to the accuracy we are considering. Hence, Eq. (5.21) is equivalent to (5.14).

What we have shown is that distortion of the vortical velocity by the mean flow is unimportant in the source term. In other words, in the equation for pressure and in the local-leading-edge region, convected and solenoidal gusts are interchangeable. Therefore the quadrupole source term for the acoustic analogy and rapid-distortion theory is identical. The suprising implication of this result is that the acoustic-analogy approach leads to the prediction of a monopole farfield behavior at low Mach number, if one approximates T_{ij} by $\rho_\infty u_i^p u_j^s$ and uses the homogeneous boundary condition $\partial p/\partial n = 0$. This conclusion follows since solving the pressure equation (5.21) is equivalent to first solving the potential equation and then differentiating to obtain pressure. The potential equation with the homogeneous boundary condition possessed a monopole farfield solution, hence, so must the pressure equation.

We will now obtain the local-leading-edge solution to the pressure equation (5.14) with the homogeneous boundary condition, to verify the prediction of the monopole for small Mach numbers. In the limit $M_\infty \to 0$, the potential field is solenoidal and the first term of the source in (5.14) (or (5.21)) vanishes. The second term can be

expanded using the following expressions for the potential and vortical velocities.

$$u_1^P - iu_2^P = \sqrt{2}\ \alpha\ \sqrt{k}\ R^{-1/2}\left[\cos\frac{\theta}{2} - i\sin\frac{\theta}{2}\right] \quad , \tag{5.26a}$$

$$(u_1^S,\ u_2^S) = (A_x,\ A_y)\ e^{i(k_x X + k_y Y)} \quad . \tag{5.26b}$$

All coordinates are Cartesian coordinates centered on the airfoil leading edge. Utilizing Eqs. (5.26a,b) in the second term of the source in (5.14), we obtain

$$\text{Source} = -\frac{\sqrt{2}\ \alpha\ \sqrt{k}}{R^{3/2}}\ e^{i(k_x X + k_y Y)}\left[D_1 \cos\frac{3\theta}{2} + D_2 \sin\frac{3\theta}{2}\right] \quad , \tag{5.27}$$

where

$$D_1 = A_x\ k_x - A_y\ k_y \qquad\qquad D_2 = A_y\ k_x + A_x\ k_y$$

A source term of the same mathematical form was encountered in the equation for H_2. (See (3.14a).) Hence, the solution to the following equations:

$$\frac{\partial^2 P}{\partial X^2} + \frac{\partial^2 P}{\partial Y^2} + w^2 P = \text{source} \quad ,$$

$$\frac{\partial P}{\partial Y}\bigg|_{Y=0} = 0 \quad ,$$

with $w = M_\infty k_x$ and the source term as in (5.27), can be obtained by analogy with (3.15). The symmetric part of the solution is

$$P_{source,sym} = \frac{e^{i\pi/4}}{8\sqrt{\pi}(k_x^2+k_y^2)} \int_{-\infty}^{\infty} \left[\frac{\cos k_y Y f_1(\lambda)}{\sqrt{\lambda+k_x'}} - \frac{i|\sin k_y Y| f_2(\lambda)}{\sqrt{\lambda+k_x}} \right] \frac{e^{hy(\lambda,X,Y)} d\lambda}{(\lambda-\lambda_1)(\lambda-\lambda_2)}$$

$$- \frac{e^{i\pi/4}}{8\sqrt{\pi}(k_x^2+k_y^2)} \int_{-\infty}^{\infty} \frac{((\lambda+k_x)f_1(\lambda)+ik_y f_2(\lambda))\ e^{a(\lambda,X,Y)}\ d\lambda}{\sqrt{\lambda+k_x}\ \sqrt{\lambda^2-w^2}\ (\lambda-\lambda_1)\ (\lambda-\lambda_2)} \quad , \tag{5.28a}$$

where

$$hy(\lambda,X,Y) = -i\lambda X - |Y|\sqrt{(\lambda+k_x)(\lambda+k_x')} \quad , \tag{5.28b}$$

$$a(\lambda,X,Y) = -i\lambda X - |Y|\sqrt{(\lambda+w)(\lambda-w)} \quad , \tag{5.28c}$$

$$f_1(\gamma) = -2D_2(\gamma+k_x)(-k_x^2+k_y^2-2k_x\gamma) - 4D_1k_y(\gamma+k_x)^2 \quad , \tag{5.28d}$$

$$f_2(\gamma) = -4ik_yD_2(\gamma+k_x)^2 + 2iD_1(\gamma+k_x)(-k_x^2+k_y^2-2k_x\gamma) \quad , \tag{5.28e}$$

and

$$\lambda_{1,2} = -\frac{k_x}{2} \pm \frac{ik_y}{2} \quad . \tag{5.28f}$$

The wavenumber k_x has a small positive imaginary part, and k_x' has a small negative imaginary part. The solution in the acoustic farfield, where $wR >> 1$, can be obtained by expanding the integral with the acoustic phase by the method of steepest descents. The result, in the limit $M_\infty \to 0$, is

$$P_{source,sym} = \frac{-i[k_x f_1(0) + ik_y f_2(0)]\, e^{iwR}}{4\,\lambda_1\,\lambda_2\,\sqrt{2M_\infty k_x}\,\sqrt{k_x R}} \qquad (5.29)$$

In the simple case of a gust with only vertical velocity fluctuations, i.e. $A_x = k_y = 0$, Eq. (5.29) reduces to

$$P_{source,sym} \sim \frac{-i\sqrt{2}\,A_y\,k_x}{\sqrt{M_\infty\,k_x\,R}} \quad , \qquad (5.30)$$

the pressure for a two-dimensional monopole.

In the limit as $M_\infty \to 0$, the sound-generating region becomes a compact source. The source is compact because the sound is produced in the local-leading-edge region, which scales on the gust wavelength. At low Mach numbers the convected wavelength is short compared to the acoustic wavelength. Equation (5.30) is the expression for the pressure many acoustic wavelengths from the airfoil leading edge. An interesting intermediate limit of the solution is the acoustic field at a distance large compared to the convected wavelength but short compared to the acoustic wavelength. The behavior in this region should resemble that due to an incompressible "monopole", i.e., a simple mass source. The logarithmic nature of the field appropriate for a two-dimensional mass source can be extracted by expanding the exact solution in (5.28a) in the following way.

In the limit as R tends to infinite and w tends to zero, with Rw still small, the acoustic solution is proportional to the following integral:

$$I = \int_{-\infty}^{\infty} \frac{(\lambda+k_x)f_1(\lambda) + i\, k_y\, f_2(\lambda)}{\sqrt{\lambda+k_x}\,\sqrt{(\lambda-i\varepsilon)(\lambda+i\varepsilon)}\,(\lambda-\lambda_1)(\lambda-\lambda_2)}$$

$$\times\, e^{-i\lambda R\cos\theta\, -R|\sin\theta|\sqrt{(\lambda-i\varepsilon)(\lambda+i\varepsilon)}}\, d\lambda\,. \qquad (5.31)$$

Differentiating (5.31) with respect to R, we have

$$\frac{dI}{dR} = \int_{-\infty}^{\infty} N(\lambda,\theta)\, e^{-i\lambda|\cos\theta - R|\sin\theta|\sqrt{(\lambda-i\varepsilon)(\lambda+i\varepsilon)}}\, d\lambda \qquad (5.32a)$$

where

$$N(\lambda,\theta) = \frac{((\lambda+k_x)f_1(\lambda) + ik_yf_2(\lambda))\,(-i\lambda\cos\theta - |\sin\theta|\sqrt{(\lambda-i\varepsilon)(\lambda+i\varepsilon)})}{\sqrt{\lambda+k_x}\,\sqrt{(\lambda-i\varepsilon)(\lambda+i\varepsilon)}\,(\lambda-\lambda_1)(\lambda-\lambda_2)}\,. \qquad (5.32b)$$

The integral in (5.32) is the second type of integral considered in Appendix B, the type with no saddle point in the exponent of the integrand. The branch cuts for two of the square roots are shown in Fig. (B.3). An additional branch cut emanating from $\lambda = -k_x$ is also required, similar to the one from $\lambda = -\delta$ shown in Fig. (B.2). (Fig. (B.2) applies to integrals with the saddle-point phase.) The expansion of (5.32) as $R \to \infty$ can be obtained according to the procedure in Appendix B integrals, except that one must account for the intersection of the branch cut from $\lambda = -k_x$ with the steepest-descent path. As shown in Appendix B for the saddle-point expansion, the error incurred by

detouring around the branch cut is exponentially small. The rest of the procedure is as outlined for integrals with the hydrodynamic phase. We find that

$$\frac{dI}{dR} \sim \frac{1\ k_x\ f_1(0) - k_y\ f_2(0)}{\sqrt{K_x}\ \lambda_1\ \lambda_2}\ \frac{1}{R} \tag{5.33}$$

The function $N(\lambda,\theta)$ approaches a constant in λ as $\lambda \to 0$; hence the asymptotic expansion is proportional to $1/R$ rather than $R^{-1/2}$ like the example of Appendix B (where the kernal function goes as $\lambda^{-1/2}$ near $\lambda = 0$.) By integrating (5.33) with respect to R, we see that the integral I, and hence the solution $P_{source,sym}$, contains the logR term characteristic of an incompressible monopole.

The monopole arising in the acoustic-analogy approach, like the one in rapid-distortion theory, can be removed by accounting for vorticity distortion on the boundary. The correct boundary condition is not $\partial p/\partial n = 0$ on the airfoil surface. By taking the substantial derivative of the boundary condition (2.4i) of rapid-distortion theory, we obtain

$$-\rho_0 \frac{D_0}{Dt}(\nabla G \cdot \bar{n}) = \rho_0 \frac{D_0 \bar{v}'}{Dt} \cdot \bar{n} \tag{5.34}$$

Utilizing the linearized momentum equation (2.4d) for the vortical velocity, and ignoring $O(\alpha^2 k)$ terms, we obtain the correct boundary condition for the pressure:

$$n_i \frac{\partial P}{\partial x_i} = \rho_\infty n_i v_j' \frac{\partial u_j^p}{\partial x_j} \tag{5.35}$$

We have gone to considerable effort to show that the acoustic analogy method with a very "reasonable" boundary condition, $\partial P/\partial n = 0$, incorrectly predicts the farfield sound at low Mach numbers. We have gone to such effort because of the popularity of the acoustic analogy. We emphasize that care must be taken in utilizing the acoustic analogy, that is, one must use the boundary condition (5.35) in order to avoid the monopole singularity. We also remark that even the "modified" acoustic analogy approach would not account for sound generation due to local scattering of acoustic waves, contained in the term H_{1c} of the rapid-distortion theory solution. The solution H_{1c} was found to be important at higher Mach numbers and smaller values of k_{np}/k_t.

5.3 Mean Loading Effects

We return to our parametric study of Eqs. (4.43). Unlike in Section 5.2, both the leading-edge and trailing-edge solutions are included. Also, airfoils with various camber distributions will be considered.

The effects of mean loading on the sound field are contained in the three parameters α_{eff}, α_g, and α_i. The first controlling parameter $\alpha_{eff} = \alpha_i - \alpha_{1c}$ is an "effective incidence angle", or, more precisely, the stength of the flow around the leading edge. For the configuration shown in Fig. (4.1), we define clockwise flow around the leading edge to be positive and counter-clockwise flow to be negative. It was found in

our local-trailing-edge analysis that the second small parameter $\alpha_g = \alpha_i + \alpha_{2c}$ is $\frac{\beta\infty}{U_\infty b}$ times the circulation, or $1/2\pi$ times the lift coefficient for the airfoil. In α_g the effects of incidence angle and camber are generally additive, since usually incidence angle and camber both contribute to the lift. In α_{eff}, however, incidence angle and camber often tend to offset one another. The camber contribution to α_{eff}, $-\alpha_{1c}$, is negative whenever the maximum displacement of the airfoil is reached in front of the mid-chord and positive when the maximum is reached behind the midchord. (See Eq. (4.4c).) For a symmetric airfoil such as a circular arc α_{1c} is zero, indicating that at zero-incidence angle the mean flow is tangent to the airfoil at the leading edge. Thus, a cambered airfoil having a maximum displacement in front of the mid-chord and a nonzero angle of attack has flow induced counterclockwise around the leading edge due to camber and clockwise due to incidence angle. In addition to the parameters α_g and α_{eff}, the incidence angle α_i appears by itself in the phase of the trailing-edge solution.

An interesting question to ask is which parameter, if any, dominates in determining the properties of the acoustic farfield. To address this question we first investigate how the total radiated power changes as a function of the mean lift on the airfoil. The airfoil total loading was varied in several ways. First, we simply increased the incidence angle for a flat plate. Second, we increased the camber on an airfoil at zero incidence. This was accomplished by multiplying

the camber line of a NACA 63 (6% maximum displacement at 30% chord) airfoil by various scaling factors. As a third example a circular-arc airfoil (5% maximum displacement) was considered at various incidence angles, both positive and negative. The last experiment was identical to the third one except this time the airfoil was the NACA 63. The four airfoils interacted with a convected disturbance having values of 7 for $k.k_t$, 0 for k_3, and 1 for k_{np}/k_t. The Mach number was 0.6.

The results are plotted versus airfoil lift coefficient in Fig. (5.22). One interesting feature of the figure is the large increase in power with increasing lift for the flat plate. The power increases by a factor of 4 over about a six degree increase in incidence angle. The opposite is true for the NACA 63 airfoil. The power decreases by a factor of 2 over the same change in lift. The power for the circular arc drops a slight amount before beginning to increase at a lift coefficient of about 0.075. The power for the variable camber airfoil monotonically decreases at a slow rate. From the plots in Fig. (5.22) it can be concluded that mean loading should not be ignored in turbomachinery noise-prediction models. It can also be concluded that mean loading alone does not accurately correlate the amount of power generated in the interaction of gusts with loaded airfoils.

Since the primary noise generation occurs in the leading-edge region, one might expect a better correlation on the strength of the flow around the leading edge, α_{eff}. To test this hypothesis, we replotted the above data against α_{eff}. As Fig. (5.23) shows, the graphs

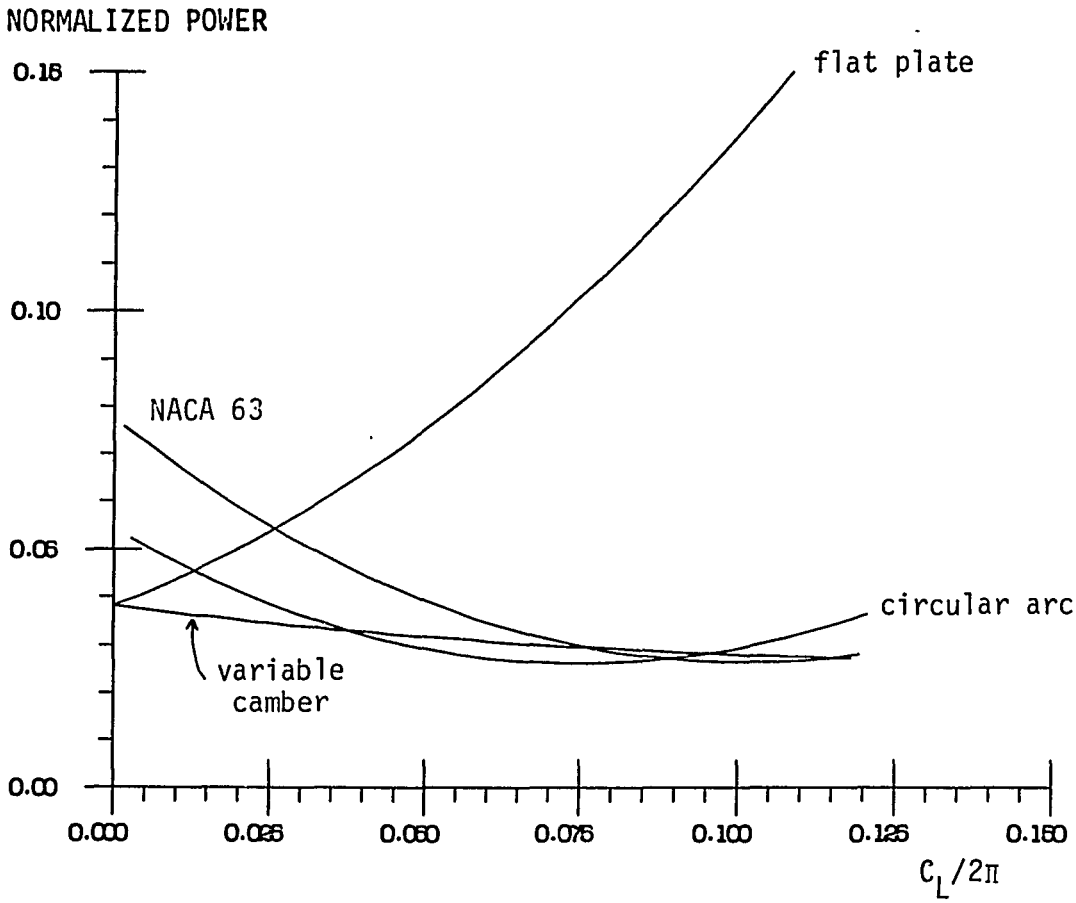

Fig. 5.22 Power vs. total mean loading. $M_\infty = .6$, $kk_t = 7$, $k_{np}/k_t = 1$.

for the four cases are nearly indistinguishable. For the conditions in which these calculations were made, α_{eff} is clearly the dominant parameter.

To examine the universality of α_{eff} as a correlating parameter, we repeated the above test at Mach numbers of 0.45 and 0.75. The results are plotted in Figs. (5.24)-(5.27). We will return in the next paragraph to the analysis of the curves; for now we observe the excellent correlation with α_{eff} in Figs. (5.25) and (5.27). The correlation holds across gust orientations as well. In Figs. (5.28) and (5.29) power calculations are shown for $k_{np/kt} = 0$. For Figs. (5.30) and (5.31), $k_{np/kt}$ is -1. In all of the calculations thus far, the high-frequency parameter $k.k_t$ was equal to 7. Figures (5.32) and (5.33) demonstrate that the correlation also holds at a relatively low frequency, where $k.k_t$ is equal to 2.1.

All of Figs. (5.22)-(5.33) can be understood from Fig. (5.34), which shows the general forms for the power vs. α_{eff} curves. The power vs. α_{eff} plots of Figs. (5.23), (5.25), (5.27), (5.29), (5.31), (5.33) are portions of larger curves such as those shown in Fig. (5.34). The portions we displayed correspond to the parts of the larger curves that are of most practical interest. The minimum points on the generic curves in Fig. (5.34) represent the point at which the sound field due to loading effects combined with the unloaded solution radiates the least power. This is not normally the point $\alpha_{eff} = 0$. It is, however, for the case where $k_{np/kt}$ equals zero. By thinking of α_{eff} as an effective incidence angle for a flat plate, the symmetry property

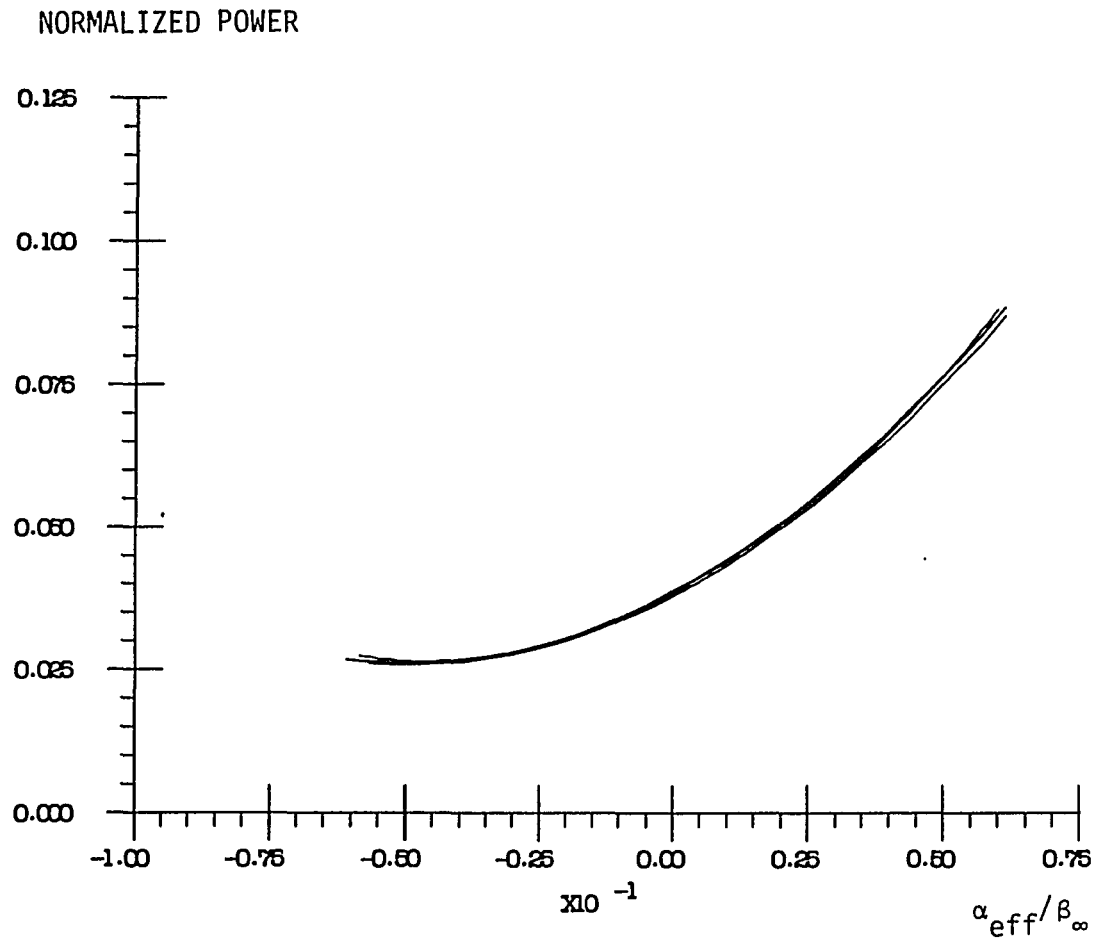

Fig. 5.23 Power vs. leading-edge flow strength. $M_\infty = .6$, $kk_t = 7$, $k_{np}/k_t = 1$.

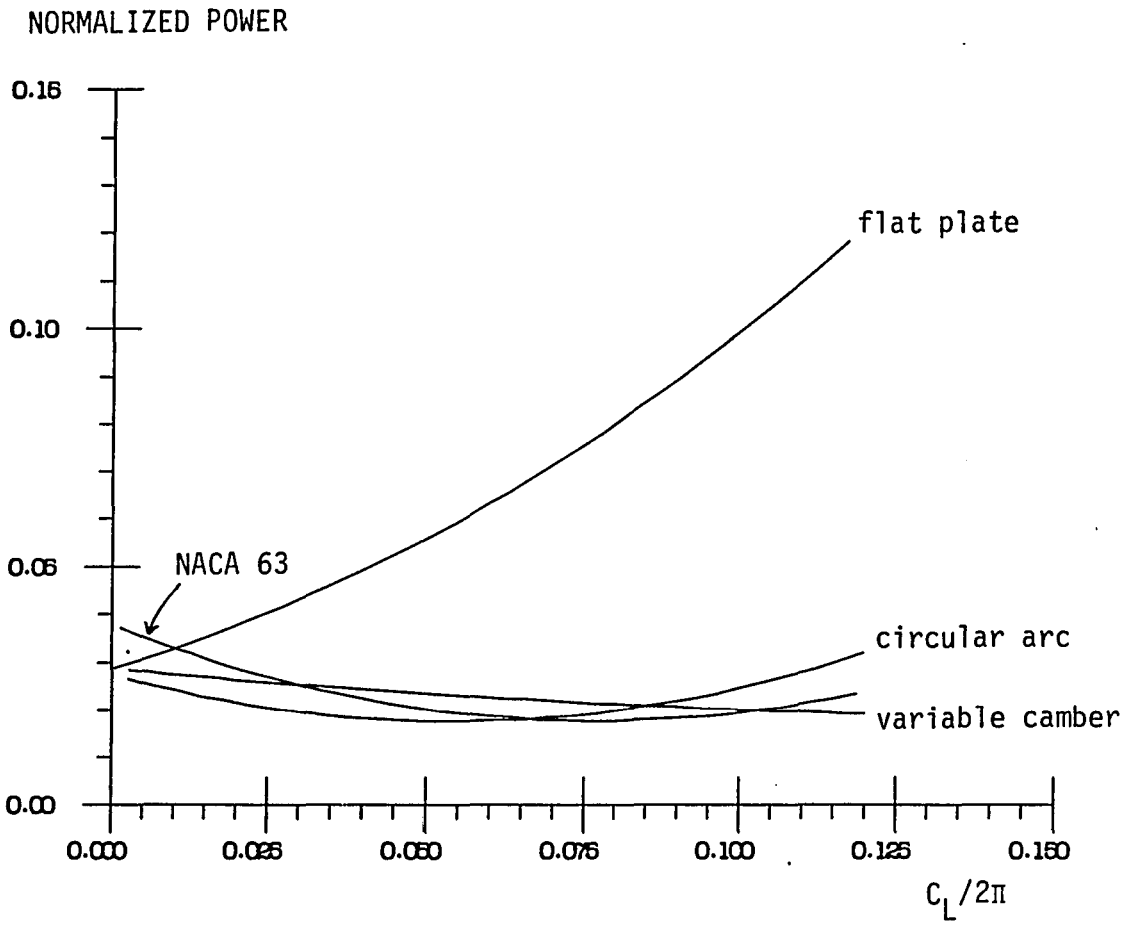

Fig. 5.24 Power vs. total mean loading. $M_\infty = .45$, $kk_t = 7$, $k_{np}/k_t = 1$.

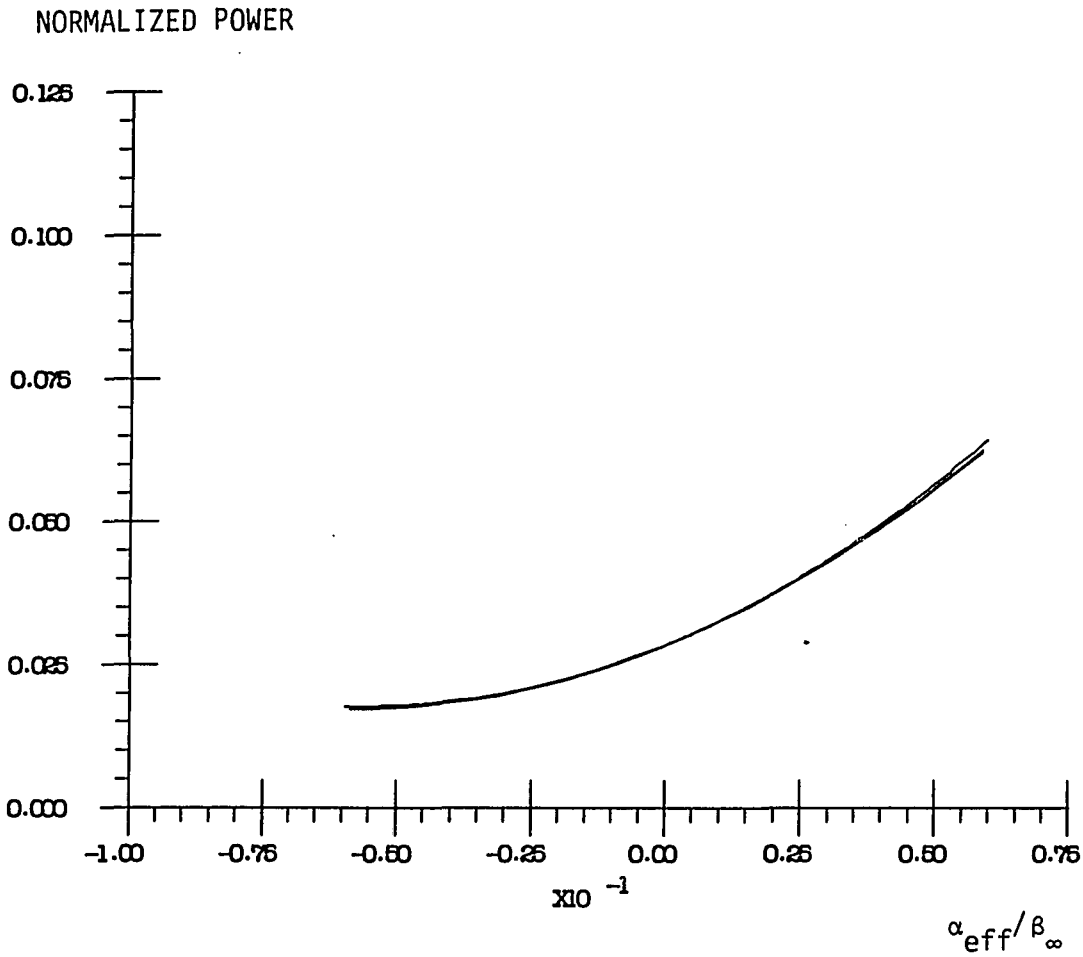

Fig. 5.25 Power vs. leading-edge flow strength. $M_{\infty} = .45$, $kk_t \doteq 7$, $k_{np}/k_t = 1$.

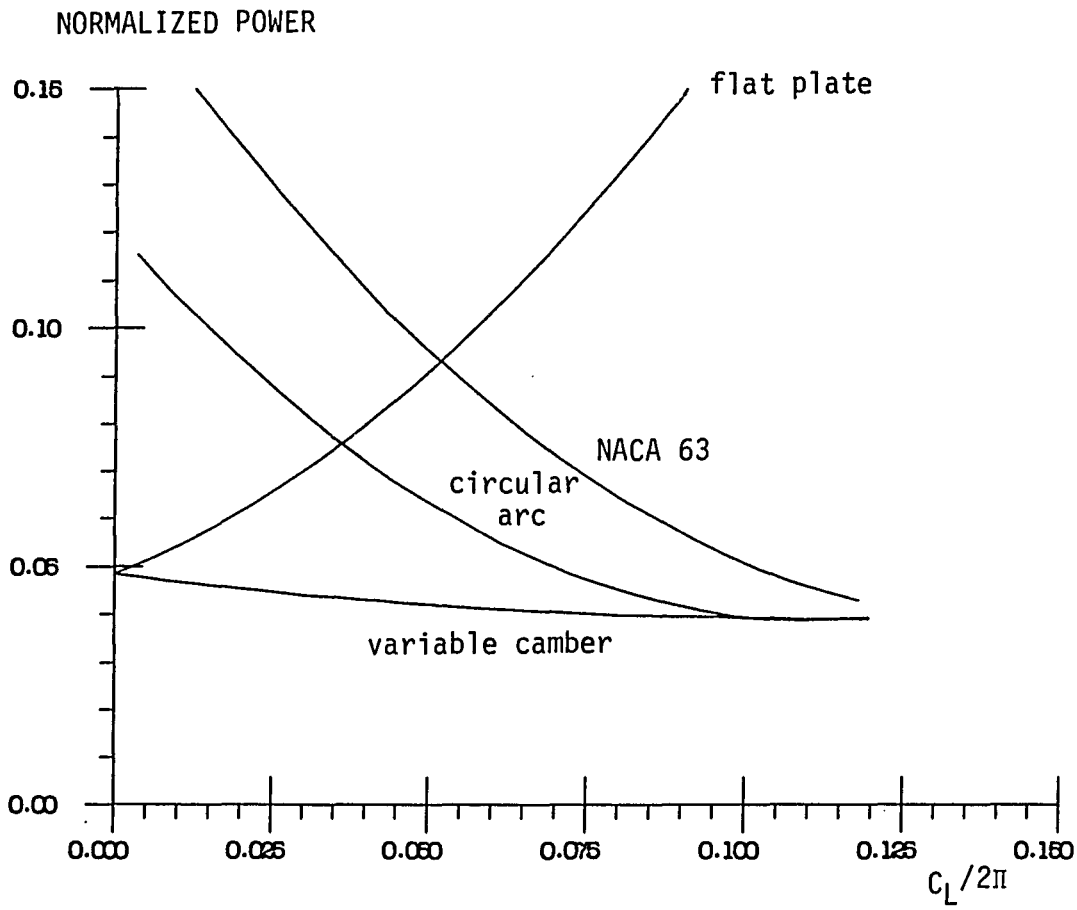

Fig. 5.26 Power vs. total mean loading. $M_\infty = .75$, $kk_t = 7$, $k_{np}/k_t = 1$.

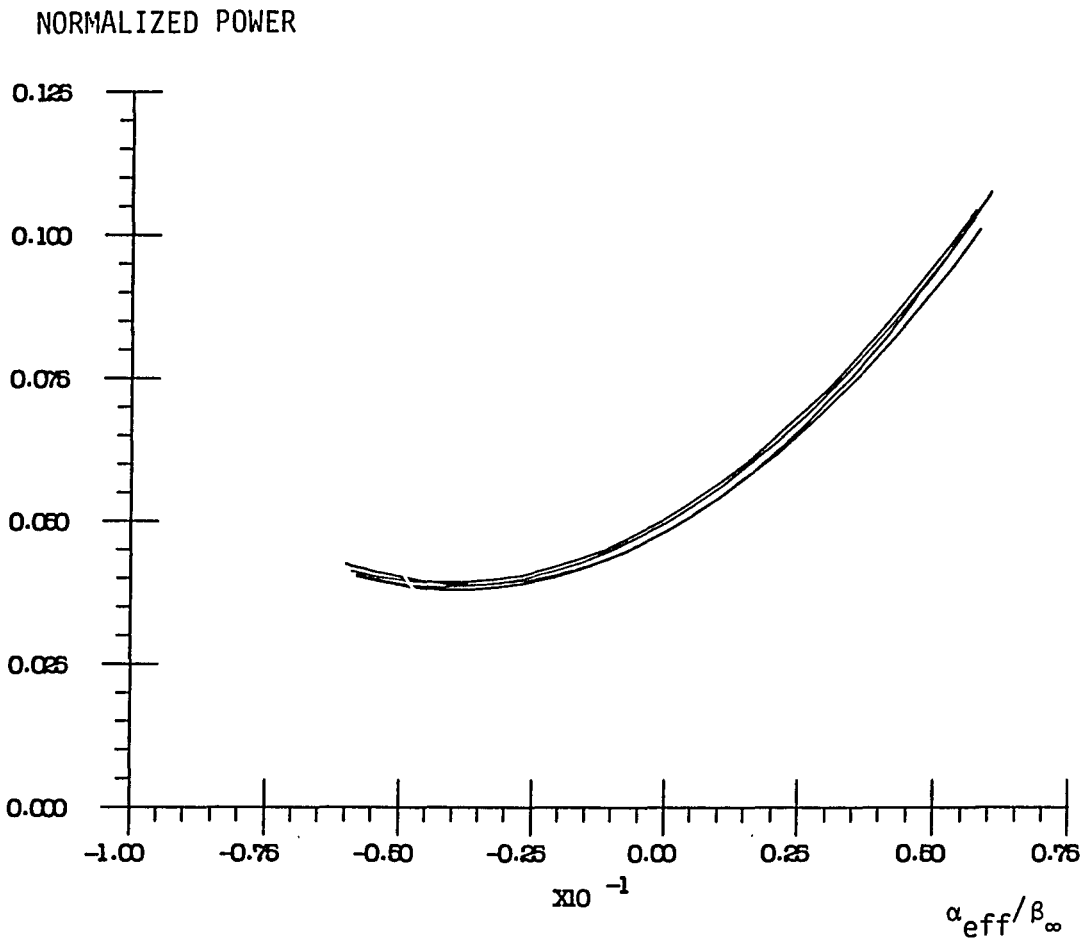

Fig. 5.27 Power vs. leading-edge flow strength. $M_{\infty} = .75$, $kk_t = 7$, $k_{np}/k_t = 1$.

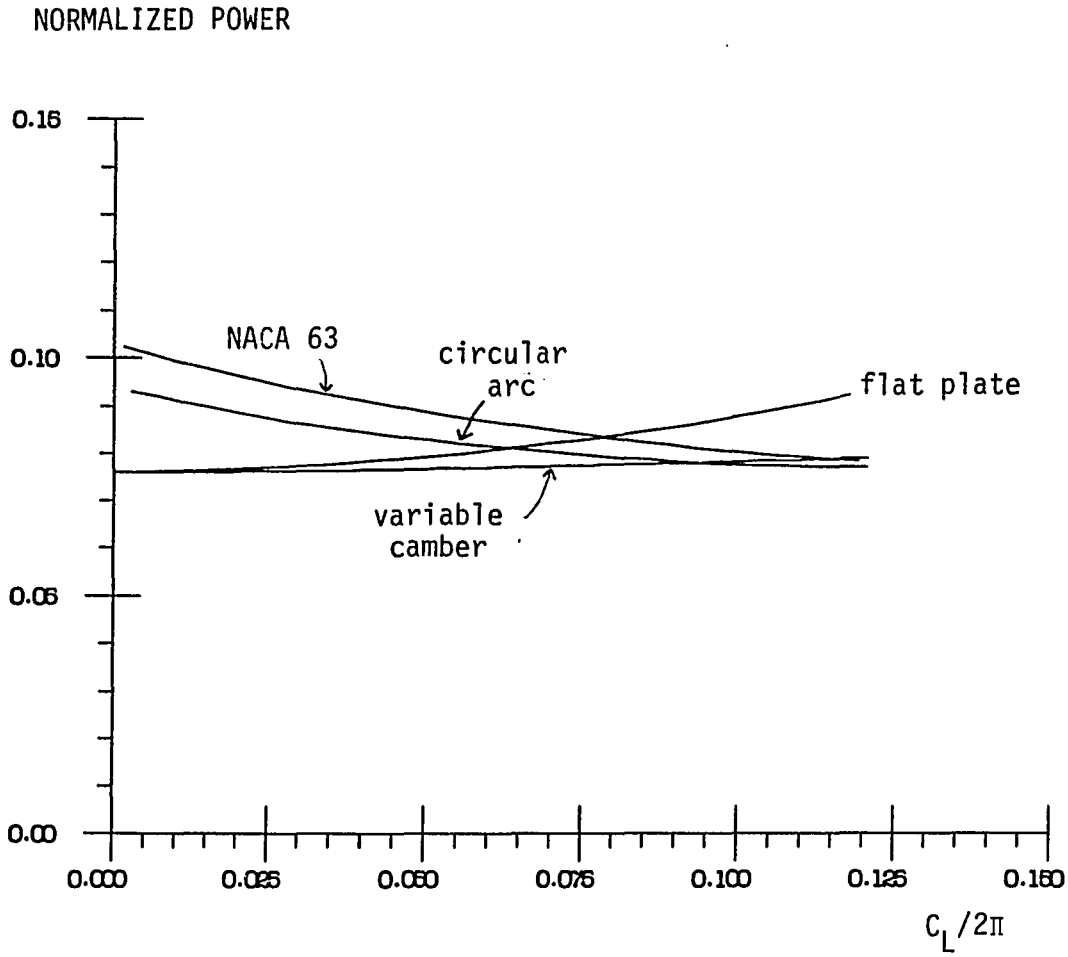

Fig. 5.28 Power vs. total mean loading. $M_\infty = .6$, $kk_t = 7$, $k_{np}/k_t = 0$.

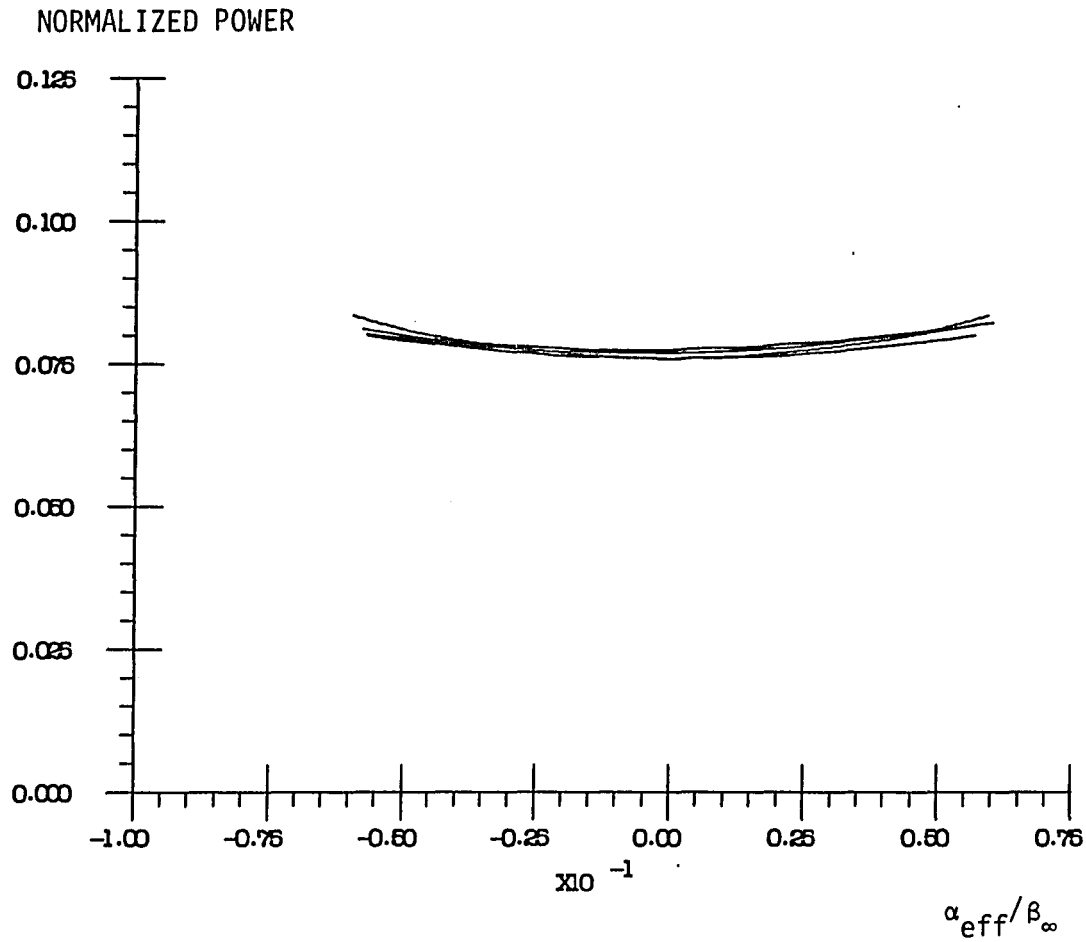

Fig. 5.29 Power vs. leading-edge flow strength. $M_\infty = .6$, $kk_t = 7$, $k_{np}/k_t = 0$.

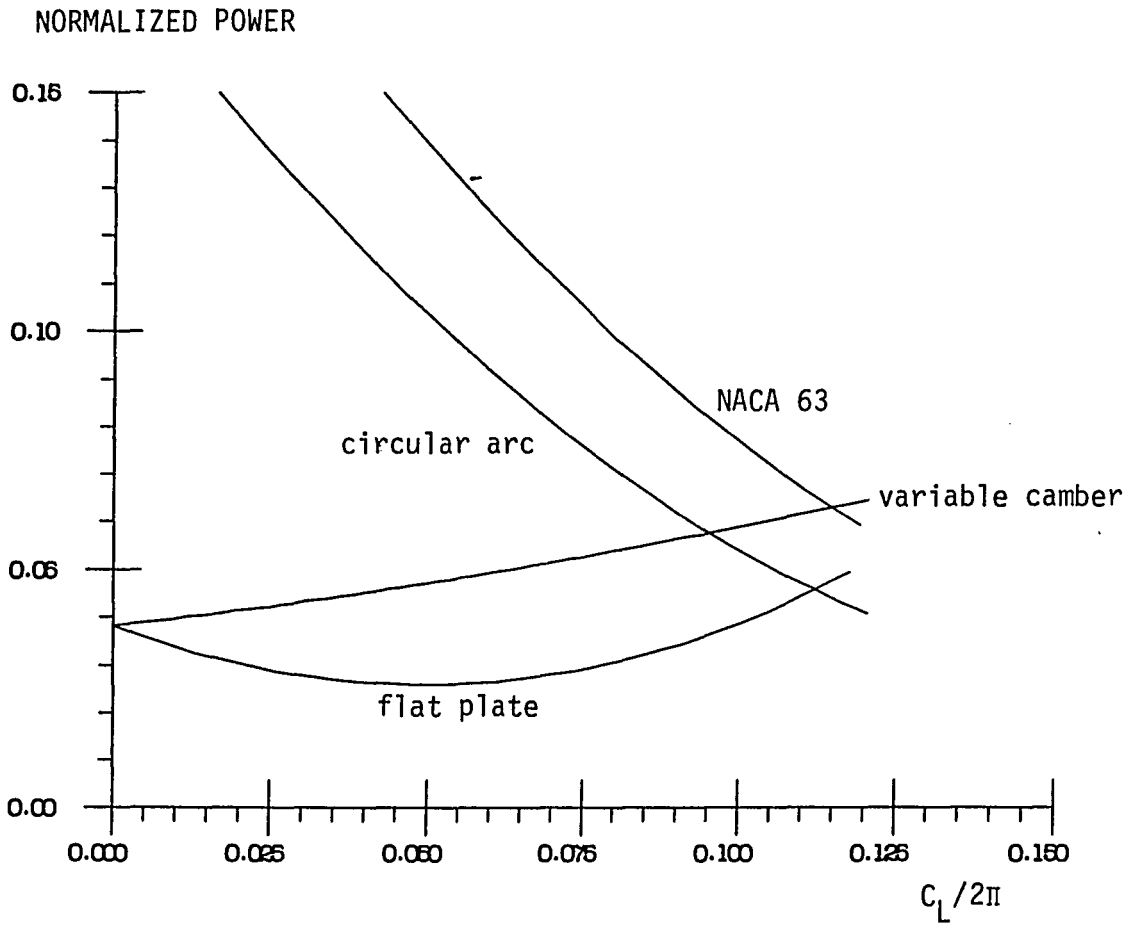

Fig. 5.30 Power vs. total mean loading. $M_\infty = .6$, $kk_t = 7$, $k_{np}/k_t = -1$.

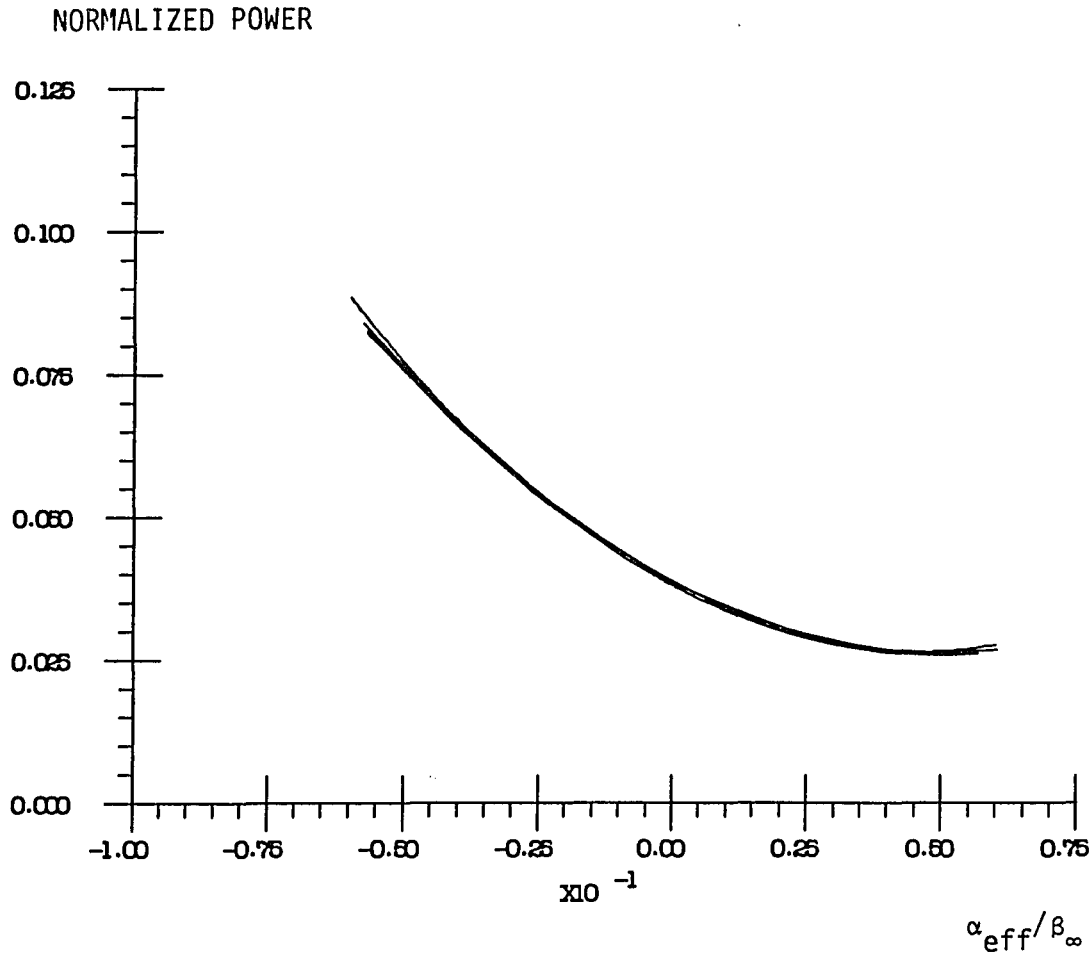

Fig. 5.31 Power vs. leading-edge flow strength. $M_\infty = .6$, $kk_t = 7$, $k_{np}/k_t = -1$.

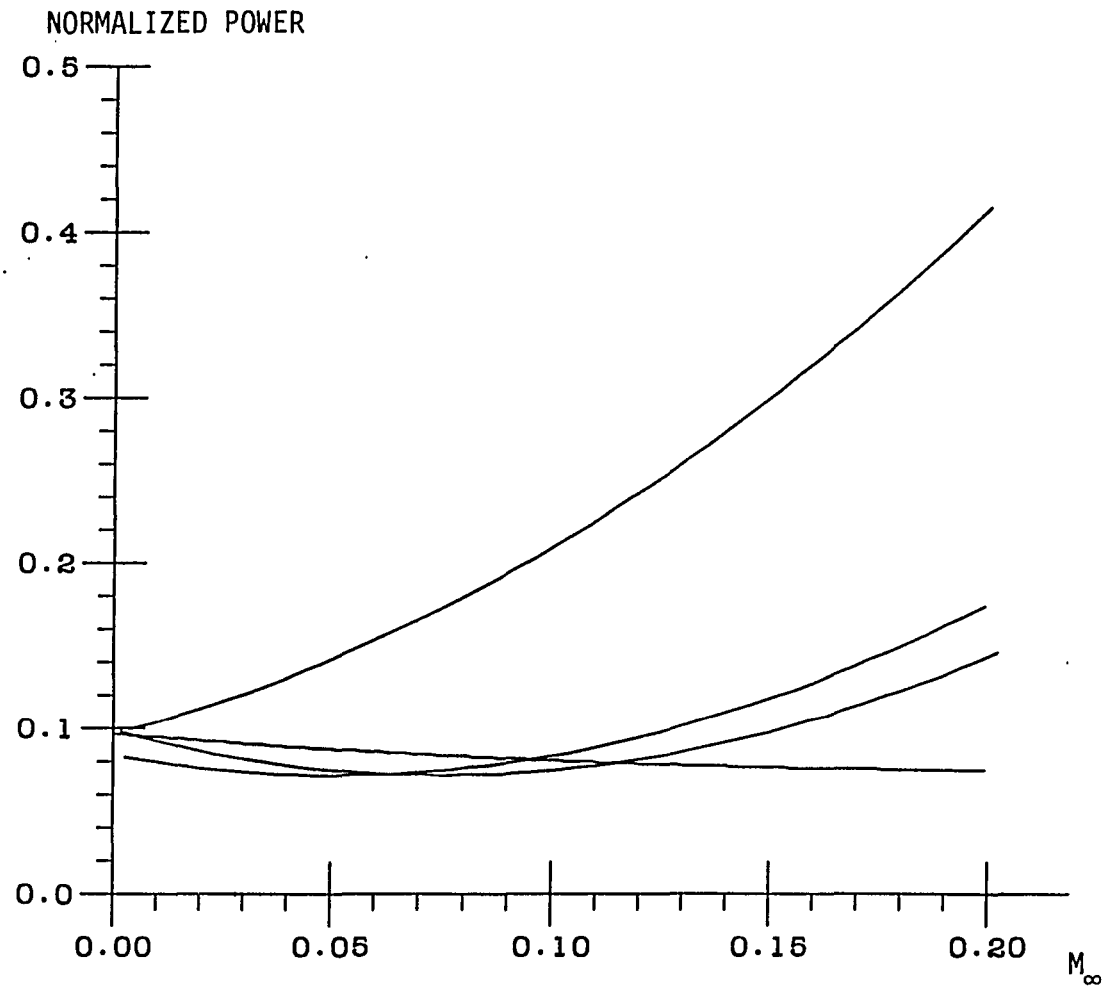

Fig. 5.32 Power vs. total mean loading. $M_\infty = .6$, $kk_t = 2.1$, $k_{np}/k_t = 1$.

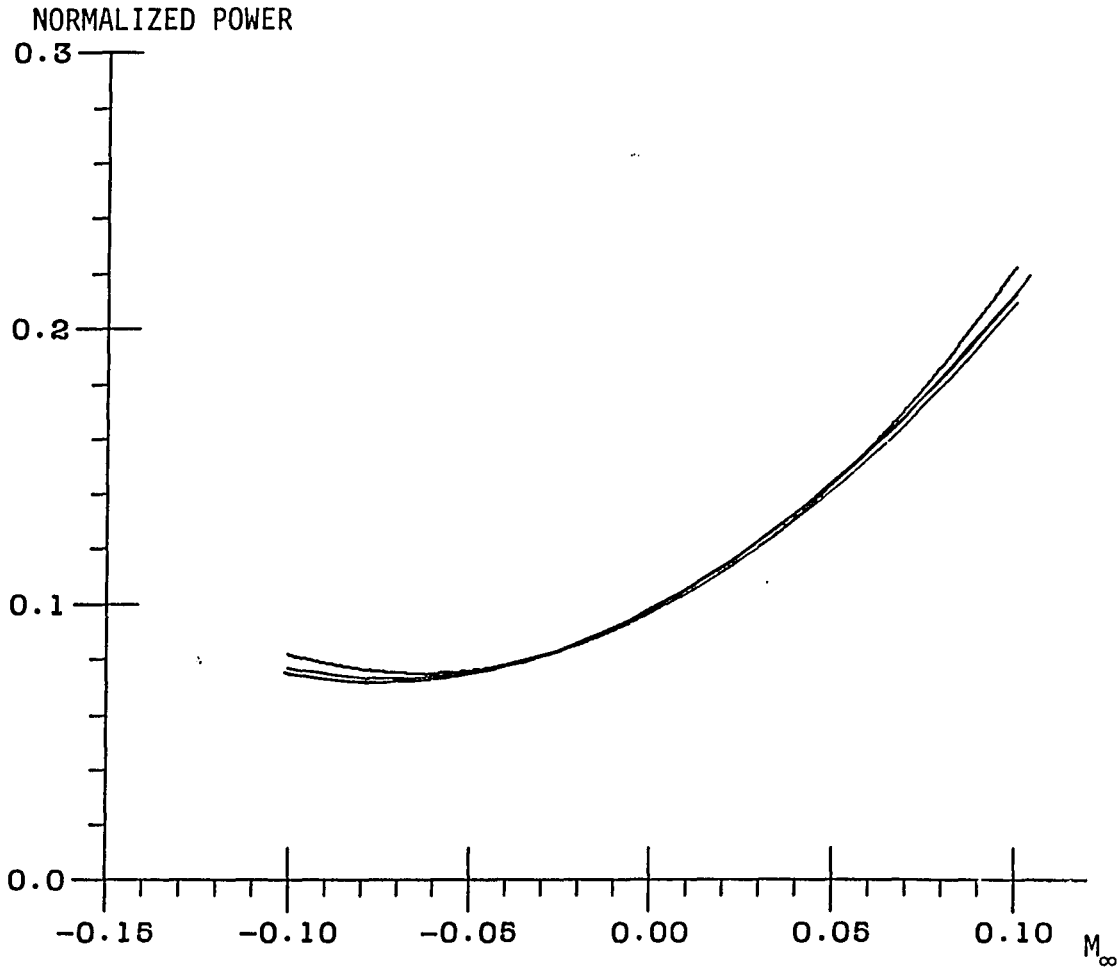

Fig. 5.33 Power vs. leading-edge flow strength. $M_\infty = .6$, $kk_t = 2.1$, $k_{np}/k_t = 1$.

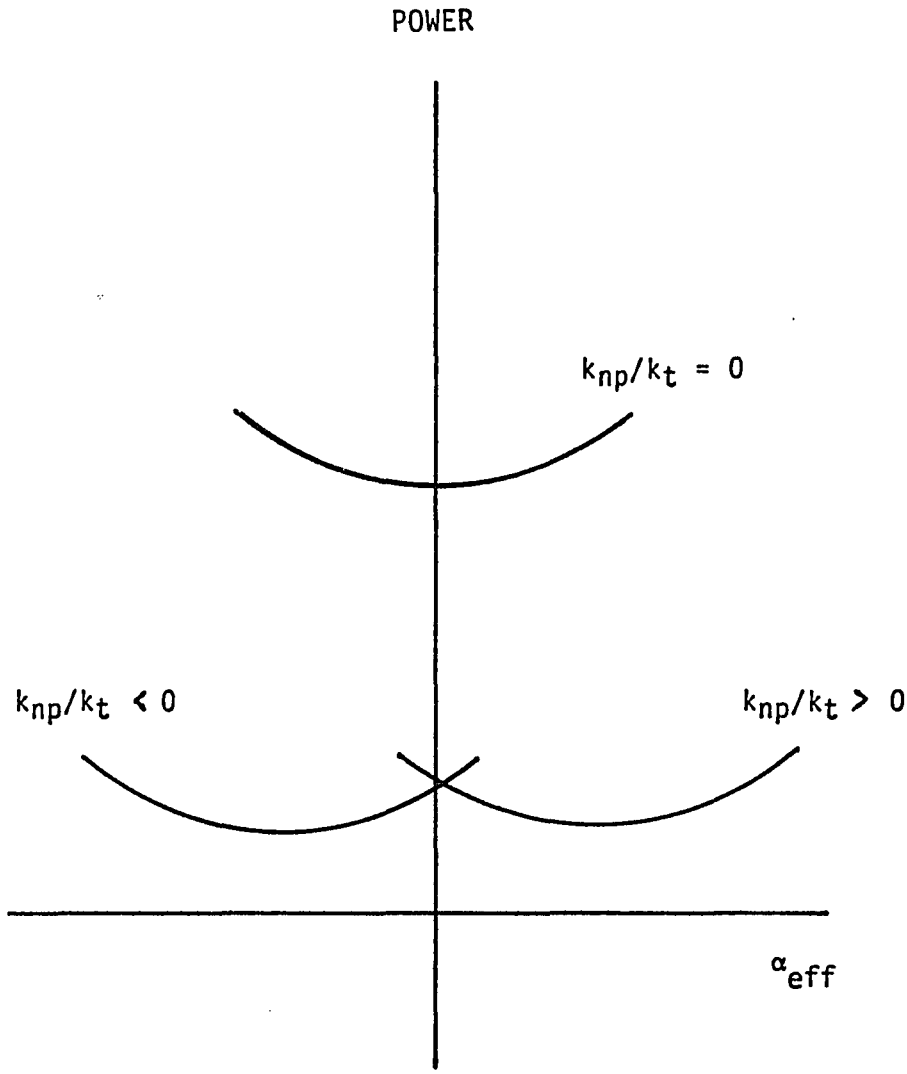

Fig. 5.34 General form for power vs. leading-edge flow strength curve.

discussed in Section 5.1 requires that the power curve possess a local minimum at $\alpha_{eff} = 0$. The minimum at $\alpha_{eff} = 0$ is apparent in Fig. (5.29). The symmetry property can be observed by examining Fig. (5.23) where $k_{np}/k_t = 1$ and Fig. (5.31) where $k_{np}/k_t = -1$. Thinking of α_{eff} as an effective incidence angle also allows us to apply all of the power results in Sections 5.1 and 5.2 to cambered airfoils. A result for a flat plate at a given incidence angle holds quite accurately for any cambered airfoil having an α_{eff} equal to the given incidence angle.

The reason for the wide amount of scatter observed when power is plotted against lift coefficient is now clear. Two airfoils having the same lift can have very different leading-edge flow strengths. Points corresponding to the same lift may even lie on opposite sides of the power vs. α_{eff} "parabola" of Fig. (5.34). For example, the variable camber airfoil at 10% maximum displacement and the flat plate at 10 degrees incidence generate approximately the same amount of lift. The leading-edge flow strength is large and positive for the flat plate and slightly negative for the cambered airfoil. Consequently, the sound power output is much greater for the flat plate. The comparison between the flat plate and the variable-camber airfoil also points out that camber is much less effective than incidence angle for changing α_{eff}. The reason is that for most practical airfoils, the point of maximum displacement is near enough to the mid-chord that the integral defining α_{lc} is small.

The strong correlation with α_{eff} implies that the trailing-edge contribution is in some sense small, since the correlation becomes

exact when the trailing edge is omitted. Under some circumstances the amplitude of the trailing-edge field is negligibly small, for the following reason. For an unloaded airfoil, the leading-edge rays above and below the airfoil are 180 degrees out of phase. Hence, the pressure jump across the trailing edge and therefore the strength of the scattered field is a maximum. When loading is introduced, the phase distortion from the nonuniform mean flow causes the waves to be less out of phase. The result is that the pressure jump for a loaded airfoil is equal to $\cos(2\pi\alpha_g kV(0))$ times that for zero loading. $V(\theta)$ is defined after Eq. (4.43). The cosine factor is maximum for $\alpha_g = 0$, and decreases as α_g moves away from 0. For $\alpha_g k = O(1)$, the decrease can be appreciable. As an example, the ratio of leading-edge to trailing-edge power outputs is 3.3 for a flat plate airfoil at no incidence encountering a gust with $k \cdot k_t = 7$ and $k_{np}/k_t = 1$. The Mach number is 0.6. Under the same conditions but with the airfoil at a six degree incidence angle, the ratio of leading-edge to trailing-edge power outputs is 5.7.

Another factor contributes to the lack of influence of the trailing edge towards the total power output. The numerous constructive and destructive interferences arising from the leading-edge-trailing-edge interaction have a small integrated effect. The power increase in one direction is cancelled by a decrease at another angle. To test this claim we plotted several directivity patterns, which are shown in Figs. (5.35) and (5.36).

Fig. (5.35a) is the pressure pattern for the sound field generated by a flat-plate airfoil at zero incidence interacting with a

gust for which $k \cdot k_t$ is 7.5, M_∞ = .6, and k_{np}/k_t is 0.5. Figs. (5.35b) and (5.35c) represent cases where α_{eff} is still zero but α_g nonzero. In (5.35b) the airfoil is a NACA 1030 (10 percent displacement at 30 percent chord) at an incidence angle of 2.75 degrees. Fig. (5.35c) applies to a NACA 1530 (15 percent displacement) airfoil at an incidence angle of 4.1 degrees. The power values for the three figures are .06, .063, and .065. In Fig. (5.35a) there is symmetry of the pattern across the x_1 axis and no downstream radiation. The symmetry is broken in Fig. (5.35b), with the mean-flow distortion on top of the airfoil adding to the phase cancellation for $x_2 > 0$ and subtracting from it for $x_2 < 0$. There is also considerable downstream radiation, because the nonuniform mean flow has created a component to the leading-edge field which is continuous across the wake. Fig. (5.35c) is a more extreme version of (5.35b). Because the loading is greater, the effect of the mean flow on the leading-edge-trailing-edge phase cancellation is enhanced. The number of lobes in the pattern below the airfoil is much less than the number above. The amount of downstream radiation has also increased.

For Figs. (5.36a,b), the Mach number is 0.6, $k \cdot k_t$ is 7.5 and k_{np}/k_t is 0.5. The leading edge flow strength is 0.05 for both figures. In Fig. (5.36a) the airfoil is a flat plate at 2.3 degrees incidence, and the radiated power is 0.093. Fig. (5.36b) corresponds to a NACA 1030 airfoil at 5 degrees incidence. The power is 0.096. The number of lobes above and below the airfoil differs little for the flat plate, but is considerable for the NACA 1030. The difference in downstream

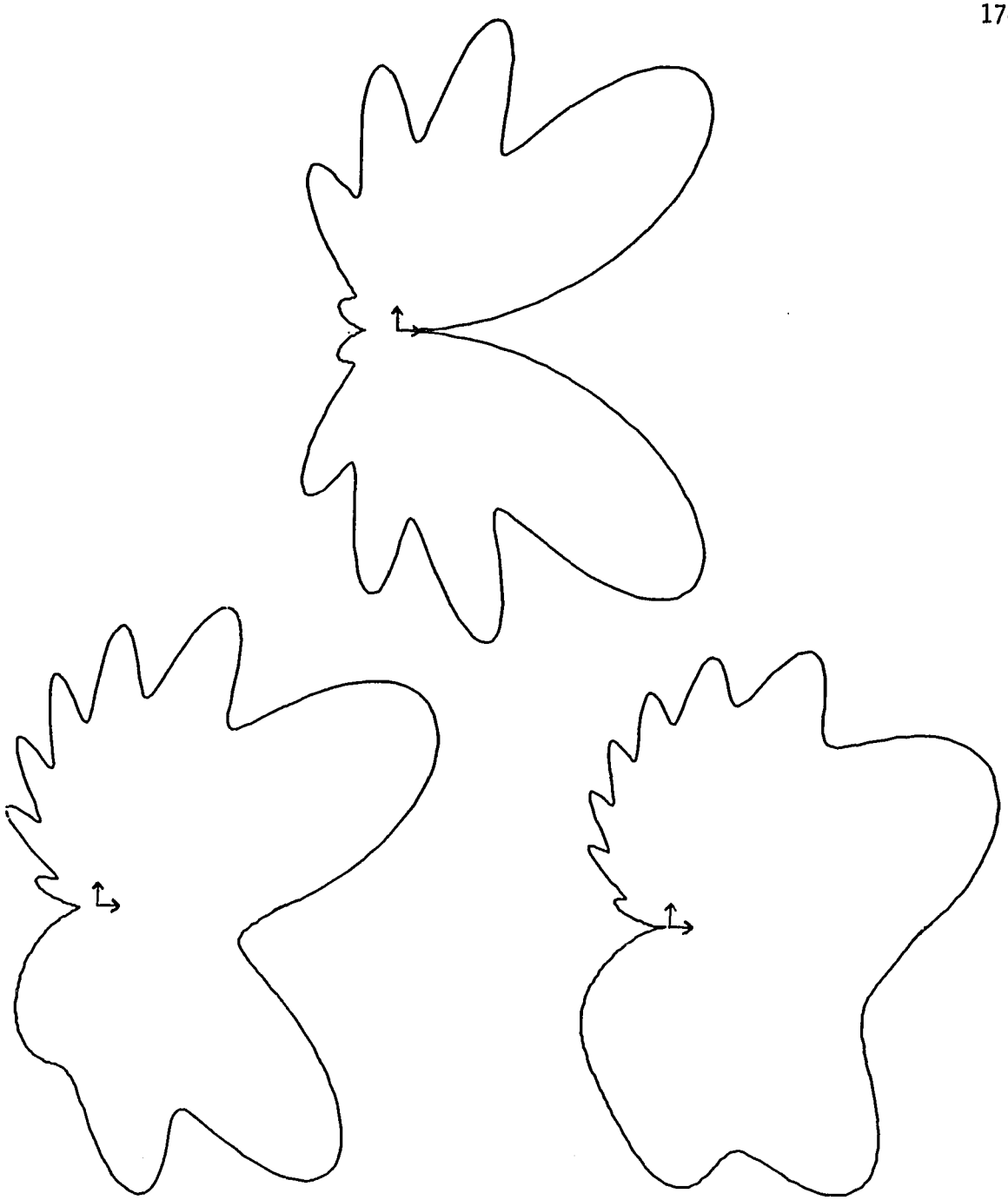

Fig. 5.35 (a,b,c) Total farfield pressure directivity patterns. $M_\infty = .6$, $k_{np}/k_t = .5$, $kk_t = 7.5$. (a) Flat plate at 0°. (b) NACA "1030" at 2.75°. (c) NACA "1530" at 4.1°.

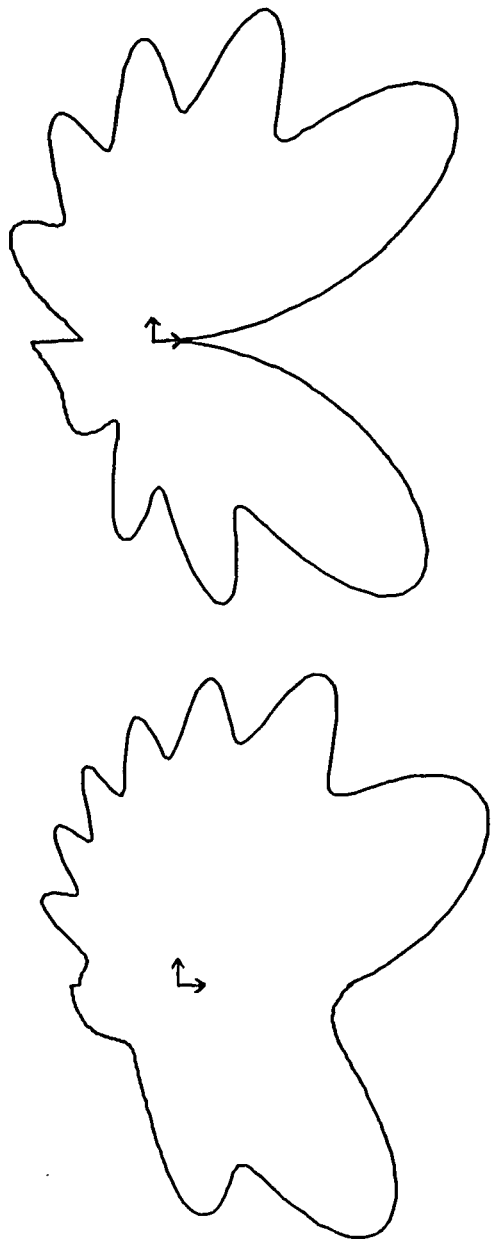

Fig. 5.36 (a,b) Total farfield pressure directivity patterns. $M_\infty = .6$, $k_{np}/k_t = .5$, $kk_t = 7.5$. (a) Flat plate at 2.3°. (b) NACA "1030" at 5°.

radiation for the two cases is also substantial. The reason for the large difference in pressure patterns for the two airfoils is the amount of total loading. The mean lift for the NACA airfoil is six times that for the flat plate.

The directivity patterns have illustrated that total lift has a small integrated effect on the sound field, but has a considerable effect on the pressure observed at a given location. Hence, if one needs to know any details of the sound field, knowledge of the total lift is important. If only a global measure is desired, the leading-edge flow strength is a good correlating parameter.

We have concluded our parametric study on the farfield solution. The important conclusions of the investigation will be summarized in the next chapter, and some suggestions will be made for further parametric studies and improvements on the ones made thus far.

CHAPTER 6

CONCLUSIONS

In this dissertation, we have investigated the effect of airfoil steady loading on the sound generated by the interaction of a zero-thickness airfoil with a high-frequency convected disturbance. Our analysis was based on Goldstein's rapid-distortion theory, which is a linearization of the inviscid equations of motion about a nonuniform mean flow. The mean flow was assumed to be two-dimensional, subsonic, and nearly uniform. The small parameter α, representing the amount of airfoil camber and incidence, and the large parameter k, representing the ratio of airfoil chord to disturbance wavelength, were utilized in a singular perturbation solution to Goldstein's equations. The product αk was assumed to be O(1).

The singular perturbation approach identified several asymptotic regions. For a flat-plate airfoil, these consisted of the local-leading-edge, local-trailing-edge, outer, and transition regions. Asymptotic solutions which retained $O(\alpha\sqrt{k}, 1/\sqrt{k})$ terms relative to the zero-loading solution, but ignored $O(\alpha, \alpha^2 k, 1/\sqrt{k})$ terms, were developed in each asymptotic region. In the transition region, a closed-form solution for the $O(\alpha\sqrt{k})$ term could be obtained only in the geometric-farfield (many chord lengths away from the airfoil). The method of matched asymptotic expansions was used to join the solutions in the individual regions.

Our solution for the flat plate revealed that essentially all of the sound generation is concentrated in the local regions, with the leading edge being the pressure source. The interaction of the convected disturbance with the leading edge produces sound through a variety of mechanisms. In addition to the blocking of the undisturbed gust by the airfoil surface(the only sound source for an unloaded airfoil), these mechanisms include the local scattering of acoustic waves, blocking of vorticity distortions by the boundary, and the interaction of the gust with the mean flow away from the boundary, as represented in the volume source.

The interaction of the convected disturbance with the trailing edge, on the other hand, produces negligible sound. This result is a consequence of the Kutta condition at the trailing edge. Due to the steady Kutta condition, the volume source is very small at the trailing edge, and due to the unsteady Kutta condition, the shed vorticity in the wake is essentially a continuation of the bound vorticity in the airfoil and no change in boundary condition is felt by the convected disturbance. Both the bound and shed vorticity in the local-trailing-edge region convect at the free-stream speed, and hence generate no pressure fluctuations. Thus, the trailing edge influences the farfield sound only by scattering the acoustic waves generated in the local-leading-edge region. Before describing the scattered field, we review the outer leading-edge field.

The propagation of the sound generated at the leading edge into the outer region is described by geometric acoustics. The normals to

the surfaces of constant phase are rays emanating from the leading edge. The phase of the acoustic waves contains an $O(\alpha k)$ (i.e., $O(1)$) distortion $\sigma_{1\ell}$ due to the propagation in a nonuniform medium. The asymptotic matching showed that the amplitude of the waves is the amplitude $L(\theta) = L_0(\theta) + \alpha\sqrt{k}\ (L_1(\theta) + L_2(\theta))$ of the local-leading-edge field.

The zero-loading amplitude $L_0(\theta)$ is antisymmetric with respect to the airfoil surface, and hence in the case of zero mean loading the waves above and below the airfoil are 180° out of phase at the trailing edge. The effect of mean loading is to change the convection and sound speeds above and below the airfoil, making the waves less out of phase at the trailing edge. The trailing-edge pressure jump associated with L_0, then, is maximum for no mean loading. Steady loading tends to decrease the pressure jump, and hence the strength of the trailing-edge scattered field, by a factor of magnitude $\cos(\alpha k)$. Since the trailing-edge field is weaker than the leading-edge field it scatters by $O(1/\sqrt{k})$, it is not necessary to consider the scattering of the sound associated with the $O(\alpha\sqrt{k})$ terms $L_1(\theta) + L_2(\theta)$. However, for simplicity in writing the final expressions, and in coding these expressions for computer analysis, we retained the $O(\alpha\sqrt{k})$ terms in the scattered field.

The scattered field arising in the local-trailing-edge region to cancel the pressure jump in the leading-edge ray-field is the source of additional rays in the outer region. The trailing-edge ray field is identical in form to the leading-edge ray field; the trailing-edge

solution contains an $O(\alpha k)$ phase distortion σ_{1t} and an amplitude $T(\theta)$ obtained by matching with the local-trailing-edge region. The ray description of the trailing-edge outer field fails at shallow angles, however. For trailing-edge angles of size $\theta_t = O(1/\sqrt{k})$ a transition region exists, which is analogous to the transition region in optical problems between illuminated and shadow regions. In the transition region, the geometric-acoustics solution gives way to one involving a Fresnel integral.

The analysis for a cambered airfoil was similar to that for a flat plate. For a general cambered airfoil, the perturbation mean-flow quantities cannot be obtained in closed form, hence closed-form solutions to the governing equations could not be found in all regions. However, in the farfield limit, we were able to obtain a complete analytical solution.

An additional asymptotic region, which we called the transition$_c$ region, is present for a cambered airfoil. It arises out of the failure of the leading-edge ray field to satisfy the boundary condition on the curved surface. The transition$_c$ region lies above and below the airfoil, in a region of angular extent $\theta = O(1/\sqrt{k})$. The transition$_c$ solution accounts for surface-curvature effects and is given in terms of an inverse cosine transform. The mathematical form of the solution is similar to the Fresnel-integral solution for the downstream transition region. We found that while the transition$_c$ solution significantly alters the acoustic field on the airfoil surface,

it produces only a higher-order effect on the scattered field from the trailing-edge and on the total farfield sound. Hence, the conclusions for a flat plate discussed in previous paragraphs also apply for a cambered airfoil. The major differences in the final solution are that for a cambered airfoil the incidence angle appearing in the amplitude for the flat plate solution is replaced by the leading-edge flow strength α_{eff}, and the incidence angle appearing in the phase is replaced by the total mean loading α_g.

The solution for the acoustic farfield was investigated through a series of parametric studies in Chapter 5. We examined the effects of varying the gust orientation, Mach number, and airfoil shape. Acoustic power calculations showed that the sound field depends strongly on gust orientation. The orientation for a two-dimensional gust was measured by the ratio k_{np}/k_t of the vertical wavenumber to horizontal wavenumber. For zero mean loading, the maximum power output occurs for k_{np}/k_t equal to zero. The point of maximum power shifts to larger values of k_{np}/k_t as the mean loading or Mach number is increased. This shift is due to changes in the field generated by the volume source and the scattering of this field by the airfoil leading edge.

To investigate the influence of changing the Mach number, we considered only the leading-edge field. This allowed us to let the Mach number approach zero without worrying about convergence of the leading-edge-trailing-edge the iteration scheme for high frequencies. Considering the leading-edge field alone also allowed us to isolate the

sound-generating mechanisms, since the trailing edge produces sound only by scattering the leading-edge field. Plots of radiated acoustic power showed that our division of loading effects into the functions H_1 and H_2 produced two terms with monopole singularities as $M_\infty \to 0$. We combined the singular parts of H_1 and H_2 into a term H_{12g}, which remained bounded with respect to the zero-loading solution H_0 as $M_\infty \to 0$. Loading effects were then represented by three terms, H_{1C}, H_{2C}, and H_{12g}. The terms H_{1C} and H_{2C} represent compressibility effects and vanish at low Mach numbers. The sound generated by the local scattering of acoustic waves by the nonuniform mean flow is contained in H_{1C}. The acoustic field produced by the interaction of mean density gradients with the convected disturbance comprises H_{2C}. The solution H_{12g} is nonzero for all Mach numbers. It accounts for the interaction of the gust with the nonuniform mean velocity and the blocking by the airfoil of the vortical velocity distortions. In general, the magnitude of H_{12g} relative to H_0 remains constant as the Mach number increases from 0 to about .5. For M_∞ greater than .5, the magnitude of H_{12g} relative to H_0 increases rapidly. The compressibility solutions are negligibly small relative to H_0 until M_∞ reaches about .4, at which point they grow in importance very rapidly. The solution H_{1C} is the dominant compressibility sound source for k_{np}/k_t less than one, while H_{2C} is stronger for k_{np}/k_t greater than one.

While examining the influence of Mach-number variation, we also compared our rapid-distortion theory approach with the acoustic analogy. A close comparison is possible in the local-leading-edge

region, since there the convected disturbance is the same in both formulations. We found that the acoustic analogy approach leads to the prediction of a monopole singularity as $M_\infty \to 0$ if one uses the homogeneous boundary condition $\partial P/\partial n = 0$. To obtain the correct result using the acoustic analogy, one must account for the blocking of the vortical velocity distortions by the airfoil in the boundary condition. The primary difference between the acoustic analogy formulation (with the correct boundary condition) and rapid-distortion theory is the solution H_{1C}. That is, acoustic analogy models which approximate T_{ij} by $\rho_0 u_i u_j$ would not account for the generation of sound by nonuniform propagation effects. We noted earlier that H_{1C} is very important at Mach numbers greater than .4 and values of k_{np}/k_t less than one.

The final section of our parametric study of the farfield solution involved mean-loading effects. Plots of acoustic power versus steady loading revealed that the radiated power changed substantially with loading, and hence that mean loading should not be ignored in noise prediction models. However, the same plots showed that the power values correlated poorly with the total loading parameter α_g. A replotting of the same results versus α_{eff}, the leading-edge flow strength, produced an excellent collapse of the points. The correlation with α_{eff} remained strong as the Mach number and gust orientation were varied.

Though total power values correlate very well with leading-edge flow strength α_{eff} alone, total loading α_g is also important in determining the details of the sound field. Pressure directivity

patterns showed that two acoustic fields can radiate the same total power but have very different pressure values at a given location. Thus, α_{eff} is an excellent global measure of the sound field, but both α_{eff} and α_g must be computed for a detailed description.

Regarding future continuations of the work in this dissertation, two important extensions are necessary to properly model turbomachinery noise. The first step is to introduce airfoil thickness. Shown in Fig. (6.1) is a thin airfoil with thickness. In turbomachinery applications, the airfoil leading-edge nose radius is small compared to the maximum thickness and very small compared to the airfoil chord. For a thin airfoil ($\tau/b \ll 1$) with a parabolic-shaped nose, the scaling $\delta/b = O(\tau/b)^2$) applies. In that case, it is reasonable to assume that the nose radius δ is roughly equal to the shift in the stagnation point from the leading edge due to mean loading. In other words, $\delta = O(\alpha^2 b)$. In the thickness problem, as throughout the dissertation, we assume $\alpha^2 b \ll \lambda$.

Much of the effort required to include airfoil thickness in the theory is associated with the extensions to the analysis in the local-leading-edge region. Since the mean flow is assumed to be a small perturbation of a uniform flow in the leading edge region, the effects of incidence angle, camber, and thickness are locally additive. The local mean flow due to thickness will produce additional nonuniform propagation effects and vorticity distortions on the airfoil surface, and hence a new solution H_3 will arise analagous to H_1 of Chapter 3. The interaction of the mean flow due to thickness with the convected

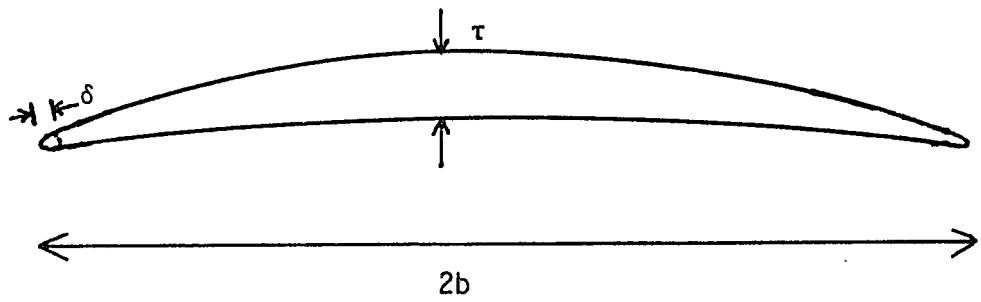

Fig. 6.1 Thin airfoil with nonzero thickness.

disturbance will produce an additional volume source term, and a new solution H_4 will arrise analagous to H_2. The effects of thickness on the farfield sound can be assessed only once H_3 and H_4 have been determined.

The remaining efforts in the thickness program will be concentrated on the development of the solution in the stagnation-point (or nose-radius) region. The matching of the stagnation-point-region solution with the local-leading-edge solution will remove any nonuniqueness associated with eigensolutions in the local-leading-edge region. Presently, these nonuniquenesses are removed by less precise criteria such as integrability conditions. In the stagnation-point region, the equations of motion cannot be linearized about the mean flow. However, since the length scale of the region is short compared to the disturbance wavelength, the flow is quasi-steady and some simplification will be possible.

The second proposed extension to the work in this dissertation is to consider an airfoil cascade rather than an isolated airfoil. The mean flow through the cascade can be obtained by a periodic conformal mapping, hence the variable coefficients appearing in Goldstein's wave equation can be obtained in a straightforward way. The local analysis of the cascade leading-edge regions would be very similar to that developed in this dissertation. The total upstream sound field could then be calculated following the procedure of Envia and Kerschen (1986). They developed an approximate solution for the sound generated by a convected gust interacting with a cascade of swept airfoils, neglecting mean loading effects. This was done by summing the fields from the infinite row of leading edges using the dirac delta function to represent the infinite summation inside an integral. The approach of Envia and Kerschen is a high-frequency approximation and should be applicable to our cascade problem.

The calculation of rearward-radiated noise for the cascade is more difficult, due to the necessity of accounting for reflection of sound off of adjacent airfoils. If surface-curvature effects can be neglected, at least to lowest order, the problem appears tractable. It is encouraging to note that surface-curvature effects arose only in higher-order terms in the present analysis. However, the level of complication produced by surface curvature can only be ascertained by an actual analysis of the problem.

When the described extensions to the model have been made, comparison of our results with experiment will be possible. For

example, using empirically-determined rotor-wake velocities as an upstream convected disturbance, we could calculate the farfield sound generated by the rotor-stator interaction in a turbomachine. Considerable experimental data exists for this interaction.

At the present, only indirect experimental evidence exists in support of our theory. This evidence lies primarily in the inability of total loading to accurately correlate sound power data. Ginder and Newby (1977) considered broadband noise generation from a variety of high-speed fans, and found that their experimental data collapsed better with the "local-leading-edge incidence angle" than with total loading. Their leading-edge incidence angle is the angle formed by the tangent to the leading edge with the mean velocity upstream. However, while the use of the leading-edge-incidence angle substantially improved the correlation, considerable scatter was still present. Our results indicate that the leading-edge flow strength is a more appropriate parameter than the geometric leading-edge incidence angle. It would be interesting to replot the data of Ginder and Newby against α_{eff}.

This dissertation, while far from being a complete noise-prediction model, has considerably extended previous analytical work in the area of turbomachinery and propeller noise. It is hoped that the closed-form solutions, together with the parametric study of Chapter 5, will provide a better understanding of how the specific mechanism of airfoil steady loading influences the total sound field.

APPENDIX A

MEAN QUANTITIES FOR A SMALL-PERTURBATION, PERFECT-GAS FLOW

This appendix concerns the calulation of the mean-flow quantities for the potential flow around an obstacle. Far upsteam the flow is uniform in the x_1 direction with magnitude U_∞, as shown in Fig. (A.1) below. The obstacle is assumed "thin", so that the mean flow around the body may be written as a small perturbation (say $O(\alpha)$) to the uniform flow. In terms of potential (as in the main text the zero subscript denotes mean quantities),

$$\phi_0 = \phi_\infty + \phi_1 \quad , \tag{A.1a}$$

where

$$\phi_\infty = U_\infty \, x_1 \tag{A.1b}$$

and

$$|\nabla \phi_1| \; / \; U_\infty = O(\alpha) \quad . \tag{A.1c}$$

The solution for the perturbation potential ϕ_1 will be derived shortly. We first show how the other mean flow perturbation quantities are related to the dimensionless perturbation speed q, defined by

$$q = \frac{1}{U_\infty} \frac{\partial \phi_1}{\partial x_1} \quad . \tag{A.2}$$

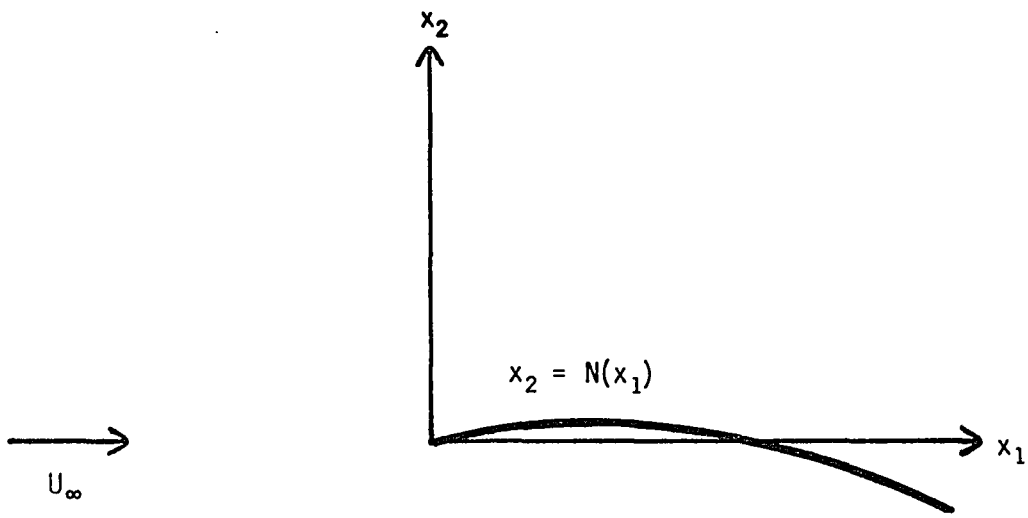

Fig. A.1 Mean flow around thin airfoil.

The total mean flow speed is

$$U_0 = \left[(U_\infty + \frac{\partial \phi_1}{\partial x_1})^2 + (\frac{\partial \phi_1}{\partial x_2})^2\right]^{1/2} = U_\infty (1 + q) + O(\alpha^2) \quad . \qquad (A.3a)$$

The following equation for the perturbation pressure can be derived from the momentum equation

$$p_1 = p_0 - p_\infty = -\rho_\infty U_\infty \frac{\partial \phi_1}{\partial x_1} = - \rho_\infty U_\infty^2 q \quad . \qquad (A.3b)$$

The entropy for the mean flow is a constant, and the density is related in a simple way to the pressure by

$$p_0 = A \rho_0^\gamma \quad , \quad \gamma = c_p/c_v \quad .$$

Writing ρ_0 as $\rho_\infty + \rho_1$, utilizing (A.3b), and expanding for small ρ_1, we obtain

$$\rho_1 = - \rho_\infty M_\infty^2 q \quad . \qquad (A.3c)$$

The speed of sound for a perfect gas is

$$a_0^2 = \frac{dp_0}{d\rho_0} = \frac{\gamma p_0}{\rho_0} \quad . \qquad (A.3d)$$

The $O(\alpha)$ sound speed correction can be found by incorporating (A.3b) and (A.3c) in (A.3d) and expanding to linear order in q. The result is

$$a_1 = - \frac{\gamma-1}{2} M_\infty^2 a_\infty q \quad . \qquad (A.3e)$$

Knowing a_1, we can easily find the first order corrections to

$$M_0 = U_0/a_0 \qquad \text{and} \qquad \beta_0 = [1 - M_0^2]^{1/2} \quad .$$

The expressions are

$$M_1 = \left[1 + \frac{\gamma-1}{2} M_\infty^2\right] m_\infty \, q \tag{A.3f}$$

and

$$\beta_1 = \left[1 + \frac{\gamma-1}{2} M_\infty^2 \right] \frac{M_\infty^2}{\beta_\infty} \, q \quad . \tag{A.3g}$$

Equations (A.3a,c,e,f,g) are used in the coefficients, source term, and boundary condition of the disturbance equations derived in Chapter 2.

We return now to the solution for the potential ϕ_1. The equations satisfied by ϕ_1 are

$$\beta_\infty^2 \frac{\partial^2 \phi_1}{\partial x_1^2} + \frac{\partial^2 \phi_1}{\partial x_2^2} = 0 \tag{A.4a}$$

and

$$\frac{\partial \phi_1}{\partial x_2} \bigg|_{x_2=0} = U_\infty \, N'(x_1) \quad , \tag{A.4b}$$

where the body shape is given by $x_2 = N(x_1)$ and the prime denotes differentiation. The condition that $\nabla\phi_1$ go to zero at infinity is also imposed. Consider next an incompressible, i.e. $M_\infty = 0$, flow over the same body with the same uniform velocity far upstream. The description of the incompressible flow problem is:

$$\frac{\partial^2 \phi_1^i}{\partial x_1^2} + \frac{\partial^2 \phi_1^i}{\partial x_2^2} = 0 \qquad \text{(A.5a)}$$

$$\left.\frac{\partial \phi_1^i}{\partial x_2}\right|_{x_2=0} = U_\infty N'(x_1) \qquad \text{(A.5b)}$$

$$\nabla \phi_1^i \to 0 \text{ at infinity} \quad . \qquad \text{(A.5c)}$$

The superscript "i" stands for "incompressible." For most body shapes of interest, there are well developed methods in potential theory to solve equations (A.5). We shall suppose that the problem has the solution

$$\phi_1^i = F_r^i(x_1, x_2) \quad . \qquad \text{(A.6)}$$

Similarly, the flow will possess a steamfunction of the form

$$\psi_1^i = F_i^i(x_1, x_2) \quad . \qquad \text{(A.7)}$$

The "r" and "i" subscripts on the two functions indicate that they are the real and imaginary parts of an analytic function.

If the Prandtl-Glauert transformation

$$x_{1,pg} = x_1 \qquad x_{2,pg} = \beta_\infty x_2 \qquad \phi_{1,pg} = \frac{1}{\beta_\infty} \phi_1 \qquad \text{(A.8)}$$

is made, the compressible problem is reduced to

$$\frac{\partial^2 \phi_{1,pg}}{\partial x_{1,pg}^2} + \frac{\partial^2 \phi_{1,pg}}{\partial x_{2,pg}^2} = 0 \qquad \text{(A.9a)}$$

$$\left.\frac{\partial \phi_{1,pg}}{\partial x_{2,pg}}\right|_{x_{2,pg}=0} = U_\infty N'(x_{1,pg}) \qquad \text{(A.9b)}$$

$$\nabla\phi_{1,pg} \to 0 \text{ at infinity} \quad , \tag{A.9c}$$

which is the incompressible problem. The solution, therefore, is

$$\phi_{1,pg} = F_r^i(x_{1,pg} \, , \, x_{2,pg}) \quad . \tag{A.9d}$$

In terms of the original variables the result becomes

$$\phi_1 = \frac{1}{\beta_\infty} F_r^i(x_1, \beta_\infty x_2) \quad . \tag{A.10a}$$

In a similar fashion, the streamfunction for the compressible problem is found to be

$$\psi_1 = \frac{1}{\beta_\infty^2} F_i^i(x_1, \beta_\infty x_2) \quad . \tag{A.10b}$$

For the compressible flow the streamfunction is defined by

$$\frac{\partial\psi_1}{\partial x_2} = \frac{\partial\phi_1}{\partial x_1} \qquad \frac{\partial\psi_1}{\partial x_1} = -\frac{1}{\beta_\infty^2} \frac{\partial\phi_1}{\partial x_2} \quad . \tag{A.11}$$

The results for the potential and streamfunction can be written compactly in complex notation. The perturbation complex potential is

$$\phi_1 + i\beta_\infty\psi_1 = \frac{1}{\beta_\infty} \left[F_r^i(x_1, \beta_\infty x_2) + i \, F_i^i(x_1, \beta_\infty x_2) \right] \quad . \tag{A.12}$$

Introducing the complex Prandtl-Glauert variable,

$$\zeta = x_1 + i\beta_\infty x_2 \quad , \tag{A.13}$$

we can write Eq. (A.12) completely in complex notation as

$$\phi_1 + i\beta_\infty \psi_1 = F(\zeta) \quad . \tag{A.14a}$$

The perturbation flow speed q is obtained from

$$q = \frac{1}{U_\infty} \text{Re} \{ F'(\zeta) \} \quad . \tag{A.14b}$$

The harmonic conjugate of q, which we label $-\mu$, is

$$-\mu = \frac{1}{U_\infty} \text{Im} \{ F'(\zeta) \} = \frac{1}{U_\infty} \text{Im} \{ -i \frac{\partial}{\partial x_{2,pg}} F(\zeta) \}$$

$$= - \frac{1}{U_\infty} \frac{\partial}{\partial x_{2,pg}} \text{Re} \{F(\zeta)\} = -\frac{1}{\beta_\infty U_\infty} \frac{\partial \phi_1}{\partial x_2} \quad . \tag{A.14c}$$

Hence physically μ is $1/\beta_\infty$ times the local mean flow angle relative to the uniform velocity at infinity.

The total potential may be conveniently represented in complex notation as well. The complex potential including O(1) and $O(\alpha)$ terms is

$$\phi_0 + i\beta_\infty \psi_0 = U_\infty (x_1 + i\beta_\infty x_2) + F(\zeta) = U_\infty \zeta + F(\zeta) \quad . \tag{A.15}$$

We make a final Prandtl-Glauert transformation, on the dependent variables:

$$\phi = \phi_0 \qquad \psi = \beta_\infty \psi_0 \quad . \tag{A.16a}$$

We also introduce the complex variable

$$z = \phi_0 + i\beta_\infty \psi_0 = \phi + i\psi \quad , \tag{A.16b}$$

so that Eq. (A.15) becomes

$$z = U_\infty \zeta + F(\zeta) \quad . \tag{A.16c}$$

In our analysis we use the variables (ϕ,ψ) of Eq. (A.16a) as the independent variables. Hence, we require the mean flow quantities, especially the complex potential and its derivatives, as funtions of ϕ and ψ. However, from equation (A.16c) we see that since

$$\zeta = z/U_\infty + O(\alpha) \quad , \tag{A.17a}$$

then

$$F(\zeta) = F(z/U_\infty) + O(\alpha) \quad . \tag{A.17b}$$

Since F is already $O(\alpha)$ and $O(\alpha^2)$ terms are neglected in our theory, equation (A.17b) may be utilized without introducing any additional error. This fact is used throughout Chapters 3 and 4.

The following example will illustrate some of the ideas of this appendix. For a flat plate airfoil of length 2b at small incidence angle α to the uniform flow, the complex potential for incompressible flow can be obtained by conformal mapping. The result is

$$\phi_0^i + i\psi_0^i = U_\infty \zeta^i + F^i(\zeta^i) + O(\alpha^2) \quad , \tag{A.18a}$$

where

$$F^i(\zeta^i) = i\,\alpha \left[\log(\zeta^i - b + \sqrt{\zeta^i(\zeta^i-2b)}\,) + \zeta^i - \sqrt{\zeta^i(\zeta^i-2b)} \right] \tag{A.18b}$$

with ζ^i equal to x_1+ix_2. The corresponding perturbation potential for the compressible problem is

$$F = \frac{1}{\beta_\infty} F'(\zeta) = \frac{i\alpha}{\beta_\infty} \left[\log(\zeta - b + \sqrt{\zeta(\zeta-2b)}\ ) + \zeta - \sqrt{\zeta(\zeta-2b)} \right] , \qquad \text{(A.19a)}$$

where

$$\zeta = x_1 + i\beta_\infty x_2 \quad . \qquad \text{(A.19b)}$$

The total compressible complex potential is

$$z = \phi + i\psi = \phi_0 + i\beta_\infty \psi_0 = U_\infty \zeta + F(\zeta) + O(\alpha^2) \quad . \qquad \text{(A.20)}$$

The perturbation flow speed for the flat plate is

$$q = \mathrm{Re}\{ \frac{i\alpha}{\beta_\infty} \left[1 - \sqrt{\frac{\zeta-2b}{\zeta}} \right] \} + O(\alpha^2) \quad . \qquad \text{(A.21a)}$$

However, in light of Eq. (A.20), we can replace ζ by z/U_∞ and incur only $O(\alpha^2)$ error. That is,

$$q = \mathrm{Re}\ \{ \frac{i\alpha}{\beta_\infty} \left[1 - \sqrt{\frac{z-U_\infty 2b}{z}} \right] \} + O(\alpha^2) \quad . \qquad \text{(A.21b)}$$

In Chapter 3, where nondimensional variables are introduced, the potential is scaled by $U_\infty b$. Equation (A.21b) in nondimensional variables becomes

$$q = \mathrm{Re}\ \{ \frac{i\alpha}{\beta_\infty} \left[1 - \sqrt{\frac{z-2}{z}} \right] \} + O(\alpha^2) \quad . \qquad \text{(A.21c)}$$

APPENDIX B

ASYMPTOTIC EXPANSION BY THE METHOD OF STEEPEST DESCENT

The purpose of this appendix is to outline the method of steepest descent for expanding integrals which arise in our analysis. Two types of integrals will be considered. The first contains the "acoustic phase" multiplied by the large parameter in the exponent; in this case the exponent possesses a saddle point and the contribution to the integral is dominated by the region near the saddle. The asymptotic structure of the first type of integral is an acoustic wave. The second type of integral contains a "hydrodynamic phase" for which there is no saddle point. The steepest descent path then consists of a pair of rays in the complex plane, and the integral over each ray is endpoint dominated. The asymptotic expansion of this integral represents a field that generates no pressure fluctuations.

We start with the integral containing the acoustic phase. We consider an integral of the form

$$I_a = \int_{-\infty}^{\infty} A(\lambda)\, e^{R(-i\lambda\cos\theta - |\sin\theta|\sqrt{\lambda^2-w^2})}\, d\lambda \quad , \tag{B.1}$$

where the path of integration is the real axis. The expansion of Eq. (B.1) as $R = kr \to \infty$ is desired.

We begin by defining

$$f(\lambda) = -i\,\lambda\cos\theta - |\sin\theta|\sqrt{\lambda^2-w^2} \quad . \tag{B.2}$$

The exponent contains one saddle point, at $\lambda = \lambda_0 = -w\cos\theta$. At $\lambda = \lambda_0$,

$$f'(\lambda_0) = 0 \quad ,$$

$$f(\lambda_0) = iw \quad ,$$

and

$$f''(\lambda_0) = -i/w\sin^2\theta \quad . \tag{B.3}$$

We transform the contour of integration to the steepest descent path, along which the imaginary part of f is constant and the real part is maximum at $\lambda = \lambda_0$. The steepest descent path passes through the saddle point at an angle of $\pi/4$ with respect to the real axis, as can be seen from the following local analysis. Near the saddle point,

$$f(\lambda) - f(\lambda_0) \simeq 1/2\ (\lambda-\lambda_0)^2\ f''(\lambda_0) \quad . \tag{B.4a}$$

Let

$$\lambda-\lambda_0 = \rho\ e^{i\gamma} \quad . \tag{B.4b}$$

Using equations (B.3) and (B.4b), we find that in the directions $\gamma = -\pi/4$ and $3\pi/4$, the left-hand side of (B.4a) is real and negative. Hence, as $R \to \infty$ the contribution to the integral along the steepest descent path is dominated by the region near $\lambda = \lambda_0$ (since there are no other saddle points.)

To calculate the asymptotic expansion we make the change of variable

$$f(\lambda) - f(\lambda_0) = -\ t^2 \quad . \tag{B.5}$$

Then

$$d\lambda \simeq \sqrt{2w}\ |\sin\theta|\ e^{-i\pi/4}\ dt \quad . \tag{B.6}$$

We then expand the amplitude function $A(\lambda)$ about $t=0$ ($\lambda=\lambda_0$) and integrate term by term. The first term of the expansion is

$$I_a \sim \sqrt{2\pi w}\ e^{-i\pi/4}\ |\sin\theta|\ f(\lambda_0)\ \frac{e^{iwR}}{\sqrt{R}} \quad . \tag{B.7}$$

This result is used often in our asymptotic analysis. For cases when $f(\lambda_0)$ is not analytic near $\lambda = \lambda_0$, Eq. (B.7) is not valid and a more involved procedure is necessary. Such a case is dealt with in Appendix C.

The equation for the steepest descent path is not required in order to obtain the asymptotic expansion of I_a. However, to be sure that the original contour can be deformed onto the steepest descent path without crossing any singularities, or picking up a contribution from the arc at infinity, some information about the steepest descent path is useful. For the exponent just considered, it turns out that the equation for the steepest descent path can be found.

The path of steepest descent is defined by

$$\mathrm{Im}\ \{\ -\ |\sin\theta|\ \sqrt{\lambda^2-w^2}\ -\ i\ \lambda\ \cos\theta\ \} = w \quad , \tag{B.8}$$

where w is the imaginary part of $f(\lambda)$ at the saddle point λ_0. Along the steepest descent path, we denote the real part of λ by x and the

imaginary part by y. Fig. (B.1) shows the geometry for defining a point P on the steepest descent path. As we see from Fig. (B.1),

$$\sqrt{\lambda^2-w^2} = -i\,[\,(w+x)^2 + y^2\,]^{1/4}\,[\,(w-x)^2 + y^2\,]^{1/4}\, e^{i(\theta_1-\theta_2)/2} \quad . \tag{B.9}$$

Upon inserting the imaginary part of (B.9) into (B.8) and rearranging terms, we have the following equation defining the steepest descent path:

$$|\sin\theta|\,[\,(w+x)^2 + y^2\,]^{1/4}\,[\,(w-x)^2 + y^2\,]^{1/4} \cos\frac{\theta_1-\theta_2}{2} = w + x\cos\theta \quad . \tag{B.10}$$

The $\cos(\theta_1-\theta_2)/2$ can be expanded by the relations

$$\cos\frac{\theta_1-\theta_2}{2} = \sqrt{\frac{1+\cos(\theta_1-\theta_2)}{2}} \tag{B.11a}$$

and

$$\cos(\theta_1-\theta_2) = \cos\theta_1\cos\theta_2 + \sin\theta_1\sin\theta_2$$

$$= \frac{w+x}{\sqrt{(w+x)^2+y^2}}\,\frac{w-x}{\sqrt{(w-x)^2+y^2}} + \frac{y}{\sqrt{(w+x)^2+y^2}}\,\frac{y}{\sqrt{(w-x)^2+y^2}} \quad . \tag{B.11b}$$

Using (B.11a,b) in (B.10), squaring, and rearranging, we have

$$\sin^2\theta\,[(w+x)^2+y^2]^{1/2}\,[(w-x)^2+y^2]^{1/2} = 2(w+x\cos\theta)^2 - (w^2-x^2+y^2)\sin^2\theta \quad . \tag{B.12}$$

After squaring one last time and cancelling the y^4 terms, we can easily solve for y^2 in terms of x:

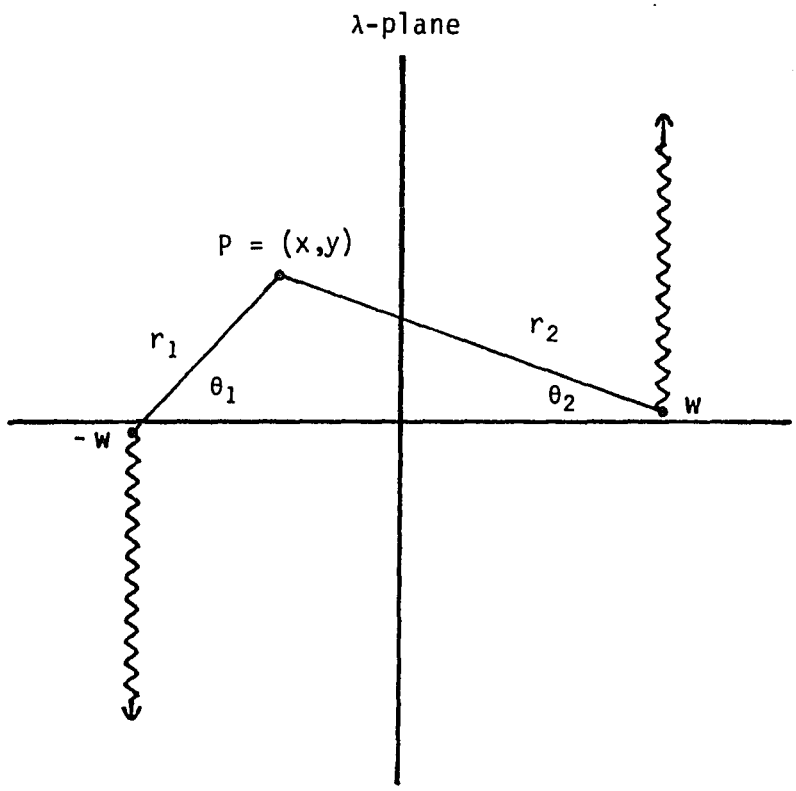

Fig. B.1 Geometry for defining point on steepest descent path.

$$y^2 = \frac{(x+w\cos\theta)^2\,(w+x\cos\theta)^2}{\sin^2\theta\,(x^2+w^2+2wx\cos\theta)} \quad .$$

The minus square root is the desired one, for it gives the proper slope (-1) of the steepest descent path at the saddle point. Hence,

$$y = -\frac{(x+w\cos\theta)\,(w+x\cos\theta)}{|\sin\theta|\,(x^2+w^2+2wx\cos\theta)^{1/2}} \qquad \text{(B-13)}$$

is the equation for the steepest descent contour.

One consequence of Eq. (B.13) is that the contour crosses the real axis at the point $x = -w/\cos\theta$ as well as at the saddle point. At the point $x = -w/\cos\theta$ the slope of the curve is

$$\frac{dy}{dx} = |\cos\theta| \quad . \qquad \text{(B.14)}$$

The behavior of the curve at infinity can also be obtained from Eq. (B.13). As $x \to \pm\infty$,

$$y \to -\frac{|x|\,\cos\theta}{|\sin\theta|} \quad . \qquad \text{(B.15)}$$

The steepest descent path can be easily drawn from the information in equations (B.13,14,15). The curve is shown in Fig. (B.2). The dashed line is a deformation of the steepest descent path around the branch cut emanating from the point $\lambda = -\delta$, to account for the cases where $A(\lambda)$ in Eq. (B.1) contains a branch point at $-\delta$. The consequence of this deformation is discussed below.

The integral along the branch cut $C_{-\delta}$ must be added to the integral along the steepest descent path to determine the asymptotic

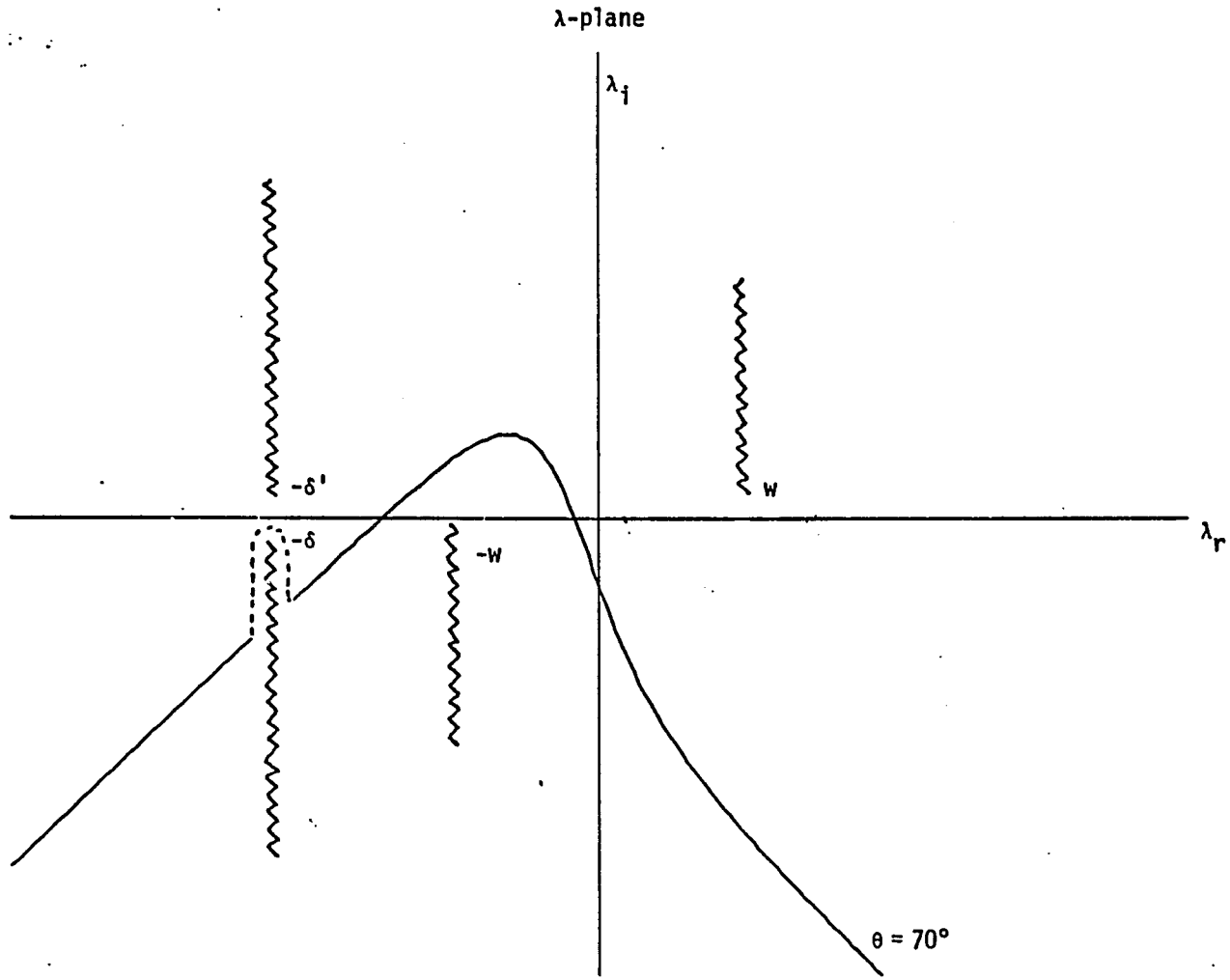

Fig. B.2 Steepest descent path for integrals with acoustic phase.

expansion of I_a in Eq. (B.1). However, we will now show that the contribution from the branch-cut integral is exponentially small. Along $C_{-\delta}$,

$$\lambda = -\delta + \rho\, e^{-i\pi/2} \quad , \quad 0 < \rho < \rho_0$$

$$\lambda - w = [(\delta+w)^2 + \rho^2]^{1/2}\, e^{i\theta_w} \quad , \quad \theta_w = -\pi + \arctan\left(\frac{\rho}{\delta+w}\right)$$

$$\lambda + w = [(\delta-w)^2 + \rho^2]^{1/2}\, e^{i\theta_{-w}} \quad , \quad \theta_{-w} = \pi + \arctan\left(\frac{\rho}{\delta-w}\right)$$

where ρ_0 is the value at which the steepest descent path crosses the branch cut. The integrand is proportional to the term

$$\exp\left\{-kr\,|\sin\theta|\,[(\delta+w)^2 + \rho^2]^{1/4}\,[(\delta-w)^2 + \rho^2]^{1/4}\cos\left(\frac{\theta_w + \theta_{-w}}{2}\right)\right\}$$

This factor attains the largest value,

$$\exp\left\{-kr\,|\sin\theta|\,[(\delta+w)^2 + \rho_0^2]^{1/4}\,[(\delta-w)^2 + \rho_0^2]^{1/4}\cos\left(\frac{\theta_{w,0} + \theta_{-w,0}}{2}\right)\right\} \quad ,$$

at the point $\rho = \rho_0$ (where $\theta_w = \theta_{w,0}$, $\theta_{-w} = \theta_{-w,0}$). Hence, the contribution from the integral along the branch cut $C_{-\delta}$ is exponentially small in $kR|\sin\theta| = k|\psi|$, and the asymptotic expansion obtained in the absence of the branch cut is unchanged.

We next consider integrals where the exponent in the integrand contains the "hydrodynamic phase." Two integrals of this type occur in the particular solution $H_{2,p}$ to Goldstein's wave equation. We illustrate the method on the first one, which has the form

$$I_h \sim \int_{-\infty}^{\infty} \frac{M(\gamma)}{\sqrt{\gamma+i\varepsilon}} e^{R(-i\gamma\cos\theta - |\sin\theta|\sqrt{\gamma-i\varepsilon}\,\sqrt{\gamma+i\varepsilon}\,)} d\gamma \quad . \quad (B.16)$$

The contour of integration is the real axis. The function $B(\gamma)$ is analytic except for simple poles away from the area of interest. The product of the square roots is simply a complex representation for $|\gamma|$. The branch cuts and contour are displayed in Fig. (B.3).

As in the saddle point method, we denote the exponent (all but the large parameter) by $f(\gamma)$:

$$f(\gamma) = -i\,\gamma\cos\theta - |\sin\theta|\,\sqrt{\gamma-i\varepsilon}\,\sqrt{\gamma+i\varepsilon} \quad . \quad (B.17)$$

We first suppose $\mathrm{Re}\{\gamma\} > 0$. In that case we see from Eq. (B.17) and Fig. (B.3) that

$$\sqrt{\gamma-i\varepsilon}\,\sqrt{\gamma+i\varepsilon} = \gamma \quad (B.18a)$$

and

$$f(\gamma) = -i\,\gamma\cos\theta - |\sin\theta|\,\gamma \quad . \quad (B.18b)$$

The real and imaginary parts of $f(\gamma)$ are

$$f_r = -|\sin\theta|\,\gamma_r + \gamma_i\cos\theta \quad (B.19a)$$

$$f_i = -\cos\theta\,\gamma_r - |\sin\theta|\,\gamma_i \quad . \quad (B.19b)$$

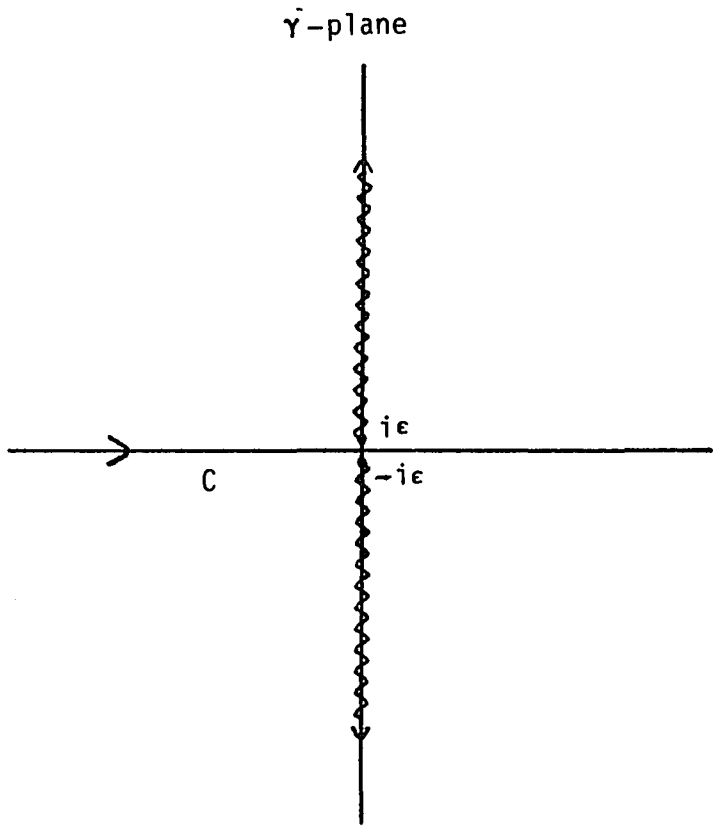

Fig. B.3 Branch cuts and contour of integration for hydrodynamic integral.

The subscripts indicate real and imaginary parts. Along the line

$$\gamma_i = - \frac{\cos\theta}{|\sin\theta|} \gamma_r \quad , \tag{B.20}$$

the imaginary part of f is 0 and the real part is negative for positive γ_r. Thus we wish to deform half of the original contour, the positive real axis, onto the ray defined by Eq. (B.20). The contribution from the connecting arc at infinity is seen to be exponentially small. The new contour is shown in Fig. (B.4), along with the left half of the steepest descent path which is found later. As one moves along the ray away from the origin the exponent becomes increasingly negative, and as $R \to \infty$ the integral is dominated by the contribution near the origin. To obtain the expansion we set

$$\gamma = \rho\, e^{i\phi_+} \quad . \tag{B.21}$$

The angle ϕ_+ is related to θ through Eq. (B.20), which implies that

$$\tan \phi_+ = - \frac{\cos\theta}{|\sin\theta|} \tag{B.22a}$$

and

$$\phi_+ = \theta - \pi/2 \qquad \text{for } 0 < \theta < \pi \tag{B.22b}$$

$$\phi_+ = 3\pi/2 - \theta \qquad \text{for } \pi < \theta < 2\pi \quad . \tag{B.22c}$$

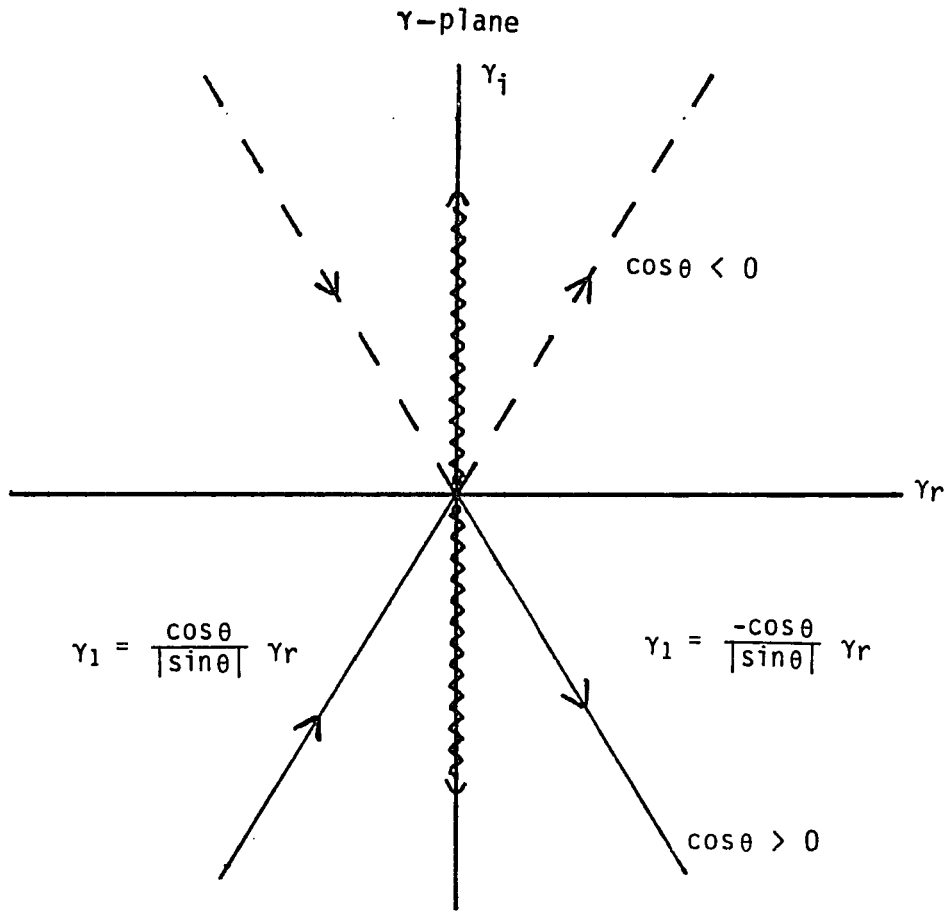

Fig. B.4 Steepest descent path for integrals with hydrodynamic phase.

In terms of ρ and ϕ_+ the original integral (B.16) may be written

$$I_h = \int_0^\infty \frac{M(\rho e^{i\phi_+})\, e^{-R\rho}\, e^{i\phi_+}\, d\rho}{\sqrt{\rho}\, e^{i\phi_+/2}}$$

$$= e^{i\phi_+/2} \int_0^\infty \frac{M(\rho e^{i\phi_+})\, e^{-R\rho}\, d\rho}{\sqrt{\rho}} \quad . \tag{B.23}$$

The asymptotic series is obtained by expanding M for small ρ and integrating term-by-term. The first term is

$$M(0)\, e^{i\phi_+/2} \sqrt{\frac{\pi}{R}} \quad . \tag{B.24}$$

We next consider the half of the original contour where $\mathrm{Re}\{\gamma\} < 0$. The procedure here is analagous to the $\mathrm{Re}\{\gamma\} > 0$ case. This time the imaginary part of f is zero and the real part negative along the line

$$\gamma_i = \frac{\cos\theta}{|\sin\theta|}\, \gamma_r \quad . \tag{B.25}$$

The steepest descent path, defined by Eq. (B.25) for $\gamma_r < 0$, is displayed in Fig. (B.4). After deforming the negative real axis onto this path, we introduce the variable of integration ρ by

$$\gamma = \rho\, e^{i\phi_-} \quad . \tag{B.26a}$$

The angle ϕ_-, determined from Eq. (B.25) and the branch cuts in Fig. (B.3) is related to θ by

$$\phi_- = \frac{3\pi}{2} - \theta \qquad \text{for} \qquad 0 < \theta < \pi \tag{B.26b}$$

$$\phi_- = \theta - \frac{\pi}{2} \qquad \text{for} \qquad \pi < \theta < 2\pi \quad . \tag{B.26c}$$

As before the integral is dominated by the contribution near the origin; hence, to obtain the asymptotic expansion we expand $M(\rho e^{i\phi_-})$ for small ρ and integrate term by term. The first term of the series is

$$- e^{i\phi_-/2} \; M(0) \sqrt{\frac{\pi}{R}} \quad . \tag{B.27}$$

The total asymptotic expansion is the sum of the integrals (B.24) and (B.27). The sum can be written as

$$I_h \sim M(0) \sqrt{\frac{\pi}{R}} \left[e^{i\phi_+/2} - e^{i\phi_-/2} \right]$$

To write ϕ_+ and ϕ_- in terms of θ we utilize equations (B.22) and (B.26). In terms of the physical variable θ the expansion is

$$I_h \sim M(0) \sqrt{\frac{\pi}{R}} \left[e^{i(\theta-\pi/2)/2} - e^{i(3\pi/2-\theta)/2} \right] \quad , \; 0<\theta<\pi \quad . \tag{B.29a}$$

$$\sim M(0) \sqrt{\frac{\pi}{R}} \left[e^{i(3\pi/2-\theta)/2} - e^{i(\theta-\pi/2)/2} \right] \quad , \; \pi<\theta<2\pi \quad . \tag{B.29b}$$

For all θ, equations (B.29a) and (B.29b) reduce to the simple result

$$I_h \sim e^{-i\pi/4} \; M(0) \sqrt{\frac{\pi}{R}} \cos\frac{\theta}{2} \quad . \tag{B.30}$$

The actual physical potential is Eq. (B.30) multiplied by $e^{i\delta\Phi}$. Since this potential has only the convected phase, it generates no pressure fluctuations.

APPENDIX C

SOLUTION FOR H_{2c}

In this appendix, we calculate the complementary solution to the antisymmetric part of the particular solution H_{2p}. The antisymmetric part of H_{2p} is

$$H_{2p,ant} = \frac{e^{i\pi/4}}{8\sqrt{\pi}\,(\delta^2+k_n^2)} \int_{-\infty}^{\infty} \left[\frac{i\, f_1(\lambda)\, \sin k_n\Psi}{\sqrt{\lambda+\delta'}} - \frac{\mathrm{sgn}\Psi\, f_2(\lambda)\, \cos k_n\Psi}{\sqrt{\lambda+\delta}} \right]$$

$$\times \frac{e^{a(\lambda,\Phi,\Psi)}\, d\lambda}{(\lambda-\lambda_1)(\lambda-\lambda_2)} + \frac{e^{i\pi/4}\, \mathrm{sgn}\Psi}{8\sqrt{\pi}\,(\delta^2+k_n^2)} \int_{-\infty}^{\infty} \frac{f_2(\lambda)\, e^{hy(\lambda,\Phi,\Psi)}\, d\lambda}{\sqrt{\lambda+\delta}\,(\lambda-\lambda_1)\,(\lambda-\lambda_2)} \quad , \qquad (C.1)$$

where $f_1(\lambda)$ and $f_2(\lambda)$ are defined in Eqs. (3.15c,d), λ_1 and λ_2 in Eq. (3.15e), and $a(\lambda,\Phi,\Psi)$ and $hy(\lambda,\Phi,\Psi)$ in Eq. (3.9b) and (3.15b). The appropriate branch cuts for the square roots and the location of the poles are shown in Fig. (3.4). The normal derivative on the airfoil associated with the particular solution is

$$\left.\frac{\partial H_{2p,ant}}{\partial \Psi}\right|_{\Psi=0} = \frac{1}{\sqrt{2\pi}} \int_{-\infty}^{\infty} B(\lambda)\, e^{-i\lambda\Phi}\, d\lambda \quad , \qquad (C.2a)$$

where

$$B(\lambda) = \frac{e^{i\pi/4}}{4\sqrt{2}\,(\delta^2+k_n^2)}\left[\sqrt{\lambda+\delta}\; f_2(\lambda) + \frac{ik_n f_1(\lambda)}{\sqrt{\lambda+\delta}} - \frac{\sqrt{\lambda^2-w^2}\; f_2(\lambda)}{\sqrt{\lambda+\delta}}\right]$$

$$\times \frac{1}{(\lambda-\lambda_1)(\lambda-\lambda_2)}. \qquad \text{(C.2b)}$$

To cancel the velocity on the airfoil we need a complementary solution satisfying

$$\left[\frac{\partial^2}{\partial\Phi^2} + \frac{\partial^2}{\partial\Psi^2} + w^2\right]H_{2C} = 0 \qquad \text{(C.3a)}$$

$$\frac{\partial H_{2C}}{\partial\Psi}\bigg|_{\Psi=0} = -\frac{1}{\sqrt{2\pi}}\int_{-\infty}^{\infty} B(\lambda)\, e^{-i\lambda\Phi}\, d\lambda \quad \text{for } \Phi > 0 \qquad \text{(C.3b)}$$

$$H_{2,c}\Big|_{\Psi=0^-}^{\Psi=0^+} = 0 \text{ for } \Phi < 0 \qquad \text{(C.3c)}$$

$$\frac{\partial H_{2C}}{\partial\Psi} \text{ continuous everywhere} \quad . \qquad \text{(C.3d)}$$

Equation (C.3) can be solved by applying a Fourier transform in Φ and integrating the resulting ordinary differential equation. The result is,

$$H_{2C} = \operatorname{sgn}\Psi \int_{-\infty}^{\infty} C_+(\lambda)\, e^{-i\lambda\Phi - |\Psi|\sqrt{\lambda^2-w^2}}\, d\lambda \quad . \qquad \text{(C.4)}$$

The plus subscript on the unknown function $C(\lambda)$ indicates that it is analytic in the upper half plane, which is necessary in order that there be no jump in potential in front of the airfoil (eq. (C.3c)). To

determine $C_+(\lambda)$ we proceed by introducing the unknown function $u(\Phi)$ defined by

$$\frac{\partial H_{2c}}{\partial \Psi} = u(\Phi) - \frac{1}{\sqrt{2\pi}} \int_{-\infty}^{\infty} B(\lambda)\, e^{-i\lambda\Phi}\, d\lambda \quad . \tag{C.5}$$

By the boundary condition (C.3b), $u(\Phi)$ is 0 for $\Phi > 0$. Transforming eq. (C.5) we have

$$-\sqrt{\lambda^2-w^2}\; C_+(\lambda) = U_-(\lambda) - B(\lambda) \tag{C.6a}$$

or

$$-\sqrt{\lambda+w}\; C_+(\lambda) = \frac{U_-(\lambda)}{\sqrt{\lambda-w}} - \frac{E(\lambda)}{\sqrt{\lambda-w}} \quad . \tag{C.6b}$$

The minus subscript on $U(\lambda)$ denotes analyticity in the lower half plane. The last term in Eq. (C.6b) will now be split into the sum of two functions, each analytic in one half plane. By observing the location of the various poles and branch points in Fig. (3.4), we see that the last term in eq. (C.6b) may be written as

$$\frac{B(\lambda)}{\sqrt{\lambda-w}} = \frac{D_-(\lambda) + D_+(\lambda)}{(\lambda-\lambda_1)(\lambda-\lambda_2)} \quad , \tag{C.7a}$$

where

$$D_-(\lambda) = e^{i\pi/4}/(4\sqrt{2}\,(\delta^2+k_n^2)) \left[\frac{\sqrt{\lambda+\delta'}\; f_2(\lambda)}{\sqrt{\lambda-w}} + \frac{i\, k_n\, f_1(\lambda)}{\sqrt{\lambda-w}\;\sqrt{\lambda+\delta'}} \right] \tag{C.7b}$$

and

$$D_+(\lambda) = - e^{i\pi/4}/(4\sqrt{2}\,(\delta^2+k_h^2)\,\frac{\sqrt{\lambda+w}\;f_2(\lambda)}{\sqrt{\lambda+\delta}} \quad . \tag{C.7c}$$

Again, the plus and minus subscripts denote the region of analyticity. It is fortunate that $B(\lambda)/\sqrt{\lambda-w}$ can be written as the sum of terms each having branch points all in the same half plane. The resulting Wiener-Hopf split is greatly simplified; it involves separating terms with only simple pole singularities. The split is

$$\frac{B(\lambda)}{\sqrt{\lambda-w}} = \left[\frac{D_-(\lambda)}{(\lambda-\lambda_1)(\lambda-\lambda_2)} - \frac{D_-(\lambda_2)}{(\lambda_2-\lambda_1)(\lambda-\lambda_2)}\right]_- + \left[\frac{D_-(\lambda_2)}{(\lambda_2-\lambda_1)(\lambda-\lambda_2)}\right]_+$$
$$+ \left[\frac{D_+(\lambda)}{(\lambda-\lambda_1)(\lambda-\lambda_2)} - \frac{D_+(\lambda_1)}{(\lambda-\lambda_1)(\lambda_1-\lambda_2)}\right]_+ + \left[\frac{D_+(\lambda_1)}{(\lambda-\lambda_1)(\lambda_1-\lambda_2)}\right]_- \quad . \tag{C.8}$$

Utilizing eq. (C.8) in (C.6b), we obtain

$$-\sqrt{\lambda+w}\;C_+(\lambda) + \frac{D_-(\lambda_2)}{(\lambda_2-\lambda_1)(\lambda-\lambda_2)} + \frac{D_+(\lambda)}{(\lambda-\lambda_1)(\lambda-\lambda_2)} - \frac{D_+(\lambda_1)}{(\lambda-\lambda_1)(\lambda_1-\lambda_2)}$$
$$= \frac{U_-(\lambda)}{\sqrt{\lambda-w}} - \frac{D_-(\lambda)}{(\lambda-\lambda_1)(\lambda-\lambda_2)} + \frac{D_-(\lambda_2)}{(\lambda_2-\lambda_1)(\lambda-\lambda_2)} - \frac{D_+(\lambda_1)}{(\lambda-\lambda_1)(\lambda_1-\lambda_2)} \quad . \tag{C.9}$$

Since the two sides of eq. (C.9) are equal on the strip $\mathrm{Im}(-w) < \mathrm{Im}(\lambda) < \mathrm{Im}(w)$, they are analytic continuations of each other and form an entire function. We turn to the edge conditions in the physical plane to determine the unknown analytic function.

The edge condition we impose is that the solution H_x be no

more singular near the origin than the zero-incidence angle solution H_0. The solution H_0 possessed a $1/\sqrt{R}$ ($R^2 = \phi^2+\psi^2$) singularity in velocity or $\sqrt{R}$ in potential as R approached zero. This same edge behavior arose naturally in the particular solution H_{2p} obtained by double Fourier transforms. Thus here we require that H_{2c} behave as $R^{1/2}$ locally, and hence that the transform function $C_+(\lambda)$ decay as $\lambda^{-3/2}$ in the upper half plane. ($U_-(\lambda)$ decays as $\lambda^{-1/2}$ in the lower half plane.)

The entire function defined by equation (C.9) can be determined by analyzing the left-hand side as λ tends to infinity in the upper half plane. The first, second, and fourth terms decay to zero and the third approaches a limiting value of

$$-4ik_nC_4 - 4i\delta C_3 \quad . \tag{C.10}$$

Hence the bounded, entire function is equal to the constant in eq. (C.10). Setting the left side of (C.9) equal to this constant and isolating $C_+(\lambda)$, we obtain

$$C_+(\lambda) = \frac{4ik_nC_4+4i\delta C_3}{\sqrt{\lambda+w}} + \frac{1}{\sqrt{\lambda+w}}$$

$$\left[\frac{D_-(\lambda_2)}{(\lambda_2-\lambda_1)(\lambda-\lambda_2)} + \frac{D_+(\lambda)}{(\lambda-\lambda_1)(\lambda-\lambda_2)} - \frac{D_+(\lambda_1)}{(\lambda-\lambda_1)(\lambda_1-\lambda_2)}\right] \quad . \tag{C.11}$$

Inserting eq. (C.11) into (C.4) and writing D_+ and D_- explicitly, we have the final form of the solution:

$$H_{2,c} = -\frac{\operatorname{sgn}\Psi\, e^{i\pi/4}}{8\sqrt{\pi}\,(\delta^2+k_\eta^2)} \int_{-\infty}^{\infty} \left[4ik_\eta C_4 + 4i\delta C_3 - \frac{\sqrt{\lambda_1+w}\; f_2(\lambda_1)}{(\lambda_1-\lambda_2)\sqrt{\lambda_1+\delta}\;(\lambda-\lambda_1)}\right.$$

$$\left. + \frac{(\lambda_2+\delta)\; f_2(\lambda_2) + i\, k_\eta\, f_1(\lambda_2)}{(\lambda_1-\lambda_2)\sqrt{\lambda_2-w}\sqrt{\lambda_2+\delta}\,(\lambda-\lambda_2)} + \frac{\sqrt{\lambda+w}\; f_2(\lambda)}{\sqrt{\lambda+\delta}\;(\lambda-\lambda_1)\;(\lambda-\lambda_2)}\right] \frac{e^{a(\lambda,\Phi,\Psi)}\, d\lambda}{\sqrt{\lambda+w}}\ . \tag{C.12}$$

APPENDIX D

UNIFORM ASYMPTOTIC EXPANSION OF TRAILING-EDGE SCATTERED FIELD

In this appendix we calculate an asymptotic expansion as $R = kr \to \infty$ for the integral

$$I = e^{iRw\cos\theta} \int_{C_\lambda} \frac{e^{R(-|\sin\theta| \sqrt{\lambda^2-w^2} - i(\lambda+w)\cos\theta)}\, d\lambda}{(\lambda+\delta)\,(\lambda+w)\,\sqrt{\lambda-w}} \quad . \tag{D.1}$$

Here C_λ is the steepest descent path in the λ-plane, drawn in Appendix B. For convenience we have deleted the "t" subscripts on the R and θ trailing-edge variables of the actual scattering problem. We have also put an $\exp(iRw\cos\theta)$ inside and outside the integral. We will develop an asymptotic expansion valid even as θ tends to zero, where the saddle point and pole coalesce and ordinary saddle point methods fail. The expansion will be found using Van Der Waerden's (1950) method.

Van Der Waerden's method begins by making the change of variable

$$u = |\sin\theta| \sqrt{\lambda^2-w^2} + i\cos\theta\,(\lambda+w) \quad . \tag{D.2a}$$

The inverse transformation is

$$\lambda = -(ui\cos\theta + w\cos^2\theta) \pm |\sin\theta| \sqrt{u-iw(1+\cos\theta)}\,\sqrt{u+iw(1-\cos\theta)} \quad . \tag{D.2b}$$

We select the minus sign for the transformation, which maps the region below the steepest descent path of the λ plane onto the u plane. The image of steepest descent path itself wraps around the branch point $u = -iw(1-\cos\theta)$, which is the image of the saddle point $\lambda = -w\cos\theta$. It is natural that the saddle point maps to a branch point, since at the saddle point the exponent u is a quadratic function of λ, or λ is a function of the square root of u. The branch points in the u plane are shown in Fig. (D.1), along with the image of the steepest descent path.

The typical procedure for finding the asymptotic expansion with this method is to expand the integrand about the branch point and integrate term by term. (There are also rules for deforming the contour around the branch cut, if one does not start with the steepest descent curve in the λ plane.) Singularities far to the left of the branch cut need not be considered, and singularities far to the right will be asymptotically negligible. Difficulties arise when a pole lies near the branch point, as is the case in our problem for small values of θ. To handle this case a variation of the method is required, which is described below.

We write the integral as

$$I = \int_{C_u} P(u)\, e^{-Ru}\, du \quad , \tag{D.3a}$$

where

$$P(u) = \frac{1}{\lambda(u) + w} \frac{1}{\sqrt{\lambda(u)-w}} \frac{1}{\lambda(u)+\delta} \frac{d\lambda}{du} \quad . \tag{D.3b}$$

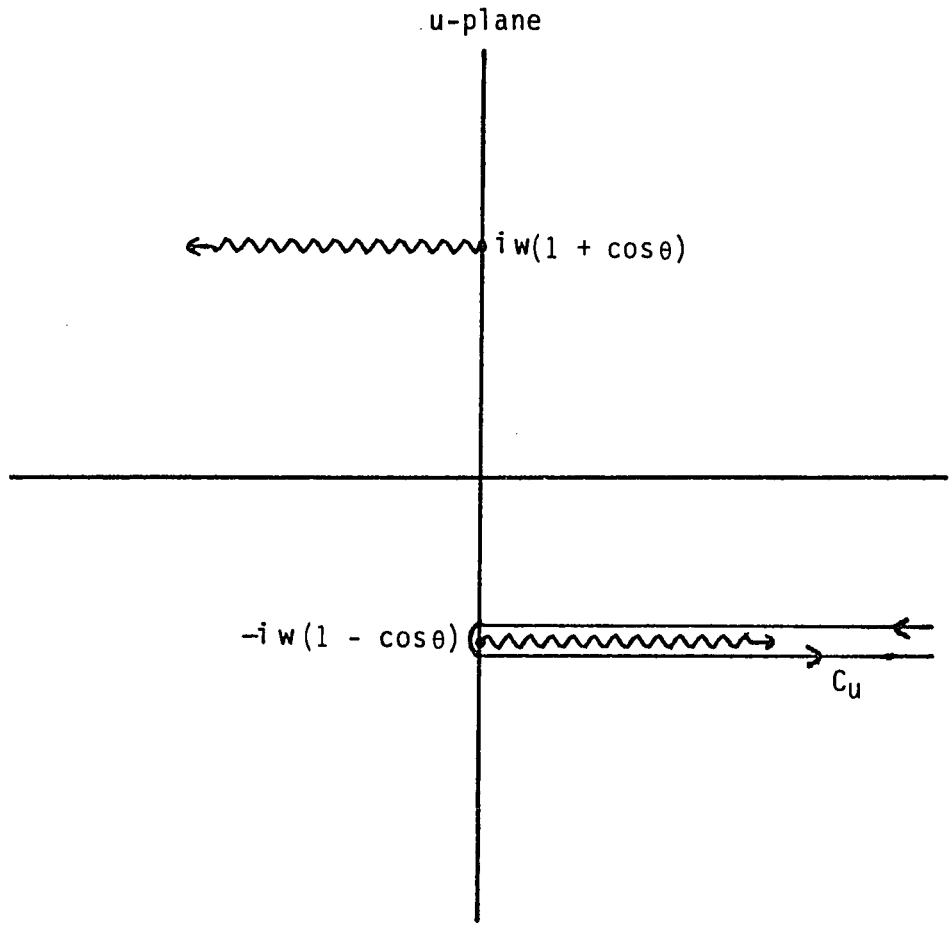

Fig. D.1 Branch cuts and path of integration in the u-plane.

The kernel P(u) has a pole at u = 0 (since $\lambda(0) = -w$) and two branch points (those of $\lambda(u)$), which for simplicity we denote as d_+ and d_-. The sign designates the location in the appropriate half plane. To proceed we temporarily make the additional change of variable

$$s = \sqrt{u-d_-} \quad .$$

The function P has poles at s = 0 and $s = b = \sqrt{-d_-}$. The poles of P can be isolated by writing

$$s\,P(s) = \frac{\beta}{s-b} + T(s) \qquad \text{(D.4a)}$$

or

$$P(s) = \frac{\beta}{s(s-b)} + \frac{T}{s} \quad . \qquad \text{(D.4b)}$$

The function T(s) is analytic at s=0 and s=b. The quantity β is the residue of sP(s) at s=0, and can be found be examining Eq. (D.4a) near s=b or u=0. The local analysis shows that

$$\beta = \frac{i}{\sqrt{2w}\ (\delta-w)} \quad . \qquad \text{(D.5)}$$

Setting $\beta = b\,\gamma$, we have

$$\gamma = \frac{e^{i\pi/4}}{w\sqrt{2(1-\cos\theta)}\ (\delta-w)} \qquad \text{(D.6a)}$$

and

$$P(s(u)) = \gamma \left[\frac{1}{s-b} - \frac{1}{s}\right] + \frac{T}{s} = \frac{\gamma}{s-b} + \frac{T-\gamma}{s} \quad . \qquad (D.6b)$$

The integral we wish to evaluate (Eq. (D.3a)) can now be written as

$$I = \int_{C_u} \frac{T-\gamma}{s} e^{-Ru}\, du + \gamma \int_{C_u} \frac{e^{-Ru}}{s-b}\, du = I_1 + I_2 \quad . \qquad (D.7)$$

The integrand of I_1 contains no pole near the branch point $u = d_-$, as we see by writing out $s(u)$:

$$I_1 = \int_{C_u} \frac{T-\gamma}{\sqrt{u-d_-}} e^{-Ru}\, du \quad . \qquad (D.8a)$$

The asymptotic expansion of I_1 can be obtained by expanding the integrand (excluding the exponential) near $u = u_-$ and integrating term by term. The first term of the expansion is

$$I_1 \sim \frac{\sqrt{2}\, e^{i\pi/4}\, e^{-Rd} \sqrt{\pi}}{w \sqrt{1-\cos\theta}\, (\delta - w\cos\theta) \sqrt{R}} + O(1/R) \quad . \qquad (D.8b)$$

It is most convenient to evaluate I_2 in the s-plane, where the integral takes the form

$$I_2 = \gamma\, e^{-Rd} \int_{\infty}^{-\infty} \frac{e^{-Rs^2}\, 2\, s\, ds}{s-b} \quad . \qquad (D.9)$$

The path of integration and the pole are shown in Fig. (D.2). Reversing the limits and extracting a minus sign, and multiplying numerator and denominator of the integrand by $s+b$, we obtain

$$I_2 = -\gamma\, e^{-Rd_-} K \quad , \qquad (D.10a)$$

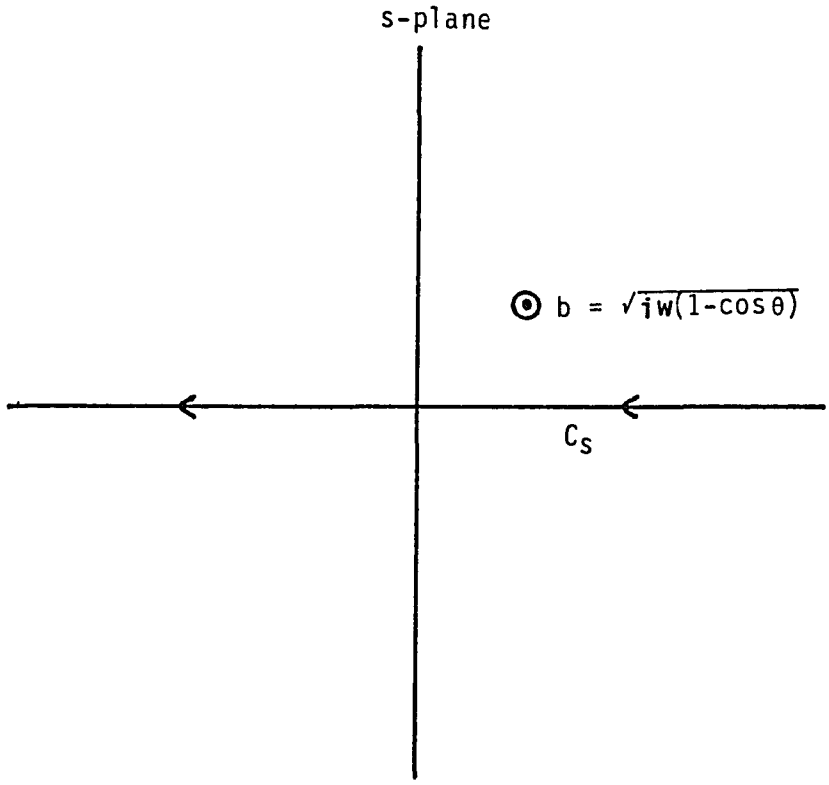

Fig. D.2 Contour of integration and pole location in the s-plane.

where

$$K = \int_{-\infty}^{\infty} \frac{2s(s+b)}{s^2-b^2} e^{-Rs^2} ds \quad . \tag{D.10b}$$

Only the even part of the integrand contributes to the integral, i.e.,

$$K = \int_{-\infty}^{\infty} \frac{2s^2}{s^2-b^2} e^{-Rs^2} ds = \int_0^{\infty} \frac{4s^2}{s^2-b^2} e^{-Rs^2} ds \quad . \tag{D.11}$$

Eq. (D.11) is one form of the final expression for K. The following sequence of steps will convert the result into a more familiar one, in terms of a complementary error function or Fresnel integral.

First, let $c = -b^2$. Multiplying K by e^{-Rc} and differentiating with respect to R, we find

$$\frac{d}{dR} e^{-Rc} K = -\int_0^{\infty} 4 s^2 e^{-R(s^2+c)} ds = -\sqrt{\pi} e^{-Rc} R^{-3/2} \quad . \tag{D.12}$$

Integrating Eq. (D.12) from R to ∞, we obtain

$$e^{-Rc} K = \sqrt{\pi} \int_R^{\infty} e^{-yc} y^{-3/2} dy \tag{D.13a}$$

or

$$K = \sqrt{\pi c}\, e^{Rc} \int_{Rc}^{\infty} e^{-x} x^{-3/2} dx \quad . \tag{D.13b}$$

The branch cut for $\sqrt{c}$ is taken along the negative real axis, so that

$$\sqrt{c} = e^{-i\pi/4} \sqrt{w(1-\cos\theta)} \quad . \tag{D.13c}$$

The final expression for K is obtained by integrating once by parts, and making the change of variable $x = -iv^2$:

$$K = \frac{2\sqrt{\pi}}{\sqrt{R}} + 4\, i\, \sqrt{\pi w(1-\cos\theta)}\; e^{Rc}\; E(\sqrt{Rw(1-\cos\theta)}) \qquad (D.14a)$$

where

$$E(a) = \int_a^\infty e^{iv^2}\, dv \quad . \qquad (D.14b)$$

We now collect the various terms comprising our original integral. Inserting Eq. (D.14) into Eq. (D.10a), adding the result to the asymptotic expansion in Eq. (D.8b), and writing out explicitly the constants γ,c, and d_-, we have

$$I \sim \frac{2^{3/2}\sqrt{\pi}\; e^{-i\pi/4}}{\sqrt{w}\;(\delta-w)}\; e^{iRw\cos\theta}\; E(\sqrt{Rw(1-\cos\theta)}) -$$

$$e^{i\pi/4}\sqrt{\frac{2\pi}{w}}\left[\frac{1}{\delta-w} - \frac{1}{\delta-w\cos\theta}\right]\frac{e^{iwR}}{\sqrt{Rw(1-\cos\theta)}} \quad + \quad O(1/R) \qquad (D.17)$$

with E(a) defined in (D.14b). This is an asymptotic expansion as $R\to\infty$ valid for all values of θ. Actually, the term containing the Fresnel integral is an exact rather than asymptotic result. As noted earlier, it is just another form for the integral of the part of P(u) containing the pole near the branch point.

When θ is O(1) the asymptotic expansion of the Fresnel integral,

$$F(a) \sim -\frac{e^{ia^2}}{2ia}$$

may be used to reduce (D.17) to

$$I \sim \frac{e^{i\pi/4}\sqrt{2\pi}\, e^{iwR}}{\sqrt{w}\,(\delta - w\cos\theta)\sqrt{Rw(1-\cos\theta)}} \quad . \tag{D.18}$$

This is the result obtained by the usual method of steepest descent.

APPENDIX E

FORMULA FOR ACOUSTIC POWER

The purpose of this appendix is to write the general formula for acoustic power in terms of our modified potential h and potential-streamline coordinates (ϕ,ψ). The formula applies in the geometric farfield, where the mean flow becomes uniform. All quantities mentioned are dimensional, as in Chapter 2, until the end of the appendix where we convert to nondimensional forms.

The definition of acoustic power, for the case of a two-dimensional mean flow, is (Goldstein, 1976b)

$$\frac{\text{Power}}{\text{span}} = \int \overline{I} \cdot \overline{n}\, ds \quad . \tag{E.1a}$$

The acoustic intensity is given by

$$\overline{I} = \left[\frac{p'}{\rho_0} + \nabla G' \cdot \overline{U}_0\right] (\rho_0 \nabla G' + \rho' \overline{U}_0) \quad , \tag{E.1b}$$

and $\overline{n}$ is the normal to a curve surrounding all of the sound sources. We assume that the curve lies entirely in the geometric farfield. Power/span denotes the amount of acoustic power radiated per unit spanwise length of the infinite-span airfoil. The quantities p', ρ', and $\nabla G'$ are the acoustic pressure, density, and particle velocity, and $\overline{U}_0$ and ρ_0 are the mean-flow velocity and density. In the farfield, the

mean density and velocity can be replaced by their values at infinity. Eq. (E.1b) then becomes (in the (ϕ,ψ) coordinate system)

$$T = \left[\frac{p'}{\rho_\infty} + U_\infty^2 \frac{\partial G'}{\partial \phi} \right] \left[\rho_\infty \nabla G' + \frac{p' U_\infty}{a_\infty^2} \bar{e}_\phi \right] \quad . \tag{E.2}$$

The vector $\bar{e}_\phi$ is the unit vector in the ϕ direction.

The acoustic pressure is given by

$$p' = -\rho_0 \frac{D_0 G'}{Dt} \quad . \tag{E.3a}$$

In terms of the modified potential h, (E.3a) is (See (2.9c) and (2.12a))

$$p' = -\rho_0 \left[\frac{\partial}{\partial t} + U_0^2 \frac{\partial}{\partial \phi} \right] \left[h \, e^{-ik(\delta M_\infty^2 \phi - k_3 x + k_t U_\infty^2 t)} \, e^{-M_\infty^2 q} \right] \tag{E.3b}$$

$$\simeq \rho_\infty U_\infty^2 \left[ik\delta h - \frac{\partial h}{\partial \phi} \right] e^{i\Gamma} \quad , \tag{E.3c}$$

where

$$\Gamma = -ik(\delta M_\infty^2 \phi - k_3 x + k_t U_\infty^2 t) \quad . \tag{E.3d}$$

Far away from the airfoil, derivatives on the cylindrical wave phase ikwr of h dominate (See (4.43) for the farfield form of h), i. e.,

$$\frac{\partial h}{\partial \phi} = ikw\cos\theta \; h + O(h/r) \quad . \tag{E.4}$$

Hence,

$$p' \simeq i\, k\, \rho_\infty\, U_\infty^2\, (\delta - w\cos\theta)\, h\, e^{i\Gamma} \quad . \tag{E.5}$$

The acoustic particle velocity is

$$\nabla G' = U_0 \frac{\partial G'}{\partial \phi}\, \bar{e}_\phi + U_0\, \beta_\infty \frac{\partial G'}{\partial \psi}\, \bar{e}_\psi \quad , \tag{E.6}$$

where $\bar{e}_\psi$ is the unit vector in the ψ direction. We have ignored the spanwise component, since it makes no contribution when the inner product with the normal to the curve in the (ϕ,ψ) plane is taken. Inserting the relation between G' and h, we have

$$\frac{\partial G'}{\partial \phi} = \left[-ik\delta M_\infty^2 h + \frac{\partial h}{\partial \phi}\right] e^{i\Gamma} \quad . \tag{E.7a}$$

Again only the derivative on the rapidly-varying phase ikwr contributes, and (E.7a) can be approximated by

$$\frac{\partial G'}{\partial \phi} = -i\, k\, (\delta\, M_\infty^2 - w\, \cos\theta)\, h\, e^{i\Gamma} \quad . \tag{E.7b}$$

Similarly,

$$\frac{\partial G'}{\partial \psi} = i\, k\, w\, \sin\theta\, h\, e^{i\Gamma} \quad . \tag{E.8}$$

The acoustic particle velocity, obtained by combining (E.7a) and (E.8) and setting $U_0 = U_\infty$ in the metrics, is

$$\nabla G' = -ikU_\infty(\delta M_\infty^2 - w\cos\theta)he^{i\Gamma}\bar{e}_\phi + U_\infty\beta_\infty ikw\sin\theta he^{i\Gamma}\, \bar{e}_\psi \quad . \tag{E.9}$$

The variables involved in the definition (E.2) for acoustic intensity are all real quantities. So, to calculate intensity we insert the real parts of (E.5) and (E.9) into (E.2). The resulting expression is

$$\mathbf{I} = \frac{1}{4}\,\rho_\infty\, U_\infty^3\, \beta_\infty^3\, k^2\, \delta\, w\, (\beta_\infty \cos\theta \bar{e}_\phi + \sin\theta \bar{e}_\psi)[ihe^{i\Gamma} - ih^* e^{-i\Gamma}]^2 \qquad (E.10)$$

The star denotes complex conjugate. We wish to calculate average rather than instantaneous power. The only term inside the square brackets which contributes to the time average is the cross-product. Using this fact, we find that

$$\bar{I}_{ave} = \frac{1}{2}\,\rho_\infty\, U_\infty^3\, \beta_\infty^3\, k^2\, \delta\, w\, (\beta_\infty \cos\theta\, \bar{e}_\phi + \sin\theta\, \bar{e}_\psi)\, hh^* \quad . \qquad (E.11)$$

A convenient curve over which to perform the integration of (E.1a) is a circle in (ϕ,ψ) space (which is an ellipse in physical space, due to the Prandtl-Glauert transformation.) The normal to the circle is

$$\bar{n} = \cos\theta\, \bar{e}_\phi + \sin\theta\, \bar{e}_\psi \quad . \qquad (E.12)$$

Hence,

$$\bar{I}_{ave} \cdot \bar{n} = \frac{1}{2}\,\rho_\infty\, U_\infty^3\, \beta_\infty^3\, k^2\, \delta\, w\, (\beta_\infty \cos^2\theta + \sin^2\theta)\, h \cdot h^* \quad . \qquad (E.13)$$

To find the total average radiated power, we put (E.13) into (E.1a) and utilize the following expression for the differential element of length in the (ϕ,ψ) plane.

$$ds = [\, h_\phi^2\, d\phi^2 + h_\psi^2\, d\psi^2\,]^{1/2} \quad . \qquad (E.14)$$

In the farfield where the mean flow is uniform the coordinate metrics (2.5) reduce to constants and we obtain

$$ds = \frac{r\, d\theta}{U_\infty \beta_\infty}\, (\beta_\infty^2 \sin^2\theta + \cos^2\theta)^{1/2} \quad . \qquad (E.15)$$

where r is the radius of the circle in the (ϕ,ψ) plane. Expression (E.2) for the power becomes

$$\frac{\text{Power}_{ave}}{\text{span}} = \frac{1}{2}\,\rho_\infty\, U_\infty^3\, \beta_\infty^2\, k^2\, \delta\, w \int_0^{2\pi} h\cdot h^*\,(\beta_\infty \cos^2\theta + \sin^2\theta)$$
$$\cdot(\beta_\infty^2 \sin^2\theta + \cos^2\theta)^{1/2}\,\frac{r\,d\theta}{U_\infty} \quad . \tag{E.16}$$

At this point all quantities are dimensional. Equation (E.16) can be easily converted to apply to the nondimensional variables in Chapters 3, 4, and 5. Recall that h and r have dimensions of potential, i.e., length times velocity, and δ and w have dimensions of inverse length times velocity. As described at the beginning of Chapter 3, we nondimensionalize h and r by bU_∞ and w and δ by $1/bU_\infty$. In terms of the dimensionless variables used throughout Chapters 3, 4, and 5, the expression for power is

$$\frac{\text{Power}_{ave}}{\text{span}} = \frac{1}{2}\,\rho_\infty\, U_\infty^3\, b\, \beta_\infty^2\, k^2\, \delta\, w \int_0^{2\pi} h\cdot h^*\,(\beta_\infty \cos^2\theta + \sin^2\theta)$$
$$\cdot(\beta_\infty^2 \sin^2\theta + \cos^2\theta)^{1/2}\, r\, d\theta \quad , \tag{E.17}$$

where b is the semichord of the airfoil. All of our calculations are made in terms of the normalized power, defined by

$$\text{Normalized Power} = \frac{\text{Power}_{ave}/\text{span}}{\frac{1}{2}\,\rho_\infty\, U_\infty^3\, b} \tag{E.18a}$$

$$= k^2\,\delta\, w\beta_\infty^2 \int_0^{2\pi} h\cdot h^*\,(\beta_\infty \cos^2\theta + \sin^2\theta)(\,\beta_\infty^2 \sin^2\theta + \cos^2\theta)^{1/2}\, r\, d\theta \; . \tag{E.19}$$

For $r >> 1$, the only radial dependence of $h \cdot h^*$ is the $1/r$ decay, which cancels with the r in the differential element of length. The integrand is then purely a function of θ, the polar angle in (ϕ,ψ) space. Equation (E.19) is utilized for the calculations presented in Chapter 5.

REFERENCES

Adamczyk, J.J., "Passage of a Swept Airfoil through an Oblique Gust," J. Aircraft, 11, 281-287 (1974).

Amiet, R.K., "Effects of Compressibility in Unsteady Arifoil Lift Theories," Proc. of a Symposium on Unsteady Aerodynamics, Univ. of Arizona (1975).

Amiet, R.K., "High-Frequency Thin-Airfoil Theory for Subsonic Flow," AIAA Journal, 14, 1076-1082 (1976).

Atassi, H.M., "Effect of Loading and Rotor Wake Characteristics on the Acoustic Field of Stator Blades," AIAA paper No. 76-566 (1976).

Babich, V.M. and N.Y. Kirpichnikova, The Boundary-Layer Method in Diffraction Problems, Springer-Verlag, New York (1979).

Cheng, H.K. and N. Rott, "Generalizations of the Inversion Formula of Thin Airfoil Theory," J. Rational Mechanics and Analysis, 3, 357-382 (1954).

Envia, E. and E.J. Kerschen, "Noise Generated by Convected Gusts Interacting with Swept Airfoil Cascades," AIAA Paper No. 86-1872 (1986).

Ffowcs-Williams, J.E. and L.H. Hall, "Aerodynamic Sound Generation by Turbulent Flow in the Vicinity of a Scattering Half-Plane," J. Fluid Mechanics, 40, 657-670 (1970).

Ffowcs-Williams, J.E. and D.L. Hawkings, "Theory Relating to the Noise of Rotating Machinery," J. Sound Vib., 10, 10-21 (1969).

Ffowcs-Williams, J.E. and D.L. Hawkings, "Sound Generation by Turbulence and Surfaces in Arbitrary Motion," Phil. Trans. of Royal Soc. A, 264, 321-342 (1969).

Ginder, R.B. and D.R. Newby, "An Improved Correlation for the Broadband Noise of High Speed Fans," J. Aircraft, 14, 844-849 (1977).

Goldstein, M.E., "Unsteady Vortical and Entropic Disturbances of Potential Flows Round Arbitrary Obstacles," J. Fluid Mechanics, 93, 209-224 (1978).

Goldstein, M.E., Aeroacoustics, McGraw-Hill, New York (1976).

Goldstein, M.E., and H. Atassi, "A Complete Second Order Theory for the Unsteady Flow about an Airfoil due to a Periodic Gust," J. Fluid Mechanics, 74, 741-765 (1976).

Goldstein, M.E., B.M. Rosenbaum, and L.U. Albers, "Sound Radiation from a High-Speed Axial-Flow Fan due to the Inlet Turbulence Quadrupole Interaction," NASA TN D-7667 (1974).

Howe, M.S., "A Review of the Theory of Trailing Edge Noise," J. Sound Vib., 61, 437-465 (1978).

Kerschen, E.J. and T.F. Balsa, "Transformation of the Equation Governing Disturbances of a Two-Dimensional Compressible Flow," AIAA Journal, 19, 1367-1370 (1981).

Kerschen, E.J. and M.R. Myers, "Perfect Gas Effects in Compressible Rapid Distortion Theory," to appear in AIAA Journal, 1986.

Kovásnay, L.S.G., "Turbulence in Supersonic Flow," J. Aero. Sci., 20, 657-674 (1953).

Landahl, M.T., "Theoretical Studies of Unsteady Transonic Flow - IV. The Oscillating Rectangular Wing with Control Surface," Aeronautical Research Institute of Sweden (FFA), Rept. 80 (1985).

Mani, R., "Isolated Rotor Noise due to Inlet Distortion or Turbulence," NASA CR 2479 (1974).

Martinez, R. and S.E. Widnall, "Unified Aerodynamic-Acoustic Theory for a Thin Rectangular Wing Encountering a Gust," AIAA Journal, 18, 636-645 (1980).

Noble, B., Methods Based on the Wiener-Hopf Technique, Pergamon Press, New York (1958).

Van Der Waerden, B.L., "On the Method of Saddle Points," App. Sci. Res., B2 (1950).

Van Dyke, M., Perturbation Methods in Fluid Mechanics, Parabolic Press, Stanford, Ca. (1975).

Woods, L.C., The Theory of Subsonic Plane Flow, Cambridge University Press, London (1961).